Informatics Control Measurement
in Economy and Environment Protection

2/2020

Informatyka Automatyka Pomiary

w gospodarce i ochronie środowiska

www.e-IAPGOS.pl

ISSN 2083-0157

Kwartalnik Naukowo-Techniczny

National University of Water and Environmental Engineering (Rivne, Ukraine)

National University of Water and Environmental Engineering (NUWEE) is one of the best technical Universities of Ukraine. For more than 100 years our University creates thriving environment for students and researchers, and provides professional engineering expertise and services to the Government and private companies.

Today our University is one of the prominent modern educational establishments of Ukraine that became Alma mater for more than 70,000 domestic and international alumni. Our advances in water management engineering, advanced water treatment and environmental technologies, latest information technologies, economics and business made the National University a truly unique place for students to excel in technical disciplines as well as in business.

The nine Institutes of the University are guided by 374 Philosophy Doctors, 72 Habilitated Doctors - Professors, 45 Academics of the Academy of Sciences of Ukraine.

The University is the largest higher education establishment in Rivne region and the leading HEE of Ukraine; it consists of 9 institutes, 5 training and consulting centres, 5 colleges. The University offers full-time and part-time studies, distance learning studies in 41 bachelor degree programs and 53 master degree programs. University also provide 24 Ph.D. and 10 Doctoral studies.

The University has extensive international relations with more than 100 higher education institutions and international organizations of 25 countries, namely of Poland, Germany, France, the USA, Georgia, the Republic of Azerbaijan, Turkmenistan, Kingdom of Morocco, Republic of Ecuador and many other countries all over the world.

NUWEE is among 20 of best Universities of Ukraine according to the ranking “Top-200 Ukraine” of the international social and political journal “Mirror of the Week”. The University was awarded the Order of Friendship of Peoples, is listed in the “Golden Book of Business Elite of Ukraine“, and is a multiple winner of ratings “Golden Fortune”, “Best Enterprises of Ukraine” in the category “Higher education” and in the field of water management.

2/2020

kwiecień – czerwiec

Wydanie pod redakcją naukową
prof. dr hab. inż. Waldemara Wójcika

INFORMATYKA AUTOMATYKA POMIARY

W GOSPODARCE i OCHRONIE ŚRODOWISKA

Informatics Control Measurement in Economy and Environment Protection

p-ISSN 2083-0157, e-ISSN 2391-6761, www.e-iapgos.pl

PRINTING HOUSE – DRUKARNIA

DjaF – Naświetlarnia B1+
ul. Kmietowicza 1/1
30-092 Kraków
http://www.djaf.pl
nakład: 100 egzemplarzy

OTHER INFORMATION – INNE INFORMACJE

Czasopismo jest indeksowane w bazach:

BazTech:	baztech.icm.edu.pl
IC Journals Master List:	www.journals.indexcopernicus.com
Google Scholar	scholar.google.pl
POL-index	pbn.nauka.gov.pl

Czasopismo *Informatyka, Automatyka, Pomiary w Gospodarce i Ochronie Środowiska* zostało objęte finansowaniem przez Ministerstwo Nauki i Szkolnictwa Wyższego w ramach programu *Wsparcie dla czasopism naukowych* w latach 2019-2020.

Czasopismo znajduje się w wykazie czasopism naukowych opublikowanym w Komunikacie Ministra Nauki i Szkolnictwa Wyższego z dnia 31 lipca 2019 r., pozycja 27864 – z przypisaną liczbą punktów przyznawanych za publikację równą 20.

Zasady publikowania artykułów, przygotowania tekstów, zasady etyczne, procedura recenzowania, wykazy recenzentów oraz pełne teksty artykułów dostępne są na stronie internetowej czasopisma:

www.e-iapgos.pl

W celu zwiększenia oddziaływania czasopisma w środowisku naukowym redakcja zaleca:

- w artykułach publikowanych w IAPGOS cytować artykuły z renomowanych czasopism międzynarodowych (szczególnie indeksowanych w bazach Web of Science oraz Scopus) używając oficjalnych skrótów nazw czasopism,
- w artykułach publikowanych w innych czasopismach (zwłaszcza indeksowanych w bazach Web of Science oraz Scopus) cytować prace publikowane w IAPGOS – zwłaszcza posługując się numerami DOI, np.:
  Kluszczyński K. *Modelowanie – umiejętność czy sztuka?* Informatyka, Automatyka, Pomiary w Gospodarce i Ochronie Środowiska – IAPGOS, 1/2016, 4–15, DOI: 10.5604/20830157.1193833.

CONTENTS – SPIS TREŚCI

http://doi.org/10.35784/iapgos.1664

TRANSISTOR-BASED TEMPERATURE MEASURING DEVICE

Oleksandra Hotra
Lublin University of Technology, Department of Electronics and Information Technologies, Lublin, Poland

Abstract*. The schematic diagrams of the temperature measuring device based on transistor structures are presented in the paper. The temperature dependence of collector current without and with linearization of the conversion function is analysed. The linearization method based on compensation current formation is proposed. This allowed to reduce the temperature measurement error up to ± 0.006°C over the temperature ranges 40… 60°C and 60… 80°C and up to 0.08°C over the temperature range 10… 90°C.*

Keywords: temperature measurement, transistor structures, linearization

TRANZYSTOROWY UKŁAD DO POMIARU TEMPERATURY

Streszczenie. *W artykule zostały przedstawione schematy miernika temperatury opartego na strukturach tranzystorowych. Została przeanalizowana zależność prądu kolektora od temperatury bez i przy zastosowaniu linearyzacji funkcji przetwarzania. Zaproponowano metodę linearyzacji opartą na formowaniu prądu kompensacyjnego, która pozwoliła zmniejszyć błąd pomiaru temperatury do ± 0,006°C w zakresach temperatury 40… 60°C i 60… 80°C oraz do ±0,08°C w zakresie 10… 90°C.*

Słowa kluczowe: pomiar temperatury, struktury tranzystorowe, linearyzacja

Introduction

The increasingly widespread implementation of cyber-physical systems (CFS), Internet of Things devices and scattered measurement systems requires the improvement of sensor devices that collect and transmit environmental and physiological information to base stations [2, 6, 13]. High-precision temperature measurements are important in many applications [7]. Temperature measurements provide valuable information when conducting medical research [1]. Continuous 24-h body core and skin temperature monitoring allows you to track circadian rhythms that carry information about the functioning of the central nervous and immune systems. Body temperature is one of the key parameters for monitoring the health of preterm infants in the neonatal intensive care unit [4]. In addition, accurate temperature monitoring can facilitate early detection of diseases, including cancer. In the case of controlled hyperthermia in cancer, it is necessary to control the temperature with an accuracy better than 0.05°C in the range of 30–50°C [8].

Temperature measurement is also important for agriculture [14, 17], construction industry [16]. However, in order to optimize the use of resources in precision agriculture, it is necessary to measure the temperature with an accuracy of no less than 0.05ºC.

Ecological, marine, and oceanographic researches, with the aim of studying physical and biological processes based on forecasting systems and sensor networks, require accuracy levels of up to 0.01°C. [12, 18]

Different types of sensors are used for temperature measurement [18]. Thermocouples and Resistance Temperature Detectors (RTDs) are the most commonly used temperature sensors in the industry. Thermocouples provide measurements over a wide temperature range from -270 to 2300°C [7], but the measurement accuracy is within the range from 0.5 to 2°C, and could be increased up to 0.1°C in the narrower range [15]. Thermocouples also require the compensation of cold-junction temperatures [10, 11]. RTDs are used over the temperature range from -260 to 850°C [9], providing a high accuracy of 0.03…1°C [7], but they are characterized by high cost. The infrared sensors operate in a wide temperature range from -40 to 3000°C, but they are characterized by low accuracy of ±2°C which is dependent on object radiation and background noise [5, 7].

Particular progress has been made in modern thermometry through the use of primary temperature transducers based on p-n junctions of transistor structures [3, 19].

The main advantage of primary temperature transducers based on transistor structures compared with thermocouples and RTDs is the high sensitivity. However, their disadvantage is the lack of linearity of the conversion function.

The informative parameters of transistor-based primary transducers are the dependence of the voltage drop across the forward bias p-n junctions and the dependence of the collector or emitter currents on the temperature change. The use of the temperature dependence of collector currents provides the highest sensitivity.

The aim of the work is to develop the high-accuracy temperature measuring device based on transistor transducer for in-situ measurements in biomedicine, pharmacy and agriculture.

1. Design of high-precision temperature measuring device

The schematic diagram of the designed temperature measuring device is shown in Fig. 1. The temperature measuring device consists of the primary temperature transducer and the secondary transducer of the primary transducer measuring current to voltage. The secondary transducer comprises the current to voltage converter (CVC), the compensator of initial output current of the primary transducer (CCPT), the former of base current of the primary transducer, the output voltage bias generator (OVBG) and the devices for output voltage linearization.

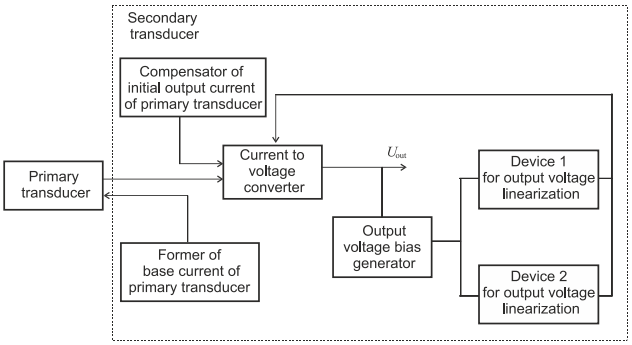

Fig. 1. Schematic diagram of the temperature measuring device

The temperature-dependent output current of the primary transducer is described by the following expression:

$$I = I_{t0} + \Delta I_t t \,, \tag{1}$$

where I_{t0} is the initial output current of the primary transducer at t = 0°C, ΔI_t is the change of output current with temperature change by 1°C, t is the measuring temperature in °C.

The compensator CCPT compensates the initial component of the output current I_{t0} and the following voltage is generated at the CVC output:

$$U_{out} = \Delta I_t t k_1 \,, \tag{2}$$

where k_1 is the conversion factor of CVC.

By choosing the coefficient k_1, the output voltage is formed, the value of which is equal to the value of the measured temperature.

The CVC output voltage through OVBG is fed to the inputs of the linearization devices. The output bias voltage generator forms the following voltage:

$$U_b = \Delta I_t t_{av} k_1 , \tag{3}$$

where t_{av} is the temperature value equal to the average temperature value of the measurement range.

The bias voltage of the OVBG is equal to the value of the output voltage of the PSN at the average temperature value of the measuring range. At $U_{out} > U_b$ the positive polarity voltage is applied to the inputs PL1 and PL2, and at $U_{out} < U_b$, the negative ones.

The output current of linearization devices is determined from the following expression:

$$I_l = (U_{out} - U_b) k_2 , \tag{4}$$

where k_2 is the conversion factor of linearization devices.

The currents of the linearization devices flow to the CVC converter and at the output the following compensating voltage is formed:

$$\Delta U_{out} = (U_{out} - U_b) k_1 k_2 . \tag{5}$$

After the corresponding substitution we get the following:

$$\Delta U_{out} = \Delta I_t k_1^2 k_2 (t - t_{av}) . \tag{6}$$

As a result of linearization, the output voltage of the PSN is described as follows:

$$U_{out} = \Delta I_t k_1 (t + k_1 k_2 (t - t_{av})) . \tag{7}$$

As can be seen, the linearization accuracy depends on the value of the coefficient k_2 and the temperature measurement range.

Schematic diagram of the designed dual-band temperature measuring device is shown in Fig. 2.

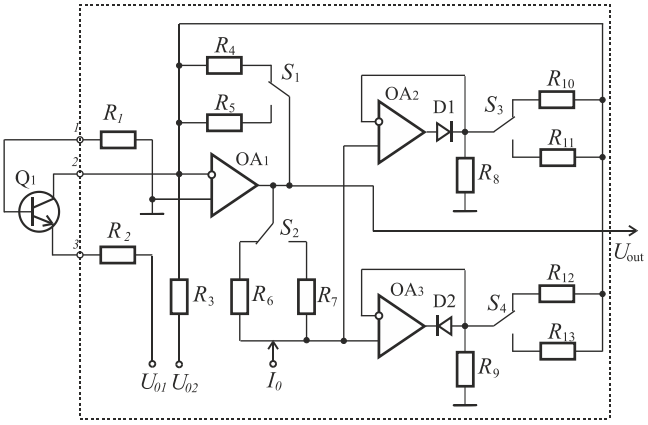

Fig. 2. Schematic diagram of the temperature measuring device

The Q_1 transistor-based primary transducer is connected to the inputs 1, 2, 3 of the secondary transducer by three lead wires. The base current of the transistor is formed by the reference voltage U_{01} and by the resistors R_1, R_2, and can be expressed as follows:

$$I_b = \frac{U_{01} - U_{R2} - U_{be}}{R_1} , \tag{8}$$

where U_{R2} is the voltage drop on resistor R_2, U_{be} is the voltage at the base-emitter junction of the transistor Q_1.

The voltage drop across resistor R_2 equals:

$$U_{R2} = (I_c + I_b) R_2 , \tag{9}$$

where I_c, I_b are collector and base currents of the transistor, respectively.

After the corresponding substitution we get:

$$I_b = \frac{U_{01} - U_{be}}{R_1 (1 + k)} , \tag{10}$$

where $k = \frac{(\beta + 1) R_2}{R_1}$, β is the gain factor of transistor.

At the temperature change the base-emitter voltage changes. The base current is determined from the following expression:

$$I_b = \frac{U_{01} - U_{be0}}{R_1 (1 + k)} + \frac{\Delta U_{be} t}{R_1 (1 + k)} \tag{11}$$

where U_{be0} is the voltage at the base-emitter junction at $t = 0°C$, ΔU_{be} is the voltage change at the base-emitter junction when the temperature changes by 1°C.

The collector current of transistor is equal:

$$I_c = \frac{U_{01} - U_{be0}}{R_1 (1 + k)} \beta + \frac{\Delta U_{be} t}{R_1 (1 + k)} \beta . \tag{12}$$

The analysis of the expression shows that the collector current contains a constant and variable component.

In order to compensate the constant component, the compensation current is used, the value of which is set by the resistor R_3, connected to the positive polarity reference voltage U_{02}. The resistance value of the resistor R_3 equals:

$$R_3 = \frac{U_{02} R_1 (1 + k)}{(U_{01} - U_{be0}) \beta} . \tag{13}$$

After compensation of the constant component of the collector current, the inverting input of the operational amplifier OA_1 receives the variable component of the collector current and the following voltage is formed at the OA_1 output:

$$U_{OA1} = \frac{\Delta U_{be} t}{R_1 (1 + k)} \beta R_4 . \tag{14}$$

By choosing the resistance value of the resistor R_4, we obtain the required value of the output voltage, proportional to the numerical value of the measured temperature.

In order to ensure the linearity of the conversion function within the temperature range $t_{min} \ldots t_{av}$, the linearization circuit based on the operational amplifier OA_3 is used, which generates the compensation current expressed by:

$$I_{com1} = \frac{U_{OA1} - U_{tav}}{R_{12}} , \tag{15}$$

where U_{tav} is the value of the voltage in the middle of the measurement range.

In order to ensure the linearity of the conversion function within the temperature range $t_{min} \ldots t_{av}$, the linearization circuit based on the operational amplifier OA_2 is used, which generates a compensation current according to the expression:

$$I_{com2} = \frac{U_{OA1} - U_{tav}}{R_{10}} . \tag{16}$$

In order to generate a voltage equal to the voltage in the middle of the measurement range U_{tav} it is used the bias on the resistor R_6, through which the reference current I_0 passes. Then the voltage U_{tav} equals:

$$U_{tav} = I_0 R_6 . \tag{17}$$

The resistor R_6 is connected in series to the output of the operational amplifier OA_1, and the following voltage is fed to the inputs of the operational amplifiers OA_2, OA_3:

$$U_{in} = U_{OA1} - I_0 R_6 . \tag{18}$$

If the following condition is met: $U_{in} < 0$, then at the output of the operational amplifier OA_3 a negative polarity voltage is generated, which is passed through the resistor R_{12} to the inverting input of the operational amplifier OA_1.

If the following condition is met: $U_{in} < 0$, then at the output of the operational amplifier OA_2 a positive polarity voltage is formed, which is passed through the resistor R_{10} to the inverting input operational amplifier OA_1.

In order to determine the required polarity of the output voltage in the output circuits of operational amplifiers OA_2, OA_3

the diodes D_1, D_2 are used. In order to reduce the influence of the diodes reverse currents on the accuracy of the formation of linearization compensation currents the resistors R_8, R_9 are used. The resistances of the resistors R_8, R_9 are much smaller than the ones of the resistors R_{10}, R_{12}.

The measurement ranges are chosen by changing the feedback resistors of the operational amplifier OA_1 (R_4, R_5), the resistors at the outputs of the operational amplifiers OA_2 and OA_3 (R_{10}, R_{11} and R_{12}, R_{13}), and the resistors at the input of the compensation circuits (R_6, R_7).

2. Investigation of the designed temperature measuring device

The investigation of the designed temperature measuring device was carried out in the Electronic Workbench, in accordance with the model shown in Fig. 3.

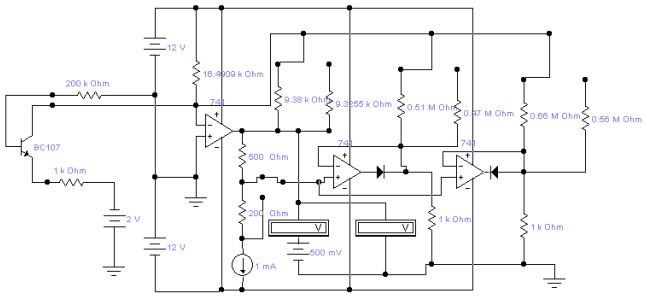

Fig. 3. Model for investigation of the designed temperature measuring device

BC107 transistor was used for investigations. The formation of collector current of the measuring temperature-dependent transistor is carried out by the reference voltage of 2 V, the base resistor of 200 kΩ and the emitter resistor of 1 kΩ. The initial collector current is compensated by a resistor connected to a positive +12 V supply voltage and to the inverting input of the input operational amplifier. The output voltage of the input operational amplifier is regulated by the resistor in the feedback. The reference DC source of 1 mA and the resistors in series (200 Ω, 500 Ω) connected to the input of the input amplifier are used to choose the required linearization range. A millivoltmeter was used to measure the output voltage of the input amplifier. A microvoltmeter and a reference voltage source were used to determine the voltage, which is equal to the nominal value of the output voltage.

The compensation of the constant component of transistor's collector current was carried out at 0°C. The calibration of the temperature measuring device was carried out at the temperature equal to the average value t_{av} of the measurement range. In this case the resistance of the resistor in the feedback of the first operational amplifier was set equal to 9.38 kΩ for the temperature range 40… 60°C and equal to 9.325 for the range 60… 80°C.

Graph dependencies of nonlinearity errors of temperature measurement for different temperature ranges are depicted in Figs. 4 and 5.

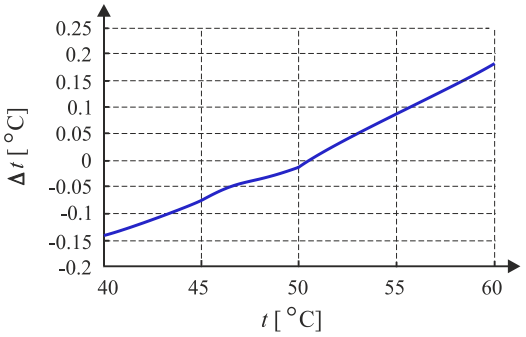

Fig. 4. Relationships between the errors of nonlinearity of temperature measurement and the temperature without linearization over the temperature range 40…60℃

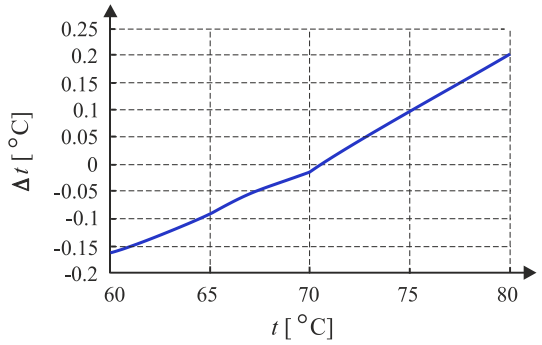

Fig. 5. Relationships between the errors of nonlinearity of temperature measurement and the temperature without linearization over the temperature range 60…80℃

The conducted analysis shows that the designed scheme of the temperature measuring device based on the transistor structure when using the temperature dependence of collector currents without linearization ensures the absolute measurement error not exceeding 0.2°C over the temperature ranges 40…60°C and 60… 80°C.

The errors of nonlinearity of temperature measurement versus temperature with linearization for different ranges are depicted in Figs. 6 and 7.

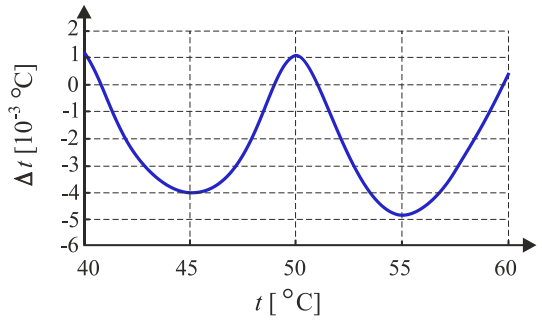

Fig. 6. Relationships between the errors of nonlinearity of temperature measurement and the temperature with linearization over the temperature range 40…60℃

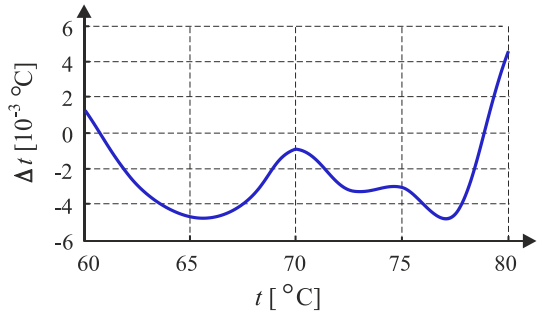

Fig. 7. Relationships between the errors of nonlinearity of temperature measurement and the temperature with linearization over the temperature range 60…80℃

As can be seen from the plots, the absolute measurement error does not exceed ±0.006°C over the temperature ranges 40… 60°C and 60… 80°C when performing linearization.

Improving of the accuracy of temperature measurements over a wider range is possible by introducing additional temperature ranges, which are chosen by additional resistors in the feedback loop of the input operational amplifier and by the output resistors of the linearization devices connected to the inverted input of the first operational amplifier.

Improving of the measurement accuracy over a wider range is also possible when compensating for nonlinearity errors at the temperature points higher than t_{av}+10°C and lower than t_{av}-10°C.

Relationships between the errors of nonlinearity of temperature measurement and the temperature during compensation at the points of 40°C and 60°C (curve 1), 30°C and 70°C (curve 2), 20°C and 80°C (curve 3) are plotted in Fig. 8.

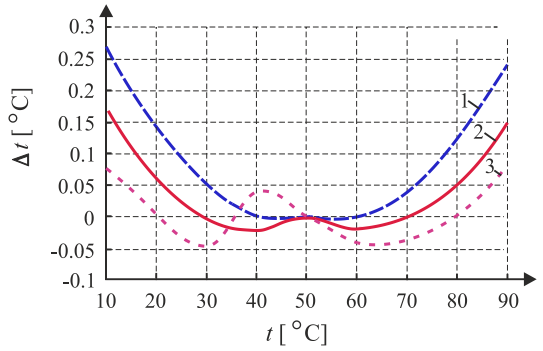

Fig. 8. Relationships between the errors of nonlinearity of temperature measurement and the temperature with linearization over the temperature range 10…90 ℃

As it can be seen from the graphical dependencies presented in Fig. 8 the absolute measurement error over the range 10… 90°C does not exceed 0.27°C for compensation at the points of 40°C and 60°C, does not exceed 0.17°C for compensation at the points of 30°C and 70°C, does not exceed 0.08°C for compensation at the points of 20°C and 80°C.

In order to improve the accuracy of temperature measurement, it is advisable to use additional compensation circuits over different measurement ranges.

3. Conclusions

The temperature measuring device based on transistor structures was developed using the temperature dependence of collector current as an informative signal, which provides the high sensitivity of temperature measurement.

In order to improve a measurement accuracy the method for nonlinearity compensation is proposed. The method is based on formation of a compensation current functionally dependent on the difference between the measured temperature value and the temperature value in the middle of the measurement range. This ensures the high measurement accuracy of ±0.006°C over the temperature ranges 40…60°C and 60… 80°C. Increasing of the temperature measurement accuracy over a wider range is possible by optimal choosing of compensation points in the middle of the measurement range. In the case of compensation at the points 20°C and 80°C, the measurement error does not exceed 0.08°C over the range 10… 90°C.

References

[1] Boano C.A., Lasagni M., Romer K., Lange T.: Accurate temperature measurements for medical research using body sensor networks. 14th IEEE International Symposium on Object/Component/Service-Oriented Real-Time Distributed Computing Workshops 2011, 189–198.

[2] Boyko O., Hotra O.: Improvement of dynamic characteristics of thermoresistive transducers with controlled heating. Przegląd Elektrotechniczny 5/2019, 110–113 [http://doi.org/10.15199/48.2019.05.27].

[3] Boyko O., Barylo G., Holyaka R., Hotra Z., Ilkanych K.: Development of signal converter of thermal sensors based on combination of thermal and capacity research methods. Eastern-European Journal of Enterprise Technologies 4/9(94)/2018, 36–42 [http://doi.org/10.15587/1729-4061.2018.139763].

[4] Chen W., Dols S., Oetomo S.B., Feijs L.: Monitoring body temperature of newborn infants at neonatal intensive care units using wearable sensors. Proceedings of the 5th International Conference on Body Area Networks, Corfu, Greece, 2010, 188–194 [http://doi.org/10.1145/2221924.2221960].

[5] Crawford D.C., Hicks B., Thompson M.J.: Which thermometer? Factors influencing best choice for intermittent clinical temperature assessment. J. Med. Eng. Technol. 30(4)/2006, 199–211.

[6] Goswami A., Bezboruah T., Sarma K.C.: Design of an embedded system for monitoring and controlling temperature and light. International Journal of Electronic Engineering Research 1(1)/2009, 27–36 [http://doi.org/10.18178/joace.4.5.331-339].

[7] Goumopoulos C.: A high precision, wireless temperature measurement system for pervasive computing applications. Sensors 18(10)/2018, 3445 [http://doi.org/10.3390/s18103445].

[8] Hans V.H.: High-precision measurement of absolute temperatures using thermistors. Proceedings of the Estonian Academy of Sciences, Engineering. 13(4)/2007, 379–383.

[9] Hotra O., Boyko O.: Analogue linearization of transfer function of resistive temperature transducers. Proceedings of SPIE 9662, 2015, 966247-1–966247-8 [http://doi.org/10.1117/12.2205449].

[10] Hotra O., Boyko O.: Compensation bridge circuit with temperature-dependent voltage divider. Przegląd Electrotechniczny 88(4A)/2012, 169–171.

[11] Hotra O., Boyko O.: Tranzystorowo-rezystancyjny układ kompensacji wpływu temperatury wolnych końców termopary. Proceedings of Electrotechnical Institute 249/2011, 21–27.

[12] Marcelli M., Piermatte V., Madonia A., Marcelli U.: Design and application of new low-cost instruments for marine environmental research. Sensors 14/2014, 23348–23364 [http://doi.org/10.3390/s141223348].

[13] Papageorgiou C., Sadriwala A., Almoalem M., Sheedy C., Hajjar A.: Environmental Control of a Greenhouse System Using NI Embedded Systems Technology. Journal of Automation and Control Engineering 4(5)/2016, 331–339.

[14] Prathyusha K., Suman M.C.: Design of embedded systems for the automation of drip irrigation. International Journal of Application or Innovation in Engineering & Management – IJAIEM 1(2), 2012. 2319–4847 [http://doi.org/10.13140/RG.2.2.18561.15207].

[15] Ross-Pinnock D., Maropoulos P.G.: Review of industrial temperature measurement technologies and research priorities for the thermal characterisation of the factories of the future. Proceedings of the Institution of Mechanical Engineers, Part B: Journal of Engineering Manufacture 230(5)/2016, 793–806.

[16] Spencer B., Al-Obeidat F.: Temperature Forecasts with Stable Accuracy in a Smart Home. 7th International Conference on Ambient Systems, Networks and Technologies / The 6th International Conference on Sustainable Energy Information Technology ANT/SEIT 2016, 726–733 [http://doi.org/10.1016/j.procs.2016.04.160].

[17] Thilagavathi G.: Online farming based on embedded systems and wireless sensor networks. International Conference on Computation of Power, Energy, Information and Communication (ICCPEIC) 2013, 71–74 [http://doi.org/10.1109/ICCPEIC.2013.6778501].

[18] Wunsch C.: Global ocean integrals and means, with trend implications. Annual review of marine science 8/2016, 1–33 [http://doi.org/10.1146/annurev-marine-122414-034040].

[19] Xie L., Gao Z.H., Gao W., Jin X.A: CMOS Temperature-to-Digital Sensor With ±0.5° Inaccuracy from -55° to 150°. IEEE 19th International Conference on Communication Technology – ICCT, 2019, 1481–1485 [http://doi.org/10.1109/ICCT46805.2019.8947211].

Prof. Oleksandra Hotra
e-mail: o.hotra@pollub.pl

Oleksandra Hotra is currently a professor in the Department of Electronics and Information Technology of Lublin University of Technology, head of Teleinformatics and Medical Diagnostics Department at Lublin University of Technology. Her areas of scientific interest cover electronic and optoelectronic sensors including materials for sensors, temperature measuring instruments, methods to improve the accuracy of temperature measurement, control measuring tools for temperature sensors, applications of NQR spectroscopy.

http://orcid.org/0000-0003-2074-347X

otrzymano/received: 21.04.2020 *przyjęto do druku/accepted: 26.06.2020*

http://doi.org/10.35784/iapgos.568

ANALYSIS OF ALL-PASS FILTERS APPLICATION TO ELIMINATE NEGATIVE EFFECTS OF LOUDNESS WAR TREND

Wojciech Surtel, Marcin Maciejewski, Krzysztof Mateusz Nowak
Lublin University of Technology, Department of Electronics and Information Technologies, Lublin, Poland

Abstract. *In this paper the influence of all-pass filters on musical material with applied hypercompression dynamics (loudness war trend) was analyzed. These filters are characterized by shifting phase in selected frequency band of signal, not by change of their amplitude levels. Because a lot of music information is present in music tracks, the dynamic range was tested together with influence of other sound parameters like selectivity or instruments' arrangement on scene, by running subjective tests on a group of respondents.*

Keywords: all-pass filters, digital filters, loudness war, dynamics compression

ANALIZA ZASTOSOWANIA FILTRÓW WSZECHPRZEPUSTOWYCH DO ELIMINACJI NEGATYWNYCH SKUTKÓW TENDENCJI LOUDNESS WAR

Streszczenie. *W artykule przeanalizowana wpływ filtrów wszechprzepustowych na materiał muzyczny z zastosowaną hiperkompresją sygnału (tendencją loudness war). Filtry tego typu, charakteryzują się przesunięciem w fazie składowych częstotliwościowych, sygnału, a nie zmianą poziomu ich amplitudy. Ze względu na dużą ilość informacji w utworach muzycznych, prócz sprawdzenia zakresu dynamiki poprzez testy obiektywne, zbadano również wpływ na inne parametry dźwięku takie jak selektywność czy rozłożenie instrumentów na scenie, poprzez testy subiektywne na grupie respondentów.*

Słowa kluczowe: filtry wszechprzepustowe, filtry cyfrowe, loudness war, kompresja dynamiki

Introduction

The concept of progressing loudness war is closely related to the dynamic compression . In the 1960s it was noticed that louder songs played by a radio stations generate better sales results. Hence, many radio stations decided to use louder versions of songs. In this type of recording, the compression of the dynamics was limited due to the characteristics of analog sound medium (magnetic tape or vinyl disc).

The launch of a CD with a much greater dynamic range and discreet representation of signal has changed the approach to music production. Recordings production could take multiple compression and signal normalization. Hence, recordings with dynamic hyper-compression began to be created.

Recordings of this type have a similar intensity of sound throughout the duration of the song. Sounds coming from more quiet instruments are amplified, so that they have a similar level of signal as other sounds in a musical track. In such production, it is easier to hear all sounds appearing in environments with high noise [12]. This trend causes a number of negative effects. They include: tiredness of ears after sustained presence in the room, reduction of the stereo scene (sound seems to come from one direction) and creation of various artifacts in the sound (clipping, aliasing, overlapping of frequency bands).

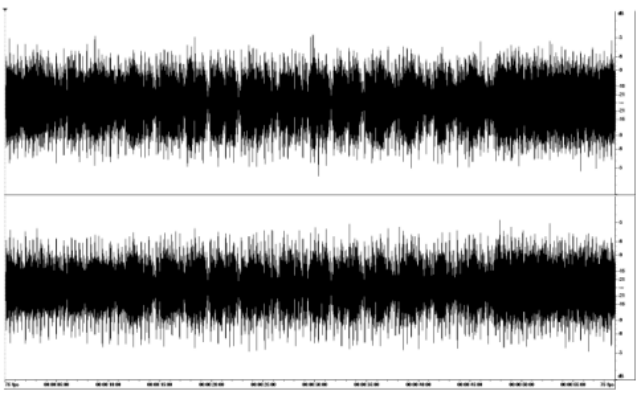

Fig. 1. Recording of the song Early Morning Wake Up Call in first vinyl editio from 1984. Despite the use of dynamic compression (similar amplitude level in the indicated fragment), the peak value of the signal is at the level of -2.77 dB, and the percussion instrument stands out from other instruments (visible sharp signal peaks)

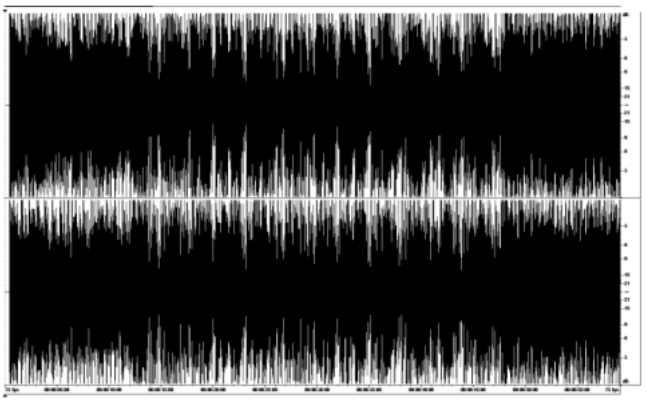

Fig. 2. Recording of the same song in remastered CD version from 2012. The peak signal level reaches the maximum value for the 16-bit file range (0 dB). There are no sharp percussion peaks (they are cut with a limiter). The recording has applied hypercompression dynamics

In addition to using loudness war in the music industry, this trend is used in movies and commercials. There are standards for the production of this type of recordings, however, they primarily comply to the maximum level of signal amplitude. There is no valid document in Europe specifying the range of sound dynamics in the presented material, thus advertisers often use hypercompression of dynamics within the boundaries of limiter in accordance with to EBU R 128 loudness recommendation [5,9]. The material thus created still retains the negative effects of the above trend.

1. The concept of removing effects of the Loudness War trend

The use of dynamic hypercompressions is an irreversible operation. In order to attenuate its negative effects the influence of various signal processors was checked. Such processors and systems for use in audio signal processing can use a variety of operation algorithms. One of them are digital filters.

Digital filters in audio technology are used to remove or cut selected frequency bands of the signal. They are used particularly for muffled or noisy recordings. Unfortunately, they change the reception of the song by modification of pitch of the sound or masking high frequencies (occurring in lossy compression). Using the filter systems and the amplification module, a system called the equalizer is created [2]. It is often used to produce effects in popular music players. However, they do not have universal appli-

cation, as the effect of its operation varies due to the type of music for which it is used.

The use of multiple signal compression cannot be reversed by using tools operating on the opposite principle. These tools (called dynamic processors) are signal amplifiers in a fixed ratio between different levels of the input signal. Using an expander (reducing the sound amplification for the given input range) can only partially reduce the negative impact of the trend. What is more, use of this tool is associated with sudden jumps in the level of noise, unnatural silence of the instruments and does not affect the clipping in any way [8].

2. Description of all-pass filters

There are various types of filters. Among these we can distinguished all-pass filters, used to shift the phase of selected frequency components or the entire frequency response. These filters differ from the others by maintaining a flat frequency response, so they do not cause differences in the pitch of the sound. They are most often used in loudspeakers and head-phones for correction of phase shifts introduced by low-pass filters. The formula for the impulse response of such a filter is [10]:

$$\left(H(e^{j\omega})\right)^2 = 1 \quad \forall\omega \tag{1}$$

where: ω – frequency.

The use of very high-order filters can lead to shifting of different signal bands over time. This most often causes blurring transients of the percussion instruments. In the case of uncom-pressed recordings, the all-pass filter may slightly change the dynamics of the song. In addition, this type of filter is used in digital devices that create a reverb effect. Making a phase shift with a large angle on the lower frequency components will result in the extension of the bass sound and the increase of his participation [3].

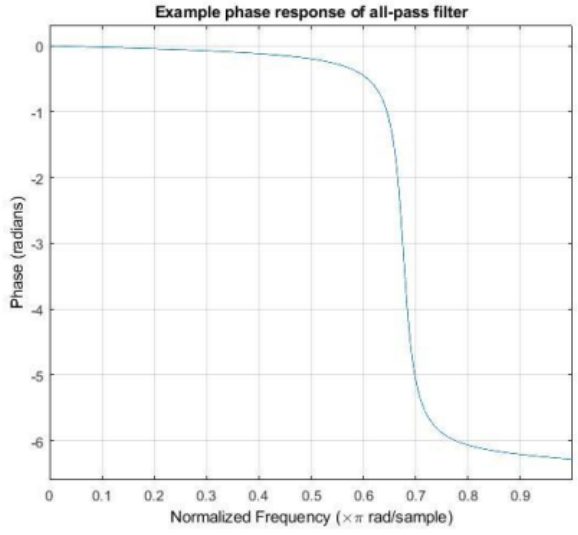

Fig. 3. Example phase characteristics of the filter with coefficients 1 and 0.9. The phase shift takes place in this case for higher frequency components by a full unit circle

3. Description of the Adobe Audition application

Adobe Audition (formerly Cool Edit Pro) is an audio editing environment created in the early 1990s. Purchased by Adobe in May 2003, it is being developed to this day. It contains many built-in digital filters and signal processors using which you can create your own characteristics. In addition, it includes fragment analysis tools and frequency or phase analysis for the audio signal. It supports many types of plugins, including the latest version of the VST3 plugin.

Version 1.5 (from May 2004) supplies is the Graphic Phase Shifter tools [1]. They are available from the Effects / Filters / Graphic Phase Shifter menu. It uses an all-pass filter with a user-defined phase characteristic. It is possible to set a the number of samples for which the fast Fourier transform will be calculated, choose the channel to shift, use the pre-made presets or save your own and use the approximation instead of the sharp transition of changes:

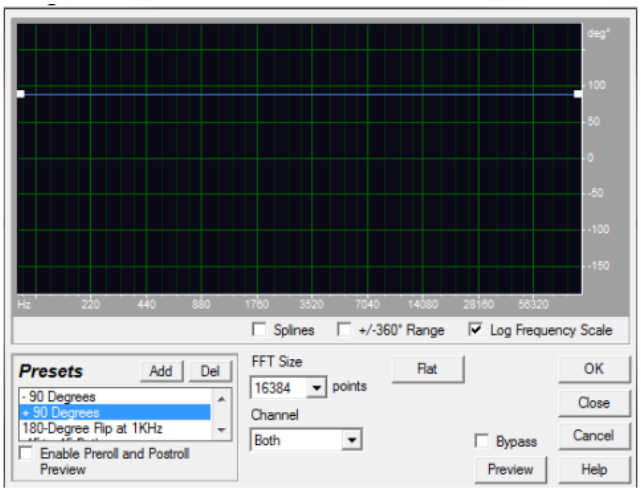

Fig. 4. View of the Graphic Phase Shifter window in Adobe Audition 1.5 with an example of a phase shift characteristic of 90° for the entire frequency spectrum.

4. Description of the experiment

As a part of the experiment, objective tests of the dynamics and subjective tests to checking impact on other parameters assessed by the group of respondents were conducted. The objective tests were performed using the Dynamic Range Meter, created by the Pleasurize Music foundation and the loudness Meter tool included in the MATLAB Audio System Toolbox. The Dynamic Range Meter uses its own algorithm, dynamic unit (abbreviation DR) and assigns a scale to it. The formula is as follows:

$$DR = \frac{1}{N}\sum_{n=0}^{N}\left(X_{max} - X_{ef}\right) \tag{2}$$

where: N – number of channels, X_{max} – signal peak in units of dBFS, X_{ef} – effective value calculated for 20% of the most amplified part of the signal in units of dBFS.

The dBFS unit represents the gain level expressed in decibels below the full scale range for the file. The DR scale has been divided into 3 ranges: good dynamics values (values from 14 DR), transient dynamics (from 8 to 13 DR) and recordings with bad dynamics (values up to 7 DR). In addition, the foundation runs a generally accessible database of phonographic recordings and their dynamics due to the publisher [4].

The loudness Meter tool uses the LRA algorithm developed by TC Electronics for the EBU R 128 recommendation. The LRA algorithm measures the dynamics of the recording based on the statistical distribution of the measured loudness. The quietest 10% and the loudest 5% of the track are not included in the final result. The unit of dynamics is in this case LU (loudness unit) and there are no specific ranges for it because, unlike DR, its value depends on the length of the song. This algorithm is often used for television and radio recordings and for matching recordings to music streaming websites [7,11].

All tests were conducted on six separate fragments of songs from various genres of music. A 30-second fragment was used for each selected song. The recordings in which hyper-compression of the dynamics in the source recording was observed were used. The result was additionally confirmed with the objective tests of the Dynamic Range Meter (values 7 and lower). The recordings were selected based on the genre variation and popularity of songs

For tests the following material was selected:

- Song ‘All Nightmare Long’ from Death Magnetic album by Metallica (thrash metal genre),
- Song ‘Thriller’ from Michael Jackson's compilation album Scream (pop genre, funk),

- Title track from album Californication by Red Hot Chili Peppers (alternative rock genre),
- Title track from the Song of Delilah album by Cedar Walton Trio (jazz genre),
- Song 'House of Wax' from Paul McCartney album Memory Almost Full (pop rock),
- Song 'Moon Child' from the album Before the Dawn Heals Us from the M83 project (genre of electronic music).

Each of the presented songs has been transformed using the all-pass filter with two settings. The first of these (Figure 5) assumes a linear increase in the phase shift between the angle of -45° and the angle of 45° for the linear frequency scale in the range from 0 to half of the material sampling frequency (44 100 Hz/2 = 22 050 Hz). The same shift was used for both channels in the stereo track. The second one (Figures 6 and 7), converts the signal by phase shift to -90° to 90° for the left channel and decreasingly for the right channel for the same range.

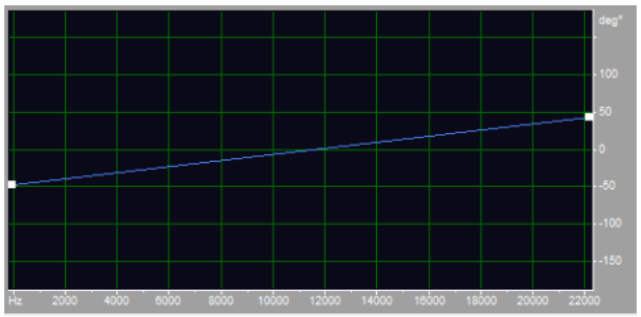

Fig. 5. Phase characteristic of the first of settings for both channels

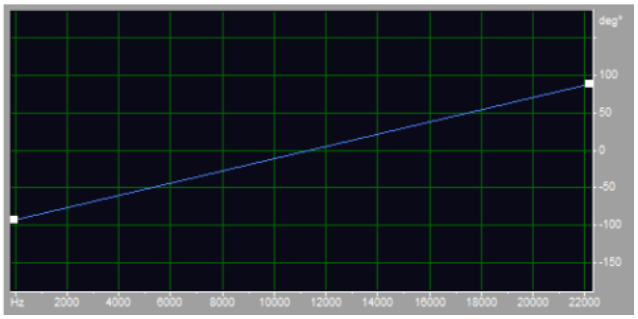

Fig. 6. Phase characteristic of the second set for the left channel

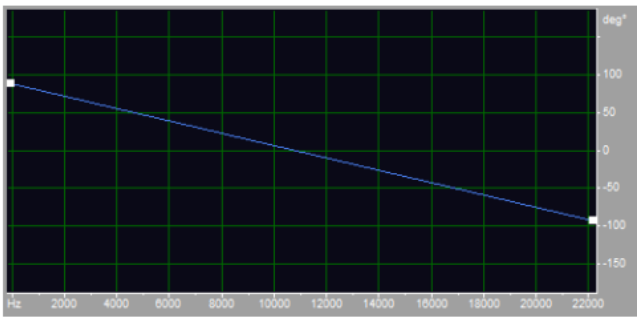

Fig. 7. Phase characteristic of the second of the settings for the right channel

Additionally, subjective tests were carried out on a group of 16 respondents, according to EBU Technical Review 274 [6], to check influence of all-pass filters on other parameters of the track. The test participants could assign grades according to recommendations as well as write their own feelings and comments on the musical material. The results of objective tests are presented in the tables below.

The results of the algorithm for measuring the dynamic range shows its growth using the phase shift. The smallest change can be observed for a jazz recording, the biggest for a metal song. Differences between the results exist due to the way drums participate in the recordings, the all-pass filter distinguished it the most by regulating the occurrence of its frequency components in time. The difference of 3 DR values, due to the use of the dBFS unit in the algorithm, is equivalent to the difference in the dynamic range of 3dB for the entire fragment (twice increase in its range). Thus, in the case of the biggest difference between the original recording and the 90° phase shift, we are dealing with a more than six-fold increase in the dynamics of the entire recording.

Table 1. The results of the fragment dynamics calculation using the Dynamic Range Meter

Fragment/version nr.	Original	45°	90°
All Nightmare Long	4	12	14
Thriller	7	13	14
Californication	4	10	10
Song of Delilah	7	9	9
House of Wax	5	9	10
Moonchild	6	10	10

Table 2. Results of dynamics calculation using the LRA algorithm obtained with MATLAB software.

Fragment/version nr.	Original	45°	90°
All Nightmare Long	1.36704729	1.36676814	1.36679966
Thriller	1.19096398	1.19275449	1.18769888
Californication	1.82118726	1.82028908	1.82093168
Song of Delilah	1.27255432	1.27282393	1.27190181
House of Wax	1.42241976	1.42180327	1.42164776
Moonchild	1.40707177	1.40800176	1.40744225

The results of the LRA algorithm show negligible changes between the original and processed fragments. This is because the influence of specific frequency components of the signal is shifted in time, and it is not cut or removed. In this case, the operation of the algorithm does not indicate that any of the filters causes an increase or decrease in the dynamics value. For versions processed with other signal processors (in particular the dynamics processor) the differences in the dynamics of the LRA algorithm are much greater. To explain the variation in the results of both algorithms for the all-pass filter, the corresponding waveforms are presented

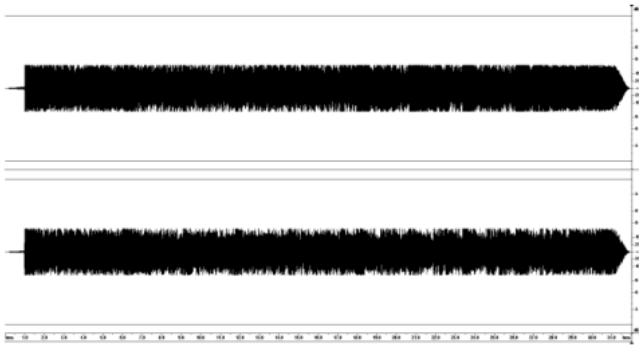

Fig. 8. The original recording of the selected fragment All Nightmare Long. The average effective values of the signal for the fragment are: -18.6 dB for the left channel and -19.96 dB for the right channel, respectively

The phase shift fragment has a significantly changed signal envelope, despite the same mean effective value of the signal for the whole fragment being compared to the same. Changes in the dynamics of the song are visible on the time courses, however, along with the increase of the dynamics of the song, you can observe unnatural peaks of the signal (in particular in places where in the original signal there were overloads). In exchange, there is no change in the amplitude of specific frequencies. Hence, the LRA algorithm did not show major changes (only differences in clipping samples).

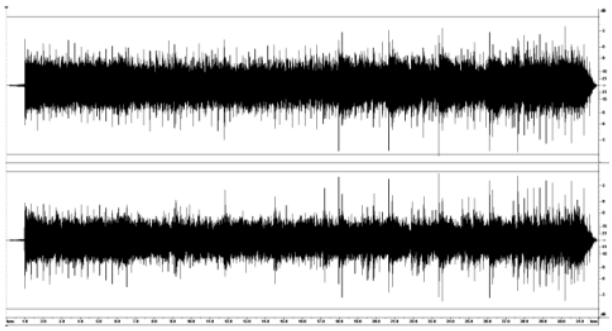

Fig. 9. The recording moved in phase according to the second setting of the selected fragment All Nightmare Long. The average effective values of the signal for the fragment are: -18.62 dB for the left channel and -19.98 dB for the right channel, respectively

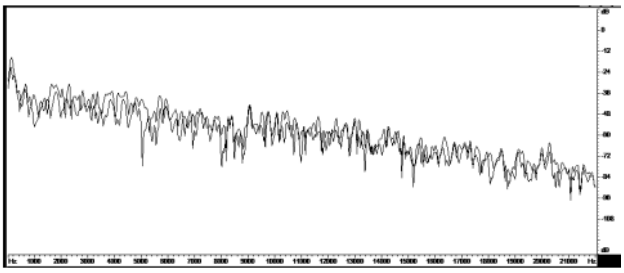

Fig. 10. Frequency analysis chart for 5 seconds of the original fragment under test, identical to the processed one

Respondents participating in the subjective test compared fragments processed to original fragments. In this case, the larger fragment with a phase shift of 45^o (average 4.8) compared to the fragment with a 90^o shift (mean 4.4) obtained a better result.

According to participants, too large phase shift caused an incorrect distribution of instruments on the stage, also manifested by changing the direction of the sound (the impression that the sound reached the listener after bouncing off the wall). The influence of guitars, in particular the bass guitar, has increased. With a shift of 90^o, this brought the instrument to the foreground. The version with a phase shift of 45^o, did not have such clear differences from the original. Some of the people showed similar comments, but they were harder to hear from the second setting.

5. Final conclusions

All-pass filters introducing a shift in the phase of frequency components of the signal change the dynamics of the recording. For a loudness-war recording, there is a local signal amplification observed through the increase in signal peaks. The dynamics of recording is especially visible for percussion instruments. Clipping objectively increases. The second objective test, however, shows that these changes do not cause differences in the gain of specific frequencies. Hence, for a smaller phase shift, these changes are difficult to hear. The positive effect (audible in audition) of the processed versions is their effect on the clipped fragments. This can be seen in Figure 9.

As it has been noticed in fragments with a larger phase shift, there are additional problems with the lower frequency components of the signal. Therefore, it would be necessary to abandon linear and symmetrical characteristics completely in relation to the middle of the range. However, this results in a smaller difference in dynamics relative to the original.

References

[1] Adobe Audition CC, https://www.adobe.com/pl/products/audition.html (access: July 2018).
[2] Altunian G.: The Difference Between a Graphic and a Parametric Equalizer. https://www.lifewire.com/graphic-vs-parametric-equalizer-3134842 (access: July 2018).
[3] Berners D.: Q: What are allpass filters and what are they used for? https://www.uaudio.com/blog/allpass-filters/ (access: July 2018).
[4] Dynamic Range DB, http://dr.loudness-war.info/ (access: July 2018).
[5] EBU R 128, Loudness normalisation and permitted maximum level of audio signals. https://tech.ebu.ch/docs/r/r128.pdf (access: July 2018) Geneva 2014.
[6] EBU Technical Review 274, Subjective assessment of audio quality – the means and methods within the EBU. https://tech.ebu.ch/docs/techreview/trev_274-hoeg.pdf (access: July 2018) Geneva 1997.
[7] EBU Tech 3342: Zakres głośności: Deskryptor uzupełniający normalizację głośności zgodnie z zaleceniem EBU R 128. https://tech.ebu.ch/docs/tech/tech3342_PL.pdf (access: July 2018) Geneva 2010.
[8] Jeffs R., Holden S., Bohn D.: Dynamics Processors -- Technology & Applications https://www.rane.com/note155.html (access: July 2018).
[9] Orpheus R.: EBU R128 – The important audio breakthrough you've never heard of https://www.iconnectivity.com/blog/2017/6/10/ebu-r128-the-important-audio-breakthrough-youve-never-heard-of (access: July 2018).
[10] Smith J.O.: Physical Audio Signal Processing, http://ccrma.stanford.edu/~jos/pasp/, online book, 2010 (access: July 2018).
[11] TC Electronics, Loudness Explained. https://www.tcelectronic.com/brand/tcelectronic/loudness-explained (access: July 2018).
[12] Vickers E.: The Loudness War: Background, Speculation and Recommendations. 129th AES Convention, San Francisco 2010.

Ph.D. Eng. Wojciech Surtel
e-mail: w.surtel@pollub.pl

Graduated from the Faculty of Electrical Engineering in Lublin Institute of Technology. From 1989 to 2011 worked in the Department of Electronics in Lublin Institute of Technology. Obtained PhD degree in 1999 in the Faculty of Electrical Engineering in Lublin Institute of Technology. Since 2011 senior lecturer in Department of Electronics and Information Technology. Fields of study include teleinformatics, telemedicine, digital data analysis.

https://orcid.org/0000-0003-1166-4083

Ph.D. Eng. Marcin Maciejewski
e-mail: m.maciejewski@pollub.pl

He graduated from the Faculty of Electrical Engineering and Computer Science at the Lublin University of Technology. Since 2011 works in the Department of Electronics and Information Technology. Completed PhD thesis in 2019. Fields of study include medical data processing, telemedicine, robotics and microcontrollers.

https://orcid.org/0000-0001-9116-5481

M.Sc. Krzysztof Mateusz Nowak
e-mail: krzysztof.mateusz.nowak94@gmail.com

He graduated from the Faculty of Electrical Engineering and Computer Science at the Lublin University of Technology in the field of Computer Science, specialization in Mobile Systems and Multimedia Techniques.

https://orcid.org/0000-0002-3117-7998

otrzymano/received: 28.10.2019 *przyjęto do druku/accepted: 26.06.2020*

http://doi.org/10.35784/iapgos.927

LOGICAL CLASSIFICATION TREES IN RECOGNITION PROBLEMS

Igor Povhan
Uzhgorod National University, Department of Software Systems, Uzhgorod, Ukraine

Abstract. *The paper is dedicated to algorithms for constructing a logical tree of classification. Nowadays, there exist many algorithms for constructing logical classification trees. However, all of them, as a rule, are reduced to the construction of a single classification tree based on the data of a fixed training sample. There are very few algorithms for constructing recognition trees that are designed for large data sets. It is obvious that such sets have objective factors associated with the peculiarities of the generation of such complex structures, methods of working with them and storage. In this paper, we focus on the description of the algorithm for constructing classification trees for a large training set and show the way to the possibility of a uniform description of a fixed class of recognition trees. A simple, effective, economical method of constructing a logical classification tree of the training sample allows you to provide the necessary speed, the level of complexity of the recognition scheme, which guarantees a simple and complete recognition of discrete objects.*

Keywords: pattern recognition problems, logical tree, graph-scheme models, recognition system

LOGICZNE DRZEWA KLASYFIKACJI W ZADANIACH ROZPOZNAWANIA

Streszczenie. *Artykuł poświęcono algorytmom konstruowania logicznych drzew klasyfikacji. Większość tych algorytmów z reguły sprowadzają się do zbudowania jednego drzewa klasyfikacyjnego na podstawie stałej próby uczącej. Należy zauważyć, że niewiele algorytmów budowania drzew klasyfikacyjnych dla prób treningowych o dużej objętości. Oczywiste jest, że mają one obiektywne czynniki związane ze specyfiką generowania takich struktur, metodami pracy z nimi i ich przechowywania. W niniejszym artykule autorzy skupiają się na opisie algorytmu konstruowania drzew klasyfikacyjnych dla dużego zbioru uczącego i wskazują możliwość jednolitego opisu stałej klasy drzew rozpoznawczych. Prosta, skuteczna i ekonomiczna metoda budowy logicznego drzewa klasyfikacyjnego dla danej próby uczącej pozwala na zapewnienie niezbędnej szybkości i stopnia złożoności schematu rozpoznawania, co gwarantuje proste i kompletne rozpoznawanie obiektów dyskretnych.*

Słowa kluczowe: zadania rozpoznawania obrazów, logiczne drzewo, schematy modeli rozpoznawania, system rozpoznawania

Introduction

As of today, various algorithms for constructing logical classification trees are known [7]. However, all of them, as a rule, are reduced to the construction of a single classification tree from the data of a fixed training sample. Note that in the literature there are very few algorithms for constructing logical trees for training samples of large volume. It is clear that this is based on objective factors associated with the features of the generation of such complex structures, methods of working with them and storage [5]. Even using the tools of Java or C#, it is necessary to provide the implementation of special data structures for working with logical trees, and ready-made libraries (LightGBM, XGBoost), although close ideologically (logical tree scheme), do not allow to implement the concept of an algorithmic classification tree, which consists of a set of vertices – different types of Autonomous classification algorithms. However, the main drawback in the construction of logical trees is the lack of algorithms and methods that would allow uniformly describe different algorithms for pattern recognition in the form of tree structures.

The ability to represent the recognition function as a logical tree has great advantages over other representations of classification schemes [4]. It should be noted that the algorithms for generating classification trees according to the training sample complement the methodology of the branched feature selection approach and allow to build simple and effective rules for the classification of discrete objects [1].

In this paper, we will focus on the description of the algorithm for constructing logical training samples for a large volume and show the way to the possibility of a uniform description of a fixed class of logical trees.

1. Statement of the recognition problem

In fact, the central task of pattern recognition is to build such a system that for each object that will be presented to it, would give the number of the class to which the object belongs [3, 4, 5]. The general problem of pattern recognition (classification) can be formulated in the following simplified form. Let on some set *M* of objects *w* a given partition *R* into a finite number *m* of subsets (classes, images) H_i ($i = 0, ..., m$):

$$M = \bigcup_{i=1}^{m} H_i \tag{1}$$

The corresponding sets $H_0, H_1, ..., H_m$ will be called images, and the elements of the set – *M* images or representatives of images $H_0, H_1, ..., H_m$. If the condition is met (1), then this split will be called complete. Objects (images) *w* are defined by sets of values of some features $x_j, j = 1,...,n$. If $w \in H_i$ we assume that this object belongs to the image H_i. In general, images $H_0, H_1, ..., H_m$ can be specified by probability distributions $p(H_0 / w), p(H_1 / w), ..., p(H_m / w)$, where $p(H_i / w)$ – the probability (or in the continuous case, the probability density) $w(w \in M)$ of belonging to the image H_i.

As a rule, in the problems of pattern recognition at the beginning is given some a priori information about *R* the nature of the partition and, depending on the nature of this information, it is customary to consider the following recognition tasks with training, without training, with self-learning. In this paper, the main attention will be paid to the problems of recognition with the previous training.

It should be noted that the fixed set of features that are characterized *w*, is always the same for all objects that are considered in solving this problem. Each feature can take values from different sets of valid feature values. For example, very often signs take values from a set $\{0,1\}$ or a sign takes a finite number of values – $\{a_1, a_2, ..., a_d\}$ the value of a sign can be a distribution function of some random variable. Objects that belong to one class are characterized by a certain commonality of their features, and objects from different classes do not have such a commonality, therefore the solution to the problem of recognition is to somehow highlight and describe this commonality or its absence.

When recognizing images, the most important, and sometimes the only given information about the partition is the training sample:

$$(A_1, H_{s,1}), (A_2, H_{s,2}), ..., (A_z, H_{s,z}) \tag{2}$$

where A_k, – certain objects (vectors), $H_{z,k}$ are the numbers of classes that contain objects A_k. Belonging of the object to a particular class is determined, as a rule, as a result of experimental studies, during which the training sample is formed.

It is on the basis of it in the problems with the previous training that the classification rule is built, and the solution is to determine the class to which the object that is being studied belongs.

The main requirement that is imposed on the training sample is the most complete and adequate description of the nature of the breakdown H_0, H_1, ..., H_m. In real tasks to fulfill this requirement is not only difficult, and sometimes impossible, because the nature of the partition may not even know the experimenter, and its full description will lead to a significant increase in the amount of training sample, and therefore – and the time spent on the learning process of the system. Therefore, the process of "error accumulation" begins at this stage, and even the most perfect recognition system in this case will be ineffective and powerless.

Each partition H_0, H_1, ..., H_m can be implemented using some finite-valued function $f_r(w)$ whose argument takes values from the set M. For example, H_0, H_1, ..., H_m it is possible to use a function $f_r(w) = i$ to split, if w necessary H_i, $i = 0, ..., m$.

It should be noted that the function $f_r(w)$, where $w \in M$, determines, in turn, some partition of the set M. Furthermore $f_r(w)$, then is only then everywhere defined in set M the plural when the corresponding partition R is complete. Thus, each partition H_0, H_1, ..., H_m can be set using a finite-valued function $f_r(w)$, and – each finite significant function $f_r(w)$ sets some partition.

For example, M – let the set of real numbers and $H_0 = \{w \mid 0 < w \le 2\}$, $H_1 = \{w \mid -2 \le w \le -1\}$, $H_3 = \{w \mid 3 \le w \le 5\}$. Moreover, $\{w \mid P(w)\}$ there is a set w for which the predicate $P(w)$ will be true. This partition can be set using an arbitrary function of the form:

$$f_r(w) = \begin{cases} \alpha_0, \, if & 0 < w \le 1 \\ \alpha_1, \, if & -2 \le w \le -1 \\ \alpha_2, \, if & 3 \le w \le 5 \end{cases}$$

Note that here $\alpha_0, \alpha_1, \alpha_2$ – arbitrary pairwise different real numbers. Thus, the same partition H_0, H_1, ..., H_m can be specified using many functions $f_r(w)$.

In general , the task of pattern recognition (classification) is to construct a function $f_r(w)$ that implements the splitting R of the set M, or to calculate the values of some predicates $P_i(w)$ (note that the decision about the object belonging to a particular class can be encoded as follows: 0 (w not allowed H_i) and 1 (w belongs H_i).

Let's define a feature of some object w as a function $f(w)$ whose arguments take values from an arbitrary set G, and $f(w)$ – from a countable set $\{0,1,..,k\}$. The function $f(w)$ can be both deterministic and probabilistic. An arbitrary function $f(w)$ defined on G, and taking a finite number of values, we called a sign. Let L be a class of signs on the lot M, and K – class diagrams. Under the scheme $S(f_1, f_2, ..., f_n)$ of the class K we understand the operator, which signs $f_1, f_2, ..., f_n$ with L puts in line some (over significant) function $\phi(x) = S(\alpha_1, ..., \alpha_n)$, defined on the set M.

As rudimentary signs there may be predicates, that is, deterministic characteristics of the host either 0 or 1. From them we will demand that they, in a sense, were the simplest (were a description of a fixed image). A sign that can be obtained in some way from the elementary features $\phi_1, \phi_2, ..., \phi_n$ we call a generalized feature.

2. The scheme of construction of a logical recognition tree

The main purpose of the algorithms of recognition methods based on the logical tree, which will be presented below, is to maximize the value of $W_M(f)$ [2, 5, 7]. The latter means that the algorithms of the logical tree should be found for the training sample (2) such a generalized sign f for $W_M(f)$ which the value is the largest possible.

Note the following, the sample (2) may have a probabilistic character, that is $(x_i, f_R(x_i))$, $(i = 1, 2, ..., M)$ pairs may appear in it according to some probability distributions $p(x/H_0)$, ..., $p(x/H_{k-1})$, but the generalized characteristic is deterministic. Thus, we pose the problem of optimal approximation of the probability sample (2) with the help of some deterministic function, which is generally represented by a generalized feature f. It is obvious that the problem makes sense when the character of images (classes) H_0, H_1, ..., H_{k-1} is close enough to deterministic. The latter will mean that the main share is occupied by those points (objects) x for which the value $\max(p(x/H_0), ..., p(x/H_{k-1}))$ is close to one. This value can vary significantly only at points (objects) that lie on the boundary of several classes H_0, H_1, ..., H_{k-1}.

Note that in practice, they mainly work with tasks where images (classes) H_0, H_1, ..., H_{k-1} have a character close to the deterministic case (for example, recognition of handwritten characters).

All algorithms that will be presented below have the following feature. Each algorithm is a process that consists of certain steps d_0, d_1, ..., d_i. Each step d_j here consists in turn of two stages (modes) – training and test.

In the training mode, a generalized feature f_i is formed on the step d_i. In the test mode, the effectiveness of $W_M(f_i)$ [5] relative to the training sample (2) is calculated for this generalized trait. If $W_M(f_i) \ge \delta$, then the learning process ends, if $W_M(f_i) < \delta$, then the transition to the step d_{i+1}; δ – a number that characterizes the evaluation of the effectiveness of training that is required by the task.

Now it is necessary to note the points regarding the nature of the sample submission (2) during training. In practice, two cases are possible:

a) The sample (2) is fixed, that is, all of It is supplied at each step of training d_i.

b) Selection (2) depends on the step d_i, which means that each step d_i of the training is fed its own sample.

The case (a) occurs when the sample (2) is the data of some experiment (for example, computer measurements), which are recorded in permanent memory. The learning algorithm in this case is a multiple sample processing (2). Note that the sample (2) can be very large. Therefore, the algorithms of processing of the sample should be such that it would be in their work sample (2) are not recorded in memory.

If there is no case (a) and stored data in permanent memory, then we have case (b). In this case, all the pairs that are processed in the step d_i are not remembered, and therefore some other series of training pairs of the form (2) are supplied in the step d_{i+1}.

Most of the methods presented below are structured so that they can be applied in both case (a) and case (b). For certainty, we further assume that there is a case (a), that is, at each step d_i the same sample (2) is supplied.

At the heart of all recognition methods in the form of a logical tree is one schematic diagram, which is called the scheme of the tree method. In this scheme, initially selected some elementary feature ϕ_1^1. This characteristic requires that the magnitude $W_M(\phi_1^1)$ is relatively (2) were possibly the greatest. Let us note once $W_M(\phi_1^1)$ that it is calculated according to the method [5, 6]. The following steps of the method of the logical tree, it is convenient to interpret with the help of a tree (Fig. 1).

In each vertex of the tree (Fig. 1) there is either some sign ϕ_i^j or a number m_i^j that belongs to the set $\{0, 1, ..., k-1\}$. Note that the number m_i^j here defines the image (class) $H_{m_i^j}$. The vertex in which it stands m_i^j is called the final vertex of the tree. From each vertex, in which there is a sign ϕ_i^j, depart two guides (arrows) which are marked 0 and 1. Guide, labeled 0, corresponds to the value $\phi_i^j = 0$ and represents the 1 value $\phi_i^j = 1$. The tree is broken conditionally behind tiers. There are signs ϕ_1^j, ϕ_2^j, ..., in j – tier.

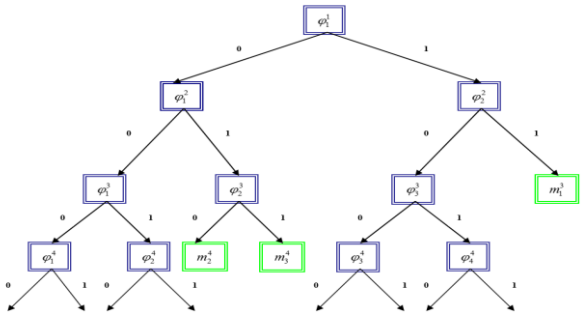

Fig. 1. Initial recognition tree

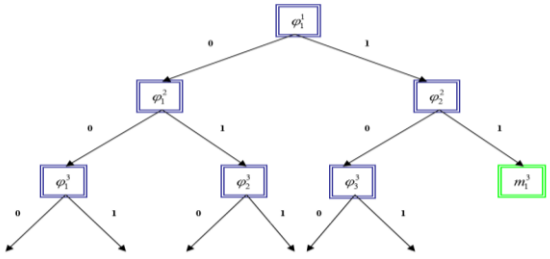

Fig. 2. Recognizer tree after three steps of the synthesis

All the features that are in all tiers, starting from the first and ending with the n – tier are those features that are obtained after the n steps (stages) of the process of building the classification tree. Moreover, the signs standing on the n – tier are those signs that are obtained at the n step (stage) of the process of building a logical tree.

Suppose that only three steps of the tree method are carried out and ϕ_1^1, ϕ_1^2, ϕ_2^2, ϕ_1^3, ϕ_2^3, ϕ_3^3 – all the signs obtained as a result of these steps. The logical tree that we get for these three steps will have the form shown in (Fig. 2).

Each related pair $(x_i, f_R(x_i))$, $(1 \le i \le M)$ of sampling (2) is the corresponding defined path of the tree (Fig. 2). This path is implemented as follows. First calculated $\phi_1^1(x_i) = r_i$. Further from the top ϕ_1^1 down the arrow, which is indicated by r_i. Let, for example $\phi_1^1(x_i) = r_1 = 0$. Then go down to the top, which is a sign ϕ_1^2. Then calculate $\phi_1^2(x_i) = r$ and go down the arrow that comes out of the vertex ϕ_1^2 and marked with the value r_2 and so on.

The path that corresponds to the pair $(x_i, f_R(x_i))$ (it is completely determined by the value x_i) is denoted by T_i. There are two possible cases:

a) Let the path T_i end with some directional arrow for example, if $\phi_1^1(x_i) = 0$, $\phi_1^2(x_i) = 0$, $\phi_1^3(x_i) = 0$ the path T_i ends with an arrow that comes out of the vertex ϕ_1^3 and is denoted by a symbol 0 (Fig. 2).

b) Let the path T_i end with some vertex where the value is m_i^j. For example, when $\phi_1^1(x_i) = 1$, $\phi_2^2(x_i) = 1$ and path T_i ends with a vertex containing a value m_1^3 (Fig. 2).

The paths in case (a) are called unfinished, and the paths in case (b) are finished.

If the path T_i that corresponds to the pair $(x_i, f_R(x_i))$ is complete and there is a value m_i^j, $(m_i^j \in \{0,1,...,k-1\})$ at the end, it means that $f_R(x_i) = m_i^j$. For example (Fig. 2) for all pairs $(x_i, f_R(x_i))$ that satisfy the condition $\phi_1^1(x_i) = \phi_2^2(x_i) = 1$, the following condition is fulfilled: $f_R(x_i) = m_1^3$. It can be said that for a value x_i that corresponds to a complete path T_i, full tree recognition is implemented (Fig. 2). That is, we can say that the pair $(x_i, f_R(x_i))$ belongs to the corresponding path T_i.

When carrying out the following steps in the construction of a classification tree are considered only unfinished journey.

Next, each path on the tree under construction will be denoted by a binary set $r_1, r_2, r_3 .... (r_i \in \{0,1\})$. For example, a binary set 010 in a tree (Fig. 2) denotes a path that ends with a final arrow, with a vertex ϕ_2^3 and a symbol 0. It is obvious that the set 000, 001, 010, 011, 100, 101 is a set of all unfinished paths on the tree (Fig. 2).

Let M_{r_1,r_2,r_3} – the number of all sample pairs $(x_i, f_R(x_i))$ (2) that belong to the unfinished tree path r_1, r_2, r_3 (Fig. 2). Let's $M^j_{r_1,r_2,r_3}$, $(0 \le j \le k-1)$ – say the number of all pairs that belong to a path r_1, r_2, r_3 and also for them the following relation is executed: $f_R(x_i) = j$. For each unfinished tree path (Fig. 2) calculate the values:

$$t^j_{r_1,r_2,r_3} = \frac{M^j_{r_1,r_2,r_3}}{M_{r_1,r_2,r_3}}, \ (j = 0,\ 1,\ ...,\ k-1) \tag{3}$$

Next, we find such a value $l(r_1, r_2, r_3)$ that:

$$l(r_1,r_2,r_3) \in \{0,1,...,k-1\}, \ t^{l(r_1,r_2,r_3)}_{r_1,r_2,r_3} = \max_j t^j_{r_1,r_2,r_3} \tag{4}$$

Substituting at the end of each path r_1, r_2, r_3 on the tree (Fig. 2) the value $l(r_1, r_2, r_3)$, we obtain the following tree (Fig. 3).

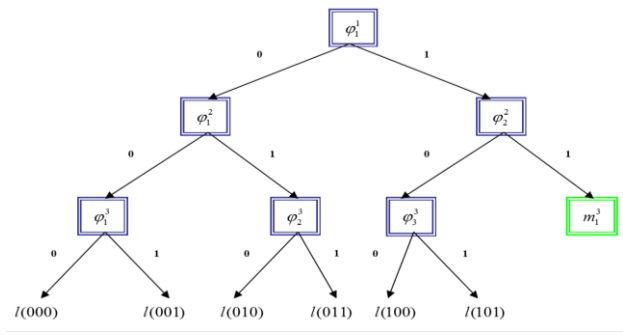

Fig. 3. Modified classification tree

3. Verification test stage

The tree (Fig. 3) implements some generalized trait $f_3(x)$ which is defined on the set G and takes values from the set $\{0,1,...,k-1\}$. The sign $f_3(x)$ is calculated as follows. First find for x the entire path T_x, which corresponds to this element. For example, if $\phi_1^1(x)=0$, $\phi_1^2(x)=1$, $\phi_2^3(x)=1$, then $T_x=011$. As values $f_3(x)$, take the element $\{0,1,...,k-1\}$ that ends the path T_x. For example, if, $T_x=011$ then $f_3(x)=l(011)$. If the object x corresponds to the completed path T_x, at the end of which there is a number m_x, $(0\le m_x\le l)$, then we assign that $f_3(x)=m_x$.

After the feature $f_3(x)$ is built, the verification test stage begins. In the test mode, the number S of all the pairs $(x_i, f_R(x_i))$ from the sample (2) for which the ratio is performed is calculated $f_R(x_i)=f_3(x)$. Next, check the condition $\frac{S}{M}\ge\delta$ here (δ – a number that characterizes the recognition efficiency which is given at the beginning). If this condition is met, the process of constructing the classification tree ends, then the generalized feature $f_3(x)$, which is represented by the tree (Fig. 3) is such that provides an approximation of the sample of the form (2). If $\frac{S}{M}<\delta$ so, the tree building process continues. When building a tree, first select recognition on the tree (Fig. 3) all those values $l(r_1,r_2,r_3)$ for which the ratio is performed $t_{r_1,r_2,r_3}^{l(r_1,r_2,r_3)}=1$. Paths r_1, r_2, r_3 that perform only the specified ratio can be considered complete.

For example let:

$t_{010}^{l(010)}=t_{011}^{l(011)}=1;\ t_{000}^{l(000)}<1;\ t_{001}^{l(001)}<1;\ t_{100}^{l(100)}<1;\ t_{101}^{l(101)}<1.$

In this case, you will get the tree view (Fig. 4) where $m_2^4=l(010),\ m_3^4=l(011)$.

All the ways, 100 and 101, but on the tree (Fig. 4) are unfinished. For each of these paths r_1, r_2, r_3 we consider sets H_{r_1,r_2,r_3}, where H_{r_1,r_2,r_3} is the set of all those pairs $(x_i, f_R(x_i))$ of the training sample that belong to the path r_1, r_2, r_3. Sets H_{r_1,r_2,r_3} can be considered as some samples. In the case of a tree (Fig. 4) we will have the following samples $H_{000}, H_{001}, H_{100}, H_{101}$.

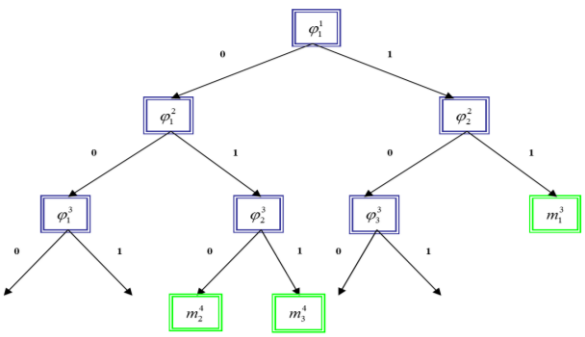

Fig. 4. General view of the final logical classification tree

4. Main results

For each sample H_{r_1,r_2,r_3}, an elementary feature ϕ_{r_1,r_2,r_3} is selected for which the value $W_{H_{r_1,r_2,r_3}}(\phi_{r_1,r_2,r_3})$ is the largest possible. The value $W_{H_{r_1,r_2,r_3}}(\phi_{r_1,r_2,r_3})$ represents the efficiency of recognition of the sample H_{r_1,r_2,r_3} using the characteristic ϕ_{r_1,r_2,r_3} [1, 6]. After selecting the features ϕ_{r_1,r_2,r_3}, we get a new tree, which is shown in (Fig. 1). Note that here $\phi_1^4=\phi_{000}$, $\phi_2^4=\phi_{001}$, $\phi_3^4=\phi_{100}$, $\phi_4^4=\phi_{101}$. Next to the tree (Fig . 1) apply the same process as to the tree (Fig. 2). It is important to note that you do not need to create a separate set of training pairs to implement each sample H_{r_1,r_2,r_3}. All these samples are implemented as follows: sample pairs (2) are submitted sequentially and only those pairs that belong to the path r_1, r_2, r_3 are taken into account. As a result of this process, sampling H_{r_1,r_2,r_3} will be implemented.

So, summarizing all the above, we can draw the following conclusions regarding the construction of logical trees:

A logical tree provides coverage of an array of educational information by fixing the sample objects in its structure. Moreover, such an approach of information storage provides-as a mechanism for further training (expansion) and error correction.

To date, in the specialized literature there is no description of algorithms and methods that would allow you to build logical trees based on large data arrays.

The use of logical trees in pattern recognition problems allows to describe recognition functions simply and compactly, which positively affects the complexity and speed of the resulting classification system.

Thus, the paper presents a step-by-step scheme for constructing a system of recognition of discrete objects based on a logical tree, and the focus of the study was a graph-scheme model of the recognition system in the form of a logical tree. Once again, we note that the results of this work are relevant for all problems of pattern recognition, in which the resulting recognition scheme can be represented as a logical tree.

References

[1] Povhan I.: General scheme for constructing the most complex logical tree of classification in pattern recognition discrete objects. Electronics and information technologies 11/2019, 112–117.

[2] Quinlan J.R.: Induction of Decision Trees. Machine Learning 1/2008, 181–222.

[3] Vasilenko Y.A, Kuhayivsky A.I, Papp S.A.: Construction and optimization of recongnizing systems. Information Technologies and Systems 1(T2)/1999, 122–125.

[4] Vasilenko Y.A., Vashchuk F.G., Povhan I.F.: Overall assessment of minimization of logical tree. European Journal of Enterprise Technologies 1(55)/2012, 29–33.

[5] Vasilenko Y.A., Vashchuk F.G., Povhan I.F.: The problem of estimating the complexity of the logic trees, recognition and general method optimization. European Journal of Enterprise Technologies 6/4(54)/2011, 24–28.

[6] Vtogoff P.E.: Incremental Induction of Decision Trees. Machine Learning 4/2009, 161−186.

[7] Zheng Z., Kohavi R., Mason L.: Real world performance of association rule algorithms. Proceedings of the Seventh ACM SIGKDD International Conference on Knowledge Discovery and Data Mining 2008, 401–406.

Ph.D. Povhan Igor
e-mail: igor.povkhan@uzhnu.edu.ua

Igor Povhan, worked as the head of the laboratory of software and hardware of the faculty of information technology in the period from 2003 to 2008. Since 2009, associate Professor of the Department of Software Systems of Uzhgorod National University. The direction of scientific work-artificial intelligence, pattern recognition theory, low-level programming.

http://orcid.org/0000-0002-7034-8702

otrzymano/received: 22.12.2019 *przyjęto do druku/accepted: 26.06.2020*

http://doi.org/10.35784/iapgos.898

RANKING OF WEBSITES CREATED WITH THE USE OF ISOWQ RANK ALGORITHM

Mariusz Duka
Silesian University of Technology, Faculty of Automatic Control, Electronic and Computer Science, Gliwice, Poland

Abstract. *The purpose of this article is to present the new ISOWQ Rank ranking algorithm for the technical assessment of website quality. For evaluation purposes, the algorithm takes into account the IT technologies used on a website, compliance of the source code with the applicable standards and the structure of the text content. The paper also includes the results of comparative ranking algorithms.*

Keywords: page ranking, ISOWQ Rank, MOZ, PageRank, SEO

RANKING WITRYN INTERNETOWYCH STWORZONY Z WYKORZYSTANIEM ALGORYTMU ISOWQ RANK

Streszczenie. *Celem artykułu jest prezentacja nowego algorytmu rankingowego ISOWQ Rank do technicznej oceny jakości strony internetowej. Algorytm do oceny bierze pod uwagę wykorzystane w serwisie WWW technologie, zgodność kodu źródłowego z obowiązującymi standardami oraz strukturę tekstu. W artykule zamieszczone są wyniki badań porównawczych algorytmów rankingowych.*

Słowa kluczowe: ranking stron, ISOWQ Rank, MOZ, PageRank, SEO

Introduction

Since 1991, when the first structures of the HTML programming language appeared, together with the first website (info.cern.ch), the Internet has been filled with over 1.4 billion websites on 233 million unique domains. Since 1995, the British company, Netcraft, has been searching Internet resources and examining IT technologies and software used to build websites on the servers of hosting service providers. Based on the analysis of the IP address and source code, Netcraft calculates the number of active websites, i.e. presenting unique content. It excludes the "under construction" web services, redirections or any domains indicating same content, e.g. ones with a registrar enabling 'the parking service'. Based on the cyclical analysis, it is estimated that almost 200 million active websites are accessible on the Internet.

A dynamic development of Internet resources is shown in Figure.1

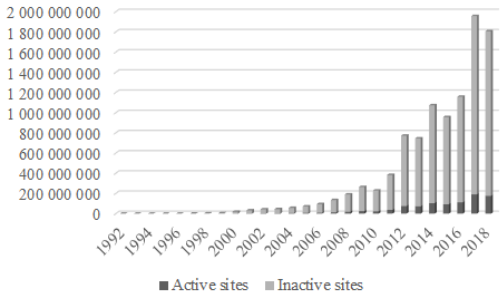

Fig. 1. The number of websites with unique content on the Internet (based on the data from Netcraft)

The growing number of websites has prompted the creation of search engines, i.e. the systems that help Internet users find specific information on the Web. The data collected in these systems is based on an analysis of Web pages in terms of their content and of the hyperlink network topology. Search engines like Google, Yahoo! or Bing, have had to develop their own algorithms to allocate value to the analysed websites to affect their ranking in the search engines results. The leading algorithm determining the quality of the website was the PageRank algorithm, developed by the creators of Google in 1998. In the following years, some other IT companies have also created their own algorithms to give websites a certain ranking value and thus determine their quality.

The popular MOZ ranking system has been created using the DA (Domain Authority) and PA (Page Authority) parameters. It is based largely on the quality of inbound links.

The quality of such links is determined by their source (catalogues, blogs, forums, social media, search engines) and their internal linking value.

This paper presents the ISOWQ Rank algorithm used in the ISOWQ (International Studies of Website Quality) ranking system, to analyse websites available under all 243 national domains (ccTLD) and the European .eu domain. Unlike the competing ranking algorithms, focusing largely on linking, such as PageRank or MOZ, the ISOWQ Rank algorithm takes into account the technologies used on the website, compliance of the source code with applicable standards (including W3C), content and text structure, as well as external rankings (MOZ, Alexa Rank). Other leading ranking systems i.e. Google PageRank, MOZ and Alexa Rank are also described here. A separate chapter presents the ISOWQ Rank algorithm and the IT system for which it was designed. The paper concludes with the presentation of the findings for the correlation between the ISOWQ Rank and MOZ.

1. Ranking methods

1.1. Google PageRank

The most well-known algorithm that determines the quality of a website is PageRank, used by Google. It was developed by Sergey Brin and Larry Page and described in the publication "The Anatomy of a Large-Scale Hypertextual Web Search Engine" [1].

The PageRank algorithm is based on the idea that the substance and quality of the site is evidenced by the number of references from other sites i.e. the value of the page measured by the number of hyperlinks pointing to that page from other pages [2].

The PageRank algorithm is calculated according to the following formula:

$$PR(A) = (1-d) + d\left(\frac{PR(T1)}{C(T1)} + \cdots + \frac{PR(Tn)}{C(Tn)}\right) \qquad (1)$$

where: *PR(A)* is the PageRank value of the side *A*, *PR(T1)* is the PageRank value of the side *T1*, *C(T1)* is the number of links pointing to the side *T1*, *d* is the dumping factor, in the range of $0<d<1$, usually accepted as 0.85. PageRank is calculated as the total value of all pages pointing to the selected page divided by the number of links on each of these pages.

The PageRank value is measured on the scale from 0 to 10, which means that the higher the value, the better the website quality. The value above 6 are usually reserved for professional sites, such as Facebook, Yahoo! or Twitter. Note that keywords, text or source code do not affect the ranking value, relevant are links only. The highest score in PageRank is usually obtained by the home page of the website. One of the reasons being, it is most often linked to and from other websites. However, there is also a

possibility that a higher score in PageRank may get another page of this website, which due to its rich content and substance, is linked more. An example of this may be a subpage containing a blog [2].

Google still uses the PageRank algorithm, but, from 2013, the data are not publicly available, which makes it go down in history for the SEO (Search Engine Optimization) industry.

1.2. MOZ DA and PA

Founded in 2004, MOZ, offers the marketing analytics tools at moz.com, It has also developed its own algorithm to give websites a ranking value. The intention of the MOZ ranking is to predict the position of a given website in search engines. Each page is awarded a so-called "authority" ranging from 0 to 100 points. The higher the authority of a domain or a page, the higher the chances of getting a good position in search engines results. The MOZ ranking is calculated for the entire website – DA (Domain Authority) and for a specific page – PA (Page Authority) [3].

In addition to analysing the quality of inbound links, the algorithm takes into account many additional factors in order to calculate the "authority". "Authority" is estimated on a 100-point logarithmic scale, which means that an increase from 20 to 30 points is much easier than that from 70 to 80 points. The algorithm structure is strictly confidential and protected by the MOZ business secrets.

1.3. Alexa Rank

Founded in 1996, Alexa Internet, currently controlled by Amazon, provides information related to Web traffic. The Alexa ranking is based on the amount of traffic generated by Internet users on a particular website. It is measured by using specific software (plugins for the Chrome or Firefox browser) and calculated on the basis of several factors, such as the number of people who visited the website and the frequency of these visits [4].

The Alexa ranking value is interpreted as an indicator of the popularity of a websites on the Internet. The lower the indicator is, the more popular a particular website is on the Internet. It is assumed that if the Alexa Rank value is below 100,000, the website is very popular among Internet users.

2. ISOWQ Rank algorithm

The ISOWQ Rank algorithm allocates a specific value to its analysed websites. It does so by measuring the three qualities. It is calculated according to the following formula:

$$IR = \frac{PM+PK+PT}{3} \quad (2)$$

where *PM* – number of points for technologies used and their ranking positions, *PK* – number of points for the source code optimisation, *PT* – the number of points for content and text structure.

The ISOWQ Rank value is calculated on a scale of 0 to 20 points. To calculate the score for the technologies used and ranking positions, ISOWQ Rank takes in to account such factors as MOZ and Alexa Rank rankings, the number of incoming links, the use of social media plugins, SSL encryption, geolocation, public e-mail addresses on the website and the registration of the hosting servers' IP addresses in DNSbl databases.

Points for the search engine optimisation are calculated using several other factors. These include: the use of HTML tags for SEO, optimization of the size of the code, the ratio of text size to the source code, the use of cascading styles and JavaScript in external files, the ratio of the number of external to internal links, the use of microformats, the number of URLs returning the error code.

The value for the content and structure of the text is affected by the size and formatting of the visible text on the page (the use of headers, highlights etc.). Text readability tests are also considered, however, as they do not apply to all languages, they are complementary. Points for PM, PK and PT is calculated only for the first 30 URLs (subpages) found in the source code of the website. The scoring can be affected by the UE factor, which is calculated on the basis of the number of internal links pointing to non-existing pages, i.e. when the server returns HTTP 4xx or 5xx error code.

The ISOWQ Rank algorithm is shown below:

ISOWQ Rank Algorithm
Input:
array T(U) with technical analysis of subpages
array P(S) with technical analysis of the web server
Output:
value in the range of <0,20>

- Create variables PM1, PM2, PK, PT, UE
- Create an auxiliary array V
- For each S_i € P calculate:
  - analyse the data
  - put for the result in PM1
- For each U_i € T, calculate penalty points for each tuple:
  - analyse the data
  - put the result in UE
- Reset the V array
- For each U_i € T calculate the score for each tuple:
  - analyse the data
  - put the result in V_i
- Insert the average value of V array into PM2
- If UE > 0, lower the PM2 value, including UE
- PM = PM1 + PM2
- If PM < 0: PM = 0 elif PM > 20: PM = 20
- Reset the V array
- For each U_i € T calculate the score for each tuple:
  - analyse the data
  - put the result in V_i
- Insert the average value of V array into PK
- If UE > 0 lower the PK value, including UE
- If PK < 0: PK = 0 elif PK > 20: PK = 20
- Reset the V array
- For each U_i € T calculate the score for each tuple:
  - if number of words in the text > 100
    - analyse the data:
    - put the result into V_i
  - elif:
    - to V_i insert 0
- Insert the average value of V array in PT
- If UE > 0 lower the PT value, including UE
- If PT < 0: PT = 0 elif PT > 20: PT = 20
- Return (PM + PK + PT) / 3

In practice, to get more than 5 points would mean that the website has met the basis technical requirements and is present in popular rankings. For example, melex.com.pl [5] obtained 8.73 ISOWQ Rank points, which should be considered a good result. Based on the analysis, it can be seen that this website also uses the YouTube service to publish video materials. It is worth noting that its code is optimised at 87%, and the <title> attribute occurs in 79% of <a> tags (hyperlinks), which again is a good value. Unfortunately, this website does not use other IT technologies such as social media plugins or the SSL encryption. Besides, the <alt> attribute only occurs in 25% of <img> tags, and public email addresses are not encoded.

Obtaining more than 10 points means that the website uses marketing techniques to communicate with other services, has many inbound links, contains a lot of text content and has a high ranking position. An example of such web service is alivia.org.pl [6] which scored 14.21 ISOWQ Rank points, indicating a very good result. It uses social media plugins, the SSL encryption, and its system is based on the modern CMS (Content Management System) – WordPress which allows the publication of the search engine – optimised text and video materials. Marketing strategies were implemented, as evidenced in the use of YouTube service. It also offers a large number of shares on Facebook and a high position in MOZ and Alexa Rank rankings. The website contains

large unique text content on every subpage. Code optimisation is at 91% and the <alt> attribute is found in 73% of <img> tags, which again is a good result.

Additional optimisation in terms of using the <title> attribute in the <a> tags and encoding email addresses would increase the chance of getting a score of 15 ISOWQ Rank points.

The score of more than 15 points is usually reserved for websites that use dominant IT technologies in Web marketing, are optimised according to SEO guidelines [7] and have high ranking positions. In practice, the score of 15 points is exceeded very rarely and is usually obtained by large web services.

An example of such website is lazienkaplus.pl [8] service, which scored 15.39 ISOWQ Rank points.

It uses social media plugins, microformats, has high positions in MOZ and Alexa Rank, has a well optimised code (93%), the <title> attribute in the <a> tag reaches 91% and the <alt> attribute in the <img> tag reaches 93%.

3. The ISOWQ ranking system

In 2010, with the increasing popularity of the SEO (Search Engine Optimisation) industry, I designed the ISOWQ (International Studies of Website Quality) ranking system as a suggestion for a new technical analysis of websites. The ISOWQ system comprises of two independent segments. The first segment consists of the subsystem responsible for automatic typing with the analysis of subsequent website while the second is responsible for the data presentation and the system user support. The user can add additional web addresses to the system and place an order for the web analysis. Both segments have direct access to the database server. In order to create the system, I have used IBM eServer x345 and Dell PowerEdge 1950 servers. I have also written the software in PHP using the PNCTL library for concurrency service [9]. The data archiving system uses MySQL and SQLite3 database engines.

In the first few years of the ISOWQ operation, all the analysed websites were hosted on the national domains only, that is, belonging to the European Union countries, the EU candidate countries, Russia with other members of the Commonwealth of Independent States, the United States of America, as well as those under the .eu domain.

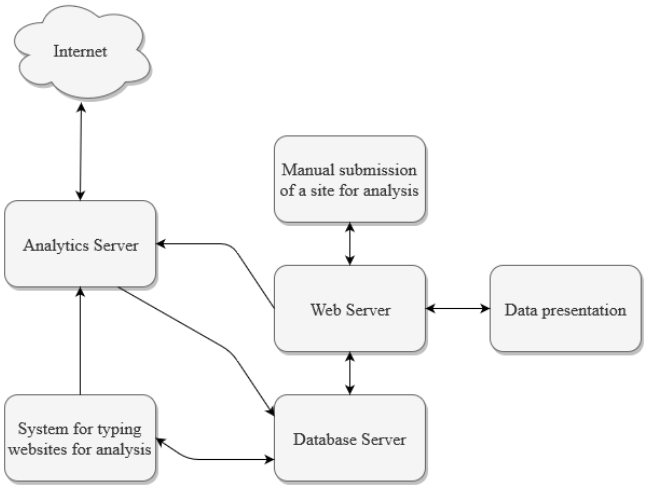

Fig. 2. The structure of ISOWQ system

Today, the main purpose of the ISOWQ system is to analyse websites operating under all (243) national domains (ccTLD). ISOWQ also produces reports to make it available publicly on the Internet. The data provided by the ISOWQ can also be used by other IT systems or be subjected to further analysis. The database contains the detailed analyses of over 1.3 million websites which creates over 25 million URLs [10].

The structure if the ISOWQ system is shown in Figure 2.

In addition to presenting the technical information online, the ISOWQ system enables the analysed website to be presented in a PDF format, with advice to specific questions regarding technical, marketing and text related aspects. Based on the collected data, one can generate many interesting combinations, e.g. regarding the use of multimedia on websites, the use of social media plugins or versions of the HTML markup language in a specific group of ccTLD domains.

Table 1 shows the summary for European national domains and the dependent territories (2016).

Table 1. The application of HTML5, YouTube and Social Media on European national domains based on the analyses conducted in 2016

Place	ccTLD	HTML5	YouTube	SM	No of audits
1	gg (Guernsey)	83,60%	19,22%	50,70%	98
2	no (Norway)	78,19%	19,29%	38,19%	1375
3	ba (Bosnia and Herzegovina)	77,49%	33,57%	8,20%	170
4	mc (Monaco)	77,49%	33,57%	8,20%	69
5	al (Albania)	65,29%	25,37%	26,71%	153
6	ax (Åland)	77,20%	15,78%	18,69%	135
7	je (Jersey)	72,56%	11,35%	25,15%	46
8	gi (Gibraltar)	62,99%	20,27%	24,68%	135
9	ad (Andorra)	56,09%	24,40%	22,92%	98
10	ch (Switzerland)	57,70%	19,10%	19,82%	1373
20	fr (France)	51,32%	9,16%	14,80%	2404
25	va (Vatican City)	62,62%	5,00%	2,50%	35
33	pl (Poland)	39,70%	8,58%	16,73%	2391
34	lv (Latvia)	39,62%	11,06%	14,04%	1456
35	eu (European Union)	40,26%	11,42%	12,05%	2235
40	gr (Greece)	35,48%	10,10%	16,24%	2302
45	ru (Russia)	39,38%	10,38%	9,28%	1546
48	de (Germany)	36,69%	10,17%	9,82%	2812
51	tr (Turkey)	39,47%	6,20%	6,58%	1890
52	mt (Malta)	36,45%	5,98%	6,90%	246

The Table above shows that in the websites with the .gg domain (analysed in 2016), HTML5 markup language was used in almost 84% of them, while those with the .pl domain used it only in 39,70%. The next interesting list in Table 2 is the share of unencrypted email addresses in the page code and registration of the IP addresses of the hosting servers as spam carriers in DNSbl databases.

Table 2. Use of IP addresses of hosting servers in DNSbl databases and the share of unencrypted email addresses in the code of websites analysed in 2016

Place	ccTLD	DNSbl	E-mail	No of audits
1	tn (Tunisia)	81,28%	57,56%	144
2	et (Ethiopia)	75,86%	52,01%	91
3	ne (Niger)	70,16%	39,05%	30
4	bt (Bhutan)	63,16%	66,39%	137
5	sd (Sudan)	59,95%	45,18%	136
6	bf (Burkina Faso)	59,71%	42,47%	75
7	sn (Senegal)	53,69%	53,11%	140
8	mm (Myanmar)	53,26%	48,83%	101
10	mv (Maldives)	49,92%	61,67%	109
28	mk (Macedonia)	31,13%	43,05%	467
29	kz (Kazakhstan)	30,88%	41,49%	557
122	pl (Poland)	9,89%	55,79%	2391
131	fr (France)	8,96%	39,70%	2404
169	lv (Latvia)	6,87%	60,63%	1456
173	de (Germany)	6,75%	60,53%	2812

The above statement shows that servers classified as a spam carrier, operate mainly in African countries. It also shows that the problem of unencrypted e-mail addresses on websites has a global dimension.

4. Comparative study of ranking algorithms

The t-Kendall ratio was used to estimate the correlation between the results obtained by MOZ and ISOWQ Rank algorithms. 10 websites were selected for the analysis and included the following technologies:

- HTML5 (+31 additional types, including HTML 2, 3, 4 and XHTML 1 and 2),
  - code analysis – meta, http-equiv, HTML tags, diagrams, microformats,
- Social media (Facebook, Twitter, Google, LinkedIn),
- Google services i.e. Ads (Adwords), Adsens, Analytics, Maps,
- JS framework (jQuery, Bootstrap +24 additional),

- Multimedia (YouTube, Flash, Silverlight),
- SSL encryption, spam protection (e-mail and DNSbl).

The study was conducted in April 2019. The scale of results has been unified to a range of 0 to 100. The results are presented in Table 3.

Table 3. Websites analysed for the purpose of research in April 2016

Website	ISOWQ Rank (0–100)	MOZ DA (0–100)
4wsk.pl [11]	55	31
alivia.org.pl [7]	71	45
argos.org.pl [12]	48	31
brightmedia.pl [13]	15	34
link2europe.pl [14]	40	30
machineryzone.pl [15]	52	30
melex.com.pl [6]	44	31
mlyny-rozdrabniacze.pl [16]	28	7
palacporaj.pl [17]	29	22
wrobywatel.pl [18]	19	14

Microsoft Excel 2016 software was used together with the "The Real Statistics Resource Pack" [19] to calculate this correlation. At the declared significance level of 0.05, the t-Kendall ratio is 0.44, which means that the algorithms have a moderate relationship with each other.

Figure 3 shows the correlation between ISOWQ Rank and MOZ DA.

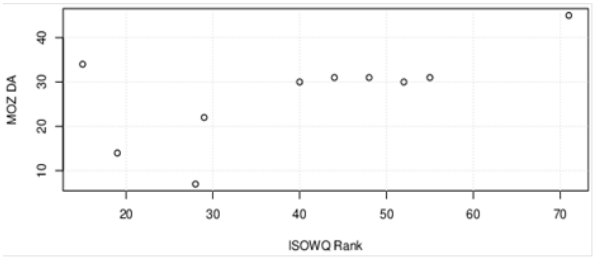

Fig. 3. Correlation between the ISOWQ Rank and MOZ DA ranking

By comparing the analyses of the ISOWQ Rank scores, it can be seen that the main differences relate to the use of social media technologies, multimedia, SSL encryption and content management system. The comparative summary of these analyses is presented in Table 4.

Table 4. A comparison of the results of different analyses for extreme scores

	brightmedia.pl	alivia.org.pl
ISOWQ Rank	3,05	14,21
MOZ DA	34	45
Alexa Rank (the higher the score the better)	1 095 670	496 768
Social media plugins usage	No	Yes
YouTube video clips usage	No	Yes
SSL (HTTPS)	No	Yes
CMS – WordPress usage	No	Yes
Source code optimisation	81%	91%
Usage of <title> attribute in the <a> tag	91%	0%

The study showed that there is a 'positive' correlation between ISOWQ Rank and MOZ, i.e. an increase in one should result in an increase in the other. This means that the technical aspect of the website (technologies used, code optimisation, text structure) is an important factor in the MOZ algorithm, whose detailed specification is not publicly available.

The 'unconventional' method of placing the text content in the code of brightmedia.pl unable the correct detection and analysis, which is reflected in the number of points for the text (PT).

Here is a snippet of source code for this site:

```
<p class="textF2" id="text1_1">Nie jesteśmy nowicjuszami,</p>
<p class="textF3" id="text1_2">nie wzięliśmy się znikąd. Mamy wiedzę</p>
<p class="textF4" id="text1_3">i doświadczenie, bo pracowaliśmy</p>
<p class="textF5" id="text1_4">w znanych agencjach dla znanych marek.</p>
```

The ISOWQ Rank algorithm did not detect any text zones in the source code above, as it considered that there was sufficient number of characters in a single paragraph in the in the <p> tag.

If the above code snippet was replaced with:

```
<p>
Nie jesteśmy nowicjuszami,<br>
nie wzięliśmy się znikąd. Mamy wiedzę<br>
i doświadczenie, bo pracowaliśmy<br>
w znanych agencjach dla znanych marek.
</p>
```

The algorithm would then detect the text zone and the website would receive a higher score for the structure, which would have a positive impact on the final ISOWQ Rank. However, based on the source code, it can be assumed that this change would negatively affect the form of presentation of the text on the page.

5. Conclusion

This paper presents the main principles of the ISOWQ system and ISOWQ Rank algorithm. The findings obtained during these analyses confirm the thesis that the use of modern IT technologies and the appropriate structure of the text are as important as the number of hyperlinks to the website. The correct detection and analysis of the text zones understood by humans is a very complicated task, especially where the text plays a secondary role. An interesting aspect of the text analysis could be the tests checking its readability level. Although most of the tests were created with the English language in mind, there are also some tailored variants to accommodate to the Polish language intricacies. The ISOWQ Rank value is moderately convergent with the MOZ ranking. Therefore, despite the lack of access to the algorithm specification (MOZ), it can be presumed that also here, as in the case of ISOWQ Rank, the technologies used and the scope of content and code optimisation are taken into account.

References

[1] Brin S., Page L.: The Anatomy of a Large-Scale Hypertextual Web Search Engine. Stanford University, Stanford 1998.
[2] Bailyn B., Bailyn E.: Outsmarting Google: SEO Secrets to Winning New Business. Que Publishing, Indianapolis 2011.
[3] https://moz.com/learn/seo/domain-authority (available: 20.06.2019).
[4] https://www.alexa.com/about (available: 20.06.2019).
[5] https://www.isowq.org/website/melex.com.pl/1439980/ (available: 02.04.2019).
[6] https://www.isowq.org/website/alivia.org.pl/1441262/ (available: 26.04.2019).
[7] https://support.google.com/webmasters/answer/35769 (available: 20.06.2019).
[8] https://www.isowq.org/website/lazienkaplus.pl/1322181/ (available: 12.04.2019).
[9] https://www.php.net/manual/en/book.pcntl.php (available: 06.12.2019).
[10] https://www.isowq.org/about (available: 06.12.2019).
[11] https://www.isowq.org/website/4wsk.pl/1443221/ (available: 08.04.2019).
[12] https://www.isowq.org/website/argos.org.pl/1441579/ (available: 05.04.2019).
[13] https://www.isowq.org/website/brightmedia.pl/1439337/ (available: 01.04.2019).
[14] https://www.isowq.org/website/link2europe.pl/1439533/ (available: 01.04.2019).
[15] https://www.isowq.org/website/machineryzone.pl/1440087/ (available: 02.04.2019).
[16] https://www.isowq.org/website/mlyny-rozdrabniacze.pl/1439111/ (available: 01.04.2019).
[17] https://www.isowq.org/website/palacporaj.pl/1439800/ (available: 02.04.2019).
[18] https://www.isowq.org/website/wrobywatel.pl/1444142/ (available: 10.04.2019).
[19] http://www.real-statistics.com/free-download/real-statistics-resource-pack (available: 10.05.2019).

M.Sc. Eng. Mariusz Duka
e-mail: mariduk781@student.polsl.pl

Ph.D. student at the Faculty of Automatic Control, Electronic and Computer Science of the Silesian University of Technology. Professionally associated with the IT industry since 1993, in particular in software design and its implementation. Author of many Web projects, including the ISOWQ (International Studies of Website Quality) ranking system. His scientific interests related to the issues of data exploring, concurrent programming and IoT.

http://orcid.org/0000-0001-5773-0459

otrzymano/received: 16.12.2019 *przyjęto do druku/accepted: 26.06.2020*

http://doi.org/10.35784/iapgos.1608

OVERVIEW OF BROADBAND INFORMATION SYSTEMS ARCHITECTURE FOR CRISIS MANAGEMENT

Jacek Wilk-Jakubowski
Kielce University of Technology, Department of Information Systems, Kielce, Poland

Abstract. *Many risks as a result of accidents, catastrophes and natural disasters can contribute to crisis situation, which according to the definition means a set of circumstances, both external and internal, that affect a given system through changes. Crisis situations are usually the result of natural disasters. Where such phenomena occur, it is important to ensure communication both at regional and national level. This is particularly important in areas affected by disasters caused by force majeure, such as earthquakes. The main aim of the article is to provide an overview of the architecture of contemporary information systems including satellite links, in order to present information on the potential possibilities of their use in the case of crisis situations.*

Keywords: information systems engineering, web services, satellite systems, crisis management, VSAT

PRZEGLĄD ARCHITEKTURY SZEROKOPASMOWYCH SYSTEMÓW INFORMACYJNYCH DO CELÓW ZARZĄDZANIA KRYZYSOWEGO

Streszczenie. *Wiele zagrożeń wynikających z wypadków, katastrof czy klęsk żywiołowych może przyczynić się do powstania sytuacji kryzysowych, przez które zgodnie z definicją rozumie się zbiór okoliczności, zarówno zewnętrznych, jak i wewnętrznych, mających wpływ na dany system poprzez zaistniałe zmiany. Sytuacje kryzysowe są zazwyczaj wynikiem klęsk żywiołowych. W przypadku wystąpienia takich zjawisk ważne jest zapewnienie odpowiedniej komunikacji zarówno na poziomie regionalnym, jak i krajowym. Jest to szczególnie istotne na obszarach dotkniętych klęskami żywiołowymi spowodowanymi siłą wyższą, takimi jak trzęsienia ziemi. Głównym celem niniejszego artykułu jest przegląd architektury współczesnych systemów informacyjnych, z uwzględnieniem sieci satelitarnych, w celu przedstawienia informacji na temat potencjalnych możliwości ich wykorzystania na potrzeby komunikacji w sytuacjach kryzysowych.*

Słowa kluczowe: inżynieria systemów informacyjnych, usługi internetowe, systemy satelitarne, zarządzanie kryzysowe, VSAT

Introduction

The Institute of Crisis Management from the US distinguishes four groups of sources of crises: (1) random factors (e.g. earthquakes, floods); (2) technical problems (e.g. accidents in production facilities); (3) human errors (e.g. communication disasters); and (4) wrong decisions at management level [2]. Such unfavorable situations may affect the operation of a person, an institution or even the entire country. For instance in the case of damage to typical terrestrial technical infrastructure, the use of wireless links (including satellite links) very often becomes the only possible way to ensure communication. Otherwise, it threatens to deepen the crisis situation [19]. Technical applications and the ability to access various types of networks play a significant role, which becomes possible with available mobile devices. Since a crisis situation has a negative impact on people's safety, it is important to use countermeasures [11, 21]. Information systems engineering allows to obtain, collect, process and distribute information by means of electronic equipment [10, 22, 24]. Along with access to the Internet, it is possible to access the content published there, as well as to use many services, such as [3, 4, 6]: (1) e-mail; (2) FTP; (3) discussion groups; (4) streaming services. In addition, the Internet allows the presentation of various data (mainly all text, audio and video) and, as a leading service, influences the availability of multimedia services in the IT environment. Thus, they include access to many other services provided over the Internet as a part of one comprehensive service, which is covered by flexible network architecture.

Satellites play an important role in providing global communication for almost decades. Along with the increase in data transmission speed in terrestrial networks, an increase in the speed offered on satellite links has been noted [27]. The reports of the Federal Communications Commission (FCC) in the US covering information on the actual speeds obtained in individual broadband communication systems have included Internet access as a satellite service since 2013 [16]. In the light of FCC reports the obtained transmission speed is often higher than the declared value (the difference is 40% for 90% of users during peak hours). In this respect this service can be ranked first in the US broadband Internet ranking [17]. What's more, the service of satellite Internet access provides the smallest speed changes depending on the time of day, with the achieved speed being at least 30% higher than the declared one and the average upload speed is 61% higher than the declared one. Therefore, access to broadband Internet using satellites can be a good option for stable Internet access due to the achieved parameters better than the parameters of traditional terrestrial links and reliability (investments in failover and redundant switching in VSAT systems cause that some networks offer 99.9921% reliability). It is worth noting that in the case of systems using satellites located in geostationary orbit, continuity of service is determined by the earth station. Only when the level of the received signal meets the assumed quality criteria (exceeds the set level for a given percentage of time per year and the worst month), it is possible to receive stable signals. While, according to the FCC report, the use of satellite services involves high system reliability and the lifetime of the satellites often exceeds the time specified in the technical specifications, it becomes difficult to repair the satellite's on-board equipment in the event of failure, which must also be calculated for the operation of the satellite system. Satellites are therefore designed with multiple layers of redundancy and backup systems. The quality levels achieved are equal to or even better than the military specifications for the manufacture, launch and exploitation of space satellites. In summary, the use of satellite systems via the connection of remote networks to the primary backbone network and cellular infrastructures allows for transmission with 99% reliability and therefore seems to be a good way to ensure communication in case of a crisis situations.

1. Selected aspects of the use of satellite links to ensure communication

In the 21st century in particular satellites are used to extend the range of operation of cable or radio networks providing access to the Internet, as well as mobile phone networks, when the range of traditional networks is insufficient. Undoubted advantages of satellite systems are: (1) ability to build global networks; (2) ability to communicate with fixed and mobile terminals; and (3) flexible provision of multiple services. Moreover, the following advantages can be indicated: (1) long-life of a satellite (usually at least 15 years); (2) low influence of the Doppler effect, because the relative speed of the satellite decreases with the increase in the orbit height; and (3) relatively constant reception level.

From a practical point of view, the use of satellite networks has also some disadvantages. One example is the propagation delay on the Earth-to-Satellite and Satellite-to-Earth links, which

makes it difficult to carry out any kind of real-time transmission. Therefore, many techniques are used to reduce the value of this delay. In practice propagation delay in corporate networks is several hundred ms, because the single jump time between the satellite and the Earth is equal to from 120 ms to 140 ms. For comparison, the delay in terrestrial networks is significantly lower and is equal to about 5 ms [27]. Thus, the delay caused by jumps: Earth-Satellite and Satellite-Earth for both receivers is significant reducing the use of the physical channel [9]. This has an impact especially on real-time voice communication. In addition, the propagation delay limits the use of systems for interactive sessions without enhancements when users constantly enter data (e.g. remote login), as well as any applications in which small packets of data are generated in response.

On the other hand, the use of satellite networks has many benefits (the cheapest way to build regional, national and intercontinental links; the possibility to build links in locations where there are a lack of adequate technical infrastructure, e.g. in sparsely populated areas, seas or oceans; no environmental degradation due to the need to build traditional communication links and many others). In the 21st century satellites are used to transmit Internet traffic wherever the use of traditional terrestrial lines is impossible or uneconomic. Apart from the need to ensure uninterrupted communication in the event of a crisis situation, satellite links can find many other applications. Offshore oil companies can be exemplified by using satellite data networks to communicate directly with platform headquarters and offshore oil tankers. There is a practical justification for using satellite networks to build networks for many entities, such as: (1) oil, mining and gas companies; (2) public entities (including government and military agencies); (3) research centers (including schools); (4) medical centers (including telemedicine); (5) enterprises offering remote surveillance systems and disaster prevention measures; (6) banks; (7) hotels; (8) shops and other entities with branches in many countries. Reliable data transmission is a key part of a computer or communication network in times of distributed systems. Such communication can be implemented in a TCP/IP network using many protocols associated with an IP multicasting. Undoubtedly, the advantage is the fact that many protocols may be used, such as: FTP, HTTP, NNTP, POP, SMTP and many others [9].

2. Architecture review of satellite broadband information systems

Many factors should be taken into account in the design of satellite systems, such as: (1) system reliability; (2) service continuity; and (3) declared signal quality parameters. Many VSAT terminals should have access to specified resources in a given percentage of time per year and per worst month. As previously indicated, satellites have a wide spectrum of applications which may also apply in domestic and corporate use. As the examples we can point out: (1) Small-Office-Home-Office (SOHO), e.g. Internet Direct to Home (DTH) systems and services dedicated to small and medium-sized enterprises (SME); (2) construction of combined local area networks (LANs); and (3) cooperation of VSATs with ground-based systems to increase network coverage and the range of services offered. However, in practical application, satellite networks should support a wide range of high-speed applications which require high quality productivity with proper use of satellite resources. To provide broadband IT services, including communications, in the event of a crisis situation, many operators' satellites can be used [12], an example is the first HTS (High Throughput Satellite) in Europe and the Mediterranean Sea with significant capacity and efficiency [13, 18]. Many computer tools are designed to simulate the parameters of this Ka-Sat satellite [14, 15].

The architecture of broadband systems offering access to multiple satellite services involves the appropriate construction of the on-board satellite equipment modules. The two main methods for handling the data stream are listed: (1) bent pipe and (2) on-board processing and switching. The choice of a specific technology depends on the purpose of the satellite system. There are one-way communication systems, which only allow to receive signals, e.g. dedicated to sending information to users located in the area of natural disaster, as well as two-way communication systems, which apart from reception allow to send data. In the event of crisis situation, access to the Internet as a leading service seems to be particularly important. The ability to use small, often portable, ground-based VSAT terminals is also a key issue. Depending on the methods for handling the data stream, radio wave propagation is accompanied by different signal degradation, which in turn is reflected in the technical infrastructure of systems. The attenuation of the signal as the basic component of signal degradation (an additional component is noise increase) is strictly dependent on, among other things, the frequency of radio waves, as well as atmospheric conditions accompanying radio wave propagation [25, 26, 28]. Thus the correct reception is dependent on the proper implementation of technical equipment [27, 29]. The use of signal retransmission systems involves a lack of signal regeneration (Fig. 1) and is therefore characterized by significant propagation attenuation (including primary attenuation due to the considerable distance between the earth station and the satellite). Antennae links are controlled by means of dedicated links and monitoring system. On the other hand, the advantage of systems allowing retransmission of data is to ensure transparent data transmission, which involves possible modification of signal structure on the Earth and translates into building new protocols without interfering with the occupied band [30].

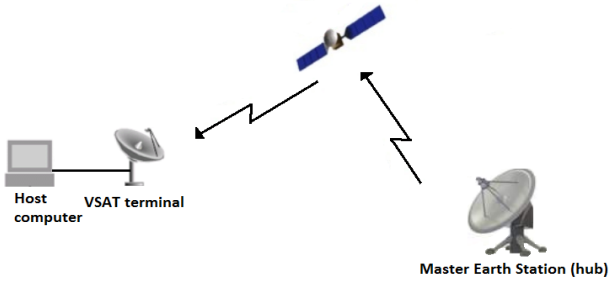

Fig. 1. Bent pipe communication with the use of a VSAT terminal

A different approach is the use of signal processing and switching techniques using satellite's on-board equipment (Fig. 2). Compared to bent pipe, the obtained link budget is much better. Such systems are mainly used for the construction of geostationary access systems, where the broadcasting (group) nature is important.

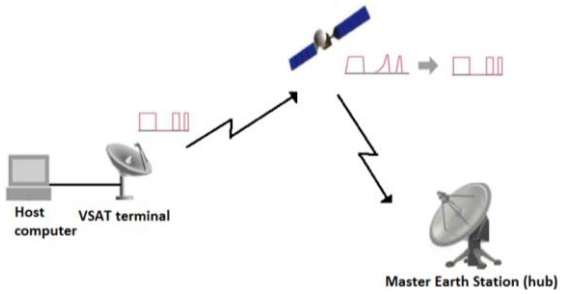

Fig. 2. Regenerative communication with the use of a VSAT terminal

As the satellite's on-board equipment processes data coming from the channels, the control of the antenna beams (spatial commutation) is possible, so that the signal can be directed to a particular beam, as shown in Fig. 3. From a technical point of view a control data can be used to build in space both switched and packet transmission networks in which the antennae have dynamically controlled beams [5, 7, 8]. In systems allowing regeneration of the signal, the link budget may be less favorable, and thus the satellite board may transmit less power. Moreover, terminal antennae may have smaller aperture due to signal regeneration, which in turn compensates greater signal degradation due to smaller antenna aperture.

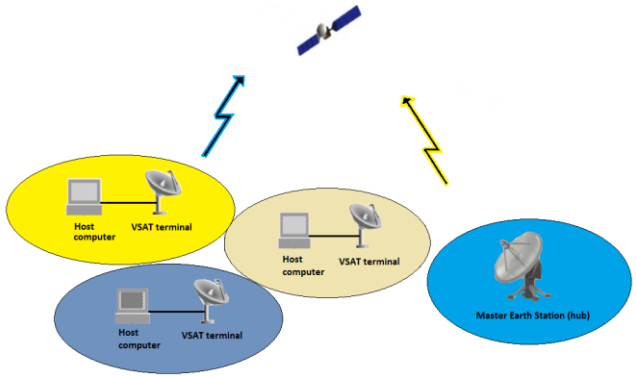

Fig. 3. On-board processing and switching communication with the use of a VSAT terminal

This is particularly important for the installation of mobile receiving terminals in the case of emergency situations. They are easy to install because of small size of the antennae. On the other hand, taking into account the technical issues, the inconvenience is the fact that the link is adjusted to the protocol, and thus the transmission is non-transparent. Therefore, it is not possible to modify the signal structures on the Earth, which makes it impossible to create new transmission protocols without interfering with the occupied band. The disadvantage of such systems is also significant delays in signal propagation (Fig. 4).

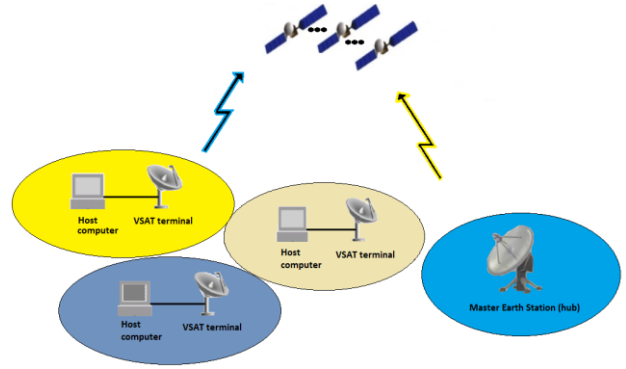

Fig. 4. On-board processing and switching communication with the use of a VSAT terminal and links between satellites

Satellite systems can serve not only as access networks, but also as access and backbone networks. If the system serves as access network, the signals from the terminal after reception by satellite are transmitted to a ground station connected to terrestrial infrastructure. The signals are sent directly to the receiver (web server) or close to it, and then via the terrestrial or satellite access network are sent to the destination. If the satellite system serves as an access and backbone network, the signals from the terminal after receiving via satellite are sent via satellite links to the satellite used by the receiver, or to the gateway which is connected to the terrestrial backbone network [30, 31]. As the examples can be indicated: (1) virtual private networks; (2) local area networks; (3) remote connection to the Internet backbone network; and (4) video conferences (e.g. with point-to-multipoint networks). Among other things, it becomes possible: (1) network caching; (2) creation of user groups (e.g. units responsible for crisis management); (3) implementation of digital audio/video transmissions; (4) real-time database updates, etc. These solutions are usually used by governmental institutions (e.g. rapid network building in the event of crisis situation), companies with branches in many countries or continents, as well as Internet and satellite service providers to ensure long distance data transmission. As has been mentioned information can be sent simultaneously by satellite to a group of users (multicast) as long as the receiving terminals are within the coverage of selected area. Taking into account the above factors, it is possible to develop satellite characteristics depending on the appropriate purpose. For instance any point-to-point applications, in addition to network resources, help mitigate congestion and increase customer ability to manage services [23].

Figure 5 contains an illustration of the link reference for a satellite network serving as a transport network. Base stations as the satellite gateways (SGs) are points of contact with the access networks or IP distribution networks.

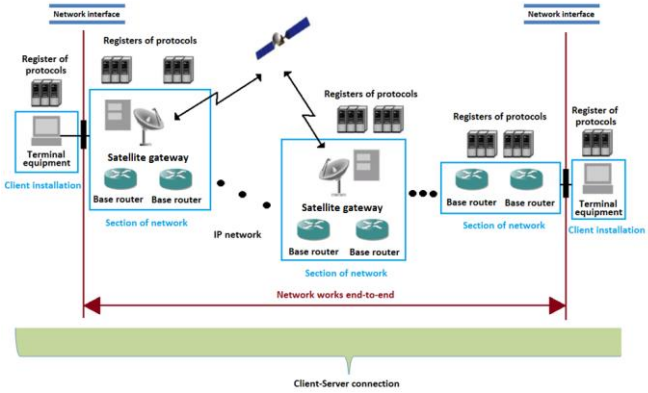

Fig. 5. Hypothetical reference link to the satellite network serving as a transport network

By the use of the IP network, which is crucial to ensure communication with an edge network, as a distribution network, it becomes possible to transmit data between the receiver and the transmitter of the terrestrial network section (Fig. 6). It is important to choose the appropriate base station (SG), which is closest to the source terminal (ST) and closest to the destination terminal (DT). It reduces undesirable signal deterioration due to long distances transmission over the IP network. The ST terminal, which is used for data transmission, is connected to the base station SG via the IP network or leased line. The satellite link can serve as the access network and distribution and access network. It is possible to use retransmission satellites for the access network. Wired or radio links can be used to build a return channel, and the satellite part as a receiver [1]. When a terminal allowing both reception and data transmission is used, then the terrestrial technical infrastructure is not included [30].

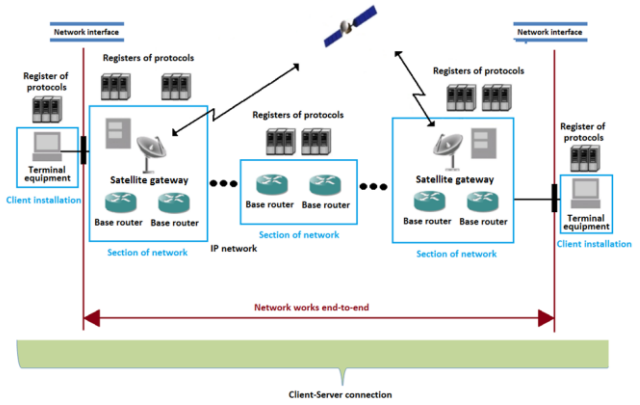

Fig. 6. Hypothetical reference link to the satellite network serving as a data distribution network in an edge network

In practice satellite networks provide access to many IT services and Internet access can be a leading service for a large number of end users. It enables the use of many tools and web applications (Fig. 7). Due to the asymmetric nature of links, the return channel from the terminal station usually sends small traffic to the service distribution point. Because the data transmission speed is not constant, it is characterized by frequent changes. Ground links can also be used for data transmission. One of the solutions for bandwidth optimization in satellite terminals is to use techniques of multiplying access to the radio channel [30].

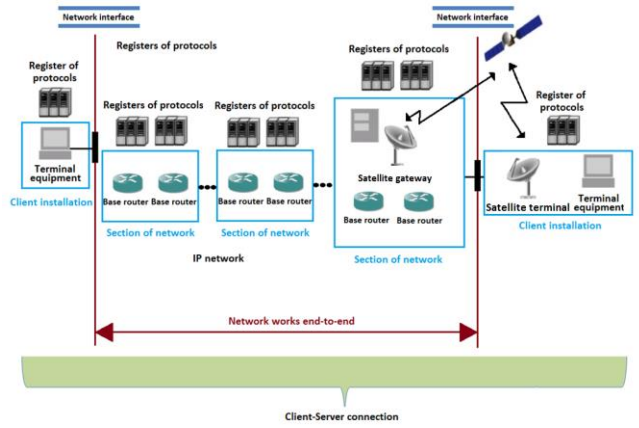

Fig. 7. Hypothetical reference link to the satellite network serving as an Internet access network

Group transmission (multicast) allows data to be transferred economically to VSAT terminals which are used as receivers. The exemplification can be streaming data and providing multimedia services using the intranet or Internet services. One of the advantages is that there is no need to collect data when providing services in real time. Both terrestrial and satellite links can be used to provide a return channel. Networks operating in PMP (Point-to-MultiPoint) mode are required to meet data link layer requirements. Higher layers are responsible for proper reception of the signal. In the case of networks designed for group and broadcast transmission, the signals are retransmitted using satellites and then received by terrestrial receiving terminals.

3. Conclusions

Satellite communication as a complex form of communication provides users the global network services with many multimedia services and is crucial in the case of damage to traditional ground technical infrastructure. As the main benefits of using satellite systems can be mentioned [20]: (1) the quickest, cheapest and least invasive way to build regional, intercontinental and global networks; (2) the ability to use links wherever this is not possible using traditional links because of: (2a) the lack of terrestrial technical infrastructure; (2b) the lack of coverage of traditional means of communication (cable and radio links); or (3) it is not economically viable; (2) easy installation and reconfiguration of the system; (3) continuous operation in crisis situations when terrestrial technical infrastructure is damaged, e.g. due to an earthquake; (4) the ability to work in many modes (including point-to-multipoint mode). Real-time network monitoring, synchronization and management are also possible. There is the ability to build local networks of connections or Internet access (for instance routers can be carried by the movements received by the satellite and sent to the network, which allows for fast data transmission in local networks). Moreover terminals can be easily moved and with the use of VSAT technology it is possible to build backup links, in addition to basic links, e.g. when satellites are the only way to ensure connectivity.

References

[1] Baras J.S., Corson S., Papademetriou S., Secka I., Suphasindhu N.: Fast asymmetric Internet over wireless satellite-terrestrial networks. CA, Monterey 1997.
[2] Barton R.M.: Crisis Management. Oxford Press Publishers, Oxford 1993.
[3] Bem D.J., Więckowski T.W., Zieliński R.J.: Radiowe systemy szerokopasmowego dostępu. Krajowe Sympozjum Telekomunikacji, Bydgoszcz 2001.
[4] Bem D.J., Więckowski T.W., Zieliński R.J.: Satelitarne systemy dostępowe 2. Przegląd Telekomunikacyjny i Wiadomości Telekomunikacyjne 8, 2001, 22–30.
[5] Bem D.J., Zieliński R.J.: Bezprzewodowa transmisja pakietowa. V Krajowa Konferencja Radiodyfuzji i Radiokomunikacji (KKRR 2000), Poznań 2000.
[6] Bem D.J., Zieliński R.J.: Satelitarne systemy dostępowe. Przegląd Telekomunikacyjny i Wiadomości Telekomunikacyjne 8/9, 2000, 593–601.
[7] Bem D.J., Zieliński R.J.: Transmisja pakietowa 1. Infotel 9, 2000, 34–36.
[8] Bem D.J., Zieliński R.J.: Transmisja pakietowa 2. Infotel 10, 2000, 20–26.
[9] Choi H-K., Qadan O., Sala D., Limb J.O., Meyers J.: Interactive Web Service via Satellite to the Home. IEEE Communications Magazine 39(3), 2001, 182–190.
[10] Collin S.M.H., Głowiński C.: Słownik komputerów i Internetu. Wydawnictwo Wilga, Warszawa 1999.
[11] Eguchi S., Kameda S., Kuroda K., Oguma H., Sasanuma M., Suematsu N.: Multi-mode portable VSAT for disaster-resilient wireless networks. Asia Pacific Microwave Conference (APMC 2014), Sendai 2014.
[12] Euroconsult: 2018 Edition, https://www.eutelsat.com/files/live/sites/eutelsat-internet/files/PDF/investors/2017-18/Eutelsat_Communications_Reference_Document_2017-18.pdf (available: 10.02.2019).
[13] Eutelsat – Ka-Sat, https://www.eutelsat.com/sites/eutelsat-internet/home/satellites/9-east.html#ka-sat (available: 05.06.2016).
[14] Eutelsat – Services, https://services.eutelsat.fr/deploy_Sorbet_SSO/pages/changeGraphParameters.do (available: 30.04.2019).
[15] Eutelsat – Services, https://services.eutelsat.fr/deploy_Sorbet_SSO/pages/displaySelectAELocation.do (available: 30.04.2019).
[16] FCC Office of Engineering and Technology i Consumer and Governmental Affairs Bureau, http://www.fcc.gov. (available: 30.04.2019).
[17] Gajewski M.: Internet satelitarny przoduje na liście usług szerokopasmowych w USA, https://www.chip.pl/2013/04/internet-satelitarny-przoduje-na-liscie-uslug-szerokopasmowych-w-usa (available: 25.04.2013).
[18] iDirect: High Throughput Satellites (HTS), http://52.3.84.67/Company/High-Throughput-Satellites.aspx (available: 04.06.2016).
[19] Księga Komunikacji Kryzysowej 2017: Postawy zarządzania informacją w kryzysie. Rządowe Centrum Bezpieczeństwa, Warszawa 2017.
[20] Pontano B.A.: Linkway™ for 21st century military communications. MILCOM 2000 Proceedings. 21st Century Military Communications. Architectures and Technologies for Information Superiority (Cat. No. 00CH37155), CA, Los Angeles 2000.
[21] Sasanuma M., Uchiyama H., Nagoya T., Furukawa M., Motohisa T.: Research and development of very small aperture terminals (VSAT) that can be installed by easy operation during disasters – Issues and the solutions for implementing simple and easy installation of VSAT earth station. IEICE 112(440), 2013, 1–3.
[22] Słownik języka polskiego: Teleinformatyka, https://sjp.pwn.pl/sjp/teleinformatyka;2577777.html (available: 23.01.2016).
[23] Souto G., Stevenson J.: Technical features of the @INTELSAT Internet product suite. IEE Colloquium on Current Developments in Intelsat (Ref. No: 1997/367), London 1997.
[24] Wilk-Jakubowski G.: Wpływ technologii informatyczno-komunikacyjnych na funkcjonowanie współczesnych społeczeństw. Grabiński T. (ed.): Rola informatyki w naukach ekonomicznych i społecznych. Innowacje i implikacje interdyscyplinarne. Wydawnictwo Wyższej Szkoły Handlowej im. B. Markowskiego w Kielcach, Kielce 2011.
[25] Wilk–Jakubowski J.Ł.: Measuring Rain Rates Exceeding the Polish Average by 0.01%. Polish Journal of Environmental Studies 27(1), 2018, 383–390.
[26] Wilk–Jakubowski J.Ł.: Predicting Satellite System Signal Degradation due to Rain in the Frequency Range of 1 to 25 GHz. Polish Journal of Environmental Studies 27(1)/2018, 391–396.
[27] Wilk–Jakubowski J.Ł.: Propagacja fal radiowych w łączności satelitarnej. Radiowaves propagation in satellite communications systems. Wydawnictwo Politechniki Świętokrzyskiej, Kielce 2018.
[28] Wilk–Jakubowski J.Ł.: Total Signal Degradation of Polish 26-50 GHz Satellite Systems Due to Rain. Polish Journal of Environmental Studies 27(1)/2018, 397–402.
[29] Wilk–Jakubowski J.Ł.: Wpływ wybranych parametrów technicznych systemu na odbiór fal radiowych. Informatyka, Automatyka, Pomiary w Gospodarce i Ochronie Środowiska 3/2018, 65–68.
[30] Zieliński R.J.: Satelitarne sieci teleinformatyczne. Wydawnictwa Naukowo-Techniczne, Warszawa 2009.
[31] Zielinski R. J.: Nowe techniki w systemach VSAT, http://absta.pl/ryszard-j-zieliskinowe-techniki-w-systemach-vsat.html (available: 25.07.2019).

Ph.D. Jacek Łukasz Wilk-Jakubowski
e-mail: j.wilk@tu.kielce.pl

Kielce University of Technology, Ph.D. (technical) Faculty of Electrical Engineering, Automatic Control and Computer Science, Department of Information Systems.
Research interests: teleinformatic systems, data transmission, signal processing, electrical engineering, wave propagation.

http://orcid.org/0000-0003-1275-948X

otrzymano/received: 01.04.2020 *przyjęto do druku/accepted: 26.06.2020*

http://doi.org/10.35784/iapgos.924

TIME-VARIANT MODEL OF HEAT-AND-MASS EXCHANGE FOR STEAM HUMIDIFIER

Igor Golinko[1], Volodymyr Drevetskiy[2]
[1]National Technical University of Ukraine "Igor Sikorsky Kyiv Polytechnic Institute", Department of Automation of Heat and Power Engineering Processes, Kiev, Ukraine,
[2]National University of Water Management and Nature Resources Use, Department of Automation, Electrical and Computer-Integrated Technologies, Rivne, Ukraine

Abstract. *The dynamical model of heat-mass exchange for a steam humidifier with lumped parameters, which can be used for synthesis of control systems by inflowing-exhaust ventilation installations, or industrial complexes of artificial microclimate, is considered. A mathematical description that represents the dynamical properties of a steam humidifier concerning the main channels of control and perturbation is presented. Numerical simulation of transient processes for the VEZA KCKP-20 humidification chamber to the influence channels was carried out. The achieved dynamical model of a humidification chamber can be the basis for the synthesis of automatic control systems and simulation of transient states. A significant advantage of the obtained mathematical model in the state space is the possibility of synthesis and analysis of a multidimensional control system.*

Keywords: dynamical model, state space, steam humidifier

NIESTACJONARNY MODEL WYMIANY CIEPŁA I MASY DLA NAWILŻACZA PAROWEGO

Streszczenie. *Rozważono model dynamiczny wymiany ciepła i masy nawilżacza parowego o parametrach skupionych, który można zastosować do syntezy układów sterowania przez instalacje wentylacyjne nadmuchowo-wywiewne lub przemysłowe kompleksy sztucznego mikroklimatu. Przedstawiono opis matematyczny przedstawiający właściwości dynamiczne nawilżacza parowego dotyczące głównych kanałów regulacji i zaburzeń. Przeprowadzono symulację numeryczną procesów przejściowych dla komory nawilżającej VEZA KCKP-20 z kanałami wpływowymi. Powstały model dynamiczny komory nawilżania może być podstawą do syntezy automatycznych układów sterowania i symulacji stanów nieustalonych. Istotną zaletą uzyskanego modelu matematycznego w przestrzeni stanu jest możliwość syntezy i analizy wielowymiarowego układu sterowania.*

Słowa kluczowe: model dynamiczny, przestrzeń stanu, nawilżacz parowy

Introduction

When heating the buildings, water and air systems are most often used. Air heating systems are used recently and have proven themselves as high-speed, with a small specific capital cost. Air heating systems use electric heaters with a distributed automatic control system [11]. For air heating of commercial and business centres, warehouses and industrial buildings, centralized ventilation and conditioning systems are used. The achievement of high performance indicators of industrial conditioning systems involves the development of adequate mathematical models of climatic equipment and their control methods.

Steam humidifying cameras have been widely used in air conditioning. Thanks to technological features, steam humidification is indispensable for creating artificial microclimate: in operating rooms; in the technology of manufacturing drugs, or semiconductor materials of the electronic industry, and so on. In contrast to the spray-type humidification chambers (the process of adiabatic or polytrophic humidification), in the case of steam humidification (the process of isothermal humidification) there is no need for additional heating of air after moisture [1].

In developing a mathematical model, the task is to determine the limits of its detalization. The dynamical model should be simple for its research and synthesis of the control system, and also take into account the features of heat-mass ex-change. Researchers use mathematical models with lumped [4, 12] and distributed [5, 6] parameters to simulate the dynamical processes of heat-mass exchange equipment. Models with lumped parameters are simpler in the calculations and make it possible to obtain an analytical solution. Models with distributed parameters apply for more exact mathematical description. An analytical modelling of equipment with distributed parameters is a rather complicated task, transcendental functions appear in the solution [5]. For such tasks numerical methods of the solution are used in practice.

1. Using dynamic models

Typically, static models of process equipment are used to design and calculate the power of a particular plant. Dynamic models of process equipment are used for the synthesis and analysis of control systems. When designing and optimizing any control system, the structure and parameters of the controller are primarily dependent on the dynamic behaviour of a controlled plant. The choice of whether a different law of control is determined by the dynamic properties of a controlled plant. The choice of a law of control is determined by the dynamic properties of a controlled plant. In automation systems, developers use: classical PI controllers, PID controllers; adaptive controllers [3, 9]; controllers with fuzzy logic [14]; controllers with fractional derivatives [10]; intelligent controllers [8]; controllers based on neural networks and many other types of controllers. In their research, experts compare the operation of control systems with different types of controllers and draw conclusions about the quality of management. In the study of control systems with different types of controllers unchanged in the system there is a controlled plant, which characterizes the dynamic behaviour of the technological apparatus and formalized in the form of differential equations controlled plant. Thus, an adequate mathematical model of a controlled plant is the basis for the synthesis and analysis of a qualitative control system.

The purpose of the publication is to develop a mathematical model of the heat-mass exchange process for a steam humidifier in the state space, which will allow the analysis of dynamic characteristics of steam generator of industrial air conditioners. An additional requirement is the convenience of using the resulting model in the MatLAB environment.

2. Dynamical model of steam humidifier

When developing a mathematical model of a steam humidifier, the model [13] was used as the base model, where the humidification chamber without a steam generator is analysed. In [13], the differential equation of the humidifier chamber material balance is considered in characteristic of relative humidity, which is linearized. Relative humidity is determined by a significant nonlinear dependence on the temperature of air [2]. As a consequence, the temperature range of the use of the linear model is small. Therefore, the material balance equations of the steam humidification chamber will be considered in characteristic of the air moisture content.

The following simplifications were made during the development of a dynamic model of a steam humidifier: heat exchange with the environment is absent, since the thermal losses of modern heaters do not exceed 5%; the model contains two main dynamic elements with lumped parameters (air space humidifying chamber and steam generator with water); the physical properties of the material flows and the heat transfer surface are brought to the averaged values of the working range. The calculation scheme of the steam humidifier is shown in Fig. 1.

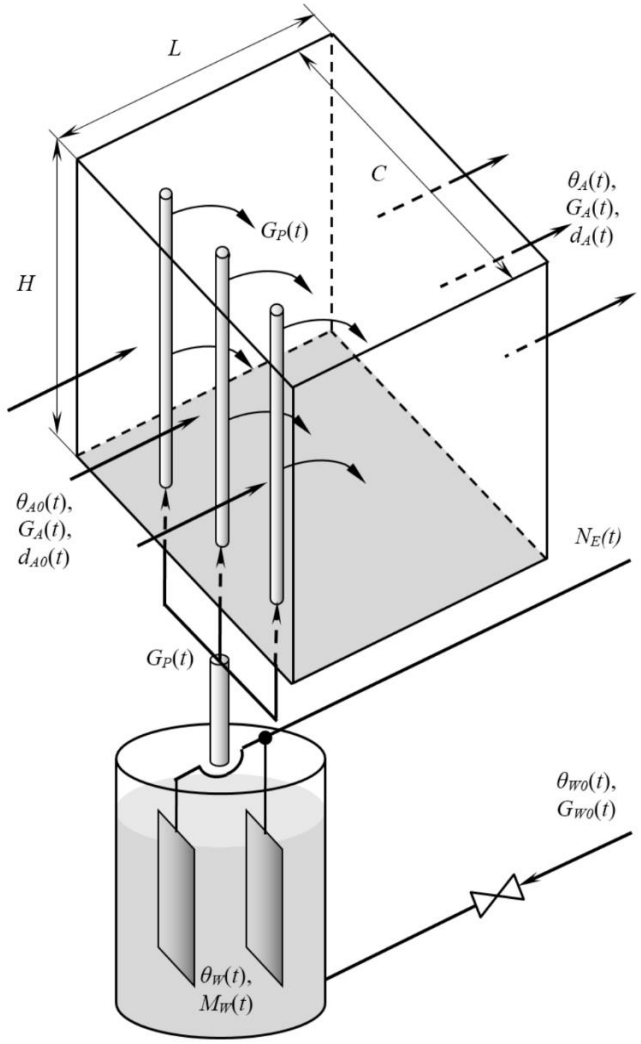

Fig. 1. Schematic diagram for simulation: $\theta_{A0}(t)$, $d_{A0}(t)$, $G_A(t)$ *temperature, moisture and input air flow;* $\theta_A(t)$, $d_A(t)$ *temperature, moisture output air;* $G_P(t)$ *steam mass flow;* $N_E(t)$ *input electric power;* $\theta_{W0}(t)$, $G_{W0}(t)$ *feed water temperature and flow;* θ_W, M_W *temperature and mass of water in the steam generator*

In the air space of the humidifying chamber with volume $V_A = H \times L \times C$ there is air with temperature $\theta_{A0}(t)$ and moisture content $d_{A0}(t)$, air flow $G_A(t)$. A steam with a mass flow $G_P(t)$ of is fed through the steam pipeline to the humidifying chamber. The steam pipeline is connected to the steam generator. The steam generator contains water, the level of which is automatically maintained by the stabilization system of the level by means of feed water with temperature $\theta_{W0}(t)$ and flow $G_{W0}(t)$. In the steam generator there are electrodes through which the electric current passes by the power $N_E(t)$, at the expense of which the steam is generated. The pair is assimilated in the air, moisturizing it to the output parameters of the air mixture $\theta_A(t)$, $d_A(t)$. Let's consider the heat and material balance for the air mixture of the humidifying chamber and the steam generator.

The heat balance for the air mixture of the humidifying chamber is:

$$G_A\left[c_A(\theta_{A0}-\theta_A)+\frac{r}{1000}(d_{A0}-d_A)\right]+ +rG_P = c_A M_A \frac{d\theta_A}{dt}, \quad (1)$$

where c_A is heat capacity of the air mixture; r is heat of vaporization; M_A is mass of moist air in volume V_A. Consider the material balance for airspace of the humidification chamber. The moisture content accumulated in the humidifier air space is defined as the difference between the mass input and output pairs

$$\frac{G_A}{1000}(d_{A0}-d_A)+G_P = V_A\frac{d\rho_A}{dt}. \quad (2)$$

The heat and material balance for the steam generator are represented by the corresponding equations:

$$G_W c_W \theta_{W0} + N_E - rG_P = c_W \frac{dM_W\theta_W}{dt} \quad (3)$$

$$G_W - G_P = \frac{dM_W}{dt} \quad (4)$$

where θ_{W0} is temperature of feed water; θ_W is water temperature in the steam generator (in operating mode $\theta_W = 100°C$); G_P, G_W is mass flows of steam and water; c_W is heat capacity of water; N_E is power of the steam generator; M_W is mass of water in the steam generator. Equations (1) – (4) represent a dynamic model of heat-mass exchange for the steam humidifier of an air conditioner:

$$\begin{cases} G_A\left[c_A(\theta_{A0}-\theta_A)+\frac{r}{1000}(d_{A0}-d_A)\right]+ +rG_P = c_A M_A\frac{d\theta_A}{dt} \\ \frac{G_A}{1000}(d_{A0}-d_A)+G_P = V_A\frac{d\rho_A}{dt} \\ G_W c_W\theta_{W0}+N_E-rG_P = c_W\frac{dM_W\theta_W}{dt} \\ G_W - G_P = \frac{dM_W}{dt} \end{cases} \quad (5)$$

The design of the steam generator includes a system for stabilizing the water level. For these reasons $\frac{dM_W}{dt} \approx 0$ and the differential equation (4) becomes algebraic $G_W - G_P \approx 0$. Also, let's take into account the constant temperature of water in the steam generator $\theta_W \approx 100°C$, from where for equation (3) $\frac{dM_W\theta_W}{dt} \approx 0$, from which it is easy to determine G_P:

$$G_P = \frac{1}{r - c_W\theta_{W0}}N_E \quad (6)$$

Thus, the system of equations (5) is simplified. After grouping similar terms for (1), (2) with regard to (6) and $G_A \approx const$, we obtain a dynamic model of the steam humidifier:

$$\begin{cases} T_A\frac{d\theta_A}{dt}+\theta_A = k_0\theta_{A0}+k_1 d_{A0}+k_2 d_A+k_3 N_E \\ T_d\frac{dd_A}{dt}+d_A = k_4 d_{A0}+k_5 N_E \end{cases} \quad (7)$$

where $T_A = \frac{M_A}{G_A}$; $T_d = \frac{\omega V_A}{G_A}$;

$$k_0 = 1;\ k_1 = \frac{r}{1000 c_A G_A};\ k_2 = -k_1$$

$$k_3 = \frac{r}{c_A G_A(r - c_W\theta_{W0})};\ k_4 = 1;\ k_5 = \frac{1000}{r - c_W\theta_{W0}}$$

The mathematical model (7) is representable in the states space:

$$\mathbf{X}' = \mathbf{AX} + \mathbf{BU} \quad (8)$$

where

$$\mathbf{X}=\begin{bmatrix}\theta_A\\ d_A\end{bmatrix};\ \mathbf{A}=\begin{bmatrix}-\frac{1}{T_A} & -\frac{k_2}{T_A}\\ 0 & -\frac{1}{T_d}\end{bmatrix};\ \mathbf{B}=\begin{bmatrix}\frac{k_0}{T_A} & \frac{k_1}{T_A} & \frac{k_3}{T_A}\\ 0 & \frac{k_4}{T_d} & \frac{k_5}{T_d}\end{bmatrix};\ \mathbf{U}=\begin{bmatrix}\theta_{A0}\\ d_{A0}\\ N_E\end{bmatrix}.$$

Applying the Laplace transform to the system (7), we obtain:

$$d_A=\frac{1}{T_d\,p+1}\left[k_4\,d_{A0}+k_5\,N_E\right] \tag{9}$$

$$\theta_A=\frac{1}{a_2p^2+a_1p+1}\left[(b_1p+b_0)\theta_{A0}+(b_3p+b_2)d_{A0}+(b_5p+b_4)N_E\right] \tag{10}$$

where $a_1=T_A+T_d$; $a_2=T_A\,T_d$; $b_0=k_0$; $b_1=k_0\,T_d$; $b_2=k_1+k_2\,k_4$; $b_3=k_1\,T_d$; $b_4=k_3+k_2\,k_5$; $b_5=k_3\,T_d$. Using the inverse Laplace transform, one can find the analytic solution (9) and (10) by the channels of control and disturbance.

Thus, a dynamic model of the steam humidifier, which can be represented as one of the equivalent dependences (7), (8), (9) or (10), is obtained.

3. An example of dynamic mode simulation for a steam humidifier

Consider the simulation of dynamic processes for the steam humidifying chamber KCKP-20 of the company "VEZA" in the complete set with the steam generator SMU-233 [2]. Tab. 1 shows the thermal physic parameters for the VEZA KCKP-20 steam humidifying chamber.

Table 1. Thermal physic parameters of the VEZA KCKP-20 steam humidifying chamber

Parameter name	Marking	Numerical value	Dimension
Dimensions of the water heater	$H\times L\times C$	1×1.4×1.9	m
Flow of air mixture	G_A	6.7	kg/sec
Power of the steam humidifier	N_E	16000	Watt
Moist air density	ρ_A	1.2	kg/m^3
Dry air density	ω	1.2	kg/m^3
Air heat capacity	c_A	1010	J/(kg·ºC)
Water heat capacity	c_W	4185	J/(kg·ºC)
Heat of vaporization	r	2256000	J/kg
Input air temperature	θ_{A0}	20	ºC
Output air temperature	θ_A	20	ºC
Input water temperature for steam generator	θ_{W0}	20	ºC
Input moisture content of air	d_{A0}	2	g/kg
Output moisture content of air	d_A	6	g/kg

Coefficients for models (8)–(10) of the steam generator were calculated in the MatLAB software environment using the `coef_SMU233.m` program:

```
H=1; L=1.4; C=1.9;
Va=H*L*C;
Ga=0.43;
pa=1.2;
w=1.2;
ca=1010;
cw=4182;
r=2256000;
TetA0=20;
TetA=20;
TetW0=20;
da0=2;
da=6;
Ta=pa*Va/Ga;
Td=w*Va/Ga;
k0=1;
k1=r/(1000*ca*Ga);
k2=-k1;
k3=r/(ca*Ga*(r-cw*TetW0));
k4=-1;
k5=1000/(r-cw*TetW0);
A=[-1/Ta,-k2/Ta;0,-1/Td];
B=[k0/Ta,k1/Ta,k3/Ta;0,k4/Td,k5/Td];
a1=Ta+Td;
a2=Ta*Td;
b0=k0;
b1=k0*Td;
b2=k1+k2*k4;
b3=k1*Td;
b4=k3+k2*k5;
b5=k3*Td;
```

The calculated coefficients are used in models (8)–(10):

$T_A=T_d=0.4788$;

$k_0=1$; $k_1=0.335$;

$k_2=-0.335$; $k_3=1.5423\cdot10^{-4}$;

$k_4=1$; $k_5=4.6033\cdot10^{-4}$;

$a_1=0.9576$; $a_2=0.2292$;

$b_0=1$; $b_1=0.4788$; $b_2=0$; $b_3=0.16$;

$b_4=0$; $b_5=7.385\cdot10^{-5}$.

$$\begin{bmatrix}\theta'_A\\ d'_A\end{bmatrix}=\begin{bmatrix}-2.0886 & -0.6998\\ 0 & -2.0886\end{bmatrix}\begin{bmatrix}\theta_A\\ d_A\end{bmatrix}+\begin{bmatrix}2.0886 & 0.6998 & 3.2212\cdot10^{-4}\\ 0 & 2.0886 & 9.6142\cdot10^{-4}\end{bmatrix}\begin{bmatrix}\theta_{A0}\\ d_{A0}\\ N_E\end{bmatrix} \tag{11}$$

$$d_A=\frac{1}{0.4788p+1}\left[d_{A0}+4.6033\cdot10^{-4}\,N_E\right] \tag{12}$$

$$\theta_A=\frac{1}{0.2292p^2+0.9576p+1}\left[(0.4788p+1)\theta_{A0}+0.16p\,d_{A0}+7.385\cdot10^{-5}\,p\,N_E\right] \tag{13}$$

Simulation modelling of the dynamic mode for the steam humidifier was carried out in the Simulink MatLAB environment using the State Space functional block. The simulation results of transients along the control channel are presented in Fig. 2. The results of the simulation of transients along disturbance channels are shown in Fig. 3.

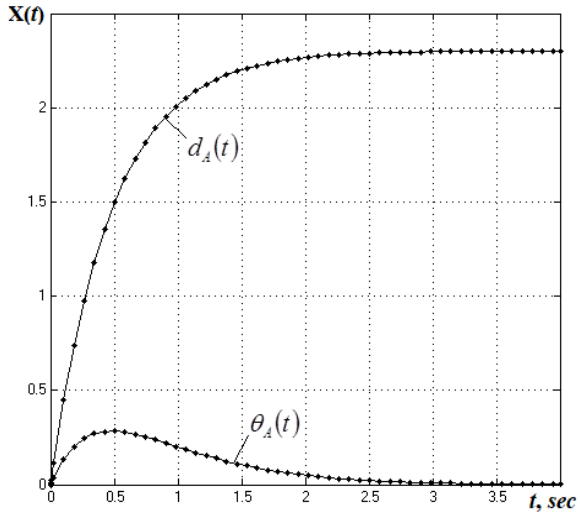

Fig. 2. Graphs of the transient processes for the control channel $N_E\rightarrow\mathbf{X}(t)$

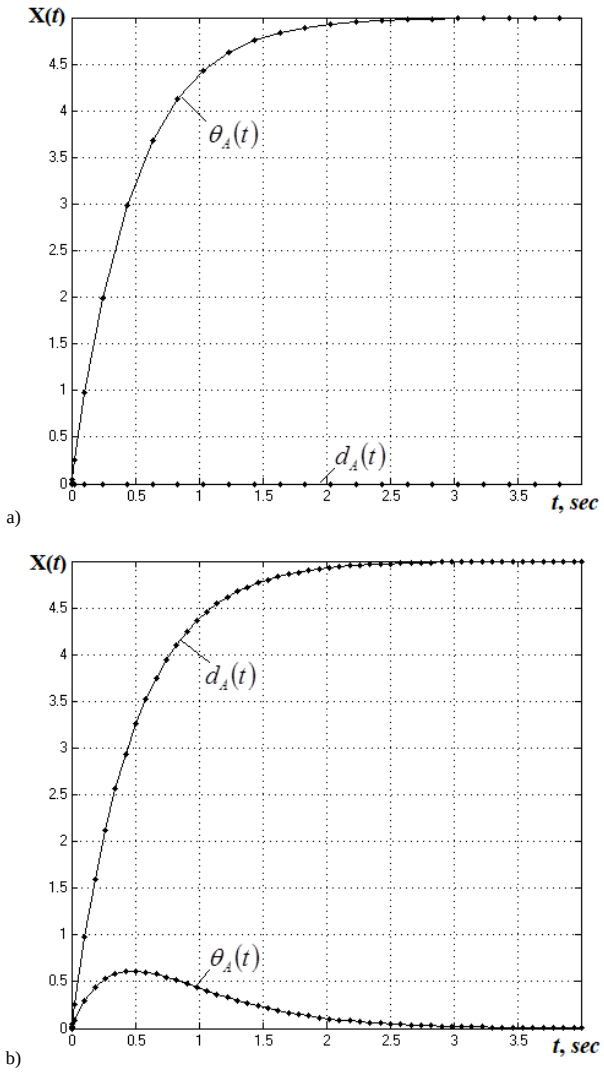

Fig. 3. Graphs of the transient processes for the perturbation channels: *a)* $\theta_{A0}(t) \to \mathbf{X}(t)$ *; b)* $d_{A0}(t) \to \mathbf{X}(t)$

The results of the simulation can be summarized as follows. The inertia of the regulation and perturbation channels is insignificant compared to the inertia of the temperature and moisture sensors. For these reasons, when designing the system for controlling steam humidifier, it is necessary to take into account the inertial properties of the temperature and moisture sensors.

4. Conclusions

In article was proposed maths model of heat-mass exchange for a steam humidifier. The proposed dynamic model takes into account mass transfer with moisture content. Existing models consider a relative humidity, so the proposed model allows us to demarcate between the nonlinear effect of temperature on air humidity. Using the new model for the synthesis of an air conditioning control system will allow to divide out between the effect of temperature at humidity.

The steam humidifier model to is offer from equivalent dependencies in: a) the differential equations form (7); b) the state space (8); c) the transfer functions form (9), (10). The mathematical dependence choice is determined by the control system synthesis method.

The proposed dynamic model is recommended to be used in the support and decision-making system at the middle level of enterprise management [7]. This will integrate the air conditioning control system into the enterprise management system. Such an approach will allow the company to transfer to a qualitatively new level of management and allow the efficient use of energy resources.

References

[1] Belova E.M.: Central Air Conditioning Systems in Buildings. Euroclimate, Moscow 2006.
[2] Conditioners Central KCKP. Catalog Equipment VEZA. 2019 http://www.veza.ru/docs/konditsionery-tsentralnye-ktskp
[3] Deacha P.: Multiobjective Multipath Adaptive Tabu Search for Optimal PID Controller Design. International Journal of Intelligent Systems and Applications 7, 2015, 51–58.
[4] Golinko I.M.: The dynamic model of heat-mass exchange for water cooling of industrial air conditioning. Science and Technology NTUU KPI 6, 2014, 27–34.
[5] Golinko I.M., Kubrak N.A.: Modeling and Optimization of Control Systems. Ruta, Kamyanets-Podilskii 2012.
[6] Golinko I.M., Ladanuk A.P., Koshelieva L.D.: Dynamic Model of the Calorifier Heat Mode. Information Technology and Computer Engineering 3, 2009, 59–63.
[7] Pankratova N., Bidyuk P., Golinko I.: Decision Support System for Microclimate Control at Large Industrial Enterprises. Proceedings of The Third International Workshop on Computer Modeling and Intelligent Systems (CMIS-2020), 489-498.
[8] Lakshmi K.V., Srinivas P., Ramesh C.: Comparative Analysis of ANN based Intelligent Controllers for Three Tank System. International Journal of Intelligent Systems and Applications 8, 2016, 34–41.
[9] Poonam S., Agarwal S.K., Narendra K.: Advanced Adaptive Particle Swarm Optimization based SVC Controller for Power System Stability. International Journal of Intelligent Systems and Applications 7, 2014, 101–110.
[10] Soukkou A., Belhour M.C., Leulmi S.: Review, Design, Optimization and Stability Analysis of Fractional-Order PID Controller. International Journal of Intelligent Systems and Applications 8, 2016, 73–96.
[11] Tkachov V., Gruhler G., Zaslavski A., Bublikov A., Protsenko S.: Development of the algorithm for the automated synchronization of energy consumption by electric heaters under condition of limited energy resource. Eastern European Journal of Enterprise Technologies 8, 2018, 51–61.
[12] Vychuzhanin V.V.: Mathematical models of non-stationary modes of air processing in the central ACS. Bulletin of the Odessa National Maritime University 23, 2007, 172–185.
[13] Vychuzhanin V.V.: Scientific and technical bases of operation of ship's central systems of comfortable air conditioning. Dissertation of technical doctor sciences, 2009.
[14] Yazdanpanah A., Piltan F., Roshanzamir A.: Design PID Baseline Fuzzy Tuning Proportional Derivative Coefficient Nonlinear Controller with Application to Continuum Robot. International Journal of Intelligent Systems and Applications 6, 2014, 90–100.

Ph.D. Igor Golinko
e-mail: conis@ukr.net

Associate professor of the sub-department of Automation Heat-and-Power Engineering processes of Heat-and-Power Engineering department, National Technical University of Ukraine "Igor Sikorsky Kyiv Polytechnic Institute", Kyiv, Ukraine.
Author of over 100 scientific papers. Engaged in scientific mathematical simulation of technical and technological processes, computer techniques and computer technologies, programming.

http://orcid.org/0000-0002-7640-4760

Prof. D.Sc.(Technical) Volodymyr Drevetskiy
e-mail: Westra@rv.uar.net

Vice President of Engineering Academy of Ukraine, Head of Automation, electrical engineering and computer integrated technologies Department, National University of Water Management and Nature Resources Use, Rivne, Ukraine.
The main scientific direction – development of methods and devices for continuous automatic monitoring of the physical and mechanical parameters of Newtonian and non-Newtonian fluids, as well as the quality of oil products. Author of over 200 scientific papers, including 51 patents, most of which are implemented in production.

http://orcid.org/0000-0001-8999-2226

otrzymano/received: 21.12.2019 *przyjęto do druku/accepted: 26.06.2020*

http://doi.org/10.35784/iapgos.930

NONSTATIONARY HEAT CONDUCTION IN MULTILAYER GLAZING SUBJECTED TO DISTRIBUTED HEAT SOURCES

Natalia Smetankina, Oleksii Postnyi
A. Pidgorny Institute for Mechanical Engineering Problems of the National Academy of Sciences of Ukraine

Abstract. *A method for calculation of nonstationary thermal fields in a multilayer glazing of vehicles under the effect of impulse film heat sources is offered. The glazing is considered as a rectangular multilayer plate made up of isotropic layers with constant thickness. Film heat sources are arranged on layers' interfaces. The heat conduction equation is solved using the Laplace transformation, series expansion and the second expansion theorem. The method offered can be used for designing a safe multilayer glazing under operational and emergency thermal and force loading in vehicles.*

Keywords: safe multilayer glazing, nonstationary heat conduction, film heat source

NIESTACJONARNE PRZEWODZENIE CIEPŁA W SZYBACH WIELOWARSTWOWYCH NARAŻONYCH NA DZIAŁANIE ROZPROSZONYCH ŹRÓDEŁ CIEPŁA

Streszczenie. *Zaproponowano metodę obliczania niestacjonarnych pól temperaturowych w wielowarstwowych szybach pojazdów pod wpływem impulsowych cienkowarstwowych źródeł ciepła. Przeszklenie jest traktowane jako prostokątna wielowarstwowa płyta złożona z izotropowych warstw o stałej grubości. Cienkowarstwowe źródła ciepła znajdują się na granicach warstw. Równanie niestacjonarnego przewodnictwa cieplnego rozwiązuje się za pomocą rozwinięcia Laplace'a w funkcji czasu, rozkładając funkcje w szeregi i stosując twierdzenie o drugim rozwinięciu. Zaproponowane podejście może być wykorzystane przy projektowaniu bezpiecznego wielowarstwowego oszklenia pojazdów w warunkach obciążeń termicznych eksploatacyjnych i awaryjnych.*

Słowa kluczowe: bezpieczne szkła wielowarstwowe, niestacjonarna przewodność cieplna, cienkowarstwowe źródło ciepła

Introduction

One of the urgent problems in modern technology is the task of reliable determination of the thermal state of structural elements. Its successful solution depends on the reliability and efficiency of the elements of different structures, which often have a heterogeneous structure.

The aircraft's modern heating glass is a complex, large, multi-layered structure. Its performance depends primarily on the strength and durability of the glass elements, the optimal parameters of adhesive layers and structural solutions that would provide the necessary heat resistance and durability of the roofing layer under cyclic loading and the action of extreme operating factors.

It should be noted that in the calculation of temperature fields in multilayer structures there are considerable mathematical difficulties. This is due to the presence of layers whose properties are significantly different, and the fulfilment of the conditions of coupling of the layers taking into account the internal heat sources.

1. Analysis of publications by research topic

Practical work on the design of protective glazing of vehicles has led to the creation of standards for multilayer safety glasses, which are designed to protect human life, ensure safety and reliability while storing and transporting material.

In modern engineering, the problem of valid identification of the thermal condition of structural components is a topical one. Models and methods of solving heat conduction and thermal elasticity problems are reviewed in [2]. Analysis of the literature has shown that uniform structures are the most investigated ones.

A review of the literature indicates that most publications are devoted to the calculation of structures under steady-state heating [4].

If the temperature field changes slowly with time, one can ignore the inertia terms in motion equations and the coupling term in the heat conduction equation, and consider the thermal elasticity problem as a quasistatic one. The monographs by Melan and Parkus [7], Gatewood [3], and Novatsky [8] have comprehensively developed the theory and solved concrete problems.

The thermal elasticity problem in the quasistatic statement has the greatest practical value. Due to insignificant dynamic effects under common nonstationary heat exchange conditions, one can ignore the coupling of mechanical and thermal energy, and solve the temperature stresses problem in two stages, viz. first solve the heat conduction equation and then determine the field of stresses using the thermal elasticity equation and the temperature distribution found.

For multilayer elements in constructions, heat conduction problems are solved by involving different kinds of hypotheses on temperature distribution over the thickness of the pack of layers. Therefore, the majority of papers use the following numerical computation methods: the finite difference method, the boundary elements method (BEM), and finite elements method (FEM).

Jane and Wu [6] used the Laplace transform and the finite difference method for solving dynamic and static thermal elasticity problems for multilayer conical shells.

Within the framework of the two-dimensional theory of thermal elasticity, Ishiguro and Tanaka [5] built a model of strain in plate-like constructions for stationary thermal flux conditions. The problem was reduced to solving a system of boundary integral equations discretized by the BEM. The technique described was used for calculating the parameters of the thermal stressed state in anisotropic rectangular plates.

Using the FEM, Oguamanam et al. [9] studied the nonlinear response of a laminated symmetrical orthogonally reinforced cylindrical panel to sudden application of a heat flux. The panel is cantilevered to a hub with limited rotation around the central axis of rotation. The temperature field thickness is constant and changes exponentially with time. The system of nonlinear equations is solved with the Newton-Raphson method jointly with the Newmark integration method.

Verijenko et al. [15], Barut et al. [1] applied the hypothesis on the piecewise-linear temperature distribution over the thickness of the multilayer pack to study stationary temperature fields in multilayer composite shells and rectangular panels in plan. The stress fields were calculated using the FEM.

Analytical methods are mathematically very involved when describing the geometrical parameters of multilayer bodies with a noncanonical configuration; the conditions of layer conjugation with account of inner heat sources, and with presence of layers with significantly differing properties.

Savoia and Reddy [11] investigated stresses in multilayer composite rectangular simply supported plates under uniform heating of the plates' outer surfaces. A polynomial and exponential temperature distribution was specified over the thickness of the pack of layers. The thermal elasticity equations were solved with the Navier method. Ootao and Tanigawa [10] used a similar

approach for calculating temperature stresses in the layers of a two-layer cylindrical composite simply supported panel.

In the paper [14] a nonstationary thermal conduction problem for layered rectangular plates at a given temperature distribution on the outer and inner surfaces is solved analytically without involving hypotheses about the temperature distribution along the plate thickness.

The unresolved problem is the development of effective methods for investigating the thermal conductivity of multilayer glazing with high parameters of thermal force loading during operational and emergency impacts.

The aim of this work is to develop a method of calculating non-stationary temperature fields in multilayer glazing of aircraft under the influence of pulsed distributed interlayer heat sources.

2. Solution method

Consider a multilayer rectangular plate assembled from I isotropic layers of constant thickness h_i, $i = 1, 2, \ldots, I$. The dimensions of the plate in the direction of X-axis and Y-axis denote A and B, respectively. The coordinate z_i is counted from the inner surface of each layer, $0 \le z_i \le h_i$. As the coordinate surface, select the front surface of the first layer of the plate, $z_1 = 0$.

We write the heat equation for the i-th layer of the plate:

$$T^i_{,t} = a_i \Delta T^i,\ i = 1, 2, \ldots, I,\ \Delta = \frac{\partial^2}{\partial x^2} + \frac{\partial^2}{\partial y^2} + \frac{\partial^2}{\partial z^2_{z_i}} \tag{1}$$

where $T^i = T^i(x, y, z_i, t)$ is temperature; $a_i = \lambda_i / (\rho_i c_i)$ is thermal diffusivity, λ_i is coefficient of thermal conductivity, ρ_i is relative density, c_i is specific heat of the i-th layer material, t is time. We accept zero initial conditions

$$T^i\Big|_{t=0} = 0,\ i = 1, 2, \ldots, I \tag{2}$$

Zero temperature is maintained on the side surface of the plate

$$T^i\Big|_{x=0,\ x=A} = T^i\Big|_{y=0,\ y=B} = 0,\ i = 1, 2, \ldots, I \tag{3}$$

On the front surfaces of the plate there is convective heat transfer with the external environment. We write down the boundary conditions

$$T^1_{,z_1} - \frac{\alpha_{\text{in}}}{\lambda_1} T^1 = -\frac{\alpha_{\text{in}}}{\lambda_1} T_{\text{in}},\ z_1 = 0 \tag{4}$$

$$T^I_{,z_I} + \frac{\alpha_{\text{out}}}{\lambda_I} T^I = \frac{\alpha_{\text{out}}}{\lambda_I} T_{\text{out}},\ z_I = h_I \tag{5}$$

and conditions for thermal conjugation of layers

$$T^i = T^{i+1},\ i = 1, 2, \ldots, I-1 \tag{6}$$

$$\lambda_i T^i_{,z_i} = \lambda_{i+1} T^{i+1}_{,z_{i+1}} + q^i_S,\ i = 1, 2, \ldots, I-1 \tag{7}$$

where α_{in}, α_{out}, $T_{\text{in}}(x, y)$, $T_{\text{out}}(x, y)$ are coefficients of convective heat transfer and ambient temperature on the front surfaces of the plate, respectively; $q^i_S(x, y)$ are intensities of film heat sources located at the contact boundary of neighboring layers.

After the Laplace transform with respect to the variable t, we obtain the operator equation

$$pT^*_i = a_i \Delta T^*_i,\ i = 1, 2, \ldots, I \tag{8}$$

where $T^*_i(x, y, z_i)$ is an image of $T^i = T^i(x, y, z_i, t)$.

The transformation of the initial (2) and boundary (3), (6) conditions is carried out by simple replacement T^i by T^*_i. The boundary conditions (4), (5) and (7) in the image space take the form

$$T^*_{1,z_1} - \frac{\alpha_{\text{in}}}{\lambda_1} T^*_1 = -\frac{1}{p}\frac{\alpha_{\text{in}}}{\lambda_1} T_{\text{in}},\ z_1 = 0 \tag{9}$$

$$T^*_{I,z_I} + \frac{\alpha_{\text{out}}}{\lambda_I} T^*_I = \frac{\alpha_{\text{out}}}{\lambda_I} T_{\text{out}},\ z_I = h_I \tag{10}$$

$$\lambda_i T^*_{i,z_i} = \lambda_{i+1} T^*_{i+1,z_{i+1}} + \frac{1}{p} q^i_S,\ i = 1, 2, \ldots, I-1 \tag{11}$$

The solution to operator equation (8) is sought in the form

$$T^*_i(x, y, z_i) = T^*(x) T^*(y) T^*_i(z_i),$$

$$\frac{d^2 T^*(x)}{dx^2} \Big/ T^*(x) + \frac{d^2 T^*(y)}{dy^2} \Big/ T^*(y) + \frac{d^2 T^*(z_i)}{dz_i^2} \Big/ T^*(z_i) = p / a_i$$

which allows us to go to a system of ordinary differential equations

$$\frac{d^2 T^*(x)}{dx^2} = -\alpha_m^2 T^*(x),\ \frac{d^2 T^*(y)}{dy^2} = -\beta_n^2 T^*(y) \tag{12}$$

$$\frac{d^2 T^*(z_i)}{dz_i^2} - \left(p / a_i + \alpha_m^2 + \beta_n^2\right) T^*(z_i) = 0 \tag{13}$$

Solving equations (12) taking into account the boundary conditions (3) on the plate contour, we obtain

$$T^*_m(x) = R_m \sin \alpha_m x,\ T^*_n(y) = Q_n \sin \beta_n y,$$

where $\alpha_m = m\pi / A$, $\beta_n = n\pi / B$.

Therefore, the solution of equation (8) is written in the form of a double series

$$T^*_i(x, y, z_i) = \frac{4}{AB} \sum_{m=1}^{\infty} \sum_{n=1}^{\infty} T^*_{imn}(z_i) \sin \alpha_m x \sin \beta_n y \tag{14}$$

Functions $T_{\text{in}}(x, y)$, $T_{\text{out}}(x, y)$ and $q^i_S(x, y)$ also expand to series

$$T_{\text{in}}(x, y) = \sum_{m=1}^{\infty} \sum_{n=1}^{\infty} T_{\text{in } mn} \sin \alpha_m x \sin \beta_n$$

$$T_{\text{out}}(x, y) = \sum_{m=1}^{\infty} \sum_{n=1}^{\infty} T_{\text{out } mn} \sin \alpha_m x \sin \beta_n \tag{15}$$

$$q^i_S(x, y) = \sum_{m=1}^{\infty} \sum_{n=1}^{\infty} q^i_{Smn} \sin \alpha_m x \sin \beta_n y \tag{16}$$

where

$$T_{\text{in } mn} = \frac{4}{AB} \int_0^A \int_0^B T_{\text{in}}(x, y) \sin \alpha_m x \sin \beta_n y\, dx\, dy,$$

$$T_{\text{out } mn} = \frac{4}{AB} \int_0^A \int_0^B T_{\text{out}}(x, y) \sin \alpha_m x \sin \beta_n y\, dx\, dy,$$

$$q^i_{Smn} = \frac{4}{AB} \int_0^A \int_0^B q^i_S(x, y) \sin \alpha_m x \sin \beta_n y\, dx\, dy.$$

The coefficient $T^*_{imn}(z_i)$ is determined by solving the transformed equation (13)

$$\frac{d^2 T^*_{imn}(z_i)}{dz_i^2} + \left(k^2 / a_i - \alpha_m^2 - \beta_n^2\right) T^*_{imn}(z_i) = 0 \tag{17}$$

where $p = -k^2$. The boundary conditions (6), (9)-(11) are also transformed taking into account (15), (16), and the general solution of equation (17) has the form

$$T^*_{imn}(z_i) = C_i \operatorname{ch} \eta_i z_i + D_i \operatorname{sh} \eta_i z_i \text{ if } k^2 / a_i - \alpha_m^2 - \beta_n^2 < 0,$$

$$T^*_{imn}(z_i) = C_i \cos \mu_i z_i + D_i \sin \mu_i z_i \text{ if } k^2 / a_i - \alpha_m^2 - \beta_n^2 > 0,$$

where $\eta_i^2 = -\left(k^2 / a_i - \alpha_m^2 - \beta_n^2\right)$, $\mu_i^2 = k^2 / a_i - \alpha_m^2 - \beta_n^2$, $i = 1, 2, \ldots, I$.

The coefficients C_i and D_i are determined from a system of linear algebraic equations, which is formed from the boundary conditions. After determining the coefficients C_i and D_i, the original of the desired function $T_{imn}(z_i, t)$ is found by the second decomposition theorem, and the solution of equation (1) has the form

$$T^i(x, y, z_i, t) = \sum_{m=1}^{\infty} \sum_{n=1}^{\infty} T_{imn}(z_i, t) \sin \alpha_m x \sin \beta_n y.$$

3. Analysis of the numerical results

Consider heating a five-layer glazing element of the airplane with dimensions A = 0.64 m, B = 0.32 m (Fig. 1). Between the first and second layers a film heat source are placed with power q^0 = 3500 W/m^2, $q_S^1(x,y) = q^0 H(t)$, where $H(t)$ is Heaviside function, x_1 = 0.07 m, x_2 = 0.57 m, y_1 = 0 m, y_2 = 0.32 m. The layers have the following thermophysical and geometric characteristics:

λ_i = 1.61 W/(m·°C), c_i = 750 J/(kg·°C),

ρ_i = 2500 kg/m^3 (i = 1, 3, 5),

λ_i = 0.17 W/(m·°C), c_i = 1500 J/(kg·°C),

ρ_i = 1200 kg/m^3 (i = 2, 4);

h_1 = 5 mm, h_2 = 3 mm, h_3 = 15 mm, h_4 = 2 mm, h_5 = 20 mm. The coefficients of convective heat transfer on the outer and inner surfaces of the glazing element and the temperature of the external and internal environment are:

α_{in} = 80 W/(m^2·°C), α_{out} = 25 W/(m^2·°C),

T_{in} = -20ºC and T_{out} = 20ºC.

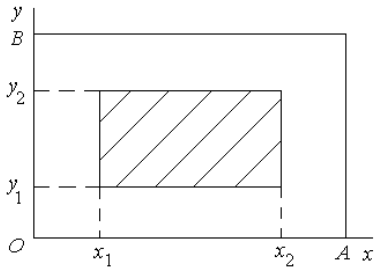

Fig. 1. The design scheme of the glazing element

The composition of the layers and the temperature distributions along the thickness of the glazing element at a point $x = A/2$, $y = B/2$ at time $t = 10^4$ s is shown at Fig. 2. Line 1 is the result of the analytical solution of the problem by the proposed method, line 2 is the result of using development of the sought functions in a series of Legendre polynomials method [12]. Comparative analysis of relations allows making the conclusion about the probability of the obtained results.

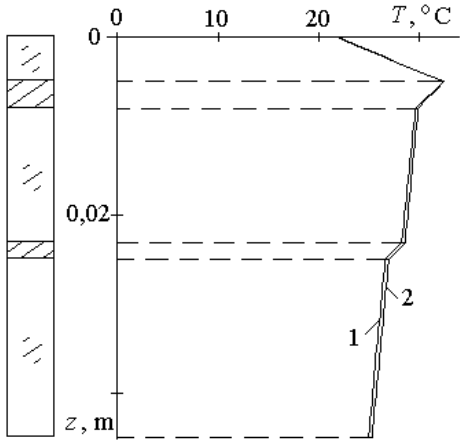

Fig. 2. Temperature distribution through the thickness of the glazing element

The temperature change in the point $x = A/2$, $y = B/2$ on different surfaces of the layers is shown at Fig. 3: line 1 – $z_1 = 0$, line 2 – $z_1 = h_1$, line 3 – $z_I = h_I$.

The dashed lines in the figure indicate the values of temperatures on the surfaces of the layers, which are solutions of a stationary problem [13]. It can be seen that from the time of the temperature field becomes stationary.

Consider now the thermal condition of a five-layer glazing element of the airplane with dimensions $A = B$ = 0.4 m containing a heat-generating film with power q^0 = 3500 W/m^2, $x_1 = y_1$ = 0.15 m, $x_2 = y_2$ = 0.35 m. As it has been specified above, we arrange the film between the first and the second layers of the element. The thicknesses, the coefficients of convective heat transfer on the outer and inner surfaces of the glazing element and the temperature of the external and internal environment are the same.

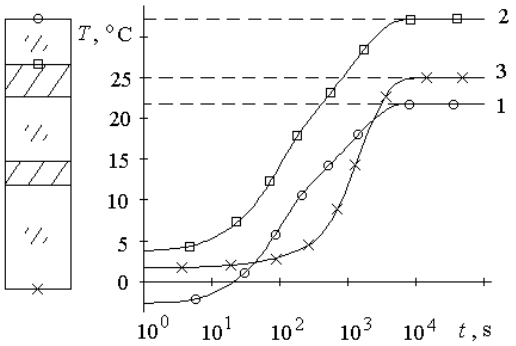

Fig. 3. Temperature changing over time

Fig. 4 shows the temperature distribution through the thickness of the element at different moments of time in the point $x = A/2$, $y = B/2$. The dash-dot line designates the position of the heat-generating film in the package of layers. At $t = 1$ s the temperature distribution is non-linear through the thickness of layers, which is appreciable especially in the third and the fifth layers. With time, the temperature distribution in all layers also becomes linear (curve 3, $t = 10^3$ s). A large temperature gradient is observed in layers close to the surface with the heat-generating film. Since $t = 5 \cdot 10^3$ s the temperature field does not practically vary, i.e. it stays steady.

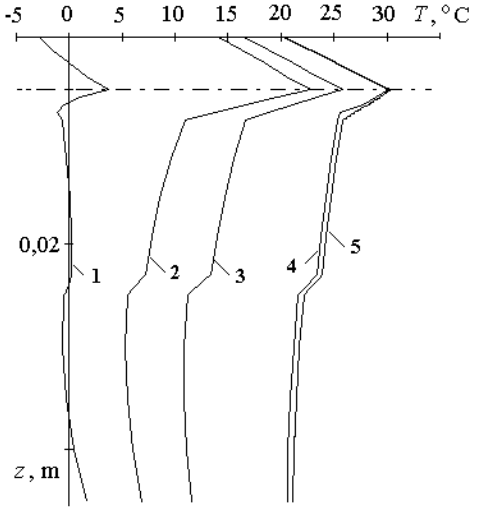

Fig. 4. Distribution of temperature through the thickness of the glazing element at different moments of time: 1 – t = 1 s, 2 – t = 5·10^2 s, 3 – t = 10^3 s, 4 – t = 5·10^3 s, 5 – t= 10^4 s

Fig. 5 shows a temperature field on the surface with the film heat source at the moment of time $t = 5 \cdot 10^3$ s.

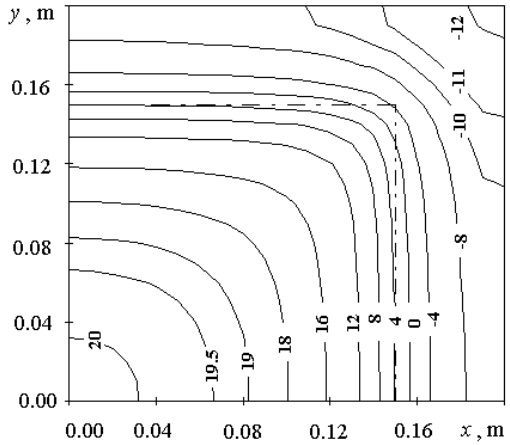

Fig. 5. Temperature field on the surface with the film heat source

4. Conclusions and prospects for further research

An analytical method for solution of the non-stationary heat conduction problem in multilayer glazing with an internal heat source is proposed. The multilayer glazing is considered as a rectangular plate made up of isotropic layers with constant thickness. Convective heat transfer occurs on outer surfaces of the plate. The temperature distribution in each layer of the plate is obtained analytically from the heat equation using the Laplace transform. As an example, we solved the nonstationary heat conduction problem for a five-layer glazing element under heating by the film heat source. The comparative analysis of the temperature distribution over the element thickness with the results of other method is carried out.

The solution of such problems has practical importance, as the results of this research can be applied to the analysis of the efficiency of deicing and demisting performances of heating systems for windshields of airplanes and different vehicles.

References

[1] Barut A., Madenci E., Tessler A.: Non-linear analysis of composite panels under non-uniform temperature distribution. Int. J. Solids and Struct 37(27)/2000, 3681–3713.
[2] Bielski W.R.: Controllability and stabilization in elasticity, heat conduction and thermoelasticity: Review of recent developments. J. of Global Optimization 17(4)/2000, 353–386.
[3] Gatewood B.E.: Thermal stresses. McGraw-Hill, New York 1957.
[4] Goldstein R.J., Ibele W.E., Patankar S.V., et al.: Heat transfer – a review of 2003 literature. Int. J. Heat Mass Transfer 49(3-4)/2006, 451–534.
[5] Ishiguro S., Tanaka M.: Analysis of two-dimensional anisotropic thermoelasticity by boundary element method. Trans. Jap. Soc. Mech. Eng. A 63(613)/1997, 1963–1970.
[6] Jane K.C., Wu Y.H.: A generalized thermoelasticity problem of multilayered conical shells. Int. J. Solids and Structures 41(9–10)/2004, 2205–2233.
[7] Melan E., Parkus H.: Warmespannungen infolge stationarer temperaturfelder. Springer-Verlag, Wien 1953.
[8] Novatsky V.: Problems of thermoelasticity. AS USSR Publishers, Moscow 1962.
[9] Oguamanam D.C.D., Hansen J.S., Heppler G.R.: Nonlinear transient response of thermally loaded laminated panels. J. Appl. Mech. Trans. ASME 71(1)/2004, 49–56.
[10] Ootao Y., Tanigawa Y.: Transient thermal stresses of angle-ply laminated cylindrical panel due to nonuniform heat supply in the circumferential direction. Compos. Structures 55(1)/2002, 95–103.
[11] Savoia M., Reddy J.N.: Three-dimensional thermal analysis of laminated composite plate. Int. J. Solids and Structures 32(5)/1995, 539–608.
[12] Shupikov A.N., Smetankina N.V., Svet Ye.V.: Nonstationary heat conduction in complex-shape laminated plates. J. Heat Transfer. Trans. ASME 129(3)/2007, 335–341.
[13] Smetankina N.V.: Non-stationary deformation, thermal elasticity and optimisation of laminated plates and cylindrical shells. Miskdruk Publishers, Kharkiv 2011.
[14] Tanigawa Y., Ootao Y., Kawamura R.: Thermal bending of laminated composite rectangular plates and nonhomogeneous plates due to partial heating. J. Thermal Stresses 14(3)/1991, 285–308.
[15] Verijenko V.E., Tauchert T.R., Shaikh C., Tabakov P.Y.: Refined theory of laminated anisotropic shells for the solution of thermal stress problems. J. Thermal Stresses 22(1)/1999, 75–100.

D.Sc. Natalia Smetankina
e-mail: nsmetankina@ukr.net

Head of the Department of Vibration and Thermostability Studies, A. Pidgorny Institute of Mechanical Engineering Problems, National Academy of Sciences of Ukraine. Scientific interests: mechanics of deformable solids, mathematical modeling, non-stationary vibrations, thermoelasticity, composites, impact, laminated structures.

http://orcid.org/0000-0001-9528-3741

M.Sc. Oleksii Postnyi
e-mail: alekh.po@gmail.com

Post-graduate student at A. Pidgorny Institute of Mechanical Engineering Problems, National Academy of Sciences of Ukraine. Scientific interests: thermoelasticity, composites, laminated structures.

http://orcid.org/0000-0002-3151-3891

otrzymano/received: 22.12.2019 *przyjęto do druku/accepted: 26.06.2020*

http://doi.org/10.35784/iapgos.1564

REAL-TIME MONITORING OF CELL CULTURES WITH NICKEL COMB CAPACITORS

Andrzej Kociubiński[1], Dawid Zarzeczny[1], Maciej Szypulski[1], Aleksandra Wilczyńska[1], Dominika Pigoń[2], Teresa Małecka-Massalska[2], Monika Prendecka[2]
[1]Lublin University of Technology, Lublin, Poland, [2]Medical University of Lublin, Lublin, Poland

Abstract. *The aim of the study was to present a method for assessing the condition of cell culture by measuring the impedance of cells cultured in the presence of nickel. For this purpose, an impedance measurement technique using nickel comb capacitors was used. The capacitor electrodes were made using a thin film magnetron sputtering. In the experimental part, the culture of cells of mouse fibroblasts on the prepared substrate was performed. The cell culture lasted 43 hours and showed that the presented technique allows it to be used to analyze the effect of nickel on cells.*

Keywords: BioMEMS, ECIS, nickel, thin films

MONITOROWANIE HODOWLI KOMÓRKOWYCH W CZASIE RZECZYWISTYM PRZY ZASTOSOWANIU NIKLOWYCH KONDENSATORÓW GRZEBIENIOWYCH

Streszczenie. *Celem pracy było przedstawienie metody oceny stanu hodowli komórkowej poprzez pomiar impedancji komórek hodowanych w obecności niklu. W tym celu zastosowano technikę pomiaru impedancji z wykorzystaniem niklowych kondensatorów grzebieniowych. Cienkowarstwowe elektrody kondensatora wykonano metodą rozpylania magnetronowego. W części eksperymentalnej przeprowadzono hodowlę komórek mysich fibroblastów na przygotowanym podłożu. Hodowla komórkowa trwała 43 godziny i wykazała, że przedstawiona technika mogłaby być zastosowana do analizy wpływu niklu na komórki.*

Słowa kluczowe: BioMEMS, ECIS, nikiel, cienkie warstwy

Introduction

Impedance measurement methods can be used to assess cell status. These techniques are non-invasive and label-free electrochemical, enabling to obtain sensitive and quantitative results. The most typical are three measurement techniques [10]:

a) impedance flow cytometry,
b) electric impedance spectroscopy,
c) electric cell-substrate impedance sensing (ECIS).

These methods are based on impedance measurement, which is defined as the complex ratio of the voltage to the current in an alternating/direct current circuit. Usually a small sinusoidal AC signal is used as excitation and the electrical current response is measured. During the measurement, biological cells are suspended in medium or adhered to a substrate. To properly analyze the cell-medium-electrode system, models of electrical circuits were created. Research work presented in this paper relates to the ECIS technique, which is based on a single-shell model, in which the cell membrane blocks the current when cells adhere to the electrodes of the substrate. Due to cell proliferation and spreading, the measured impedance changes [4]. The possibility of long-term monitoring of cell culture means that it is a method which can be widely used in biological research.

1. ECIS to monitor cell status

The technique of monitoring cell culture using impedance measurement in the ECIS system is based on the use of thin-film capacitors produced on a biocompatible substrate. This technique has already been used for various types of researches: cell apoptosis [2], cell proliferation [11], drug screening [6], toxicity testing [9], cancer research [5] and stem cell differentiation [3].

Figure 1 shows typical resistance and capacitance characteristics (impedance components) for a cell culture cycle on the example of animal fibroblasts. When cells are added to the medium, the number of cells is increased by cell growth and division. Impedance increases as a result of the increase of electrodes area covered with a non-conductive cell membrane (phase 1). The number of cells is closely related to the corresponding normalized impedance value [1]. Cell proliferation and cell apoptosis or necrosis change the morphology of the cells that cover the electrodes, and thus can be detected quantitatively. During phase 2, cell culture stabilizes. And in phase 3, cells die, their adhesion decreases, therefore in the measurement circuit electrical resistance decreases, and capacity increases.

The fabrication of electrodes requires the use of microelectronic technologies, because their size should be about the size of biological cells (~10 µm in diameter). The biocompatible test substrate with capacitor electrodes is the main sensor element of the ECIS system. Polyethylene terephthalate (PET) and polycarbonate (PC) are used as the starting substrate. Thin film electrodes are usually fabricated of gold or platinum due to their biocompatible properties and good electrochemical parameters.

The measuring capabilities of the ECIS system also allow testing the effect of the presence of various metals on cell cultures. However, it is necessary to produce dedicated test substrates with thin-film capacitors made of various materials. Some other metals offer different chemical, physical and electrical properties than gold and platinum, which are also the expensive materials. In biomedical microdevices, metal elements are also made of nickel, aluminum, tungsten, silver alloys, aluminum alloys and Indium-Tin Oxide (ITO) [7].

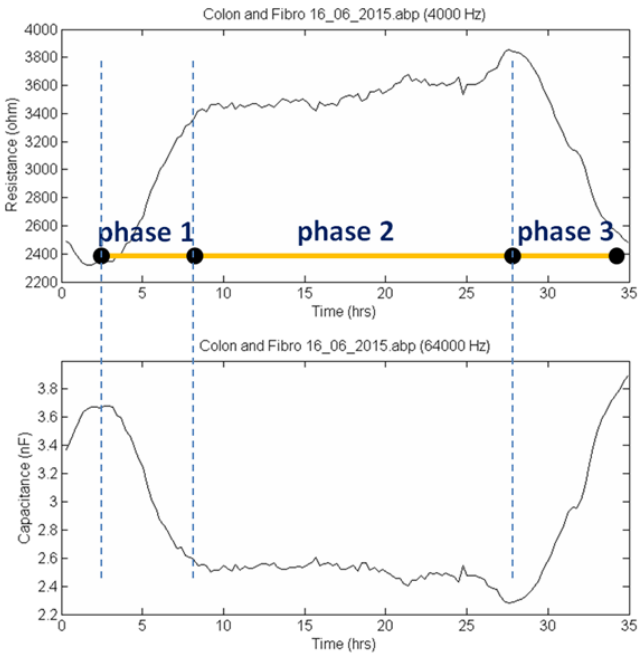

Fig. 1. Resistance (top) and capacitance (bottom) characteristics of mouse fibroblast cells measured by a standard ECIS sensor array at 4 kHz and 64 kHz, respectively

The main problem in the selection of material in biomedical applications is the assessment of the impact of its presence on the tested cells or substances [8]. Biocompatibility is a very important issue, especially for implants intended for long-term use. The materials used in BioMEMS devices usually have lower requirements, but also need to be tested for toxicity, degradation, corrosion and dissolution at ambient temperature. There are many applications in which the contact of substances of biological origin with metallization is short-lived and often one-off, e.g. physiological and biochemical sensors, devices for drug delivery. In such cases, it seems advisable to use a cheaper material, even if it is less biocompatible than gold or platinum typically used. The aim of this work is to perform a test culture on the made substrate with nickel electrodes, expecting that the obtained results of electrical parameters should be similar to a typical cell culture on a commercial substrate with gold electrodes. The prepared substrates can be used to test the effect of metal on biological substances using the ECIS measuring platform to monitor the condition of cells cultured in the presence of nickel electrodes. In addition, they will replace highly biocompatible materials with a less biocompatible but cheaper replacement.

2. Technology and experimental cultures

2.1. Technology of nickel electrode array

As part of an experiment analyzing the effect on a cell culture of a material other than gold or platinum, a test substrate with nickel capacitors was produced. The preparation of test substrates required a number of works in the field of thin film structure manufacturing technology. First, technological masks have been designed based on an electrode array with eight wells. The individual electrodes were made as comb capacitors in which the width of a single finger was 200 µm.

The biocompatible substrate was cut out of 2 mm thick polycarbonate. The key step was the deposition of a nickel layer (100 nm) in the magnetron sputtering process using a Kurt J. Lesker NANO 36™ device. The magnetron sputtering technique is based on the phenomenon of individual particles deposition of material evaporated from the source under the influence of ionized energy by a strong electric field of gas. A vacuum is required to perform the deposition process. During the process, high temperatures are not used that would damage the base material (melting or polymerization). In this case, the process temperature does not exceed 60–70°C. Standard semiconductor technology uses a silicon monocrystalline substrate and the process temperatures reach above 1000°C.

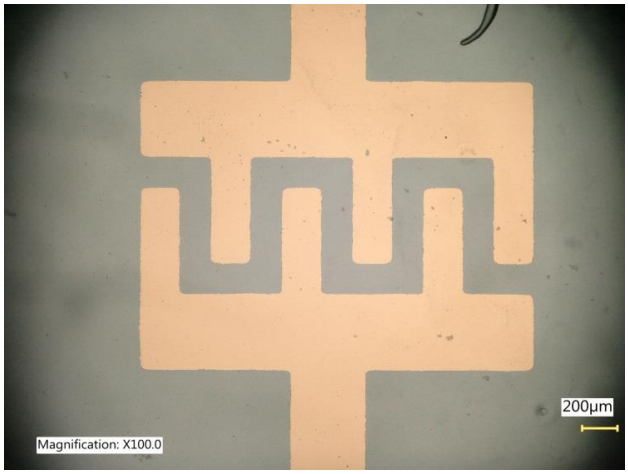

Fig. 2. Nickel comb capacitor on a biocompatible polycarbonate substrate

Positiv 20 photosensitive emulsion was used for the photolithography process. The emulsion was heated and exposed by UV radiation through the mask. Next, the etching of the metallization layer were carried out. Finally, the substrate was washed with deionized water in an ultrasonic cleaner (Fig. 2).

Special wells were placed on the electrodes and fixed using a biocompatible silicone. Each of the 8 wells with a volume of 0.6 cm^3 and a substrate area of 0.8 cm^2 contains a single comb active electrode (Fig. 3). The wells were exposed bactericidal ultraviolet radiation to sterilize the set.

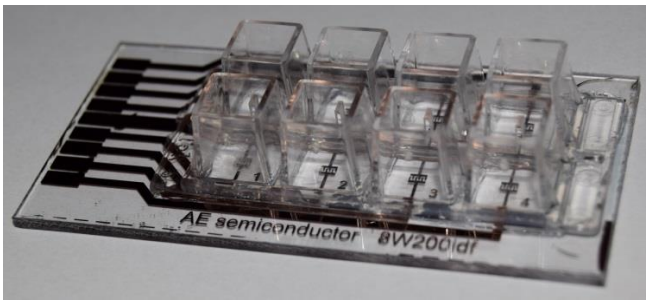

Fig. 3. The final nickel electrode array with 8 wells

2.2. Preparation of the cell culture test

An experimental culture of animal cells was performed on the prepared testing substrate. For this purpose, cells of mouse fibroblast cell line were used. It was NCTC clone 929 [L cell, L-929, derivative of Strain L] (ATCC® CCL-1™) derived from ATCC organization which were cultured according to the instruction manual in complete Eagle MEM medium (Sigma Aldrich) supplemented with 10% Fetal Bovine Serum (FBS) Good HI, in an Galaxy 170R incubator, under controlled growth conditions, constant humidity and air saturation of 5% CO_2 (Fig. 4).

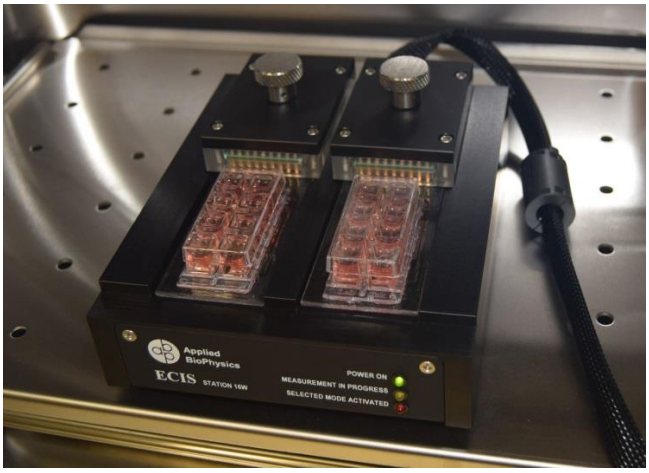

Fig. 4. The electrode array placed in the ECIS holder in the climatic chamber

The stabilization of conditions lasted 24 hours after placing the medium in the wells. Inoculation of arrays was carried out by 0.3 cm^3 per well of cell suspension at ~1.2×10^5 cell/cm^3. When the cells will be introduced to the well, they drift to the bottom of the dish where they attach and then spread on both the nickel electrodes and the polycarbonate surfaces.

3. Results and discussion

3.1. The results of electrical parameters measurements

During the experiment, the results of measuring resistance, capacitance and impedance were collected for a signal frequency in the range 62.5 Hz – 64 kHz. The experiment lasted for 43 hours. However, only the results obtained for the first 18 hours are interpretable. The obtained values were normalized and presented as their changes during cell culture. Each parameter reading is plotted as a point, in ohms for resistance and impedance or nanofarads for capacitance, in dependence of time.

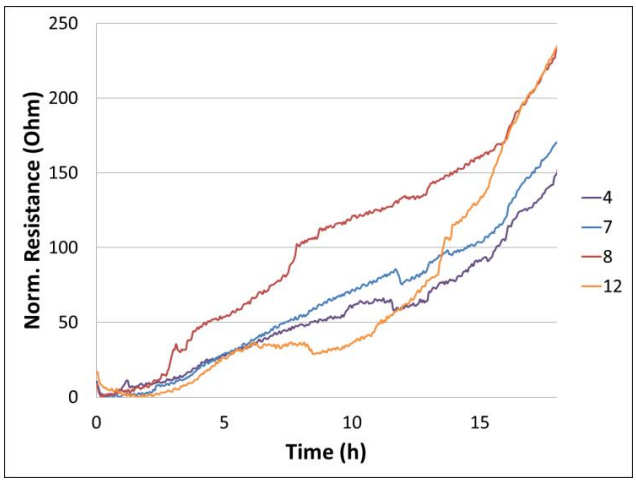

Fig. 5. Resistance response measured by a nickel sensor array at 62.5 Hz for 18 hours

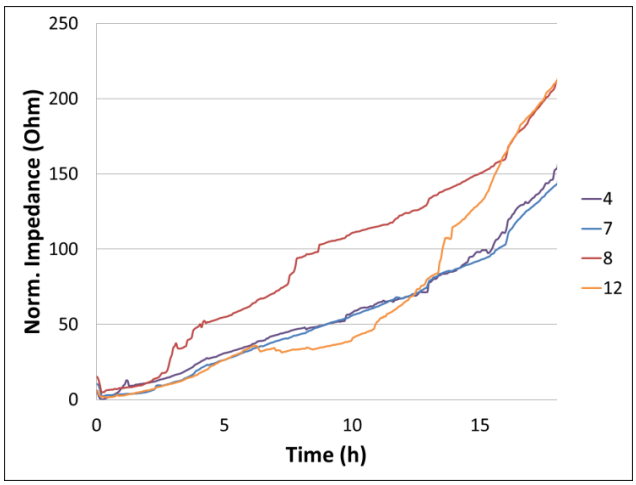

Fig. 6. Impedance response measured by a nickel sensor array at 4 kHz for 18 hours

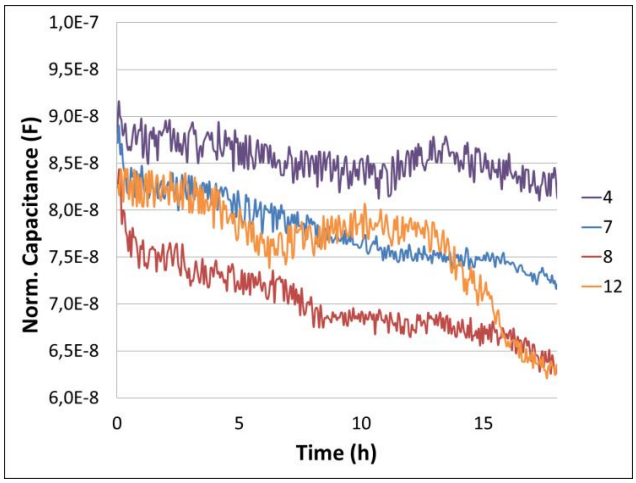

Fig. 7. Capacitance response measured by a nickel sensor array at 64 kHz for 18 hours

Fig. 5 shows the values of the resistance as a function of frequency for four typical electrodes It was found that resistance increased to ~150–200 ohms in the first 18 hours. This indicates relatively good cell viability and proliferative potential. The resistance represents the quality and function of the cell barrier and therefore takes into consideration the resistance towards para- and trans-cellular current flow. Similar fluctuations were observed for impedance at 4 kHz (Fig. 6).

At much higher frequency, the current start to flow through the cells because of the high capacitance of the cell membranes. Capacitance measurement results refer to an overall measure of electrode coverage. The decrease in capacity (Fig. 7) achieved during the initial 18 hours with increasing resistance should be interpreted as cell proliferation and in this respect both values complement each other and should be analyzed in parallel as a standard.

3.2. Metallization layer damage

After more than 20 hours of the cells growing, there was a sharp increase in resistance (Fig. 8) and impedance. Cell culture was continued for up to 43 hours despite receiving unusual results.

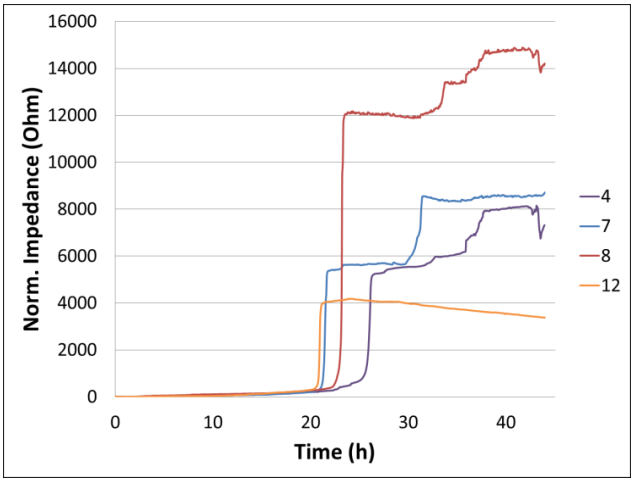

Fig. 8. Impedance response measured by a nickel sensor array at 4 kHz for 45 hours

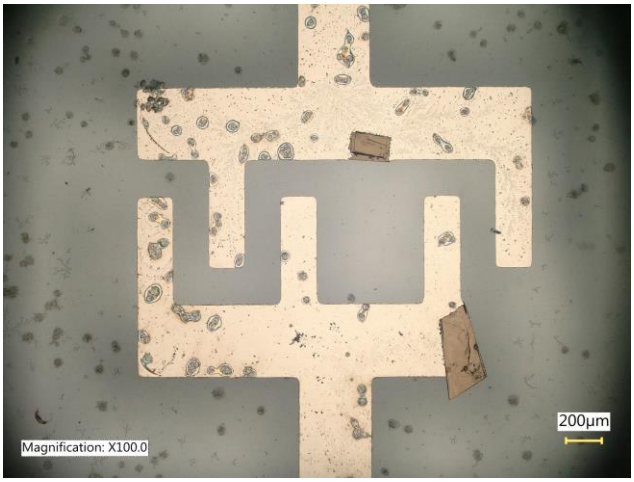

Fig. 9. Damaged nickel capacitor electrode without cells in the reference well after 67 hours (24 h stabilization of medium conditions and 43 h cell culture)

Fig. 10. Damaged nickel capacitor electrode with cells after 67 h (24 h stabilization of medium conditions and 43 h cell culture)

After the experiment microscopic images of the capacitor electrodes were taken (Fig. 9–10). They showed that during cell culture the metallization layer lost its adhesion to the substrate, which resulted in a rapid increase in the measured resistance.

However, during this time the second phase is visible, i.e. the stabilization of cell culture. After about 42 hours, the third phase (4 and 8 wells) begins, which is characterized by a decrease in the value of the measured resistance.

4. Conclusions and future work

In this paper, the developed measuring substrate technology with thin-film nickel capacitors is demonstrated. The substrates were checked for compatibility with the ECIS system. To verify that the presence of nickel would allow monitoring of vital functions of cells, the L929 cell line was performed. The obtained results of the electrical parameters show that after adding the cells to the wells, a typical cell culture cycle can be observed. This indicates the possibility of use of a substrate with nickel capacitors to analyze the effect of this metal on cell culture. And in the future it will allow the use of cheaper material in many applications.

References

[1] Arias L.R., Carla A.P., Yang L.: Real-Time Electrical Impedance Detection of Cellular Activities of Oral Cancer Cells. Biosensors and Bioelectronics 25(10), 2010, 2225–2231 [http://doi.org/10.1016/j.bios.2010.02.029].

[2] Arndt S., Seebach J., Psathaki K., Galla H.J., Wegener J.: Bioelectrical Impedance Assay to Monitor Changes in Cell Shape during Apoptosis. Biosensors and Bioelectronics 19(6), 2004, 583–594 [http://doi.org/10.1016/S0956-5663(03)00269-0].

[3] Bagnaninchi P.O., Drummond N.: Real-Time Label-Free Monitoring of Adipose-Derived Stem Cell Differentiation with Electric Cell-Substrate Impedance Sensing. Proceedings of the National Academy of Sciences of the United States of America 108(16), 2011, 6462–6467 [http://doi.org/10.1073/pnas.1018260108].

[4] Giaever I., Keese C.R.: A Morphological Biosensor for Mammalian Cells. Nature 366(6455), 1993, 591–592 [http://doi.org/10.1038/366591a0].

[5] Hong J., Kandasamy K., Marimuthu M., Choi M.S., Kim S.: Electrical Cell-Substrate Impedance Sensing as a Non-Invasive Tool for Cancer Cell Study. The Analyst 136(2), 2011, 237–245 [http://doi.org/10.1039/C0AN00560F].

[6] Hug T.S.: Biophysical Methods for Monitoring Cell-Substrate Interactions in Drug Discovery. ASSAY and Drug Development Technologies 1(3), 2003, 479–488 [http://doi.org/10.1089/154065803322163795].

[7] Scholten K., Meng E.: Materials for Microfabricated Implantable Devices: A Review. Lab on a Chip 15(22), 2015, 4256–4272 [http://doi.org/10.1039/C5LC00809C].

[8] Stensaas S.S., Stensaas L.J.: Histopathological Evaluation of Materials Implanted in the Cerebral Cortex. Acta Neuropathologica 41(2), 1978, 145–155 [http://doi.org/10.1007/BF00689766].

[9] Xiao C., Luong J.H.T.: On-Line Monitoring of Cell Growth and Cytotoxicity Using Electric Cell-Substrate Impedance Sensing (ECIS). Biotechnology Progress 19(3), 2003, 1000–1005 [http://doi.org/10.1021/bp025733x].

[10] Xu Y., Xie X., Duan Y., Wang L., Cheng Z., Cheng J.: A Review of Impedance Measurements of Whole Cells. Biosensors and Bioelectronics 77(March), 2016, 824–836 [http://doi.org/10.1016/J.BIOS.2015.10.027].

[11] Zudaire E., Cuesta N., Murty V., Woodson K., Adams L., Gonzalez N., Martínez A., Narayan G., Kirsch I., Franklin W., Hirsch F., Birrer M., Cuttitta F.: The Aryl Hydrocarbon Receptor Repressor Is a Putative Tumor Suppressor Gene in Multiple Human Cancers. Journal of Clinical Investigation 118(2), 2008, 640–650 [http://doi.org/10.1172/JCI30024].

Ph.D. Andrzej Kociubiński
e-mail: akociub@semiconductor.pl

He received the M.Sc. and Ph.D. degrees in electronic engineering from Warsaw University of Technology, Poland. In 2007 he joined the Lublin University of Technology (Poland), where he was involved in research on semiconductor technology. His research interest is concentrated on semiconductor devices and technology. His recent activities are related to microsystems for biomedical applications.

http://orcid.org/0000-0002-0377-8243

M.Sc. Eng. Dawid Zarzeczny
e-mail: dawid.adrian.zarzeczny@gmail.com

He graduated in Mechatronics at the Lublin University of Technology. Ph.D. student at the Lublin University of Technology at the Department of Electronics and Information Technology. His research area focuses on microeletronics, semiconductor technology and biomedical engineering. He is the author or co-author over 16 articles in the field of in the field of designing microelectronic devices and testing the electrical properties of cells culture.

http://orcid.org/0000-0003-2029-9962

M. Sc. Eng. Maciej Szypulski
e-mail: szypulski.maciej@gmail.com

A graduate of Mechatronics at the Lublin University of Technology (2017). Currently a PhD student at the Lublin University of Technology. His main scientific interests are the use of MEMS technologies in applications in the field of bioengineering for local temperature change.

http://orcid.org/0000-0002-6227-3624

Eng. Aleksandra Wilczyńska
e-mail: aleksandra.wilczynska9@gmail.com

Master student of mechatronics at the Faculty of Electrical and Computer Science of the Lublin University of Technology. She received Eng. biomedical engineering degrees at the Faculty of Mechanical Engineering of the Lublin University of Technology.

http://orcid.org/0000-0002-5630-1078

M.Sc. Dominika Pigoń
e-mail: dominikapigon@umlub.pl

She received the M.Sc. in biology with microbiology specialization at Maria Curie-Skłodowska University, Lublin, Poland in 2017.

The same year she joined the Medical University of Lublin (Poland), where she is involved in research on cell cultures lifetime monitoring by ECIS (Electric Cell-substrate Impedance Sensing). Her research interest is concentrated on anticancer activity of natural compounds.

http://orcid.org/0000-0002-7545-3237

Prof. Teresa Małecka-Massalska
e-mail: tmalecka@gmail.com

Internal medicine and rheumatology specialist, head of the Human Physiology Department, Medical University of Lublin, Poland (2014–present), a research fellow at Renal Research Institute, Beth-Israel Dialysis Center, Dialysis Department, New York, author and translator of the books for biomedical engineering students. Since 2009 she has been involved into the research of malnutrition in patients with head and neck cancers and since 2016 in ECIS which is an advanced in vitro impedance measuring system to determinate behavior of the cells in physiological conditions.

http://orcid.org/0000-0003-3384-0324

Ph.D. Monika Prendecka
e-mail: m.prendecka@gmail.com

Assistant professor at the Medical University of Lublin, Physiology Department. She graduated as M.Sc. in 1997 in biochemistry and then Ph.D. in 2003 at the Maria Curie-Skłodowska University in Lublin. She completed post-graduate studies "Project management of the research and development", "Public relations in scientific research" and "Manager of research projects" at the Higher School of Economy and Innovation in Lublin. She does research about biological properties of fungal extracts is their antitumor activity by the monitoring of the electric parameters in cell cultures.

http://orcid.org/0000-0001-9414-4344

otrzymano/received: 20.03.2020 *przyjęto do druku/accepted: 26.06.2020*

http://doi.org/10.35784/iapgos.1569

AN OVERVIEW OF CLASSIFICATION METHODS FROM DERMOSCOPY IMAGES IN SKIN LESION DIAGNOSTIC

Magdalena Michalska[1], Oksana Boyko[2]
[1]Lublin University of Technology, Department of Electronics and Information Technology, Lublin, Poland, [2]Danylo Halytsky Lviv National Medical University, Department of Medical Informatics, Lviv, Ukraine

Abstract. *The article contains a review of selected classification methods of dermatoscopic images with human skin lesions, taking into account various stages of dermatological disease. The described algorithms are widely used in the diagnosis of skin lesions, such as artificial neural networks (CNN, DCNN), random forests, SVM, kNN classifier, AdaBoost MC and their modifications. The effectiveness, specificity and accuracy of classifications based on the same data sets were also compared and analyzed.*

Keywords: dermatoscopic images, classification methods, neural networks, SVM, skin cancer, skin lesions

PRZEGLĄD METOD KLASYFIKACJI OBRAZÓW DERMATOSKOPOWYCH WYKORZYSTYWANYCH W DIAGNOSTYCE ZMIAN SKÓRNYCH

Streszczenie. *Artykuł zawiera przegląd wybranych metod klasyfikacji obrazów dermatoskopowych zmian skórnych człowieka z uwzględnieniem różnych etapów choroby dermatologicznej. Opisane algorytmy są szeroko wykorzystywane w diagnostyce zmian skórnych, takie jak sztuczne sieci neuronowe (CNN, DCNN), random forests, SVM, klasyfikator kNN, AdaBoost MC i ich modyfikacje. Porównana i przeanalizowana została również skuteczność, specyficznośc i dokładność klasyfikatów w oparciu o te same zestawy danych*.

Słowa kluczowe: obrazy dermatoskopowe, metody klasyfikacji, sztuczne sieci neuronowe, SVM, nowotwór skóry, zmiany skórne

Introduction

Nowadays, the classical classification methods of dermatoscopic images used by generations of doctors are becoming insufficient. These include the ABCD, Hunter, Menzies method [25], 7-point checklist [4], TDS, Chaos-Clue [29], scale Glasgow, scale Hunter and many others [3, 7, 22]. They do not allow to effectively diagnose cancer and save human health and even life [5].

Classic pattern analysis gives the opportunity to describe skin lesions for diagnostic purposes, five basic elements are enough: lines, circles, pseudopodia, papules and dots. Each of these elements can be part of the pattern. To create a pattern, it is necessary to repeat the same structure multiple times. The presence of specific colors and the number of colors is of great importance in dermatoscopy. The Hunter scale gives a score in the range of zero to thirteen points. Clinical symptoms suggesting suspected melanoma are often grouped in two systems: the ABCD scale and the seven-point Glasgow scale. Chaos – Clue is a simple method for quickly assessing suspected pigmented skin lesions with a dermatoscopy. Its use can lead to a better diagnosis of melanoma and other skin cancers [29]. Figure 1 presents the most important stages of this algorithm.

Therefore, automated diagnostic systems have been developed to assist doctors in the diagnostic process. The images used in programs are subjected to the process of removing artifacts, segmentation of changes, extraction of features, optimization and finally classification of the skin lesions. Most often, the lesions is characterized by the type of damage, color, arrangement, shape, texture and border irregularity. Currently, the classification of skin lesions uses automatic recognition of lesions or known anomalies occurring in a given population. These methods are also intended to classify a given birthmark as a pattern with a colored texture.

Classification means that elements of set $X = \{fx_1, x_2, \ldots, x_n\}$ are assigned elements of set $Y = \{fy_1, y_2, \ldots, y_n\}$, for $i = 1, \ldots, n$, where n is a number of objects. The set X is called the set of feature vectors x_i, but Y is a set of classes $y_{i..}$ The classifier construction process consists of preparation of learning data, test subset, classification and calculation of classification efficiency.

One of the first ways to classify was discriminant analysis [18]. Next appeared artificial neural networks (ANNs) [14, 20], decision trees [21], support vector machine (SVM) [11, 12], logistic regression [8], ensemble learners [2, 30]. Many different classifiers have been used to classify dermatoscopic skin images. Skin melanoma is classified using kNN classifier [9]. The AdaBoost MC algorithm [1] is considered optimal and reliable.

The types of machine learning algorithms are commonly divided into 4 categories: supervised learning, unsupervised learning, semi-supervised learning and reinforcement learning. The mostly common supervised learning algorithms are nearest neighbor, naive Bayes, decision trees, linear regression, logistic regression, linear discriminant analysis, SVM, neural networks, similarity learning. Algorithms try to model relationships and dependencies between the target prediction output and the input features. They predict the output values for new data based on those relationships which it learned from the previous data sets.

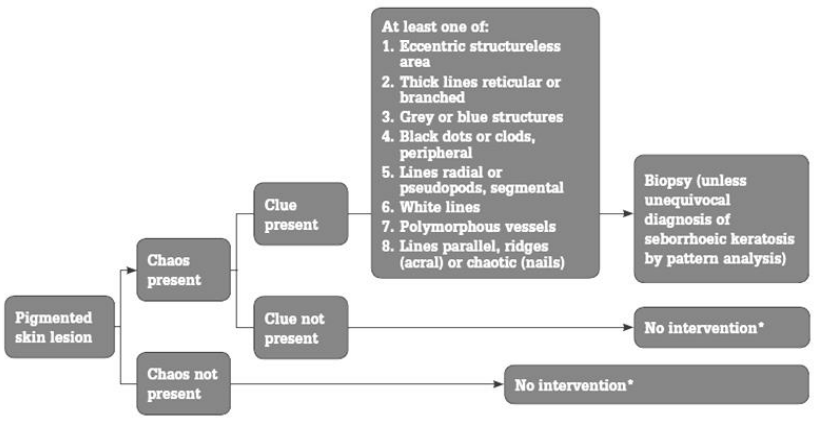

Fig. 1. Algorytm działania metody Chaos – Clue [29]

The most current methods in the field of melanoma classification use artificial neural networks of increasingly complex structure. The most commonly used include artificial neural networks, logistic regression, decision making using trees and supervised machine learning algorithms.

1. Supervised machine learning algorithm in classification

Support Vector Machines (SVM) is supervised learning model with associated learning algorithm. SVM is most commonly used in classification problems [27, 31]. In the algorithm, each data element is a point in n-dimensional space (where n is the number of features), the value of each feature is a coordinate value. Then elements classification is performed by finding the hyperplane, which differentiates on the best way two classes. The optimal separating hyperplane (OSH) is a hyperplane which margins are the largest.

In [31] the proposed classification model uses HSV, LBP and HOG functions, that are passed to the SVM classifier. The function extraction process has been divided into three parts, features of color, texture and shape of melanoma. Then the feature vector of all these three features was joined to obtain a complex feature vector. The process is repeated for all images in the data set and vector features are marked according to their accepted classes. The labeled feature vectors are fed to the SVM classifier to effectively train the algorithm. In tests, all functions are extracted from the new image and the feature vector is fed to SVM to predict classes. The scheme of described activities is presented in Figure 2.

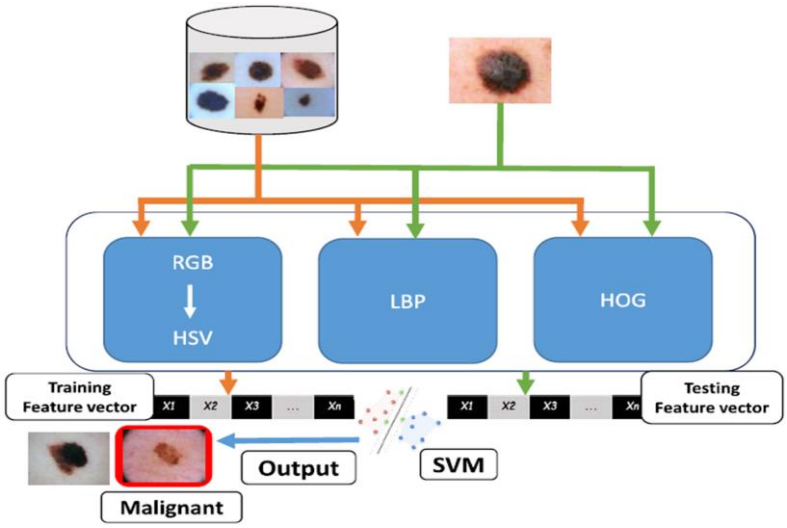

Fig. 2. Diagram of activities using SVM in the classification of dermatoscopic images [31]

2. Classifiers based on Convolutional Neural Network (CNN)

Neural networks are used in many fields of computer science, especially in image processing. Nowadays, various modifications are becoming more and more common. They are used to classify images [15, 17, 23, 31, 33].

More and more scientists are comparing skin diseases diagnostics effectiveness of computer algorithms with experienced doctors. Classification of skin lesions enabling identification of the most common tumors using CNN was used in [16]. The network was trained directly from a data set containing over 129,000 clinical images, using only pixels and skin disease labels as input.

The effects have been compared with the diagnoses of over 20 dermatologists. The doctor's diagnoses were confirmed by an additional skin lesion biopsy. The diagnosed cases were malignant melanomas and benign skin birthmarks. CNN achieves performance comparable to that of expert dermatologists, 22 and 21 experienced doctors participated in the study. Figure 2 demonstrates artificial intelligence possibilities in classification of skin cancer comparable to dermatologists. The charts include results of physician diagnostics and algorithm for 130 melanoma images and 111 dermatoscopic images. The average of dermatologists was also included. It turns out that when diagnosing melanoma, doctors have comparable diagnostic effectiveness to the proposed algorithm. In contrast, their diagnostic ability decreases for dermal pictures containing various stages of skin diseases.

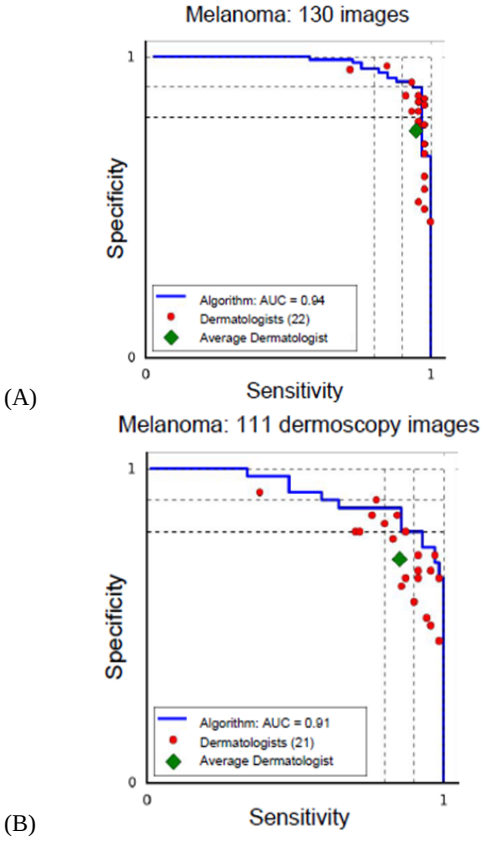

Fig. 3. ROI curves for CNN algorithm and dermatologist: (A) data with 130 images of melanoma, (B) date with 111 images of melanoma [16]

3. Classifiers based on Deep Convolutional Neural Networks (DCNN)

Neural networks different models modifications are increasingly common. They contain deep learning algorithms [13], deep convolutional neural networks (VGGNet convolutional neural network architecture and the transfer learning paradigm) [28], synergic deep learning (SDL). They show great effectiveness in the diagnosis of skin lesions.

In [34] was proposed a model combining synergistic models (SDL) and (DCNN). The proposed model (Figure 4) consists of three modules: an input layer, double DCNN-A/B components and synergistic network. The input layer takes a few images as input. Each DCNN component is for self-study under the supervision of class labels. The synergistic network checks if the pair of input images belongs to the same category and provides feedback.

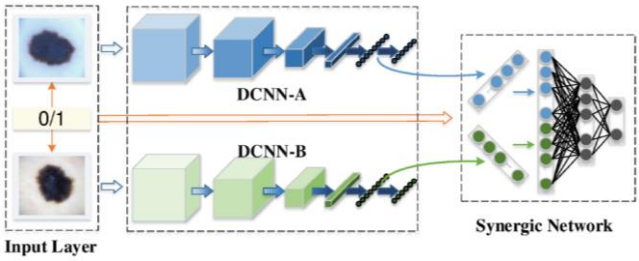

Fig. 4. Proposed model architecture of constructed input layer, double DCNN components (DCNN-A/B) and synergic network [34]

4. Effectiveness of selected classification methods

Many scientists [6, 10, 19, 24, 26, 32] test the effectiveness of available or modified classifiers on various dermatoscopic data. For they research, scientits use a large number of dermatoscopic images using many new modifiers of classifiers.

Figure 5 presents ROC curves (Receiver Operationg Characteristic), which are the tool for joint assessment of the classifier, its sensitivity and specificity. It included AdaBoost MC, ML - SVM, ML - KNN algorithms. The larger area under the ROC curve usually allows for more accurate classification of objects.

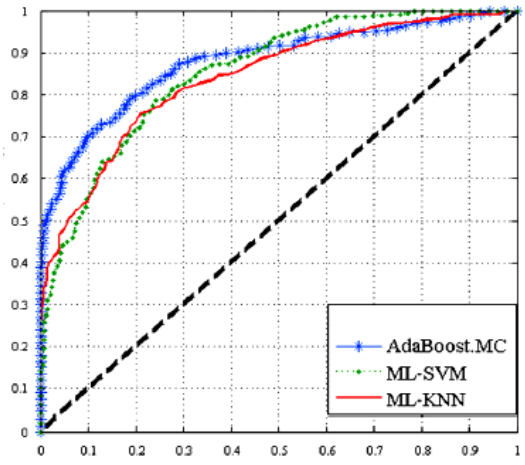

Fig. 5. ROC curves for AdaBoost MC, ML- SVM, ML- KNN algorithms [1]

It is important that the classification algorithms are tested on the same data sets. For this reason, many publications are cited that use different data sets to compare the classifier. Table 1 compares the classifications based on the two models Caucasians (1) and Xanthou (2). Random forests and KNN algorithms showed a specificity above 96%.

Table 1. Results of classifiers based on different models [32]

Classifiers	Sensitivity (%)		Specificity (%)		Accuracy (%)	
	1	2	1	2	1	2
Random forests	73.33	80.00	95.83	**96.25**	88.33	90.83
KNN	51.67	77.50	**97.50**	**96.25**	82.22	90.00
Adaboost	71.67	80.00	95.83	92.50	87.78	88.33
RBF SVM	75.00	87.50	94.17	93.50	87.78	91.67
S – SVM	75.00	85.00	93.33	91.25	87.22	89.17
DCNN	83.33	95.00	95.00	93.75	91.11	94.17

At dermatoscopic images are many artifacts, is not easy to use effective classification algorithm. In [1] pattern based on CASH is very accurate. Skin lesions were classified by pattern detectors classes such as reticular, globural, homogeneous, parallel, cobblestone, starbust, multicomponent. Table 2 presents sensitivity, specificity, accuracy, average standard deviation training error (E) during learning by AdaBoost.MC. Reticular and globural patern detectors have reached a specificity value above 97% for the dermatoscopic image dataset chosen by scientists.

Table 2. Pattern classification of dermatoscopic lessions made by AdaBoost.MC [1]

Patern detector	Sensitivity (%)	Specificity (%)	E	Accuracy (%)
reticular	87.11	**97.96**	0.459	0.981
globural	86.25	**97.21**	0.477	0.997
cobblestone	87.76	93.23	0.555	0.990
homogeneous	90.47	95.10	0.697	0.996
parallel	85.25	89.50	0.524	0.989
starbust	89.62	90.14	0.634	0.966
multicomponent	98.50	93.11	0.344	0.989

In [23] SVM has been compared with the Random algorithm classifier. The best accuracy of class recognition on the database has been achieved in the SVM classifier. SVM associated with attriutes selected by the Fisher method. Scientists have received total accuracy equal to 93.8 % for recognizing melanoma from the other lesions of human skin, sensitivity in recognition of melanoma is equal to 95.2 % and specificity 92.4 %.

5. Discussion and conclusions

In experiments, verification of extraction, reduction of features, classification, performance was tested using various classifiers. These methods are tested on various data sets from around the world. Experimental results strongly suggest that the proposed classifiers are particularly beneficial in distinguishing between malignant and benign lesions. Any classification problem can be solved with more than one classifier. It is important that they are not hypersensitive to damage lesions, eliminate less important functions, reduce the dimension of the function and choose the optimal set.

An effective algorithm should well minimize the object classification error presented in the image. However, the error cannot be completely eliminated. Image elements or the entire image is classified based on a finite set of its features. To improve classification efficiency, it is important to combine available methods.

Equipped with software with classifiers, mobile devices can potentially extend the scope of diagnosis. It is anticipated that many new algorithms will be created in the future. It is important to provide universal access to the necessary diagnostic care. The classification results provided by the tested models over the years prove to be more accurate in the process of diagnosis of skin lesions.

References

[1] Abbas Q., Celebi M.E., Serrano C., Fondo´n Garcı´ I., Maa G.: Pattern classification of dermoscopy images: A perceptually uniform model. Pattern Recognition 46, 2013, 86–97.

[2] Abedini M., Chen Q., Codella N.C.F., Garnavi R., Sun X.: Accurate and scalable system for automatic detection of malignant melanoma. Dermoscopy Image Analysis. CRC Press, Boca Raton 2015.

[3] Alendar F., Kittler H, Helppikangas H., Alendar T.: Clear definitions,simple terminology, no metaphoric terms. Expert Rev. Dermatol. 3, 2008, 27–29.

[4] Argenziano G., Fabbrocini G., Carli P., De Giorgi V., Sammarco E., Delfino M.: Epiluminescence microscopy for the diagnosis of doubtful melanocytic skin lesions, comparison of the ABCD rule of dermatoscopy and a new 7-point checklist based on pattern analysis. Archives of Dermatology 134, 1998, 1563–1570.

[5] Argenziano G., Soyer H.P., Chimenti S., Talamini R., Corona R., Sera F.: Dermoscopy of pigmented skin lesions: results of a consensus meeting via the Internet. Journal of American Academy of Dermatology 48(5), 2003, 679–693.

[6] Barata, C., Ruela, M.: Two Systems for the detection of melanomas in dermoscopy images using texture and color features. IEEE Systems Journal 8(3), 2014, 965–979.

[7] Blum H., Ellwanger U.: Digital image analysis for diagnosis of cutaneous melanoma, development of a highly effective computer algorithm based on analysis of 837 melanocytic lesions. British Journal of Dermatology 151(5), 2004, 1029–1038.

[8] Blum H., Luedtke H., Ellwanger U., Schwabe R., Rassner G., Garbe C.: Digital image analysis for diagnosis of cutaneous melanoma, development of a highly effective computer algorithm based on analysis of 837 melanocytic lesions. Computerized Medical Imaging and Graphics 31(6), 2007, 362–373.

[9] Burroni M., Corona R., Dell'Eva G., Sera F.: Melanoma computer -aided diagnosis reliability and feasibility study. Clinical Cancer Research 10(6), 2004, 1881–1886.

[10] Celebi M.E., Aslandogan Y.A., Stoecker W.V., Iyatomi H., Oka H., Chen X.: Unsupervised border detection in dermoscopy images. Skin Res Technol. 13, 2007, 1–9.

[11] Celebi M. E., Kingravi H.A., Uddin B., Iyatomi H., Aslandogan Y.A., Stoecker W.V., Moss R.H.: A methodological approach to the classification of dermoscopy images. Computerized Medical Imaging and Graphics 31(6), 2007, 362–373.

[12] Celebi M.E., Kingravia H.A., Uddina B., Iyatomid H., Aslandogana Y.A., Stoeckerb W.V., Mossc R.H.: A methodological approach to the classification of dermoscopy images. Comput Med Imaging Graph. 31(6), 2007, 362–373.

[13] Codella N., Cai J., Abedini M., Garnavi R., Halpern A., Smith J. R.: Deep learning, sparse coding, and SVM for melanoma recognition in dermoscopy images, Machine Learning in Medical Imaging. Springer, Munich 2015.

[14] Ercal F., Chawla A., Stoecker W.V., Lee H.-C., Moss R.H.: Neural network diagnosis of malignant melanoma from color images. IEEE Transactions on Biomedical Engineering 41(9), 1994, 837–845.

[15] Esteva, A.: Dermatologist-level classification of skin cancer with deep neural networks. Nat. Res. 542(7639), 2017, 115–118.

[16] Esteva A., Kuprel B., Novo R.A., Ko J., Swetter S. M., Bla H.M, Thrun S.: Dermatologist-level classification of skin cancer with deep neural networks. Nature 542, 2017, 115–118.

[17] Ge Z., Demyanov S., Chakravorty R., Bowling A., Garnavi R.: Skin disease recognition using deep saliency features and multimodal learning of dermoscopy and clinical images. Springer Cham LNCS 10435, 2017, 250–258.

[18] Green A., Martin N., McKenzie G., Pfitzner J., Quintarelli F., Thomas B. W., O'Rourke M., Knight N.: Computer image analysis of pigmented skin lesions, Melanoma research 1(4), 1991, 231–236.

[19] Gutman D., Codella N., Celebi E., Helba B., Marchetti M., Mishra N., Halpern A.: Skin lesion analysis toward melanoma detection: A Challenge at the International Symposium on Biomedical Imaging (ISBI) 2016, International Skin Imaging Collaboration (ISIC). eprint arXiv:1605.01397.

[20] Husemann R., Tölg S., Seelen W.V., Altmeyer P., Frosch P.J., Stücker M., Hoffmann K., El-Gammal S.: Computerised diagnosis of skin cancer using neural networks. Skin Cancer and UV Radiation. Springer, Berlin 1997.

[21] Kahofer P., Hofmann-Wellenhof R., Smolle J.: Tissue counter analysis of dermatoscopic images of melanocytic skin tumours: preliminary findings. Melanoma research 12(1), 2002, 71–75.

[22] Kittler H., Riedl E., Rosendahl C., Cameron A.: Dermatoscopy of unpigmented lesions of the skin: A new classification of vessel morphology based on pattern analysis. Dermatopathology: Practical & Conceptual 14(4), 2018, 3.

[23] Kruk M., Świderski B., Osowski S., Kurek J., Słowińska M., Walecka I.: Melanoma recognition using extended set of descriptors and classifiers. J Image Video Proc. 43, 2015 [https://doi.org/10.1186/s13640-015-0099-9].

[24] Menzies S.W., Bischof L, Talbot H, Gutenev A, Avramidis M, Wong L.: The performance of SolarScan: An automated dermoscopy image analysis instrument for the diagnosis of primary melanoma. Arch Dermatol. 141(11), 2005, 1388–1396.

[25] Menzies S., Ingvar C., Crotty K., McCarthy W.: Frequency and morphologic characteristics of invasive melanomas lacking specific surface microscopic features. Archives of Dermatology 132, 1996, 1178–1182.

[26] Michalska M.: Klasyfikacja zmian skórnych z obrazów dermatoskopwych, Wybrane zagadnienia z zakresu elektrotechniki, inżynierii biomedycznej i budownictwa. Prace doktorantów Politechniki Lubelskiej 2019, 108–120.

[27] Piątkowska W., Martyna J., Nowak L.: A decision support system based on the semantic analysis of melanoma images using multi-elitist PSO and SVM. Proceedings of the 7th International Conference on Machine Learning and Data Mining in Pattern Recognition MLDM'11 1, 2011, 362–374.

[28] Romero-Lopez A., Giro-i-Nieto X., Burdick J., Marques O.: Skin lesion classification from dermoscopic images using deep learning techniques. Proc. of Biomedical Engineering 2017 [https://doi.org/10.2316/P.2017.852-053].

[29] Rosendahl C., Cameron A., McColl I., Wilkinson I.: Dermatoscopy in routine practice. Chaos and Clues. Australian Family Physician 41(7), 2012.

[30] Schaefer G., Krawczyk B., Celebi M.E., Iyatomi H.: An ensemble classification approach for melanoma diagnosis, Memetic Computing 6(4), 2014, 233–240.

[31] Shahid M., Khan S.: Dermoscopy images classification based on color, texture and shape features using SVM. The 3rd International Conference on Next Generation Computing (INC GC2017b), 243–245.

[32] Xie F., Fan H., Li Y., Jiang Z., Meng R., Bovik A.: Melanoma classification on dermoscopy images using a neural network ensemble model. IEEE Transationa on Medical Imaging 36(3), 2017, 849–858.

[33] Yu L., Chen H., Dou,Q., Qin J., Heng P.A.: Automated melanoma recognition in dermoscopy images via very deep residual networks. IEEE Trans. Med. Imaging 36(4), 2017, 994–1004.

[34] Zhang J., Xie Y., Wu Q., Xia Y.: Skin lesion classification in dermoscopy images using synergic deep learning. Springer Nature Switzerland, LNCS 11071, 2018, 12–20.

M.Sc. Magdalena Michalska
e-mail: magdalena.michalska@pollub.edu.pl

Ph.D. student at Lublin University of Technology. Recent graduate Warsaw University of Technology The Faculty Electronics and Information Technology. Her research interests include medical image processing, 3D modelling, optoelectronics, spectrophotometry. Author of more than 10 publications.

http://orcid.org/0000-0002-0874-3285

Dr. Tech. Sc. Oksana Boyko
e-mail: oxana_bojko@ukr.net

Oksana Boyko graduated from Lviv Polytechnic State University with a master's degree in Applied Mathematics. Since 2011 she is the Head of the Medical Informatics Department of Danylo Halytsky Lviv National Medical University.
Her research interests include mathematical modelling, biomedical sensors and embedded systems, medical information systems. She is the author of over 200 scientific and methodological works.

http://orcid.org/0000-0002-8810-8969

otrzymano/received: 22.03.2020 *przyjęto do druku/accepted: 26.06.2020*

http://doi.org/10.35784/iapgos.923

SOFTWARE DEVELOPMENT FOR SMART HOME PROCESS CONTROL

Vitalii Kopeliuk[1], Vira Voronytska[1], Volodymyr Havryliuk[2]
[1]Rivne State University of Humanities, Department of Applied Math and Computer Science, Rivne, Ukraine, [2]International University of Economics and Humanities Academician Stepan Demianchuk, Department of Information Systems and Computing Methods, Rivne, Ukraine

Abstract*. Here we make an overview of the main stages of software development for server management system of "smart" building with a central controller via a mobile device. We have developed our own version of the concept.*

Keywords: Arduino, Internet of things, microcontroller, smart home, client-server architecture, sensors

OPRACOWANIE OPROGRAMOWANIA DO STEROWANIA PROCESAMI W BUDYNKU INTELIGENTNYM

Streszczenie. *Rozpatrzono etap podstawowy opracowania oprogramowania dla systemu sterowania inteligentnym budynkiem z centralnym kontrolerem, przez urządzenie mobilne. Zaproponowano własną wersję rozwiązania.*

Słowa kluczowe: Arduino, Internet rzeczy, mikrokontroler, inteligentny budynek, architektura klient-serwer, czujniki

Introduction

Smart Home (Home automation, smart home) is one of the most promising areas of information and communication technologies. Such type of systems connects all of the electrical devices of the house in one functional system which can be operated by a user with display-controller or with certain algorithms. Optimizing energy consumption today is one of the key objectives of the Smart Home systems.

Number of system types in this area is increasing: there are wireless technologies for the integration of devices into a single network, new kinds of sensors. At the same time, increased demand for Smart Home product makes the following problems extremely relevant:

- insufficient standardization and compatibility of different protocols;
- system reliability;
- safety and security systems from unauthorized access;
- costs and complexity of deployment.

This paper examines the main existing approaches to building Smart Home systems, analyzes network protocols and technologies used to build local networks, describes their advantages and disadvantages. In addition it investigates ways to improve existing solutions in this area. It justifies the choice of protocols, technologies and approaches for building Smart Home systems that are capable of solving main disadvantages.

The aim of this work is to build a device management system for the smart home, that will consist of the following elements:

- monitoring and controlling device (Smart Monitor),
- server that collects data from all devices in the local network and makes decisions regarding changes in the configuration of the network and switching devices on and/or off depending on the current state of the system.

1. Internet of things and cloud computing

At present time the vast majority of smart home systems do not have the function of remote control via the Internet. Meanwhile, mobile devices with constant network access have now become commonplace, they are practically everywhere. In 1999, the founder of the Research Center of Auto-ID Center at MIT Kevin Ashton proposed the term Internet of Things (Internet of Things). The basic idea is that the way a new generation of things will not only be "intelligent", but also will be connected in a network – Internet of Things [6]. The concept implies that devices such as smartphones, tablets, TVs, and various sensors and controlled devices with wireless modules, such as Wi-Fi and Bluetooth, can interact with each other as well as with users by using these modules. Due to the massive proliferation of mobile devices, the remote control of such systems as Internet of things, has become possible. Remote control has obvious advantages. The main one is of course security. When all of the inhabitants are not in the house, it is possible to remotely monitor the state of the house using cameras together with sensors and controllers.

Equally important is to increase user comfort when using smart home system. Often smart home control systems use scripts to manage light and heat automatically. However, some users prefer not to use these options. And the presence of the remote control option, for example, may himself at the approach to the house he needs to include devices (turn on lights, appliances, and include pre-heating or air conditioning). Implementation of remote access is possible through the use of cloud computing, where users are provided with universal access network computing resources, services and applications. There are several models of cloud computing. The most suitable model for a given problem definition is SaaS (software as a service). This model is based on providing customers access to software over the Internet. The main advantage of the SaaS model for end users is the absence of a need to install and update software, and caring about performance equipment, which operates the application. When using cloud computing systems smart home there are two options. First one is when the controller (server) for managing smart home devices is located not in the house, but on a cloud. In this case smart home system can be accessed from any point where internet access in available. As for the second option, controller can be located in the building, and the software is installed on a cloud. Also, in the second case, only additional modulus, that provide access to the internet are required, which reduces the requirements to the system. Also in the case of implementing remote control to the already existing system of smart home, there is no need to replace any equipment, it is enough to provide access for the controller to the cloud server. Direct remote control of the smart home systems can be done either via a web browser or through a special mobile application. One more important thing. Many modern devices that are used in smart homes, have their own specific protocols of the data transmission and can interact with internet services only via their own specific API's. So often it is impossible to expand the system of a smart home by adding extra devices, such as smart refrigerator, for example, since they are requiring completely different data transmission system. However, cloud-based system gives a general interface for controlling all of the devices via cloud. In this case all the devices interact with each other via cloud. The application of cloud technologies in the smart home will make them much more flexible, and will reduce maintenance costs and system expansion with any smart refrigerator, or other devices working on other data transmission protocols. However, with cloud service that will provide a common interface management of all systems and different devices will interact with each other through the cloud, it is possible to use devices from different manufacturers with different data transmission protocols. The application of cloud technologies in smart home will make them much more flexible, and will

reduce maintenance costs and system expansion. which any smart refrigerator, or add the devices working on other data transmission protocols. However, with cloud service that will provide a common interface management of all systems and different devices will interact with each other through the cloud, it is possible to use devices from different manufacturers with different data transmission protocols. The application of cloud technologies in smart home will make them much more flexible, and will reduce maintenance costs and system expansion. Is the ability to use devices from different manufacturers with different data transmission protocols.

2. Microservices

Microservice style of architecture [5] is an approach to developing a holistic applications as a set of small services, each of which runs on its own process and connect with others through lightweight mechanisms such as RPC or HTTP. Services are built according to a specific task and can be independent to be deployed by automated systems. There is some minimum centralized management of such services.

Traditional server systems are usually built as monoliths – logically separate executable programs. And this approach is natural: the whole logic of request processing works in a single process that allows you to use existing tools programming languages to divide an application into classes, functions, and namespaces. The monolith can be scaled horizontally by running multiple instances outside the load balancer.

Monolithic software is quite successful, but it has its disadvantages. Change cycles monoliths are bound together, that is, changing a small part of the system requires reassembly (compilation) and deployment. Over time, it becomes difficult maintain a good modular structure while keeping changes relevant specific module, only inside it. It is necessary to scale everything monolith instead of individual parts that require more resources.

Microservices can also be deployed and scaled independently. They also provide clear boundaries between modules, even allowing implement separate subsystems in different programming languages. That's it delimiting helps to manage the complexity of the codebase, as each the module will have a public API that will contain only the required functionality, and everything else will be encapsulated and not relevant for the development of other services, which depend on it.

The main disadvantage of microservice architecture is the increase in complexity error handling. Unlike a monolith, every call to a service can fail. Therefore, it is necessary to develop mechanisms for monitoring the condition services, check the various metrics of their functioning as well automate the restoration of the microservice if it fails.

The positive thing is that there are failures in microservice architecture largely isolated. If meeting the request requires a call many services and some of them are unavailable, perhaps less complete response (graceful degradation).

Difficulties can also be caused by providing consistency the deployment of dependent microservices, and the need for management transactions that interact with multiple subsystems.

Internal communication between servers occurs in binary TCP format for performance reasons, but from the point code view, each service provides a public API that encapsulates the creation messages to the corresponding service [4].

Apart from the division of responsibilities, the main advantage is the opportunity horizontal scaling of each service separately. For example, if the flow of operational data is greatly accelerated without increasing the flow administrative data, you can scale the corresponding DBMS (Database Management System) separately.

3. Cloud server interaction with smart home devices

In order to interact with the cloud server, smart home devices need to select protocol for sending messages. Currently there are several dozens of data transfer protocols that allow communication IoT devices. In our implementation we preferred protocol MQTT (Fig. 1).

MQTT (Message Queue Telemetry Transport) - Simplified network protocol that runs on top of TCP/IP. It is used to exchange information between devices on the basis of publish-subscribe. The first version of the protocol was developed by Dr. Andy Stanford Clark (IBM) and Arlen Nipper (Arcom) in 1999 and published under license royalty-free. MQTT 3.1.1 specification was standardized OASIS consortium in 2014.

The main advantages of the protocol are:

- the pattern of interaction on the basis of publish-subscribe solutions most suitable for working with different kinds of sensors,
- easy to use. This software unit does not contain any unnecessary functionality and can be easily embedded into any complex system,
- it is easy to administer,
- provides work in constant communication loss or other problems on the line,
- there are no restrictions on the format of the data.

MQTT requires broker messages. The broker is responsible for distributing messages to all devices that are signed in this newsletter. MQTT defines methods (so-called "verb") to indicate the desired action that should be performed on the identified resource, which can be either existing data or data that is generated dynamically, depending on the server implementation. Often resource corresponds to a given file or it is a result of a file processing on a server.

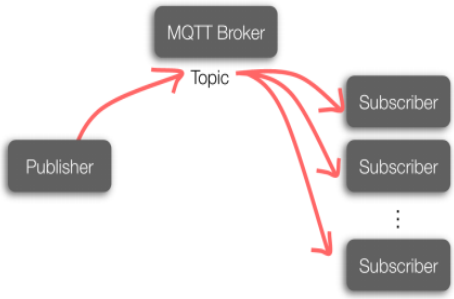

Fig. 1. MQTT broker scheme

Here are examples of the following methods:

Connect. Connect: Waiting for a connection to the server.

Disconnect. Disconnect: Waiting until the customer MQTT finish any work that must be done, and the session TCP/IP is broken.

Subscribe. Subscribe: Pending completion of Subscribe method.

UnSubscribe. Unsubscribe: server asks the client to unsubscribe from one or more topics.

Publish. Post: immediately returns to the application flow after customer requests pass MQTT.

Currently there are several open Brokers MQTT: Emqttd, ActiveMQ, Apollo, Mosquitto, RabbitMQ and others. They differ only in their feature set, and some add-ons over the standard version of the protocol MQTT.

4. The operating data reception subsystem

Because data arrives at high speed and can occur bursts of traffic, you need to have a buffer between the database and the front servers for provide load balancing. For this platform architecture involves using a message queue.

Message queues define an asynchronous communication protocol. this is means that the sender and recipient of the message should not interact with message queue at the same time. Messages that are queued stored until received by the receiver.

An important feature of the message queue is to ensure resilience and reliability, which are implemented using various data storage strategies. To increase the reliability of message delivery, it is possible to save them on drive before they are received by the recipient. Even if the receiver program or message queue will stop working due to failure, messages will be safe and will be available to recipients, only the system will be operational again.

Using Message Queuing can support much more messages. In general, applying queue architecture is a good strategy for organizing asynchronous processing of big data.

We formulate the requirements for the message queue:

- **High performance**. Need to provide high speed writing messages to the queue.
- **Horizontal scalability**. Increase through put system ability by increasing the number of servers.
- **Ability to save messages to disk**. Need to reduce the amount of data lost when the message queue server is down. This is very necessary when reading data from the queue in large packets with large intervals - in this case, in the absence of permanent storage You can lose a lot of data.
- **Replication**. For some increase in data storage guarantees and maintaining the availability of the message queue for recipients in case of shutdown part of the servers.
- **Ability to configure storage reliability messages**. That is, how many servers are replicated and how often saved to disk. Needed in order to adjust the system so that it is more reliable to store messages from devices that have a long period between data transfer operations. With a heavy load, it should be possible to loosen such guarantees.
- **The ability to divide messages into groups by topic.** In this way, can send recipients of messages that implement a specific for a certain type of device logic, to receive messages with a specific queue in which the relevant data is placed.

5. Software smart home central controller

The system of interaction between devices in the "smart" house built (Fig. 2) on the architecture of the central controller (server). Therefore all requests coming from client applications are added to the message queue and only then turn to the commands that will be distributed to the microcontroller (in the case of multiple rooms/facilities).

Also, for the additional reliability, all the data is synchronized with cloud server, which helps to easily track errors. Such architecture has many advantages:

- Prior processing of user requests; only those requests that have been processed on a server will be sent to the microcontrollers; this helps to enable multi-user mode as well as organize all of the commands in a queue without any errors.
- Removing the burden of the microcontroller since it has a limited set of memory, saving a large amount of requests on it might influence the quality of the performance. When server is used microcontroller receives only a final command to execute, which are of a type ON-OFF.
- Scalability. When microcontroller-application system is used, we are having a problem with switching between the tasks for different devices in different rooms of the house. When a central server is used, it will take care of this problem by statically describing all of the controllers. Final user only has to define desired settings.
- Enhanced security system. Given the low processing power of microcontroller, in order to organize more or less reliable encryption on it is impossible. Unlike microcontrollers server has sufficient resources to perform encryption/decryption information.

Despite the obvious advantages, systems of this kind have also a number of disadvantages:

- Need of an extra device to perform the functions of the server. That adds complexity to the system and its maintenance.
- Need of an additional software for the organization of the server.

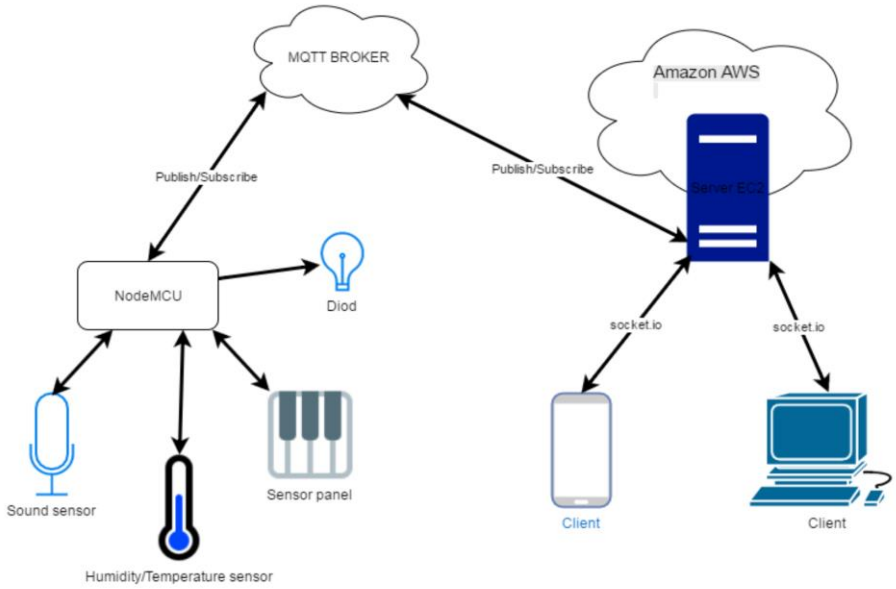

Fig. 2. An example of the finished system

6. Conclusion

We developed our own software for server management system of "smart" building via mobile device with a central controller, which is the main module of communication between the application and domestic electronic devices. We also developed basic functions such as storage configuration and information link between devices, encryption system, communication with cloud storage, energy forecasting, and more.

The developed platform meets the set functional and non-functional requirements and contains the implementation of the following subsystems: acceptance, storage, processing of operational data; authentication and security; work with administrative data; monitoring. This allows it to be used as such dedicated user groups: devices, administrators, analysts, and security administrators.

Such distributed service oriented service has been proposed and implemented (microservice) platform architecture that delivers high performance and almost endless scalability. This allows you to increase power systems for servicing device networks of all sizes and for increasing the capabilities of the data analytics subsystem. Effective implementation system components to optimize hardware costs platform.

The platform also guarantees a significant level of resiliency, which reduces the probability of losing operational data and providing a high level of it availability. The investigated and implemented aspects of security provide sufficient level of data protection during transmission and protect the system from the various information attacks.

During the development, the platforms were properly and properly selected modern systems, protocols, data formats, libraries and databases are applied data. Third-party solutions have open source that simplifies system expansion, has economic and other benefits.

Various aspects of the chosen architectural features were described in detail solutions: from justifying high-level division into functional modules to features of effective implementation of I/O and the influence of the selected scheme authentication for scalable platform architecture.

Unlike existing platforms, the solution developed is good expandable in the sense that it can be easily adapted to analytics data coming from different devices and sensors, setting the chains data processing. Data protocols and formats were chosen not only in light of them efficiency, and also given the convenience and ease of extending the platform.

Other key features of the platform are monitoring and the functionality of securely transferring service information between devices and by administrators. These capabilities allow you to effectively manage your network devices, and flexibly configure alerting tools possible problems and promptly respond to them.

There are architectural and technical solutions proposed and applied in the work versatile enough to allow them to be built various big data processing systems and other platforms for the Internet things specializing in narrower areas.

References

[1] Aberer K.: Smart Earth: From Pervasive Observation to Trusted Information. International Conference on Mobile Data Management, Mannheim, 2007, 3–7
[2] Darianian M., Michael M.P.: Smart Home Mobile RFID-Based Internet-of-Things Systems and Services. International Conference on Advanced Computer Theory and Engineering, Phuket, 2008, 116–120.
[3] EPCglobal.EPC information services (EPCIS) version 1.0.1 specification. EP-Cglobal, Lawrenceville 2007.
[4] Garg V.K.: Elements of Distributed Computing. John Wiley & Sons, New York 2002.
[5] Marz N., Warren J.: Big Data: Principles and best practices of scalable realtime data systems. Manning, Shelter Island 2015.
[6] Sathi A.: Big Data Analytics: Disruptive Technologies for Changing the Game. Mc Press, Boise 2012.
[7] Tamer Özsu M., Valduriez P.: Principles of Distributed Database Systems. Springer, New York 2011.
[8] Tel G.: Introduction to Distributed Algorithms. University Press, Cambridge 2000.

Vitalii Kopeliuk
e-mail: vkopeluk@gmail.com

Master Student at the Department of applied math and computer science of Rivne State University of Humanities, Rivne, Ukraine.

Robotics, computer technology and computer technology, programming, programming of microcontrollers, artificial intelligence.

http://orcid.org/0000-0002-3538-7028

M.Sc. Vira Voronytska
e-mail: vera.voronitska@gmail.com

Senior Lecturer at the Department of applied math and computer science of Rivne State University of Humanities, Rivne, Ukraine.

Development of sites, development of multimedia courses, computer science and computer technologies, programming.

http://orcid.org/0000-0003-0014-1121

Ph.D. Volodymyr Havryliuk
e-mail: V.i.Havrilyuk@gmail.com

Associate professor at the Department of Information Systems and Computing Methods International University of Economics and Humanities Academician Stepan Demianchuk, Rivne, Ukraine. Engaged in applied and computational mathematics, mathematical modeling of technological processes, numerical modeling and analysis, differential equations in applied mathematics, physics and engineering, computer science and computer technologies, programming.

http://orcid.org/0000-0003-3377-6465

otrzymano/received: 21.12.2019 *przyjęto do druku/accepted: 26.06.2020*

http://doi.org/10.35784/iapgos.933

EXERGY-BASED CONTROL STRATEGY IN A DWELLING VENTILATION SYSTEM WITH HEAT RECOVERY

Volodymyr Voloshchuk, Mariya Polishchuk
National Technical University of Ukraine "Igor Sikorsky Kyiv Polytechnic Institute", Department of Automation of Thermal Processes, Kyiv, Ukraine

Abstract. *The paper presents energy and exergy analysis of a typical dwelling ventilation system with heat recovery for Ukrainian climatic conditions using a quasi-steady state approach over 24-hour time-steps. Evaluation of such systems on the base of the first law of thermodynamics demonstrates that heat recovery is beneficial for the whole variety of operational modes. Such methodology identifies as a thermodynamic inefficiency only energy losses to the surroundings with the exhaust air. The exergy-based analysis can detect additional inefficiencies due to irreversibilities within the components of the system. As a result the exergetic investigations show that for the ventilation systems there are operating conditions for which heat recovery increases exergy of fuel expended to provide the ventilation air compared to cases without bringing any recovery of heat and additional power consumption to drive the air flow by the fans. For the specified system, in case of switching ventilation unit to the operation mode of lower values of spent fuel exergy it is possible to provide annual saving of the primary energy sources from 5 to 15%.*

Keywords: ventilation system, exergy analysis, control, heat recovery, exergy saving

OPARTA NA EGZERGI STRATEGIA STEROWANIA SYSTEMEM WENTYLACJI MIESZKAŃ Z ODZYSKIEM CIEPŁA

Streszczenie. *W pracy przedstawiono analizę energetyczną i egzergetyczną typowego systemu wentylacji mieszkań z odzyskiem ciepła dla ukraińskich warunków klimatycznych z zastosowaniem podejścia quasi-stabilnego w 24-godzinnych krokach czasowych. Ocena takich systemów w oparciu o pierwsze prawo termodynamiki wykazuje, że odzysk ciepła jest korzystny dla całego szeregu trybów pracy. Taka metodologia identyfikuje jako nieefektywne termodynamicznie tylko straty energii do otoczenia wraz z powietrzem wylotowym. Analiza egzergetyczna może wykryć dodatkowe nieefektywności wynikające z nieodwracalności elementów systemu. W rezultacie badania egzergetyczne wykazują, że w systemach wentylacyjnych występują warunki pracy, dla których odzysk ciepła zwiększa egzergię paliwa zużytego do dostarczenia powietrza wentylacyjnego w porównaniu do przypadków, w których nie występuje żaden odzysk ciepła i dodatkowe zużycie energii elektrycznej do napędzania przepływu powietrza przez wentylatory. Dla określonego systemu, w przypadku przełączenia urządzenia wentylacyjnego na tryb pracy o niższych wartościach egzergii zużytego paliwa możliwe jest zapewnienie rocznych oszczędności pierwotnych źródeł energii od 5 do 15%.*

Słowa kluczowe: system wentylacji, analiza egzergii, kontrola, odzysk ciepła, oszczędność egzergii

Introduction

Heat/energy recovery from exhaust air in dwelling ventilation systems provides a possibility to reduce energy consumption [4]. From viewpoint of the energy conservation statement which is based on the first law of thermodynamics such systems are effective. Due to recovery of heat from the exhausted stream heat losses to the environment are decreased. These are the only detectable energy losses (i.e., inefficiencies) in an energy analysis. The main drawback of this evaluation is that it fails to provide the full information about the real thermodynamic inefficiencies in a system.

Exergy-based methods reveal the location, magnitude of thermodynamic inefficiencies and the effects that cause them. As a results exergetic techniques can be successfully applied in evaluating the potential for improving the efficiency of the system.

Over the last two decades special attention is being paid to the so called low exergy (LowEx) heating and cooling systems [2]. LowEx systems are defined as systems that allow the use of low valued energy as the energy source. Such strategy provides matching the quality of supplied energy with the demand. This implicitly accounts thermodynamic inefficiencies in the given system. The application of exergy-based methods in buildings to identify and reduce this quality mismatch has aroused great interest among some scientists in recent years [2].

In a dwelling ventilation system with heat recovery to drive fans for air distribution electricity is consumed. The quality of electrical energy is much higher compared with the same amount of recovered thermal energy. Exergy-based approach which is based on the second law of thermodynamics provides a possibility to evaluate the level of energy quality and improve control of dwelling ventilation system by decreasing consumption of the most valuable types of energy.

The paper [8] presents steady-state energy and exergy analyses for dwelling ventilation with and without air-to-air heat recovery and discusses the relative influence of heat and electricity on the exergy demand by ventilation airflows in winter conditions of Netherlands. It has been shown that from an exergy viewpoint, it could make sense to use the heat recovery unit only when environmental air temperature is low enough to compensate the additional need for electricity. When the air temperature is not too low, electricity input could be decreased by letting ventilation air bypass the heat recovery unit or by operating the heat recovery unit at low ventilation airflow rate, depending on outdoor temperatures and indoor occupancy conditions.

The authors [5] in contrast to traditional performance parameters also applied exergy analysis and nonequilibrium thermodynamics to characterize the performance of heat recovery ventilator and a structurally similar membrane energy recovery one. They showed that the exergy efficiency can be used to identify the range of operating conditions for which the recovered heat and moisture are not enough to compensate power consumed by ventilation fans, and for which it is more beneficial to bypass the energy recovery unit.

The work [1] addresses the trade-off of heat recovery and fan power consumption in the ventilation system based on primary energy, carbon dioxide emission, household consumer energy price and exergy frameworks for a broad range of operating conditions in the different climates in Europe. The paper shows that the profitability concerning operating energy recovery ventilation as opposed to simple mechanical exhaust or natural ventilation strongly depends on the type of conversion coefficient between electrical energy and fuel combustion for heating, building performance, climatic conditions of a region, investment and maintenance cost.

On the annual energy and exergy performance the paper [3] shows that addition of a mechanical ventilation system with heat recovery increases the energy efficiency, however, it decreases the exergy efficiency. The authors conclude that the use of a separate mechanical ventilation system in a house should be considered with caution, and recommended only when other means for controlling the indoor air quality cannot be applied.

The results presented in considered papers are based on the exergy values at room or primary energy levels without focusing on the efficiency of energy conversion and delivery processes steps. The conclusions may be more sophisticated and practical if the exergy-based parameters are considered in all subsystems of energy conversion system which provides a possibility to identify

and calculate the location, magnitude and causes of thermodynamic inefficiencies in an energy conversion system.

The scope of the paper is to demonstrate benefits of application of exergy-based approach for better control strategy in a dwelling ventilation system taking into account all intermediate steps from primary energy transformation to final energy consumption in climate conditions of Ukraine.

1. Methodology

The Figure 1 provides a schematic illustration of the analyzed system from primary energy conversion to the building envelope. The dwelling ventilation system consists of a heat recovery unit, two fans and two additional heaters. In case of heat recovery from the exhausted air stream the system increases the electricity consumption by ventilation fans to compensate additional pressure drops in the air-to-air heat exchanger. If the outdoor air temperature is too low the ventilation air is first preheated with the additional hot water preheater. The second hot water heater is used only if the temperature of ventilation air, after the heat recovery, is lower than the indoor air temperature. If streams bypass the recovery unit the outdoor air is heated in the both hot water heaters and fan power required to drive the air flow is decreased.

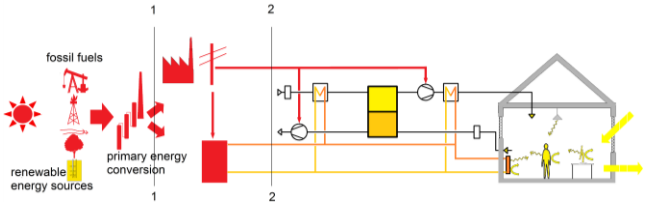

Fig. 1. Energy supply chain for space heating in a buildings from primary energy transformation to final energy, including all intermediate steps up to the supply of the heating demand

Two control layers are considered to analyze the amount of fuel exergy (representing the resources in terms of exergy) expended to provide the product exergy (representing the desired result, ventilation air, in terms of exergy) [6] (see Figure 1).

For investigation of variable operational modes of the system due to fluctuating in outdoor conditions a mathematical model for energy and exergy assesment has been developed using 24-hour time step quasi-stationary approach. The model is based on mass, energy and exergy balances for the specified dwelling, ventilation and heating system.

The analysis is performed for a typical Ukrainian individual house. The dwelling has one floor with a gross floor area of 90 m^2 and a volume of 225 m^3. For the reference case weighted average insulation value of non-glazed external surfaces is 0.5 W/(m^2·K). U-value of windows including frames is 2 W/(m^2·K). Infiltration rate is regarded as 1 h^{-1}. Internal heat gains are defined with a constant value of 10 W/m^2 [10]. Setpoint for the indoor temperature is 18ºC. The fraction of east and west oriented glazing is 30%, of the south one – 50%, of the north one – 20%. Heat recovery efficiency of the ventilation system is equal 55%. Heating needs in the both hot water heaters are covered by a heat pump system. Low temperature energy utilised in the evaporator of the heat pump is not taken into account in calculations.

For the control layer 2 the exergy of fuel is calculated using the formula

$$E_{F,2}(\tau) = E_{F,PH}(\tau) + E_{F,H}(\tau) + E_{F,fun}(\tau) \quad (1)$$

where

$$E_{F,PH}(\tau) = En_{PH}(\tau) \cdot \left\{1 - \frac{T_0(\tau)}{T_{in}(\tau) - T_{out}(\tau)} ln\left(\frac{T_{in}(\tau)}{T_{out}(\tau)}\right)\right\} \quad (2)$$

$$E_{F,PH}(\tau) = En_{H}(\tau) \cdot \left\{1 - \frac{T_0(\tau)}{T_{in}(\tau) - T_{out}(\tau)} ln\left(\frac{T_{in}(\tau)}{T_{out}(\tau)}\right)\right\} \quad (3)$$

τ – time step, τ = 24 hr; En_{PH}, En_H – daily energy consumed in the hot water preheater and heater of the ventilation air, kW·h; T_0 – temperature of outside air, K; T_{in} – heater and preheater inlet temperature of water, K; T_{out} – heater and preheater outlet temperature of water, K; $E_{F,fun}$ – electricity consumed by the fans, kW·h.

For the control layer 1 representing the primary energy inlet the exergy of fuel is calculated using the formula

$$E_{F,1}(\tau) = \frac{E_{F,HP}(\tau) + E_{F,fun}(\tau)}{\varepsilon} \quad (4)$$

where

$$E_{F,HP}(\tau) = \frac{En_{PH}(\tau) + En_{H}(\tau)}{COP(\tau)} \quad (5)$$

ε – exergy efficiency of electricity generation on thermal power plant, ε = 0.37 [9]; $COP(\tau)$ – coefficient of performance of the heat pump system, calculated on the base of [7].

The values of *COP* are highly dependent on the temperature difference between the source and sink. Because of variation of operational conditions within building the calculated *COP* values varied within the range from 2.5 to 4.5.

Primary energy sources are based on fossil fuels [2]. For simplicity the quality factors of different kinds of fossil fuels are equal to 1.0.

2. Results and discussions

Figure 2 presents the results of application the energy balance approach for the calculations of consumed energy for providing ventilation air within the range of outside temperatures -20 … 14ºC. In this case the control layer 2 is considered.

It is clearly observed that for the analysed layer heat recovery from ventilation airflow plays an increasingly important role in minimising energy needs. According to the obtained results energy consumed for providing ventilation air with recovering heat from the exhausted air (line 1) is lower compared to cases without energy recovering (line 2) for the investigated variety of outside temperatures. But it should be noted that the energy analysis identifies only an energy transport to the surroundings as a thermodynamic inefficiency. Such approach does not provide information about all existing thermodynamic inefficiencies within the system. The necessary data can be obtained on the base of exergy analysis.

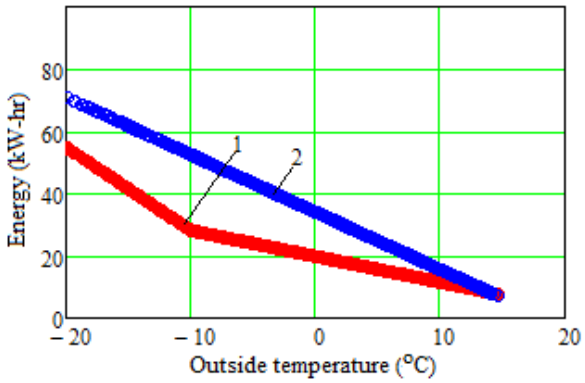

Fig. 2. Energy consumed for providing ventilation air versus outside temperature for the control layer 2: 1 – with heat recovery; 2 – without heat recovery

Figure 3 illustrates values of the exergy of fuel expended to provide the ventilation air for the control layer 2 as a function of outside temperature. The line 1 represents the mode of using heat recovery system. The line 2 belongs to the mode when the air streams bypass the recovery unit. It can be observed that the lines 1 and 2 intersect at the environmental air temperature equal to -6ºC. For this temperature the values of exergy of fuel for the two different modes are equal. So, at the environmental air temperatures lower than -6ºC the exergy of fuel expended to provide the ventilation air is lower for the mode 1 (heat recovery application). If the outside air temperatures are higher than -6ºC it is more beneficial to bypass the recovery unit.

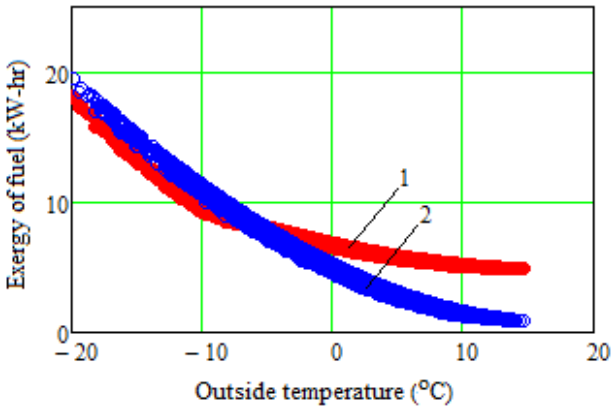

Fig. 3. Exergy of fuel expended to provide the ventilation air versus outside temperature for the control layer 2: 1 – with heat recovery; 2 – without heat recovery

Figure 4 presents results of calculating values of the exergy of fuel spent in the ventilation system as a function of outside air temperature for the control layer 1 which is associated with primary energy sources inlet. The line 1 belongs to the mode of heat recovery and the line 2 – to the mode of bypassing the recovery unit. For the control layer 1, if the outside air temperatures are lower than 0ºC the exergy associated with fuel is lower for the mode 1 (heat recovery application). On the contrary, if the outside temperatures are higher than 0ºC it is makes sense to bypass the recovery unit because the exergy of fuel for this mode is lower than for the mode of heat recovery.

Taking into account that the quality factors of different kinds of fossil fuels is equal to 1.0 it can be concluded that energy spent in providing ventilation air for the control layer 1 is the same as the spent fuel exergy.

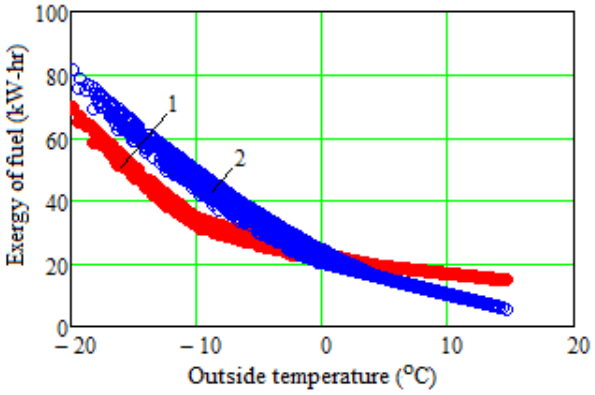

Fig. 4. Exergy of fuel expended to provide the ventilation air versus outside temperature for the control layer 1: 1 – with heat recovery; 2 – without heat recovery

Energy and exergy flows from the primary energy sources to the indoor ventilation air through the entire dwelling ventilation system are illustrated in Figures 5 and 6. These results are presented for the outdoor temperature 10ºC and -10ºC respectively. The diagrams clearly show advantages of the exergy analysis as compared with the energy one. From the primary energy inlet (layer 1) to the indoor ventilation air the value of exergy flow is decreased due to thermodynamic inefficiencies. And the steps with the biggest decrease of exergy can be identified. The energy approach does not provide such information.

In case of the outdoor temperature equal to 10ºC higher exergy destruction (19 kW·h - 5 kW·h = 14 kW·h) belong to the system with heat recovery in the step of energy conversion between the layers 1 and 2. But during energy conversion from the layer 2 to the indoor ventilation air exergy destruction is also quite high and equal to 5 kW·h - 0.2 kW·h ≈ 5 kW·h. For the system without recovering energy from the exhaust air (bypassing mode) exergy destructions are lower for the both energy conversion steps and this mode is more beneficial.

If the outdoor temperature is equal to -10ºC (see Figure 6) it is more efficient to use heat recovery. For this operational mode within the both energy conversion steps (from the layer 1 to layer the 2 and from the layer 2 to the indoor ventilation air) exergy destructions are equal to 27 and 7 kW·h respectively which is lower compared with the case of bypassing the recovery unit.

In case of applying energetic analysis it is quite difficult to identify the more efficient mode since it is impossible to detect any thermodynamic inefficiencies in the system.

For example, as can be seen from Figure 5 for the outdoor temperature 10ºC, in case of using heat recovery (dashed line 1), for the layer 2 inlet energy flow is equal 12 kW·h but the outlet one representing indoor ventilation air is equal to 15 kW·h. The increase of 3 kW·h of energy is due to recovered heat from the exhaust air. But if heat recovering is not used (dashed line 2) 1 kW·h of energy losses are observed. So, using energetic approach the investigator can make a wrong conclusion about applying heat recovery. But, as a result, for such operational mode the primary energy consumption will be equal to 19 kW·h which is higher by 8 kW·h compared with the mode of bypassing the recovery unit.

So, only the exergy analysis can provide correct information which can be used to find improvement potentials for operational modes.

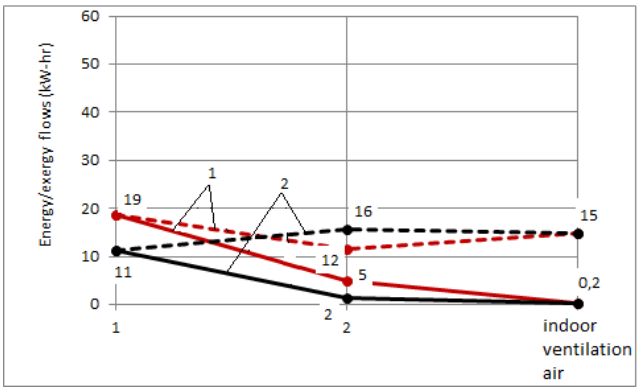

Fig. 5. Energy and exergy flows of the dwelling ventilation system from the primary energy source to the indoor ventilation air for outside air temperature 10ºC: 1 – with heat recovery; 2 – without heat recovery; solid lines – exergy flows, dashed lines – energy flows

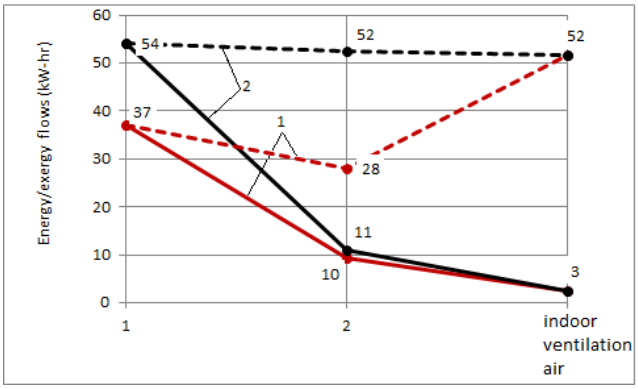

Fig. 6. Energy and exergy flows of the dwelling ventilation system from the primary energy source to the indoor ventilation air for outside air temperature -10ºC: 1 – with heat recovery; 2 – without heat recovery; solid lines – exergy flows, dashed lines – energy flows

For the more detailed analysis of the causes of thermodynamic inefficiencies from the layer 2 to the indoor ventilation air of the investigated system the differentiated values of exergy flows of the dwelling ventilation system for outside air temperature 10ºC are presented in Figure 7. It can be clearly observed that in comparison to the case of bypassing the recovery unit ventilation with heat recovering demonstrates higher thermodynamic inefficiency due to irreversibilities associated with the fan power consumed to drive the air flow through the recovery system.

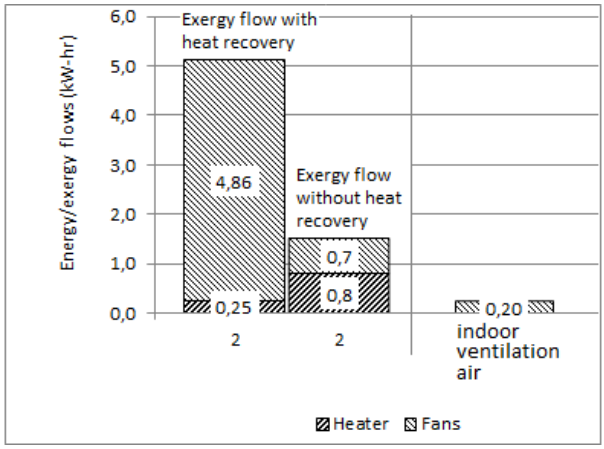

Fig. 7. Differentiated exergy flows of the dwelling ventilation system from the layer 2 to the indoor ventilation air for outside air temperature 10°C

The results presented above reveal a potential to improve the efficiency of the dwelling ventilation system through the implementation of an exergy-based control strategy, which tries to fulfill the demand of the ventilation system with low-quality energy sources involving the bypassing mode of heat recovery unit. The results of such strategy are presented in Figure 8 for the layer 1 which demonstrates the primary energy sources consumption.

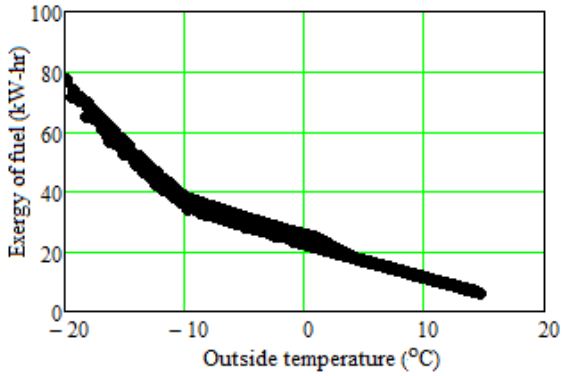

Fig. 8. Exergy of fuel expended to provide the ventilation air versus outside temperature for the control layer 1 through the implementation of the exergy-based control strategy

Figure 9 demonstrates the values of annual fuel exergy saving over 27-year period for the control layer 1 (primary energy sources) of the reference system in case of applying the proposed exergy-based control approach.

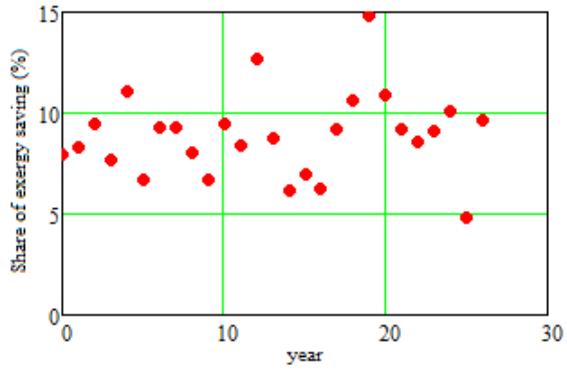

Fig. 9. Annual values of saving exergy associated with fuel for the control layer 1

It can be observed from Figure 9 that in comparison to the conventional operating dwelling ventilation system with heat recovery (recovering energy from the exhausted air stream for the all range of operating modes) it is possible to save annually from 5 to 15% of the primary high quality energy by bypassing the recovery unit in cases when the recovered exergy of heat is not enough to compensate the fan power consumed to drive the air flow through the recovery unit.

3. Conclusions

The present paper proposes the exergy-based optimal control strategy the identifying the range of operating conditions within which the dwelling ventilation system with heat recovery consumes more the high-quality energy sources (electricity) compared to the conditions for which bypassing the recovery unit is applied. Detailed explanation of the necessity of such strategy application is provided.

For the climate conditions and typical buildings of Ukraine it has been found that implementation of the proposed exergy-based control strategy provides a possibility of saving annually from 5 to 15% of the primary high quality energy sources.

References

[1] Gjennestad M.Aa., Aursand E., Magnanelli E., Pharoah J.: Performance analysis of heat and energy recovery ventilators using exergy analysis and nonequilibrium thermodynamics. Energy and Buildings 170, 2018, 195–205.
[2] Hepbasli A.: Low exergy (LowEx) heating and cooling systems for sustainable buildings and societies. Renewable and Sustainable Energy Reviews 16(1), 2012, 73–104.
[3] Jensen J.K., Ommen T., Reinholdt L., Markussen W.B., Elmegaard B.: Heat pump COP, part 2: Generalized COP estimation of heat pump processes. Proceedings of the 13th IIR-Gustav Lorentzen Conference on Natural Refrigerants 2, 2018, 1136–1145.
[4] Laverge J., Janssens A.: Heat recovery ventilation operation traded off against natural and simple exhaust ventilation in Europe by primary energy factor, carbon dioxide emission, household consumer price and exergy. Energy and Buildings 50, 2012, 315–323.
[5] Mert Cuce P., Riffat S.: A comprehensive review of heat recovery systems for building applications. Renewable and Sustainable Energy Reviews 47, 2015, 665–682.
[6] Rosen M.A., Dincer I.: Effect of varying dead-state properties on energy and exergy analyses of thermal systems. International Journal of Thermal Sciences 43, 2004, 121–133.
[7] Sakulpipatsin P., Boelman E., Cauberg J.J.M.: Exergy analysis as an assessment tool of heat recovery of dwelling ventilation systems. Int. J. of Ventilation 6(1), 2007, 77–85.
[8] Tsatsaronis G.: Definitions and nomenclature in exergy analysis and exergoeconomics. Energy 32, 2007, 249–253.
[9] Zmeureanu R., Wu X.Y.: Energy and exergy performance of residential heating systems with separate mechanical ventilation, Energy 32(3), 2007, 187–195.
[10] National Standard of Ukraine: Instruction for development of energy passport of buildings under new construction and reconstruction: DSTU-N B A.2.2-5:2007. Minregionbud of Ukraine, Kiev 2008.

Prof. Volodymyr Voloshchuk
e-mail: Vl.Volodya@gmail.com

He is a professor of the department of automation of thermal processes in National Technical University of Ukraine "Igor Sikorsky Kyiv Polytechnic Institute". The scientific activity is devoted to development and implementation of mathematical and computer modeling of thermal processes, exergy-based design, assessment, optimization and control of thermal systems.

http://orcid.org/0000-0003-0687-8968

M.Sc. Mariya Polishchuk
e-mail: atep_mariya@ukr.net

She is a Ph.D. student of the department of automation of thermal processes in National Technical University of Ukraine "Igor Sikorsky Kyiv Polytechnic Institute". The research interests lie in the field of mathematical and computer modeling of thermal processes and control theory.

http://orcid.org/0000-0003-2273-3750

otrzymano/received: 22.12.2019 *przyjęto do druku/accepted: 26.06.2020*

http://doi.org/10.35784/iapgos.932

ANALYSIS OF THE ELECTRICITY METERING SYSTEM FOR OWN ELECTRIC SUBSTATION NEEDS

Sergiy Stets, Andriy Stets
National University of Water and Environmental Engineering Institute of Automatics, Cybernetics and Computer Engineering, Rivne, Ukraine

Abstract. *In the article the researches of the use of electronic meters with standard nominal parameters for metering of substation own electric energy in the schemes of high and low voltage networks simultaneously with the use of the corresponding calculated coefficients on voltage for the purpose of operational control and determination of the reliability of measurement of electricity parameters.*

Keywords: electricity metering, meter, electrical substation

ANALIZA SYSTEMU POMIAROWEGO ENERGII ELEKTRYCZNEJ NA POTRZEBY WŁASNE STACJI ELEKTROENERGETYCZNEJ

Streszczenie. *W artykule przedstawiono badania wykorzystania liczników elektronicznych o standardowych parametrach nominalnych do pomiaru energii elektrycznej własnej stacji elektroenergetycznej w obwodach wysokiego i niskiego napięcia przy jednoczesnym zastosowaniu odpowiednich obliczonych współczynników napięciowych dla potrzeb sterowania pracą i określania wiarygodności pomiaru parametrów elektrycznych.*

Słowa kluczowe: pomiar energii elektrycznej, licznik, podstacja elektryczna

Introduction

The main areas of modern electricity development are infrastructure improvement, digital layer overlay, and business process modernization during power generation, transmission, distribution, supply and use, as defined by the Smart Grid concept.

Central to solving these problems in the Smart Grid concept is provided by Smart Meters and based on them Smart Metering Systems, which in Ukraine traditionally refer to an automated commercial electricity metering system.

With the creation of the Wholesale Electricity Market of Ukraine, where differentiation of electricity metering is carried out on an hourly basis, and its calculations are made on a daily basis, automated systems of commercial metering of electricity have become the basic tool for determining the volume of electricity sales. The 21st century is characterized by the mass introduction and integration of automated commercial electricity metering systems into a distributed hierarchical commercial metering system of the Wholesale Electricity Market of Ukraine. Since 2016, calculations on the Wholesale Electricity Market of Ukraine have been made entirely on the basis of the displays of automated systems of commercial metering of electricity.

In the conditions of liberalization of the electricity market, automated systems of control, metering and management of energy use are almost crucial in solving the problems of increasing the efficiency of generation, transmission, distribution and use of electricity. Only with the application of highly reliable full-scale multifunctional automated systems of commercial metering of electricity of energy market entities that co-ordinate in a single information system and provide solutions for demand management and market calculations, in particular, based on the cost of ancillary services, to improve the efficiency of electricity use by end consumers.

The gradual transition of the wholesale electricity market of Ukraine from the “single buyer” market model to the liberalized electricity market [1, 3, 6] will require the formation of appropriate information support for electricity billing. These are fundamentally new approaches to the definition of commercial metering data in a context where the price of electricity consists of the prices of a certain range of electricity products and the value of ancillary services, first of all, of balancing the market, which are sold and bought within the market. Under these conditions, fundamentally new requirements for hardware and software, which form data for electricity billing, as well as for the rules for their construction, implementation and application, are put forward.

To reduce the technological costs of electricity, it is important to mattering and analyze electricity consumption for own needs. According to the sectoral guidance document (SGD) “Electricity expenditure for own and economic needs of power station and networks” the mattering of electricity consumed for own needs of substations must be carried out by separate metering devices. Usually, inductive three-phase, two- or three-element (depending on the type of network of the given voltage level) meters of active electricity are used. The relevance of the introduction of automated electricity metering systems at the substations in accordance with the requirements of the Concept of construction of automated electricity metering systems in the conditions of the energy market within the automated dispatching control systems, implies the use of modern multifunctional electronic electricity meters. The automated dispatching system is assembled on-site from mass-produced measuring equipment and has standard technical parameters [2].

1. The aim and objectives of the study

Most substations have electricity metering for a three-element, high-voltage network (35/10(6) kV), i.e. meters are supplied with a secondary voltage of 100 V from the measuring transformer. An exception is the mattering for electricity for own needs, which is carried out by meters for three or four-wire low voltage network on the side of 0.4(0.23) kV own transformers. In this regard, the introduction of automated control systems containing microprocessor-based measuring equipment in the form of electronic meters raises the question of the possibility of using these meters to mattering for the electricity of a three-wire high-voltage network also for the mattering of low-voltage electricity 0.4(0.23) kV used for the substation's own needs and operational control of its parameters.

The transition to the use of automated commercial metering systems in conjunction with automated dispatching systems is the most promising avenue for their development, as these systems are interoperable in terms of operational control over power consumption and capacity. At the same time, the automated system at each level provides for the use of a wide range of unified software using microprocessor technologies. For such a measuring complex, the main technical task is to collect data from electronic meters along the information lines. However, the question remains as to the possibility of applying and unifying types of meters with the same technical parameters at the local substation level (as measuring equipment within the automated control system) in the presence of connections of different voltage class: 35/10(6) kV high-voltage switches and own needs. 0.4(0.23) kV.

It is known that high-voltage metering points on the high-voltage side of 35/10(6) kV are installed at the substations for consumer switches, and low-voltage metering points are only on the side of 0.4(0.23) kV of the transformers of own needs for

metering of electricity consumed on their own substation needs. These metering points are equipped with induction meters, which must be replaced by electronic ones when implementing automated systems. Multifunctional electrical meters on the high-voltage side are programmable electronic devices that have a flexible metering system that is customizable by software such as the Astaris SL7000 Smart or ZMD400AR/CR + ZFD400AR/CR Landis+Gyr Dialog. These meters can be programmed to operate in three- or four-wire high or low voltage networks, for direct or transformer start-up, and can be used as part of automated commercial metering systems. At 110(35)/10(6) kV substations, high-voltage metering points are generally not commercial, i.e. they serve for technical mattering [4, 5].

Low-voltage mattering of own needs is used both to control the consumption of electricity for own needs, as well as to analyze the balance and its technological costs for transmission by electrical networks. Accordingly, an automated electricity metering system within an automated dispatching system that implements the function of operational control of electricity and power need not be commercial. Therefore, the use of the above electronic devices intended for high voltage metering with a flexible metering system as a measuring technique within an automated control system is not always appropriate, given their high cost.

For the automated electricity metering system within the automated control system, for the purpose of high-voltage metering, the same type of multifunctional electronic meters are used for a three-wire high-voltage network without a flexible metering system (for example, NR-03 ADDED0.Z-U) with standard technical parameters protocol of information exchange, the voltage circuits of which are calculated for the nominal secondary voltage 3×57.7/100 V. The function of operational control and analysis is implemented power consumption in high-switches, but does not solve the problem of keeping those same counters electricity consumed for own needs substations on the low side of 0.4(0.23) kV transformers own needs.

Because modern multifunction meters have a flexible measuring system, which can be parameterized, it is logical to assume that electronic meters with standard nominal parameters can be used in the schemes of high and low voltage networks, subject to certain conditions and by applying the corresponding voltage coefficients [5]. Given the impossibility or impracticality of using these meters as part of an automated control system, the task is to research the possibility of using microprocessor-based measuring equipment in the form of electronic meters with standard technical characteristics for the mattering of electricity as a whole, consumed as a high power consumed substation needs at low voltage.

2. Solving the problem

The main purpose of the research is to find out the possibility of solving this problem in the technical plan, namely to research the reliability of metering of electricity (power) consumed for own needs on the side of 0.4(0.23) kV own transformer 10(6)/0.4(0.23) kV, electronic meters with a nominal voltage of 3×57.7/100 V taking into mattering the corresponding design factor.

In the implementation of automated dispatching control system at the substations high-voltage switches as microprocessor-based measuring equipment for measurement (accumulation) and data transmission use electronic multifunctional three-element electricity meters NP-03 ADDED0,3-U. 3×57.7/100 V. For the purpose of research, these meters were also installed at the points of mattering of own needs on the side of 0.4(0.23) kV. The use of three-element electronic meters instead of two-element inductors made it possible to record not only in the three-wire 0.23 kV network but also in the four-wire 0.4 kV network of own needs, where electricity consumption can occur each phase separately, requiring the presence of three measuring transformers, and three items in the counter.

To mattering for the needs of the voltage circuits of the NP-03 model meters, a secondary voltage of 100 V was supplied from the measuring transformers of the voltage, and the phasing was carried out so that the vector of the secondary linear voltage of the measuring transformer coincided with the corresponding linear voltage of 0.4(0.23) kV from the transformer own needs. Since the winding of the higher voltage of the measuring voltage transformer is connected to the star and the lower voltage to the star with the output zero point, the angle of displacement between the vectors of the linear voltages of the windings of the higher and lower voltage is zero. This connection group of the measuring transformer of the voltage transformer coincided with the group of connection of the transformer of own needs 10(6)/0.4 kV on the low side. The lower voltage winding of the 10(6)/0.23 kV self-contained transformer is connected in a "triangle", therefore, depending on the winding performance, an angular displacement may occur between the higher voltage and lower voltage linear vectors. For a three-wire, 0.23 kV power supply system using two current transformers, the connection of three-element meters to the metering scheme was made by connecting the current circuit of the middle element of the meter to the sum of the currents of phases A and C with reverse polarity. For the 0.4 kV four-wire network, where three current transformers are used, all three meter elements were connected. It should be noted that the technical decision on the reorganization of the specified metering points cannot be fulfilled if 0.4(0.23) kV direct-inductionmeters are used in the schemes, since electronic transformer-based meters are rated at 3×57.7 / 100 V and current 3×5 A cannot be incorporated directly into the scheme, i.e. without the use of separate circuits of current and voltage. Therefore, in the technical plan we have a scheme of semi-direct switching with the use for the circuits of the counter voltage, which corresponds to its technical parameters [6].

After the determination of 0.4(0.23) kV of the transformer of own needs, from the metering points of electricity consumed by the substation for own needs, from the digital interfaces of the HP-03 meters, separate parameters of the electrical network were taken out with the help of the appropriate software reliability of the measuring system as a whole. For convenience, the instantaneous values of the parameters recorded by the meters in the secondary circuits of the measuring current and voltage transformers for each phase were taken separately, without the use of calculated coefficients.

Measurement data obtained with the software from the substation meters are given in Table 1.

The results obtained show that the secondary circuits of the meters are powered by a voltage of 100 V from the measuring transformers of the voltage, and since the information was read from the interface of the three-element meter, we have, on all counting points, an average phase voltage of about 60 V (nominal phase voltage of the counter is 57.7 V). It should be noted that the load of some current collectors is reactive. As you can see, when consuming electricity for the substation's own needs with a linear voltage of 0.4 kV, there may be a situation where the load is asymmetrical and connected to only two (one) phases of the four-wire network, and in the other one (two) phase the load current is absent. In this three-phase metering scheme, three measuring current transformers are used and current circuits are connected to the star, so in the absence of load current in one of the phases in the zero wire, the unbalance current flows, and the three-element counter conducts a phase analysis of the power supply parameters in the loaded phases. In contrast to the 0.4 kV four-wire network, two measuring current transformers are used for the three-wire 0.23 kV network, the current circuits of which are connected in “incomplete star” and the zero pole connected to the middle element of the counter with reverse polarity. the sum of currents of phases A and C flows.

Table 1. The results of the phase measurements of the parameters of the power network of own needs

# of substation	Voltage TV by phases U_f, V			Amperage by phases I_f, A			Active power P_f, W			Reactive power Q_f, VAr		
	«A»	«B»	«C»	«A»	«B»	«C»	«A»	«B»	«C»	«A»	«B»	«C»
Mattering points on the low side of own needs with a linear voltage of 0,4 kV												
1	60.7	61.2	61.0	0.8	0.1	0	48.6	7.0	2.4	3.6	3.3	-0.3
2	62.6	63.1	63.1	0	0.3	0.1	0	19.9	5.1	0	0	5.8
3	62.4	62.7	62.3	0.1	0.3	0.6	8.6	18.2	35.5	0	0	0
4	60.0	60.0	59.6	0	1.4	0.3	2.2	82.6	10.0	0.5	6.1	15.1
Metering points on the low side of own needs with a linear voltage of 0,23 kV												
5	59.9	59.1	59.0	0.6	0.7	0.7	30.3	38.4	34.1	15.8	15.1	22.1
6	60.1	60.1	59.3	1.3	1.5	1.5	74.8	87.2	86.6	10.5	2.4	17.5
7	59.2	59.7	59.2	0.2	0.1	0.1	1.8	-0.9	3.0	10.3	7.4	6.5
8	59.7	59.2	59.9	0	0.1	0.1	2.8	7.4	4.9	0	0	4.2
9	61.9	61.8	61.7	1.6	1.8	1.4	95.9	108.3	82.7	-10	10.8	10.6

Accordingly, in the asymmetric nature of the load, i.e. in the absence of current in one of the phases, due to the asymmetry, the vector diagram of currents and the total active power of the network (as well as reactive) will be unreliable. From the received data it is clear that only with symmetrical nature of the load can the most reliable data be obtained while mattering for the electrical parameters of the network.

The analysis of the work of the reorganized metering points as external measuring devices within the automated control system "SCADA IMS" occurred after reading the electrical parameters obtained at the lower level of the substations of the district network from the RS-485 interfaces via the RTU-560 output buffer Modbus information. Since the process of obtaining this information is automated and consists of recording data from electricity meters throughout the mattering period, it is important to analyze the reliability of the measurement information, as well as the synchronicity of measurements at the metering points. It should be borne in mind that in the reports of the most automated control system, the read data is time-bound and contains the real values (unlike the data in Table 1), that is, they take into mattering all the calculated current and voltage factors, related to the mattering of the parameters of the mains through measuring current transformers and measuring transformers of voltage. I_f the meters are connected to voltage transformers and current transformers (transformer switching), when determining electricity consumption (power) according to their readings, it is necessary to use the calculated coefficient, which takes into mattering the transformation coefficients of these measuring transformers:

$$K_p = \frac{U_1}{U_2} \times \frac{I_1}{I_2} = K_U \times K_I \quad (1)$$

where U_1, U_2 is the rated voltage of the primary and secondary windings of the measuring voltage transformer, respectively; I_1, I_2 is the rated current of the primary and secondary windings of the measuring current transformer, respectively, A.

In this case, after reorganization of the points of mattering of own needs on the side of 0.4(0.23) kV, it should be taken into mattering that instead of the nominal voltage U_{nom} = 400(230) V. In own needs the secondary voltage U_2 = 100 V from the measuring transformer is supplied voltages, and the nominal parameters of the low-voltage measuring current transformers and the transformation factor in the power network did not change. Since the metering needs to be reduced to 0.4(0.23) kV, formula (1) takes on a slightly different form:

$$K_p = \frac{U_1^{"}}{U_2} \times \frac{I_1}{I_2} = K_U^{"} \times K_I \quad (2)$$

where $U"_1$ – nominal voltage of the transformer, V.

Electricity consumption can be determined by integrating power over time, so information from an automated dispatching system regarding load schedules for reorganized metering points used for own needs was used for convenience. Moreover, in the reports of the automated control system, the primary values of the network parameters (current, power) were obtained, that is, taking into mattering the calculated coefficients.

The substation's own energy sources include mainly current collectors that provide heating and lighting for the equipment. Therefore, to simplify the calculations, it is conventionally assumed that the power factor is equal to one and the phase voltage is the same for each phase, i.e. $U_f = U_A = U_B = U_C$. In addition, the reorganization of the metering points of the transformation needs the transformation factor of the measuring current transformers does not change, and a new voltage factor $K"_U$ is introduced. the sum of the capacities of the individual phases, taking into mattering the calculated coefficient (3).

Since the automated dispatching system in the automatic mode controls the condition of the equipment and the modes of consumption, an important criterion is the promptness of obtaining information. Accordingly, in addition to averaged values of currents and capacities, instantaneous values were used to analyze the measurement results, which reflected the operational situation directly in real time on the layout of a substation. For the purpose of comparative analysis of the data received from the automated system of dispatching data management and real parameters of the grid, the calculations were performed according to the formula. All results of measurements in the automated control system and calculations for individual substations of district grids are given in Table 2.

As we can see, for a power supply network with a voltage of 0.4(0.23) kV, the load is asymmetrical. In this case, averaged over a certain period of time, data (both current and power) differ little from the instantaneous values, that is, we have a uniform load schedule for electrical equipment of our own needs. Basically, the data obtained from the automated control system of the three-phase power network are close to the calculated values (the largest difference is 0.5 kW). For Substation #7 we have an unreliable value of active power, which may be due to the non-observance of the above conditions of ensuring the reliability of the data of the metering of electricity consumed for own needs of the substation.

$$P = K_p(P_A + P_B + P_C) = K_P(U_A I_A K_I \cos\varphi_A + U_B I_B K_I \cos\varphi_B + U_C I_C K_I \cos\varphi_C) = K_U^{"} U_f (I_A + I_B + I_C) \quad (3)$$

where $K"_U$ - coefficient taking into mattering the use of measuring equipment voltage 3×57.7/100 V in the network voltage 400(230)V; U_f – phase voltage measured by the meter, V; I_A, I_B, I_C are the primary values of currents (taking into mattering the transformation factor of measuring current transformers) for each phase, respectively, A.

Table. 2. The results of measurements of the parameters of the power network of substations' own needs in the automated control system

# of substation	Transformation factor		Measured values in an automated dispatching control system						Estimated value ΣP, kW
			Instant				Averaged over an interval of 30 minutes		
			Amperage I_{nom}, A			ΣP, kW	I_{nom}, A	ΣP, kW	
	K''_U	K_I	Phase A	Phase B	Phase C		Phase B		
1	230/100	150/5	40.2	30.3	22.2	12.85	30.2	12.76	12.3
2	230/100	200/5	43.4	26.7	34.7	12.75	26.6	12.48	13.9
3	230/100	200/5	29.1	26.1	46.6	11.07	26.1	10.90	13.5
4	230/100	150/5	27.8	13.7	18.9	7.75	13.6	7.71	8.0
5	400/100	100/5	11.6	16.3	11.5	9.38	15.6	9.6	9.1
6	230/100	600/5	56.5	41.5	81.6	23.6	41.0	23.14	23.8
7	230/100	200/5	31.6	42.2	42.4	0.07	41.9	0.03	15.4
8	230/100	300/5	20.7	26.2	12.7	7.98	29.2	8.94	7.9
9	400/100	400/5	54.1	70.4	46.4	40.64	70.6	40.68	39.4
	400/100	400/5	0.8	1.3	1.0	0.47	1.24	0.46	0.72
10	230/100	100/5	20.7	16.9	12.2	6.66	17.0	6.62	6.6
11	400/100	50/5	14.2	20.1	8.8	10.39	20.0	10.29	9.9
12	400/100	50/5	11.9	0	15.0	6.40	0	6.34	6.2
13	230/100	100/5	7.3	9.5	6.0	5.31	9.4	5.26	3.0
14	230/100	50/5	13.3	14.7	5.9	4.43	16.2	4.78	4.5

3. Conclusions

Analyzing the results of the studies, we can conclude:

- mattering of the electricity of own needs on the side of 0.4(0.23) kV by inclusion in the measurement scheme of electronic meters with a nominal voltage of 100 V is possible solely for the purpose of operational control of the parameters of active electricity, if the use of meters with a flexible system of measurement is impossible or impractical:
- the real values of the electricity parameters can be determined by a factor that takes into mattering the fact that the meters at a voltage of 100 V in the network with a voltage of 400 (230) V;
- if the metering of the electricity consumed for the substation's own needs is carried out by direct switches, the mattering of own needs by electronic meters with a rated voltage of 100 V on the side of 0.4(0.23) kV is impossible;
- for reliable and accurate operational control of electricity parameters at any load nature, in the presence of measuring equipment in the automated control system of only electronic meters with a rated voltage of 100 V, it is necessary to consider the possibility of mattering on the high side 10 (6) kV of the transformer of own needs;
- only three-element multifunctional electronic meters should be used as a measuring equipment for the automated control system as a means of measuring equipment on the side of 0.4(0.23) kV;
- in the case of unbalanced load mode, the obtained values of the parameters of the reactive electricity will be unreliable;
- to ensure the accuracy of mattering and operational control of the parameters of electricity, the following conditions must be observed: self-contained transformers and voltage transformers connected to the same bus section must be used; self-contained transformers and voltage measuring transformers must have the same connection group (allow for angular displacement of vectors); the load of own needs should be evenly distributed across all phases.

References

[1] Chauhan et al.: Real Time Energy Management System for Smart Buildings to Minimize the Electricity Bill. International Journal of Emerging Electric Power Systems 18(3), 2018, 1–15.

[2] Kaplan C.E.: Simplified Model and Genetic Algorithm Based Simulated Annealing Approach for Excitation Current Estimation of Synchronous Motor. Advances in electrical and computer engineering 18(4), 2018, 75–84.

[3] Lakrih S., Diouri J.: Combined Frequency Equivalent Model for Power Transmission Network Dynamic Behavior Analysis. International Journal of Emerging Electric Power Systems 19(2), 2018, 20170104.

[4] Popkov D.M., Lunyaka A.V, Krzhevytskyi V.S.: Implementation of Automated Electrical Accounting and Control Systems in the Example of Odesaoblenergo. Collection of scientific works Odessa National Academy of Food Technologies 53(3)/2017, 45–48.

[5] Scrabets F.P.: Electricity Supply: Tutorial. NSU 2015.

[6] Zhao W.Ye., et al.: A Grouping Strategy Based on Prime Factorization for Capacitor Voltage Balancing of the Modular Multilevel Converter, 2018, 570–580.

Ph.D. Serhiy Stets
e-mail: s.e.stets@nuwm.edu.ua

Associate professor of the Department of Automation, Electrical and Computer Integrated Technologies of National University of Water and Environmental Engineering. The basic directions of scientific work are: automation of systems of measurement and control of technological processes, development and research of mathematical models of objects and systems of automatic control, development and research of automated systems of management of hydro-mining of minerals and soil moisture.

http://orcid.org/0000-0003-0063-5009

B.Sc. Andii Stets
e-mail: stets_ak19@nuwm.edu.ua

Student of Department of Applied Mathematics of National University of Water and Environmental Engineering.
The main area of scientific work is the development, programming and research of mathematical models of objects and systems of automatic control.

http://orcid.org/0000-0002-8271-647X

otrzymano/received: 22.12.2019 *przyjęto do druku/accepted: 26.06.2020*

http://doi.org/10.35784/iapgos.1835

RESEARCH ON THE COMBUSTION PROCESS USING TIME SERIES

Żaklin Grądz
Lublin University of Technology, Department of Electronics and Information Technology, Lublin, Poland

Abstract. *In the combustion process, one of the most important tasks is related to maintaining its stability. Numerous methods of monitoring, diagnostics, and analysis of the measurement data are used for this purpose. The information recorded in the combustion chamber constitute one-dimensional time series. In the case of non-stationary time series, which can be transformed into the stationary form, the autoregressive integrated moving average process can be employed. The paper presented the issue of forecasting the changes in flame luminosity. The investigations discussed in the work were carried out with the ARIMA model (p,d,q). The presented forecasts of changes in flame luminosity reflect the actual processes, which enables to employ them in diagnostics and control of the combustion process.*

Keywords: time series, ARIMA model, flame luminosity

BADANIA PROCESU SPALANIA Z WYKORZYSTANIEM SZEREGÓW CZASOWYCH

Streszczenie. *W procesie spalania jednym z najważniejszych zadań jest zachowanie jego stabilności. Do tego celu wykorzystywanych jest wiele metod z zakresu monitorowania, diagnostyki i analizy danych pomiarowych. Zarejestrowane w komorze spalania informacje są jednowymiarowymi szeregami czasowymi. W przypadku niestacjonarnych szeregów czasowych, które można przekształcić do formy stacjonarnej, znalazły zastosowanie scałkowane procesy autoregresji i średniej ruchomej. W artykule przedstawiono problematykę prognozowania zmian intensywności świecenia płomienia. Badania zaprezentowane w pracy zostały przeprowadzone z wykorzystaniem modelu ARIMA(p,d,q). Przedstawione prognozy zmian intensywność świecenia płomienia odwzorowują rzeczywiste przebiegi, co pozwala wykorzystać je w diagnostyce i sterowaniu procesem spalania.*

Słowa kluczowe: szereg czasowy, model ARIMA, jasność świecenia płomienia

Introduction

Coal constitutes the main source of energy used in the energy economy. The need to protect the natural environment against its exploitation and increasing pollution necessitates implementation of Renewable Energy Sources in the energy sector [6, 8, 16, 19]. The application of biomass in the combustion process technologies contributes, i.a., to a reduction in the generation of sulphur and nitrogen oxides. The co-combustion of coal and biomass is usually realized through a direct co-combustion, involving simultaneous burning of the mixture in a combustion chamber [7, 15, 20, 25].

Combustion is a complex process. Its diagnostic is aimed at ensuring the stability of the process. The monitoring of the combustion process is implemented using optoelectronic systems, which enable acquiring measurement data from the flame in a non-invasive way [5, 9, 17, 18]. Since the obtained signal contains numerous variables characterizing the combustion process, it can be analyses using different methods [10, 21–24].

The measurement data recorded using a fiber optic probe are available in discrete, equal time steps – 1000 samples per second. They form a time series which reflects the changes occurring in flame during the combustion process. Identifying the transition from the stable to the unstable state, which may occur due to the changes in the process parameters or disturbances, is essential in the diagnostics of the combustion process. Conducting the forecast of changes in flame luminosity enables to detect such state.

The forecasting of future time series values can be carried out with the ARIMA model. In the autoregressive integrated moving average process, it is possible to employ non-stationary time series, which can be transformed into the stationary form. The selection of model parameters can be performed using the dependences of the autocorrelation function. The analysis of the selected model can be considered using Akaike's Information Criterion (AIC) and Bayesian Information Criterion (BIC), mean square error, as well as the significance criterion of model parameters [1, 3, 14].

The paper discusses one-dimensional time series of changes in flame luminosity for the selected cases of the combustion process: the first variant concerned 100% pulverized coal, whereas the second – a mixture of 80% coal and 20% biomass. The measurements were performed for different flame zones. The data from the first zone, which contained the most information, were presented. For the discussed cases, such parameters as the number of collected samples or measurement time were identical. The analysis of data was performed in time domain using autoregressive integrated moving average process. Using the ARIMA model, the time series for the flame luminosity data were presented and single-step, multi-step as well as interval forecasts were subsequently conducted on their basis. In the case of the interval forecasts, they were determined with 95% probability. This means that the forecast value of one-dimensional time series belongs to the confidence interval [18]. Due to the high correlation between the measurements and one-step forecasts, these models can be employed for the diagnostics as well as control of the combustion process. The application and forecasting using the ARIMA model was presented in literature [2, 4, 11–13].

1. Diagnostic system and data acquisition

The measurements of flame luminosity were conducted using fiber optic measurement probe which constitutes an element of the diagnostic system. This device was placed in the combustion chamber, where it acquired the data on the combustion process from the flame. The measurements were performed for four different flame zones (see Fig. 1).

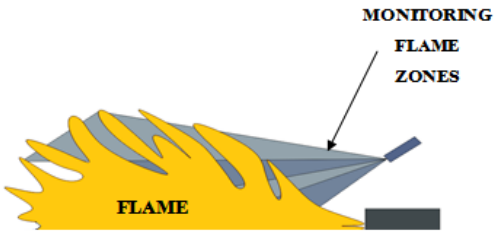

Fig. 1. Flame zones

The measurement data recorded by the flame monitoring system present the changes in flame luminosity in the form of a one-dimensional time series. The investigations were performed for two variants – pure coal and a mixture of 80% coal and 20% biomass, at constant parameters, constant thermal power of 400 kW and excess air coefficient λ=0.85. In both cases, the recorded data are characterized with identical measurement time and number of collected samples, i.e. over two millions for each configuration.

The figure below presents the time series of changes in flame luminosity for 100% pulverized coal (Fig. 2a) and mixture with biomass (Fig. 2b) recorded in the same flame zone.

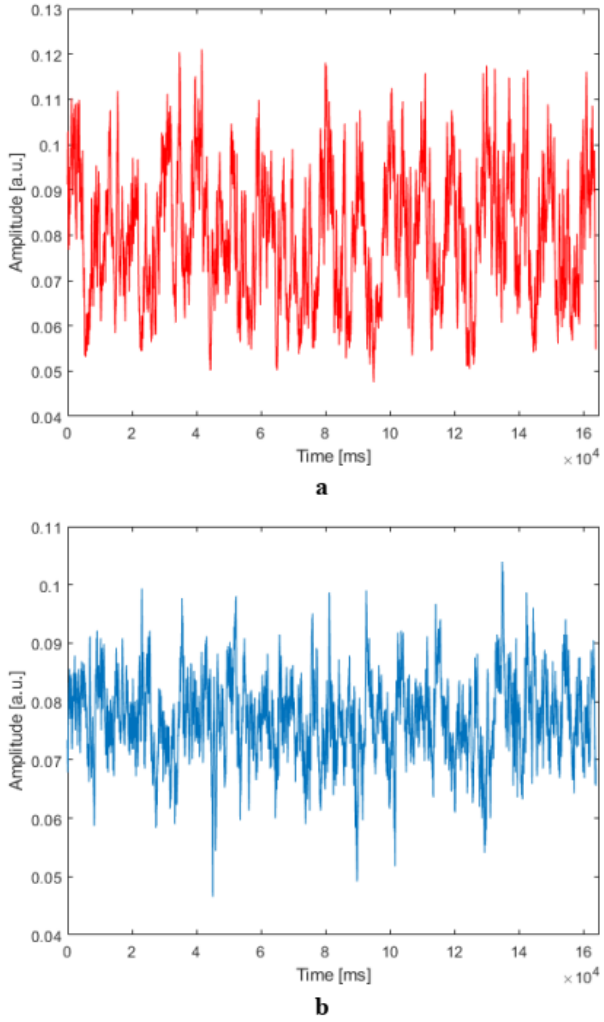

Fig. 2. Time series of changes in flame luminosity of a) coal, b) mixture of coal and biomass

2. Model ARIMA

ARIMA (Autoregressive Integrated Moving Average) models are frequently employed in the time series forecasting processes [18–22]. The basis for the model includes the autoregressive (AR) and moving average (MA) processes. This model finds application in the case of non-stationary time series, which may be transformed into stationary ones using, e.g. logarithmic transformations or differencing. The ARIMA model (p,d,q) is described by the components determining [18]:

- p – number of autoregressive parameters,
- d – order of differencing,
- q – number of parameters in the moving average.

Its generalized form is expressed with the dependence [18]:

$$\varphi^*(B)z_t = \varphi(B)\nabla^d z_t = \theta_0 + \theta(B)a_t, \quad (1)$$

where,

$$\varphi(B) = 1 - \varphi_1 B - \varphi_2 B^2 - \ldots - \varphi_p B^p, \quad (2)$$

$$\theta(B) = 1 - \theta_1 B - \theta_2 B^2 - \ldots - \theta_q B^q, \quad (3)$$

$$\varphi^*(B) = \nabla^d \varphi(B) \quad (4)$$

The variables represent [18]:

- $\varphi(B)$ – autoregressive operator
- $\varphi^*(B)$ – non-stationary autoregressive operator,
- $\theta(B)$ – moving average operator,
- ∇ – differencing operator.

On the basis of the methodology presented by Box&Jankins, the time series identification model involves: identification, estimation of parameters, and model verification.

3. Research results

For the analysis of time series and forecasting, 16384 (2^{14}) observations of changes in flame luminosity were conducted for the pulverized coal and the mixture of coal and biomass. The assessment of series shape for both configurations was performed and logarithmized in order to stabilize the series. The selection of ARIMA model parameters (p,d,q) was based on the analysis of autocorrelation plots. For the considered time series, the Autocorrelation function (ACF) and Partial Autocorrelation Function (PACF) plots were drawn (Fig. 4).

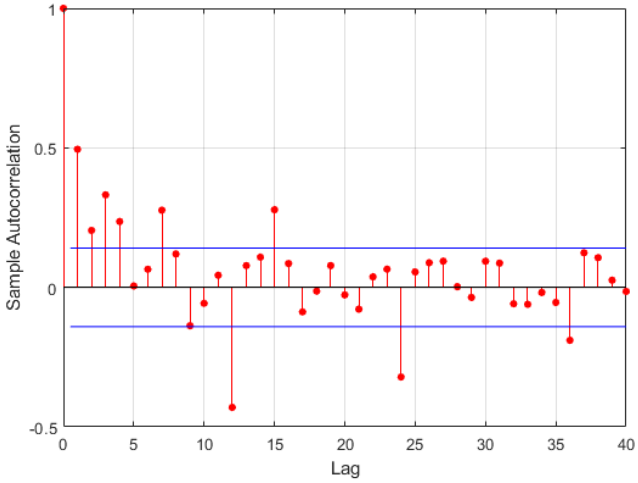

Fig. 3. Autocorrelation function of changes in flame luminosity for the mixture of pulverized coal and biomass

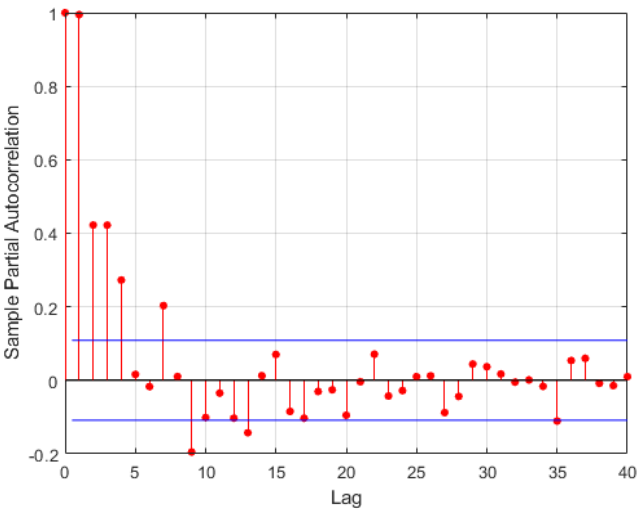

Fig. 4. Partial autocorrelation function of changes in flame luminosity for the mixture of pulverized coal and biomass

Then, the Box&Jankins methodology was employed to determine the p, d, and q parameters of the ARIMA model. When analyzing the number of statistically significant ACF parameters, the number of lags in the autoregressive model was determined, which amounted to p = 4 for the first series configuration and p = 7 for the mixture of coal and biomass. Using the same approach, the number of lags in the moving average was determined on the basis of the PACF parameters, amounting to q = 4 (pulverized coal) and q = 4 (mixture of coal and biomass). The differencing degree was set at d = 1 for both considered variants. Simultaneously, this means that in order to transform the time series into the stationary form, another differencing operation has to be performed.

On the basis of the determined parameters, several ARIMA model configurations were devised: (1,1,1); (4,1,4); (4,1,5) for 100% pulverized coal and (4,1,1); (3,1,4); (7,1,4) for the mixture.

Table 1. Values of information criteria for particular ARIMA models

	Akaike's Information Criterion (AIC)	Bayesian Information Criterion (BIC)
ARIMA model for 100% pulverized coal		
p = 1,d = 1,q = 1	-1,9041e+06	-1,9040e+06
p = 4,d = 1,q = 4	-1,9911e+06	-1,9910e+06
p = 4,d = 1,q = 5	-1,9679e+06	-1,9679e+06
ARIMA model for mixture of 80% coal and 20% biomass		
p = 1,d = 1,q = 1	-1,8464e+06	-1,8464e+06
p = 3,d = 1,q = 4	-1,9118e+06	-1,9117e+06
p = 7,d = 1,q = 4	-2,0054e+06	-2,0053e+06

In order to select the best ARIMA model parameters, the Akaike's Information and Bayesian Information criteria were employed. Table 1 presents the results of analysis for particular models.

While comparing the results presented in table 1, it was checked for which of the presented variants the value of information criterions was the lowest. As a result, the ARIMA model (4,1,4) was selected for the pure coal time series and ARIMA (7,1,4) was picked for the mixture of coal and biomass.

The next step involved conducting forecasts for the assumed model. Figures 5 and 6 present the one-step and multi-step forecasts and interval forecast for 95% probability of the analyzed time series of changes in flame luminosity for pulverized coal and the mixture of coal and biomass.

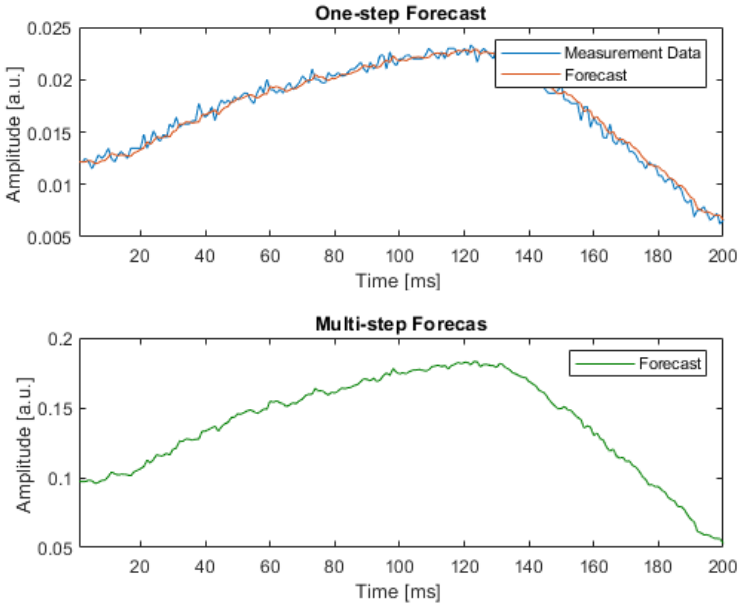

Fig. 5. Selected measurement data and one-step and multi-step forecasts of changes in flame luminosity for pulverized coal using the ARIMA model (4,1,4)

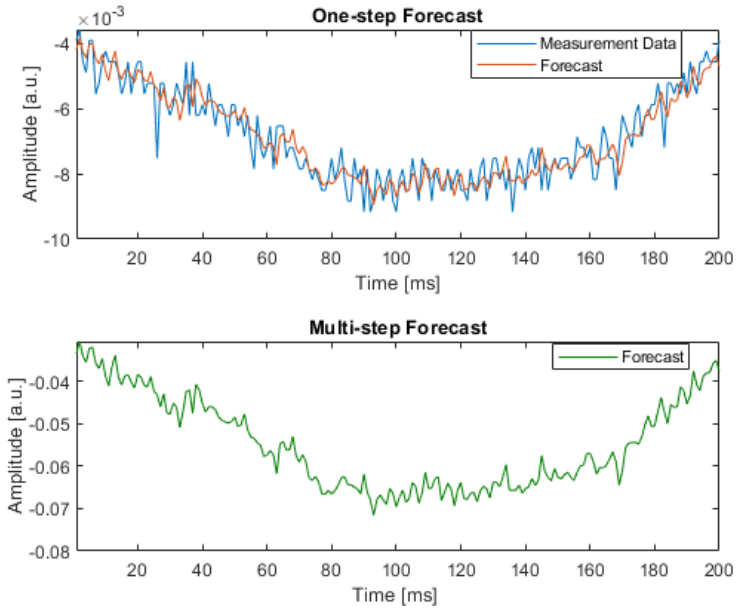

Fig. 6. Selected measurement data and one-step and multi-step forecasts of changes in flame luminosity for the mixture of 80% coal and 20% biomass using the ARIMA model (7,1,4)

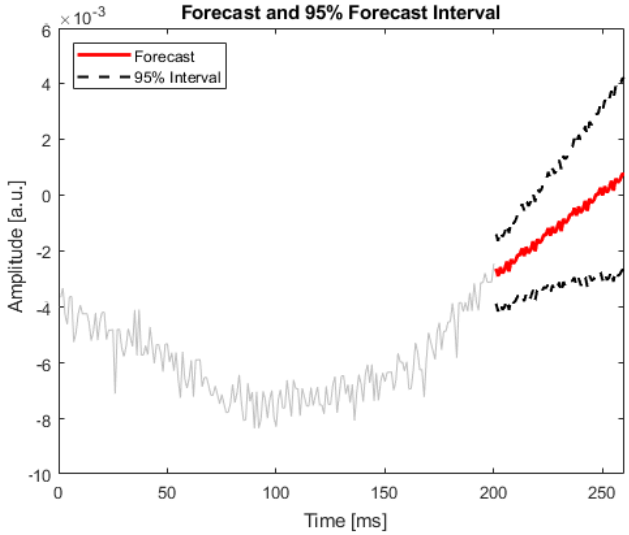

Fig. 7. Selected measurement data and interval forecast of changes in flame luminosity for mixture of 80% coal and 20% biomass using the ARIMA model (7,1,4)

The time series for 200 observations were plotted in order to present the forecast results in detail. The multi-step forecasts presented above were prepared for $l = 2$ offsets. When comparing forecasting charts, it should be noted that the multi-step forecast is far away from the measured data. The interval forecasts shown on plots present the interval to which the time series value corresponds with 95% probability. While comparing the shape of measurement data characteristics with a one-step forecast, a high correlation can be seen. The ARIMA model can be successfully used for diagnosing and controlling the combustion process. One-step forecasts, owing to their accuracy, are best suited for the analysis of changes occurring in flames during the combustion process.

4. Conclusions

The analysis of changes occurring in the flame during the combustion of pulverized coal or co-combustion of its mixtures, can be performed using numerous methods. The acquisition of data from the flame requires the application of specialist diagnostic systems, such as fiber optic measurement probe. These devices are resistant to high temperatures or possible dusting. The acquisition of measurement data using measurement systems enables recording large amounts of information on the changes occurring in flame. In the monitoring system, the data acquisition process is performed in the following steps: obtaining the data from the flame in the optical form, passing the data to the optoelectronic block, and transforming the information into the electronic form. Afterwards, the measurement data are subjected to further processing and analyses.

The measurement data were presented in the form of time series in two variants: I – pulverized coal and II – mixture of coal and biomass.

The paper presented the process of forecasting the changes in flame luminosity using the ARIMA model. Verification of the selected models using the quantitative criterion indicated that the forecasts should be performed using the ARIMA model (4,1,4) in the first variant and model p = 7, d = 2, q = 4 for the second variant. One-step and multi-step forecasts for $l = 2$ offsets and interval forecasts with 95% probability were prepared for the analyzed time series. The conducted one-step forecasts of changes in flame luminosity indicate high correlation with the real data. Forecasting can be successfully employed for the diagnostics of the combustion process, both for the time series of pure coal and its mixture with biomass.

References

[1] Box G.E.P, Jenkins G.M.: Analiza szeregów czasowych Prognozowanie i sterowanie, Warszawa 1983.
[2] Díaz-Robles L.A., Ortega J.C., Fu J.S. et al.: A hybrid ARIMA and artificial neural networks model to forecast particulate matter in urban areas: the case of Temuco, Chile. Atmospheric Environment 42(35), 2008, 8331–8340.
[3] Ding S., Dang Y.G., Li X.M., Wang J.J., Zhao K.: Forecasting Chinese CO2 emissions from fuel combustion using a novel grey multivariable model. Journal of Cleaner Production 162, 2017, 1527–1538.
[4] Jiang S., Yang C., Guo J., Ding Z.: ARIMA forecasting of China's coal consumption, price and investment by 2030. Energy Sources, Part B: Economics, Planning, and Policy 13(3), 2018, 190–195.
[5] Komada P.: Analiza procesu termicznej przeróbki biomasy. Monografie – Polska Akademia Nauk. Komitet Inżynierii Środowiska, Warszawa 2019.
[6] Korbicz J., Kościelny J.M., Kowalczuk Z., Cholewa W.: Diagnostyka procesów, Modele, Metody sztucznej inteligencji, Zastosowania. Wydawnictwo Naukowo-Techniczne, Warszawa 2002.
[7] Kordylewski W. i inni.: Spalanie i paliwa. Politechnika Wrocławska, Wrocław 2008.
[8] Kotyra A., Wojcik W., Gromaszek K., Smolarz A., Jagiełło, K.: Assessment of biomass-coal co-combustion on the basis of flame image. Przegląd Elektrotechniczny 88(11b), 2012, 241–243.
[9] Kotyra A., Wójcik W., Gromaszek K., Bazil G.: Application of flame image series analysis in estimation of biomass and coal combustion operating point. Przegląd Elektrotechniczny 8(92)2016, 129–132.
[10] Lu G., Yan Y., Colechin M.: A digital imaging based multifunctional flame monitoring system. IEEE Transactions on instrumentation and measurement, 53(4), 2004, 1152–1158.
[11] Mahla S.K., Parmar K.S., Singh J., Dhir A., Sandhu S.S., Chauhan B.S.: Trend and time series analysis by ARIMA model to predict the emissions and performance characteristics of biogas fueled compression ignition engine. Energy Sources, Part A: Recovery, Utilization, and Environmental Effects, 1–12.
[12] Ong C.S., Huang J.J., Tzeng G.H.: Model identification of ARIMA family using genetic algorithms. Applied Mathematics and Computation 164(3), 2005, 885–912.
[13] Sanchez A.B., Ordonez C., Lasheras F.S., Juez F.J.D., Roca-Pardinas J.: Forecasting SO_2 Pollution Incidents by means of Elman Artificial Neural Networks and ARIMA Models, Abstract and Applied Analysis 2013, Article ID 238259.
[14] Savchuk T. O., Kozachuk A., Gromaszek K., Sugurova L.: Forecasting the state of technogenic emergency situation on the railway transport using data mining technologies. Przegląd Elektrotechniczny 1, 2014, 50–54.
[15] Sawicki D., Kotyra A., Perdesh K.: Ekstrakcja cech obrazów płomienia współspalania węgla i biomasy z wykorzystaniem wizyjnego systemu diagnostycznego. Przegląd Elektrotechniczny 92(8), 2016, 133–136.
[16] Sawicki D., Kotyra A., Akhmetova A., Baglan I., Suleymenov A.: Using Optical Methods for Process State Classification of Co-firing of Coal and Biomass. Annual Set The Environment Protection 2(18), 2016, 404–415.
[17] Sawicki D., Kotyra A.: A quality factor of co-firing pulverized coal and biomass. Przegląd Elektrotechniczny 92(11), 2016, 140–143.
[18] Smolarz A., Wójcik W., Gromaszek K., Komada P., Lytvynenko V.I., Mussabekov N., Toigozhinova A.: Artificial intelligence methods in diagnostics of coal-biomass blends cocombustion in pulverised coal burners. Environmental Engineering V, 2017, 311–317.
[19] Wójcik W., Gromaszek K., Shegebayeva Z., Suleimenov B., Burlibay A.: Optimal control for combustion process. Przegląd Elektrotechniczny 90(4), 2014, 157–160.
[20] Wójcik W., Gromaszek K., Smailova S.: Using optical signals for pulverised coal combustion process optimal control to increase economic efficiency of the boiler. Actual Problems of Economics 4, 2013, 307–311.
[21] Wojcik W., Kotyra A., Komada P., Golec T.: Fiber optic system detecting the type of burned fuel in power boilers. Proc. of SPIE 5125, 2003.
[22] Wójcik W.: Application of fibre-optic flame monitoring systems to diagnostics of combustion process in power boilers. Bulletin of the Polish Academy of Sciences – Technical Sciences 56(2), 2008, 177–195.
[23] Wójcik W.: Światłowodowy układ do monitorowania procesu spalania, PAK 53(11), 2007, 24–28.
[24] Zhou H., Li Y., Tang Q., Lu G., Yan Y.: Combining flame monitoring techniques and support vector machine for the online identification of coal blends. Journal of Zhejiang University – Science A 18(9), 2017, 677–689.
[25] Zyska T., Wójcik W., Imanbek B., Zhirnova O.: Diagnostyka stanu czujnika termoelektrycznego w procesie zgazowania biomasy. Rocznik Ochrona Środowiska 18(2)/2016, 652–666.

M.Sc. Żaklin Grądz
e-mail: z.gradz@pollub.pl

Assistant in the Department of Electronics and Information Technology of Lublin University of Technology and Ph.D. student at the Electrical Engineering and Computer Science Faculty. Scientific activity includes the analysis of the combustion process in terms of its monitoring and diagnostics.

http://orcid.org/0000-0003-1902-4953

otrzymano/received: 08.05.2020 *przyjęto do druku/accepted: 26.06.2020*

http://doi.org/10.35784/iapgos.928

RESEARCH AND SIMULATION OF THE LOCAL NAVIGATION SYSTEM OF TERRESTRIAL MOBILE ROBOT

Andrii Rudyk[1], Viktoriia Rudyk[2], Mykhailo Matei[2]
[1]National University of Water and Environmental Engineering, Department of Automation, Electrical Engineering and Computer-Integrated Technologies, Rivne, Ukraine,
[2]Kyiv National University of Construction and Architecture, Faculty of Automation and Information Technology, Kyiv, Ukraine

Abstract. *The algorithm of complex information processing in the local navigation system of a terrestrial mobile robot and its physical model is developed. Experimental researches of this physical model have been carried out, as a result of which qualitative characteristics of the developed local navigation system have been determined. The trajectory of the object, based on the calculated navigation parameters, has a configuration identical to the actually passed route (adequate functioning of the system as a course indicator). The error in determining the coordinates of an offline object has value $0.012t^2$ (1.2 m per 10 s) when moving linearly and $0.022t^2$ (2.2 m per 10 s) when maneuvering. The orientation angles are worked out with precision $(0.1\div0.3)^o$ for roll and pitch angles and $(2\div3)^o$ for the angle of the course. Precise characteristics of the developed physical model LNS for determining orientation angles and motion parameters MR similar to the passport serial data SINS, and in some cases due to navigation features MR show even better accuracy.*

Keywords: local navigation system, mobile robot, algorithm of complex information processing, generalized Kalman filter, offline mode

BADANIA I MODELOWANIE LOKALNEGO SYSTEMU NAWIGACJI NAZIEMNEJ ROBOTA MOBILNEGO

Streszczenie. *Opracowano algorytm złożonego przetwarzania informacji w lokalnym systemie nawigacji naziemnego mobilnego robota i jego modelu fizycznego. Przeprowadzono eksperymentalne badania tego modelu fizycznego, w wyniku których określono cechy jakościowe opracowanego lokalnego systemu nawigacji. Trajektoria obiektu, określona na podstawie obliczonych parametrów nawigacyjnych, ma konfigurację identyczną z rzeczywistą przebytą trasą (system działa poprawnie jako wskaźnik). Błąd w określaniu współrzędnych obiektu offline wynosi $0{,}012t^2$ (1,2 m w 10 s) podczas ruchu liniowego i $0{,}022t^2$ (2,2 m w 10 s) podczas manewrowania. Kąty orientacji są obliczane z dokładnością $(0{,}1\div0{,}3)^o$ dla kątów przechyłu i pochylenia oraz $(2\div3)^o$ dla kąta kursu. Dokładne cechy opracowanego modelu fizycznego systemu do określania kątów orientacji i parametrów ruchu robota mobilnego są podobne do danych paszportowych seryjnych BINS, a w niektórych przypadkach, ze względu na cechy nawigacji robotów mobilnych, wykazują jeszcze lepszą dokładność.*

Słowa kluczowe: lokalny system nawigacji, robot mobilny, zintegrowany algorytm przetwarzania informacji, uogólniony filtr Kalmana, tryb offline

Introduction

Navigation in mobile robotics has a number of features that do not allow to effectively use the navigation equipment of other mobile objects. Therefore, to create navigation systems for mobile robots (MR) it is necessary to use several different navigation aids with their complexation and parallel processing of information taking into account the peculiarities of the object dynamics and kinematics [2].

1. Local navigation of mobile robots

There are two types of navigation of autonomous MR – global and local. The main task of global navigation systems is to formulate a plan of movement on a given digital map. Local navigation systems plan and control the execution of maneuvers that are part of moving along formed route. Local navigation is a scheme for navigating autonomous MR, which determines the relative coordinates of the object and its displacement parameters on a short time interval of up to 10 minutes. The main tasks of local navigation are [4]:

– determination of relative Cartesian coordinates and parameters of MR motion;
– planning and control of MR maneuvers implementation, of which consists moving along the formed route;
– adjusting the global navigation system to determine the absolute coordinates of the MR.

An example of using a Local Navigation System (LNS) is a safe trajectory control for moving in a confined space and MR navigation in the absence of data from external navigation sources (failure of GPS based positional adjustment system). Therefore, when developing LNS, such requirements are put [12]:

– ability to determine orientation angles (course, pitch, roll) of MR and its velocity and acceleration to form the desired trajectory;
– continuous delivery of navigation information;
– accuracy of calculation of MR coordinates at short time intervals;
– system autonomy, resistance to effect of obstacle and vibration;
– small overall dimensions and power consumption.

From the analysis of literary sources it is known that LNS MR can be implemented using active (inertial navigation, systems of technical vision) and passive (satellite, radio beacons and markers) navigation schemes [3, 11]. However, most of the advantages has inertial navigation, the main advantages of which are autonomy, no influence of weather conditions and radio electronic suppression, as well as secrecy (they do not generate electromagnetic radiation that can give off the presence of MR).

2. Structure and mathematical model of LNS

In [12], taking into account the above requirements, the structural diagram of the LNS is presented in Fig. 1. In this structure, the IMU is used to obtain information on the six degrees of MR freedom, each of consists of three accelerometers (A_x, A_y, A_z) and gyroscopes (G_x, G_y, G_z) or at least six accelerometers providing the navigation system with information on angular and linear displacements of MR [13]. Because the duration of autonomous use of such a navigation system is a short time interval of up to 10 minutes [10], then the exact characteristics of the inertial sensors are less important than the requirements for the equipment of autonomous objects – the size and price characteristics, reliability, resistance to shock, vibration, etc. In this regard, MEMS inertial sensors are often used to implement such systems [14, 15].

IMU prints data packets on on-board computer that contain information about angular velocities and imaginary system accelerations for each axes of the linked coordinate system (LCS). The data packets are fed to the input packet processing module (IPPM), where data packet integrity take place, component partitioning, and computing module (CM) validation useful information about angular velocities $(\omega_x, \omega_y, \omega_z)$ and imaginary accelerations (a_x, a_y, a_z) system in LCS. In CM, which consists of a recalculation unit (RU) and navigation algorithm calculation modules (NACM) and orientation algorithm (OACM) occurs processes of filtering and calculating the navigation parameters of MR – angles of course, pitch and roll (α, β, χ) and passed distance, speed and acceleration (s, v, n) [9]. The utilized IMU in LNS was a custom made device.

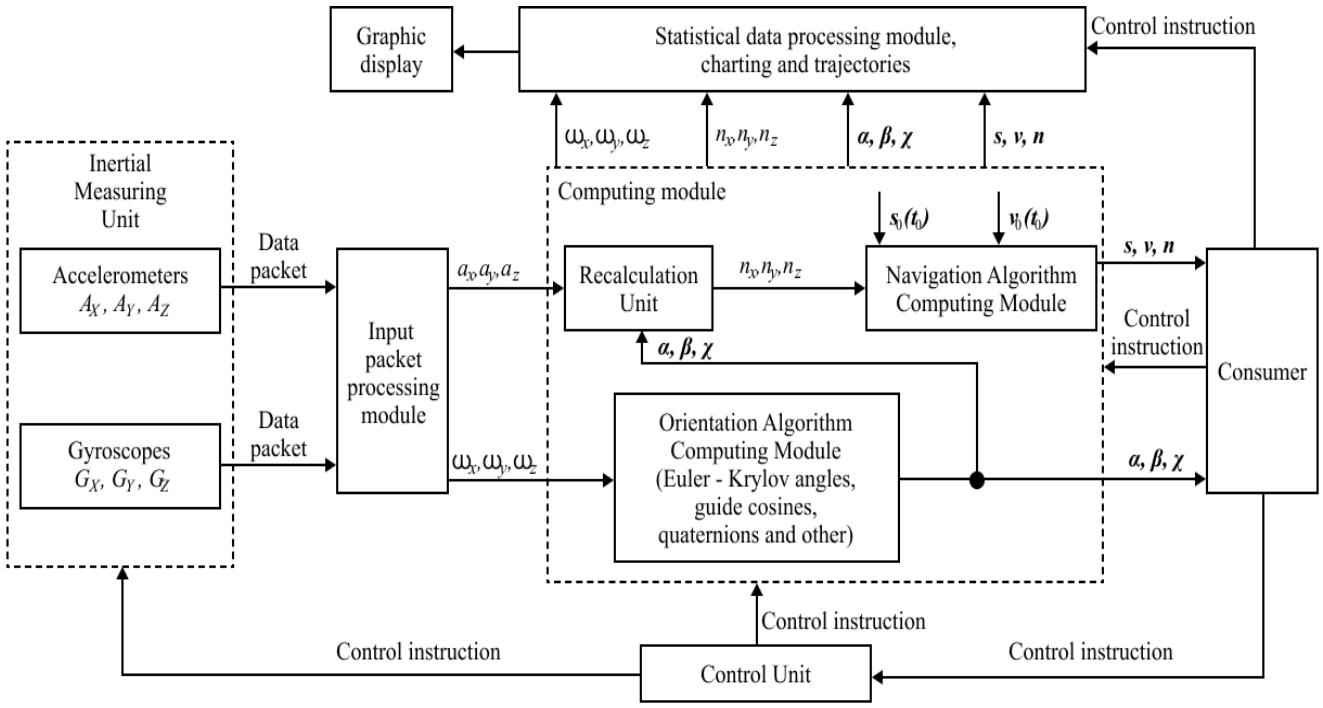

Fig. 1. Structural diagram of the local navigation system

Obtained navigation information, depending on the CM settings and the control commands from the consumer, can be issued in a different form to the graphical display using module of statistical data processing, charting and trajectories. The information from the IMU sensors in the processed IPPM form is stored in the CM memory for subsequent playback and data analysis [1]. The LNS control unit that controls the operation of the IMU and CM can be commanded by the consumer.

When moving MR, most of the wheels, we will take into account a number of features that affect the definition of navigation parameters: no lateral wear; small ranges of changes pitch and roll angles within short time intervals; the independence of the angular velocity of rotation about the vertical axis MR from the angular velocities of rotation about other axes; small linear speed of MR movement. With these features in mind, we will use the following mathematical model MR in the developed autonomous LNS:

$$\dot{\alpha} = \omega_z; \quad \dot{\beta} = \omega_x \cos\chi + \omega_z \sin\chi; \quad n_x = a_x \cos\chi + a_z \sin\chi;$$
$$\dot{\chi} = \omega_y; \quad n_y = a_x \sin\beta \sin\chi + a_y \cos\beta - a_z \sin\beta \cos\chi;$$
$$n_z = -a_x \cos\beta \sin\chi + a_y \sin\beta + a_z \cos\beta \cos\chi - g;$$
$$v(t_1) = v_0(t_0) + \int_{t_0}^{t_1} n_y dt; \quad s(t_1) = s_0(t_0) + \int_{t_0}^{t_1}\int_{t_0}^{t_1} n_y dt,$$

where n_x, n_y, n_z – projections of true acceleration on the axis of the moving trajectory coordinate system (MTCS); $v_0(t_0), s_0(t_0)$ – initial velocity values and coordinates at time t_0 (initial conditions).

To account for the accumulation of SINS integration errors [17] we supplement the system mathematical model with equations that relate the measured values of the angular velocities and the components of MR imagined acceleration with their true values $\omega_j^m = \omega_j + \varepsilon_j$ and $a_j^m = a_j + \psi_j$, where ω_j^m, a_j^m – values of angular velocities and components of the imagined acceleration of MR, that are determined by sensors; ω_j, a_j – the true values of the angular velocities and the components of the imagined acceleration MR; ε_j, ψ_j – measurement errors; $j = \{x, y, z\}$.

3. Development of the algorithm of complex information processing

Because all measured and observed quantities are related by nonlinear dependencies, to determine the vector of the MR state by the vector of measurement of inertial sensors at each moment of time is used nonlinear filtering algorithm – generalized Kalman filter (GKF) [5]. In this case, the task of estimating the vector state x_i comes down to filtering the Markov sequence $x_i = \Phi_i(x_{i-1}) + \vartheta_i$ by the measurements taken at each *i*-th time $y_i = \varphi_i(x_i) + \lambda_i$ in the Gaussian nature of generating noises ϑ_i and measurement errors λ_i. Function $\Phi_i(x_{i-1})$ characterizes the dynamics of the state vector change, and the function $\phi_i(x_i)$ – measurement vector connection y_i with him.

GKF is based on a Gaussian approximation of posterior density in the Taylor series expansion of functions $\Phi_i(x_{i-1})$ and $\varphi_i(x_i)$ (x_{l1}, x_{l2} – points of linearization):

$$\Phi_i(x_{i-1}) \approx \Phi_i(x_{l1}) + \frac{\partial \Phi_i(x_{l1})}{\partial x_{i-1}^T}(x_{i-1} - x_{l1}) \quad (1)$$

$$\phi_i(x_i) \approx \phi_i(x_{l2}) + \frac{\partial \phi_i(x_{l2})}{\partial x_i^T}(x_i - x_{l2}) \quad (2)$$

As points of linearization in (1) and (2) is used vector state estimation of the previous and posterior estimation of the current steps: $x_{l1} = \tilde{x}_{i-1}, x_{l2} = \tilde{x}_{i/i-1}$.

Thus, the mathematical apparatus of one iteration of the GKF algorithm consists in the sequential determination of the following quantities:

– aposteriori evaluation of the state vector

$$\tilde{x}_{i/i-1} = \Phi_i(x_{l1}) + \frac{\partial \Phi_i(x_{l1})}{\partial x_{i-1}^T}(\tilde{x}_{i-1} - x_{l1}) \quad (3)$$

– covariance matrix of the state vector posterior estimation

$$P_{i/i-1}(x_{l1}) = \frac{\partial \Phi_i(x_{l1})}{\partial x_{i-1}^T} P_{i-1} \left(\frac{\partial \Phi_i(x_{l1})}{\partial x_{i-1}^T} \right)^T + Q_i \quad (4)$$

where Q_i – matrix of intensity of generating noises;

– covariance matrix of the current state vector estimator

$$P_i\left(x_{l1}, x_{l2}\right)=\left(\left(P_{i/i-1}\left(x_{l1}\right)\right)^{-1}+\left(\frac{\partial\phi_i\left(x_{l2}\right)}{\partial x_i^T}\right)^T R_i \frac{\partial\phi_i\left(x_{l2}\right)}{\partial x_i^T}\right)^{-1} \quad (5)$$

– Kalman filter gain coefficient

$$K_i\left(x_{l1}, x_{l2}\right)=P_i\left(x_{l1}, x_{l2}\right)\left(\frac{\partial\phi_i\left(x_{l2}\right)}{\partial x_i^T}\right)^T R_i \quad (6)$$

where R_i – measurement noise intensity matrix;

– current assessment of the state vector

$$\tilde{x}_i=\tilde{x}_{i/i-1}+K_i\left(x_{l1}, x_{l2}\right)\left(y_i-\phi_i\left(x_{l2}\right)-\frac{\partial\phi_i\left(x_{l2}\right)}{\partial x_i^T}\left(\tilde{x}_{i/i-1}-x_{l2}\right)\right) \quad (7)$$

On the basis of the mathematical model of Local Navigation System, the type used in (3)–(7) matrices and vectors. The measurement vector is thus shaped $y_i=\left(\omega_{xi}, \omega_{yi}, \omega_{zi}, a_{xi}, a_{yi}, a_{zi}\right)^T$, and a 21-dimensional state vector consist of values from mathematical model equations, changing velocity of the filtered values $\ddot{\alpha}, \ddot{\beta}, \ddot{\chi}$ and $\ddot{n}_x, \ddot{n}_y, \ddot{n}_z$, which are necessary to determine the dynamics matrix $\Phi_i\left(x_{i-1}\right)$. Because information about these parameters is not available, they are modeled by generating noise in the form of Markov stationary processes [6–8]. Finally, the system dynamics matrix $\Phi_i\left(\tilde{x}_{i-1}\right)$, link of the measurement vector to the system state vector $\varphi_i\left(\tilde{x}_{i/i-1}\right)$ covariance Q_i generating noises ϑ_i and covariances R_i measurement noise λ_i described by (8)–(11). In this formulas $E_j=exp\left(-\Delta t/\tau_j\right)$, τ_j – time constants for modeling the rate of change of filtered quantities that characterize the possible frequency of their change; $\Delta t=t_i-t_{i-1}$ – discretization period; Q_j – the intensity of white noise by which the rate of change of the filtered values is simulated; N_j – intensity of measurement noise.

The following is a list of parameters that must be defined or specified to enable the use of the resulting matrices in the generalized Kalman filter filtering algorithm [16]: the initial values of the state vector x_0 and covariance matrices P_0; the value of the discretization period Δt; value of time constants of simulated Markov processes τ_j; intensity of generating noises Q_j and measurement noise N_j. The optimal values of these parameters are selected in the research of the physical model.

$$\Phi_i\left(\tilde{x}_{i-1}\right)=\begin{vmatrix}
1 & \Delta t & 0 & 0 & 0 & 0 & 0 & 0 & 0 & 0 & 0 & 0 & 0 & 0 & 0 & 0 & 0 & 0 & 0 & 0 & 0\\
0 & 1 & \Delta t & 0 & 0 & 0 & 0 & 0 & 0 & 0 & 0 & 0 & 0 & 0 & 0 & 0 & 0 & 0 & 0 & 0 & 0\\
0 & 0 & E_\alpha & 0 & 0 & 0 & 0 & 0 & 0 & 0 & 0 & 0 & 0 & 0 & 0 & 0 & 0 & 0 & 0 & 0 & 0\\
0 & 0 & 0 & 1 & \Delta t & 0 & 0 & 0 & 0 & 0 & 0 & 0 & 0 & 0 & 0 & 0 & 0 & 0 & 0 & 0 & 0\\
0 & 0 & 0 & 0 & 1 & \Delta t & 0 & 0 & 0 & 0 & 0 & 0 & 0 & 0 & 0 & 0 & 0 & 0 & 0 & 0 & 0\\
0 & 0 & 0 & 0 & 0 & E_\beta & 0 & 0 & 0 & 0 & 0 & 0 & 0 & 0 & 0 & 0 & 0 & 0 & 0 & 0 & 0\\
0 & 0 & 0 & 0 & 0 & 0 & 1 & \Delta t & 0 & 0 & 0 & 0 & 0 & 0 & 0 & 0 & 0 & 0 & 0 & 0 & 0\\
0 & 0 & 0 & 0 & 0 & 0 & 0 & 1 & \Delta t & 0 & 0 & 0 & 0 & 0 & 0 & 0 & 0 & 0 & 0 & 0 & 0\\
0 & 0 & 0 & 0 & 0 & 0 & 0 & 0 & E_\chi & 0 & 0 & 0 & 0 & 0 & 0 & 0 & 0 & 0 & 0 & 0 & 0\\
0 & 0 & 0 & 0 & 0 & 0 & 0 & 0 & 0 & 1 & 0 & 0 & 0 & 0 & 0 & 0 & 0 & 0 & 0 & 0 & 0\\
0 & 0 & 0 & 0 & 0 & 0 & 0 & 0 & 0 & 0 & 1 & 0 & 0 & 0 & 0 & 0 & 0 & 0 & 0 & 0 & 0\\
0 & 0 & 0 & 0 & 0 & 0 & 0 & 0 & 0 & 0 & 0 & 1 & 0 & 0 & 0 & 0 & 0 & 0 & 0 & 0 & 0\\
0 & 0 & 0 & 0 & 0 & 0 & 0 & 0 & 0 & 0 & 0 & 0 & 1 & \Delta t & 0 & 0 & 0 & 0 & 0 & 0 & 0\\
0 & 0 & 0 & 0 & 0 & 0 & 0 & 0 & 0 & 0 & 0 & 0 & 0 & E_{n_x} & 0 & 0 & 0 & 0 & 0 & 0 & 0\\
0 & 0 & 0 & 0 & 0 & 0 & 0 & 0 & 0 & 0 & 0 & 0 & 0 & 0 & 1 & \Delta t & 0 & 0 & 0 & 0 & 0\\
0 & 0 & 0 & 0 & 0 & 0 & 0 & 0 & 0 & 0 & 0 & 0 & 0 & 0 & 0 & E_{n_y} & 0 & 0 & 0 & 0 & 0\\
0 & 0 & 0 & 0 & 0 & 0 & 0 & 0 & 0 & 0 & 0 & 0 & 0 & 0 & 0 & 0 & 1 & \Delta t & 0 & 0 & 0\\
0 & 0 & 0 & 0 & 0 & 0 & 0 & 0 & 0 & 0 & 0 & 0 & 0 & 0 & 0 & 0 & 0 & E_{n_z} & 0 & 0 & 0\\
0 & 0 & 0 & 0 & 0 & 0 & 0 & 0 & 0 & 0 & 0 & 0 & 0 & 0 & 0 & 0 & 0 & 0 & 1 & 0 & 0\\
0 & 0 & 0 & 0 & 0 & 0 & 0 & 0 & 0 & 0 & 0 & 0 & 0 & 0 & 0 & 0 & 0 & 0 & 0 & 1 & 0\\
0 & 0 & 0 & 0 & 0 & 0 & 0 & 0 & 0 & 0 & 0 & 0 & 0 & 0 & 0 & 0 & 0 & 0 & 0 & 0 & 1
\end{vmatrix} \cdot \tilde{x}_{i-1} \quad (8)$$

$$Q_i=diag\begin{bmatrix}0 & 0 & \left(1-E_\alpha^2\right)Q_\alpha & 0 & 0 & \left(1-E_\beta^2\right)Q_\beta & 0 & 0 & \left(1-E_\chi^2\right)Q_\chi & 0 & 0 & 0\\ 0 & \left(1-E_{n_x}^2\right)Q_{n_x} & 0 & \left(1-E_{n_y}^2\right)Q_{n_y} & 0 & \left(1-E_{n_z}^2\right)Q_{n_z} & 0 & 0 & 0\end{bmatrix} \quad (9)$$

$$\phi_i\left(\tilde{x}_{i/i-1}\right)=\begin{vmatrix}
\dfrac{\dot{\beta}_{i/i-1}-\dot{\alpha}_{i/i-1}\sin\chi_{i/i-1}}{\cos\chi_{i/i-1}}+\varepsilon_{xi/i-1}\\
\dot{\chi}_{i/i-1}+\varepsilon_{yi/i-1}\\
\dot{\alpha}_{i/i-1}+\varepsilon_{zi/i-1}\\
n_{xi/i-1}\cos\chi_{i/i-1}+\left(n_{yi/i-1}\sin\beta_{i/i-1}-\left(n_{zi/i-1}+g\right)\cos\beta_{i/i-1}\right)\sin\chi_{i/i-1}+\psi_{xi/i-1}\\
n_{yi/i-1}\cos\beta_{i/i-1}+\left(n_{zi/i-1}+g\right)\sin\beta_{i/i-1}+\psi_{yi/i-1}\\
n_{zi/i-1}\sin\chi_{i/i-1}+\left(n_{yi/i-1}\sin\beta_{i/i-1}-\left(n_{zi/i-1}+g\right)\cos\beta_{i/i-1}\right)\cos\chi_{i/i-1}+\psi_{zi/i-1}
\end{vmatrix} \quad (10)$$

$$R_i=diag\begin{bmatrix}N_\alpha & N_\beta & N_\chi & N_{n_x} & N_{n_y} & N_{n_z}\end{bmatrix} \quad (11)$$

4. Investigation of the physical model of LNS

For experimental tuning of LNS parameters and verification of the proposed algorithm for calculation accuracy of MR navigation parameters, a physical model of the system was implemented, which is a combination of IMU (MEMS chip triaxial accelerometer and magnetometer type LSM303DHL and triaxial gyroscope type L3G42000D) and a GPS receiver with a built-in antenna and designed to determine the coordinates of the object and the orientation angles of the object. Using such a system without a GPS receiver is similar to autonomous mode.

To implement the functions Computing module, Input packet processing module and Control unit (Fig. 1) has been developed software that performs such functions in accordance with the block diagram LNS: receiving and processing IMU data packets; calculation of navigational parameters of MR by the implemented algorithm of information processing; saving the MR motion parameters obtained from the IMU during the experiment, in Statistical data processing module, charting and trajectories (SDPMCT) for further reproduction, processing and analysis of results.

Based on the work results, the authors developed two options for the implementation of inertial orientation microsystems based on the Kalman filter: for the MR control circuit (Fig. 2a) and for the backup orientation system (Fig. 2b). These orientation systems have been successfully tested and have shown stable operation during long-term operation (5 hours or more). The technical characteristics of orientation systems are shown in table 1.

Table 1. Technical characteristics of inertial orientation microsystems

Characteristic	Value	
	Based on Kalman filter	Backup system
Supply voltage, V	7 … 12	9, ±15
Supply current, A	0.35	0.5 (9 V); 0.1 (±15 V)
Measured angular velocities range, °/s	±400	±100
Measured accelerations range, *g*	0 … 6	0 … 10
Angle detection range: – course, ° – pitch, ° – roll, °	 0 … 360 ±90 ±180	 – ±90 ±180
The maximum error course angle determining: – linearly moving, ° – when maneuvering, °	 1.85 2.8	 – –
The maximum error pitch angle determining: – linearly moving, ° – when maneuvering, °	 1.9 2.95	 2.0 3.1
The maximum error roll angle determining: – linearly moving, ° – when maneuvering, °	 2.1 2.8	 2.2 2.9
Weight, gram	100	750
Overall dimensions, mm	50×50×50	80, Ø118

Experimental researches of the physical model were conducted in a brick room with a minimum number of metal surfaces and in the open space (uniform asphalt pavement). The length of the MR trajectory was up to 80 m when moving in a straight line and up to 35 m when maneuvering.

In the GPS receiver algorithmically compensates systematic errors from the receiver clock offset relative to the system scale and from ionospheric and tropospheric signal delays on the propagation path. However, there are random errors due to the influence of internal noise of the receiver, which in the conditions of "open sky" lead to random errors in determining the coordinates with a standard deviation (2–3) m. Deterioration of the accuracy of satellite measurements due to the "shading" of the sky by tall buildings and multi-beam signal propagation leads to an increase in standard deviations of the coordinates up to 7 m and the modulus of absolute speed up to 0.25 m/s.

At the rectilinear movement of MR (at a constant angle of a course) exact characteristics are better, than at maneuvering. However, over time, the error in determining the longitudinal component of velocity and coordinates gradually increases and reaches the characteristic errors of GNSS [8].

When maneuvering, any nonlinearity of the trajectory shape is characterized by a change in the course angle. Significant changes in the course angle when turning lead to an increase of errors in determining the coordinates of the MR. When maneuvering on a trajectory with the shape of a circle, the course angle changes linearly, and the standard deviation of the error of determining the coordinates is almost constant.

In the researches, the maximum time of satellite loss was 5 minutes with a minimum duration of the initial full-constellation correction of 1 minute. Therefore, the question of the initial installation of SINS is relevant.

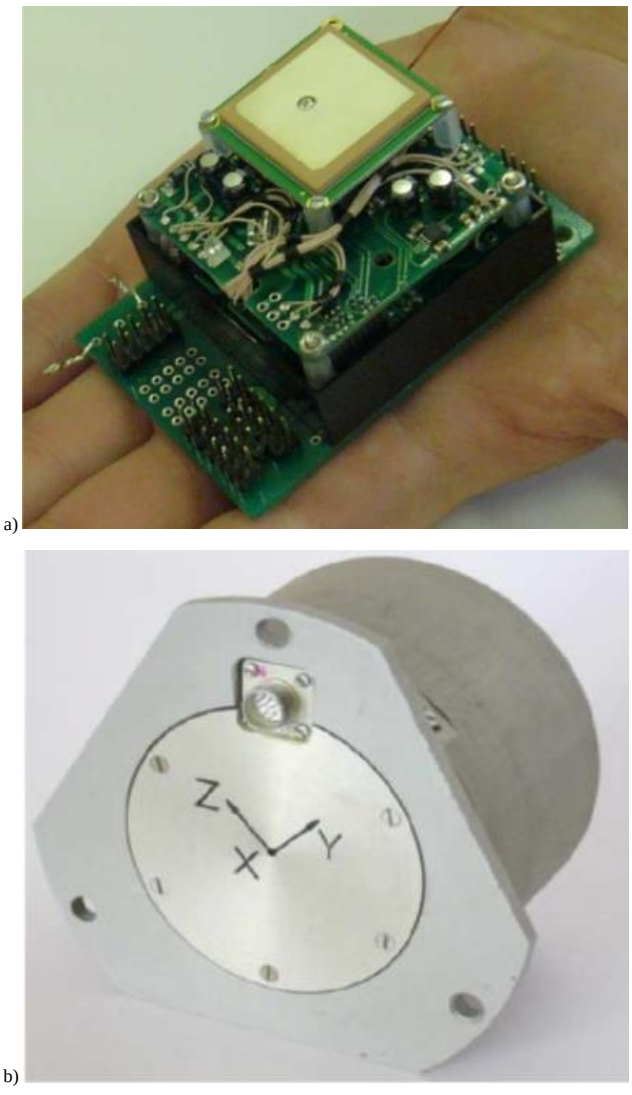

Fig. 2. Implementation of inertial orientation microsystems based on Kalman filter: for the MR control circuit (a) and for the backup orientation system (b)

The results of experimental researches of the physical model are shown in Fig. 3 and Fig. 4, which allows us to draw conclusions about the following qualitative characteristics of the developed LNS:

– trajectory of the object based on the calculated navigation parameters, has a configuration identical to the actually completed route (adequate LNS operation as a course pointer);

– the error of determining the coordinates of the LNS object in offline has a value $0.012t^2$ (1.2 m per 10 s) when moving linearly and $0.022t^2$ (2.2 m per 10 s) when maneuvering;
– refinement of the MR orientation angles is accurate $(0.1 \div 0.3)^o$ for roll and pitch angles and $(2 \div 3)^o$ for the angle of the course;
– accurate characteristics of the developed physical model LNS for determining the orientation angles and MR motion parameters are similar to the serial SINS passport data, and in some cases at the expense of navigation features MR show slightly better accuracy.

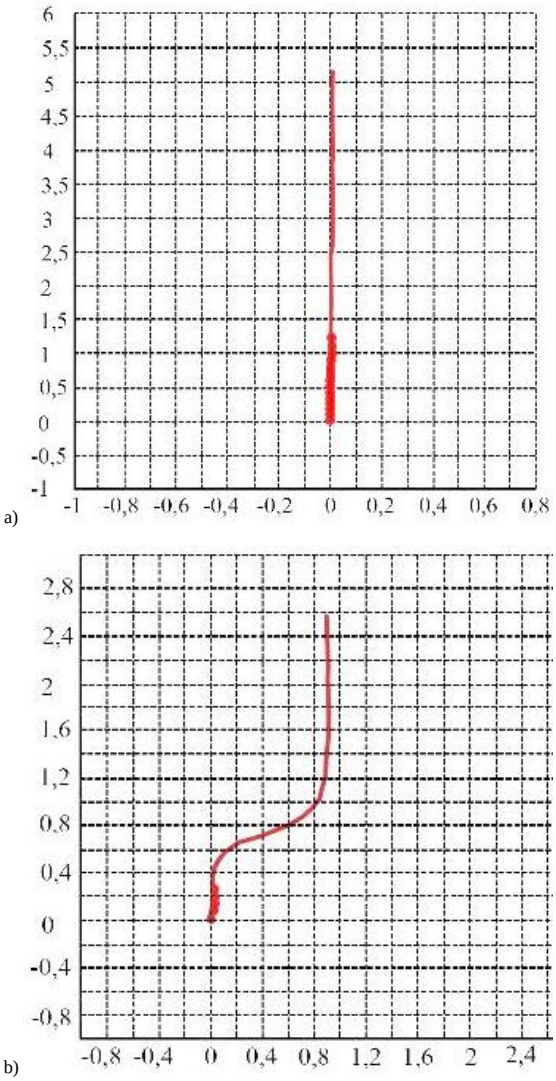

Fig. 3. Actual object trajectories obtained by a physical model in the case of straight-line displacement (a) and maneuvering (b)

According to certain qualitative characteristics of the physical model we can make the following conclusions about using the developed LNS:

– autonomous use of LNS indoors is possible at short time intervals (5÷10) s; in open areas, autonomous using time is up to 60 s, and the provided accuracy is comparable to accuracy of GPS;
– the use of this LNS in the navigation system is acceptable and has some advantages over the known analogues.

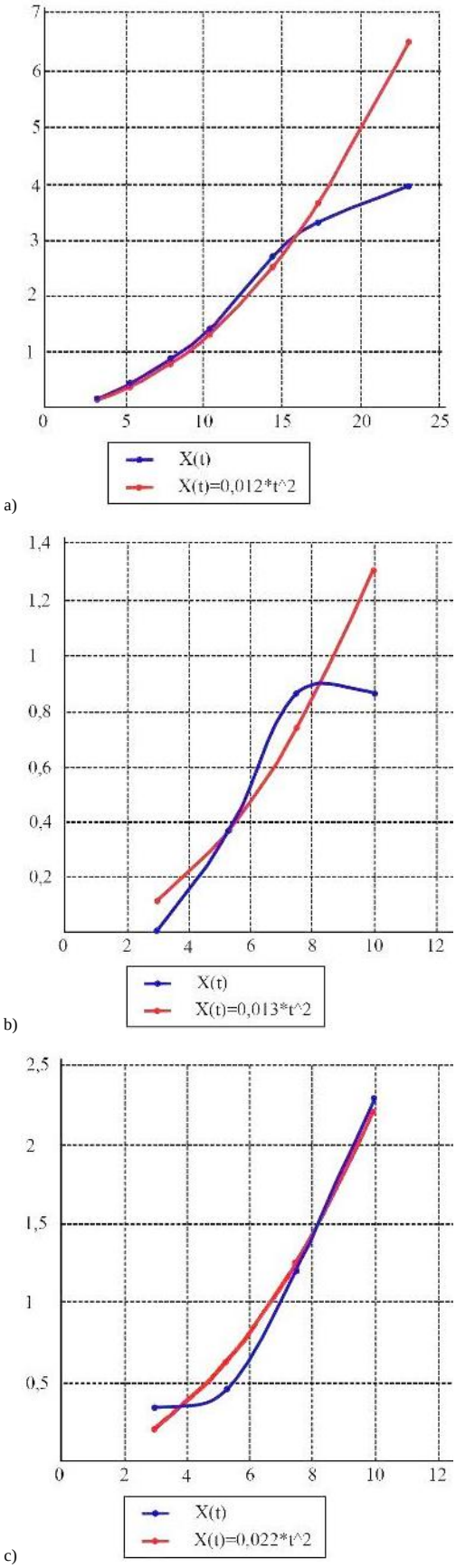

Fig. 4. Dependencies of object coordinate errors (observed deviation of the robot actual route from the measured IMU readings) over time (blue curves) and approximating functions (red curves) when moving linearly (a) and when maneuvering (b, c)

5. Conclusions

The results of investigations of the physical model of the developed LNS confirm the possibility of its use in the navigation complex of terrestrial MR. The system provides accuracy in determining the coordinates of the object and its orientation angles and it allows you to use the developed system as a stand-alone system to control maneuvers when moving the MR along a safe route for short intervals, and in combination with other navigation devices (GPS, odometers, rangefinders, etc.). In the future it is planned to improve the mathematical model and algorithm of information and software processing to calculate the navigation parameters of an object to improve the accuracy of the system, as well as the practical implementation of the advanced system and integrate it into the navigation complex for terrestrial MR.

References

[1] Arvanitakis I., Giannousakis K., Tzes A.: Mobile robot navigation in unknown environment based on exploration principles. Control Applications (CCA), IEEE Conference on. IEEE, 2016, 493–498.

[2] Corke P.: An introduction to inertial and vision sensing. International Journal of Robotics Research 6(26), 2007, 519–535.

[3] Farrell J.A.: Aided Navigation: GPS with High Rate Sensors. McGraw-Hill, New York 2008.

[4] Gang L., Wang J.: PRM path planning optimization algorithm research. Wseas Transactions on Systems and Control 11, 2016, 81–86.

[5] Grewal M.S., Weill L.R., Andrews A.P.: Global Position Systems, Inertial Navigation and Integration. John Wiley & Sons, New York 2001.

[6] Grewal M.S., Andrews A.P.: Kalman filtering: theory and practice using MATLAB. J. Wiley & Sons. Inc., New York 2001.

[7] Groves P.D.: Principles of GNSS, Inertial and Multisensor Integrated Navigation Systems. Artech House 2008.

[8] Ingle V.K., Proakis J.G.: Digital Signal Processing Using MATLAB. V.4. PWS Publishing Company, Boston 2009.

[9] Ko D.W., Kim Y.N., Lee J.H., Suh I.H.: A scene-based dependable indoor navigation system. Intelligent Robots and Systems (IROS), IEEE/RSJ International Conference on. IEEE, 2016, 1530–1537.

[10] Kvasnikov V.P., Rudyk A.V.: Practical estimation of errors of single-channel strapdown inertial navigation system on MEMS sensors in a short time interval. Visnyk of Ukraine Engineering Academy 1, 2017, 98–105.

[11] Rudyk A.V.: Methods for evaluating the spatial position of objects. Integrated Intelligent Robotics (IIRTC-2016), 2016, 31–33.

[12] Rudyk A.V.: Development of a local navigation system for a terrestrial mobile robot. Modern problems of radio electronics, telecommunications and instrumentation, Vinnytsia 2017, 75–76.

[13] Rudyk A.V.: Comparative analysis of the accuracy characteristics of classical and accelerometric inertial navigation systems. Measurement, control and diagnostics in technical systems, Vinnytsia 2017, 209–210.

[14] Rudyk A.V.: Analysis of the errors of MEMS accelerometers by the Allan variation method. Visnyk of Zhytomyr State Technological University. Series: Technical Sciences 1, 2017, 100–109.

[15] Titterton D.H., Weston J.L.: Strapdown Inertial Navigation Technology. Stevenage: Institution of Electrical Engineers York, 2004.

[16] Wang L., Zhao L., Huo G., Li R., Hou Z., Luo P., et al.: Visual semantic navigation based on deep learning for indoor mobile robots. Complexity, 2018. Article ID: 1627185.

[17] Weiping Jiang, Li Wang, Xiaoji Niu, Zhang Quan, Zhang Hui, Tang Min: High-precision image aided inertial navigation with known features: observability analysis and performance evaluation. Sensors 14(10), 2014, 19371–19401.

Prof. D.Sc.(Technical) Andrii Rudyk
e-mail: a.v.rudyk@nuwm.edu.ua

Professor of Automation, electrical engineering and computer integrated technologies Department, National University of Water and Environmental Engineering, Rivne, Ukraine.
The main scientific direction – development of methods and devices for measuring motion parameters of mobile robots. Author over 150 scientific papers, including 12 patents.

http://orcid.org/0000-0002-5981-3124

Student Viktoriia Rudyk
e-mail: vikka2612@gmail.com

Student of Kyiv National University of Construction and Architecture, Faculty of Automation and Information Technology, Kyiv, Ukraine.
Engaged in scientific mathematical simulation of various processes, computer techniques and computer technologies, programming. Author over 20 scientific papers.

http://orcid.org/0000-0001-8014-1054

Student Mykhailo Matei
e-mail: nomiso432@gmail.com

Student of Kyiv National University of Construction and Architecture, Faculty of Automation and Information Technology, Kyiv, Ukraine.
Engaged in scientific mathematical simulation of various processes, computer techniques and computer technologies, programming. Author over 10 scientific papers.

http://orcid.org/0000-0002-5151-5122

otrzymano/received: 22.12.2019 *przyjęto do druku/accepted: 26.06.2020*

http://doi.org/10.35784/iapgos.1617

DESIGN OF MULTIFUNCTION SIMULATOR FOR ENGINE ROOM PERSONNEL TRAINING

Artem Ivanov[1], Igor Kolosov[2], Vadim Danyk[1], Sergey Voronenko[1], Yurii Lebedenko[3], Hanna Rudakova[3]
[1]Kherson State Maritime Academy, Department of Ship Electrical Equipment and Automatic Devices Operation, Kherson, Ukraine, [2]Marlow Navigation Ukraine, Odessa, Ukraine, [3]Kherson National Technical University, Department of Automation, Robotics and Mechatronics, Kherson, Ukraine

Abstract. *International requirements for improving energy efficiency and environmental protection and the necessary goals for their implementation in the marine industry are an actual problem. To integrate state-of-the-industry technologies and marine specialists education, the training complex is proposed. It is based on the platform of a hardware-software complex with the ability to integrate training equipment, simulators and software. That makes such a training complex multitask, universal, and flexible in achieving a variety of tasks and goals. The complex also implements high-quality education and training of marine specialists, conducting research after processing working out the results of engineering modelling of structural, thermal power, hydraulic, electrical, electronic, multi-physical and other solutions. The need to use the training complex allows us to form the necessary competence of the engine team personnel, develop methods and criteria for assessing competence, evaluate and demonstrate practical skills.*

Keywords: power systems, standards activities, energy efficiency, training, performance evaluation

PROJEKTOWANIE WIELOFUNKCYJNEGO SYMULATORA DO SZKOLENIA PERSONELU MASZYNOWNI

Streszczenie. *Międzynarodowe wymogi dotyczące poprawy efektywności energetycznej i ochrony środowiska oraz cele niezbędne do ich wdrożenia w przemyśle morskim stanowią aktualny problem. W celu zintegrowania najnowocześniejszych technologii i kształcenia specjalistów z branży morskiej proponuje się utworzenie kompleksu szkoleniowego. Jest on oparty na platformie kompleksu sprzętowo-programowego z możliwością integracji sprzętu szkoleniowego, symulatorów i oprogramowania. To sprawia, że taki kompleks jest wielozadaniowy, uniwersalny i elastyczny w realizacji różnorodnych zadań i celów. Ponadto kompleks realizuje wysokiej jakości kształcenie i szkolenie specjalistów morskich, prowadząc badania po opracowaniu wyników modelowania inżynierskiego rozwiązań konstrukcyjnych, cieplnych, hydraulicznych, elektrycznych, elektronicznych, i innych. Wykorzystanie kompleksu szkoleniowego pozwala na kształtowanie niezbędnych kompetencji personelu zespołu inżynierskiego, opracowanie metod i kryteriów oceny kompetencji, ocenę i wykazanie umiejętności praktycznych.*

Słowa kluczowe: systemy zasilania, działania w zakresie standaryzacji, efektywność energetyczna, szkolenia, ocena wydajności

Introduction

With the advancements in technology and the need to perform a wide range of various tasks and functions in the marine industry, a huge number of different in classes and purpose types of ships are used.

The operational profile of vessels has become more diverse and the implementation of numerous tasks leads to an increase of ship's power plants power and the difficulty in performing various marine operations. Because of this, the trade-off between efficiency and adaptability to perform various tasks has led to the appearance of various types of the ship's propulsion systems [1].

Those ship propulsion architectures contain mechanical propulsion, electrical propulsion or a hybrid combination of both; generating electricity with internal combustion engines, fuel cells, energy storage or a hybrid combination; alternating or direct currents electrical distribution systems. Most notably, such technologies require implementation in order to increase energy efficiency and environmental protection.

Taking into account all of the above-mentioned requirements and goals which are necessary for implementation into the marine industry, the actual problem is the integration of state-of-the-industry technologies and the appropriate training of marine specialists.

1. International requirements for marine industry

International Maritime Organization (IMO) – Marpol regulations have set targets for reducing the Energy Efficiency Design Index (EEDI) for marine vessels, which should significantly reduce fuel consumption and emissions into the environment and, therefore, IMO – Marpol increased control and enforcing these advances [7].

On January 1, 2015, Annex VI of MARPOL 73/78 entered into force on the issue of limiting emissions of combustion products into the atmosphere, which defines the limit of sulfur content in marine fuel at the level of 0.1% [6]. This annex, in particular, lists the sea basins, which are called SECA (Sox Emission Control Areas). Those are sulfur compound emission control zones, where, oxide emissions of sulfur are controlled and the restrictions on its content in marine fuel are functioned.

In addition to Marpol, as part of the IMO, one of the Marine Environment Protection Committee (MEPC) adopted the resolution "Ship energy efficiency management plan (SEEMP)" [8]. Based on SEEMP, a guide on the best practices for the fuel-efficient operation of ships was developed. It includes a list of energy efficiency measures for fuel-efficient operations; power management; development software for calculating fuel consumption, controlling emissions, optimizing goal-setting operations to improve and track progress. This guide also includes renewable energy sources (wind energy, solar or photovoltaic cells), which have improved significantly in recent years and should be considered for use on ships; the possibility of obtaining fuel of improved quality to minimize the amount of fuel needed to provide a given output power and much more.

SEEMP provides a feasible approach for monitoring vessel and fleet performance. The goal of SEEMP is to create a mechanism for improving the energy efficiency of ship operations. The structure of SEEMP includes planning, implementation and monitoring:

Planning is the most important stage of SEEMP, since it primarily determines the current state of the ship's energy consumption and the expected improvement in ship's energy efficiency. It includes ship special measures (speed optimization, weather routing, and maintenance), company-specific measures (ship-repair yards, shipowners, operators, charterers, cargo owners, ports and traffic management services) and the development of human resources (raising awareness and providing the necessary personnel training both onshore and onboard).

In the Implementation process, after the vessel and the company have identified the measures that should be implemented, it is important to create a system for implementing certain measures and developing energy management procedures by defining tasks and assigning them to the qualified personnel.

Monitoring is a stage, the basis of which is continuous and consistent data collection. To ensure meaningful and consistent monitoring, a monitoring system, including procedures for collecting data and appointing responsible personnel, should be developed.

To evaluate the effectiveness of decisions made by staff, it is necessary that the SEEMP structure has a Self-Assessment phase and improvement as the last stage of the management cycle. This phase should provide significant feedback for the upcoming first stage. The purpose of the self-assessment is to assess the effectiveness of the planned measures and their implementation in order to deeper reveal and understanding of the overall characteristics of the ship operation.

2. Training of marine personnel

For marine personnel to acquire the skills working with ship systems, training complexes are widely used.

Simulator training enables the use of both ready-made solutions and models of ship systems, as well as the creation of scenarios and specific training tasks, such as:

- to reproduce the operational capabilities of the appropriate ship's equipment as close as possible to the conditions of a real ship with physical reality;
- to reproduce a variety of conditions, which may include an accident, unusual or emergency situations, as well as situations that are potentially and really possible with ship's propulsion systems operation;
- to create the conditions for human behaviour with sufficient reality allowing the person to undergo training and to acquire the necessary skills;
- to monitor, observe and record the actions of people, undergoing the training, to conduct their effective debriefing and playback exercises;
- to simulate abnormal situations and equipment fault.

In Fig. 1 the structure of training of marine specialists on simulators is shown.

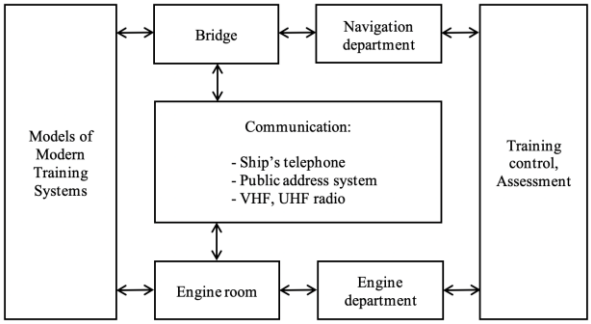

Fig. 1 The structure of training of marine specialists on simulators

Flexible training on simulators forms not only theoretical and practical skills among students, but also allows them to show personal qualities when training as part of a bridge - engine room team. For such purposes, IMO has developed a number of model courses, which are recommended to be included to the training program.

For example, model course 4.05 "Energy-Efficient Operation of Ships," 2014 edition [10], is designed to facilitate training to improve the energy efficiency of ship operation. The course contributes to achieving the IMO environmental goals set out in resolutions A.947 (23) and A.998 (25) by disseminating the "Best Practice" in the maritime industry, which reduces greenhouse gas (GHG) emissions and the negative impact of shipping on global climate change. Thus, the course content reflects the guidance for the development of the "Ship Energy Efficiency Management Plan (SEEMP)," MEPC Resolution 63.

The requirements and chapter III of International Convention on Standards of Training, Certification and Watchkeeping for Seafarers (STCW) with Manila amendments include the standards and requirements for the competence of engine room personnel at the operational and management levels [5]. In this case IMO developed a number of recommended model courses (7.02 [11], 7.04 [12], 7.08 [13], 2.07 [9]), which describe in detail the principles of training, methods of demonstration and lists of competencies that engine room personnel must be fully consistent with.

The competency tables also describe the minimum knowledge, understanding and professional skills regarding state-of-the-industry ship's systems for controlling propulsion systems, including electric propulsion.

Nowadays, there are many famous manufacturers of virtual marine simulators such as "Kongsberg" [14], "Transas (Wartsila)" [17] and others. Such simulators include a wide range of virtual simulators to provide effective training for cadets and marine crew in order to develop vital skills that promote safety, profitability and stability during work at sea.

The entire training process takes place on virtual systems of simulators and provides good theoretical knowledge. Unfortunately, during the training, there is no sense of physical realism of the real ship equipment, which cadets and crew members have to work on in the future.

Marine simulators must satisfy the international requirements and standards for conduct training and competency assessment. The world's largest international association of Classification Societies (IACS) member DNV GL, which is a leading provider of classification, certification, verification and training services, has developed a standard for marine simulations [4]. The purpose of the standard is to ensure that the simulations provided by the simulator include an appropriate level of physical and behavioral realism in accordance with the requirements for training and competency assessment. To ensure physical and behavioral realism, as indicated in [4], the simulator must be like real equipment to a certain extent to allow the delegates to demonstrate appropriate skills. Such realism should include the capabilities, limitations and possible errors of such equipment. The standard describes the classes of simulators and their application areas; a list of competencies that should be covered during training on these simulators; requirements and a list of ship systems.

The concept of conducting combined training and competency assessment simultaneously on the virtual and real simulator will allow to improve qualitatively the training process and the competence of delegates.

3. Multifunctional simulator

Based on the IMO model courses and recommendations for training on virtual and real simulators, the structure of a specialized multifunctional simulator (Fig. 2) and a hardware-software complex for engineering modelling are given. In addition, high-quality education and training of marine specialists, as well as scientific research are proposed.

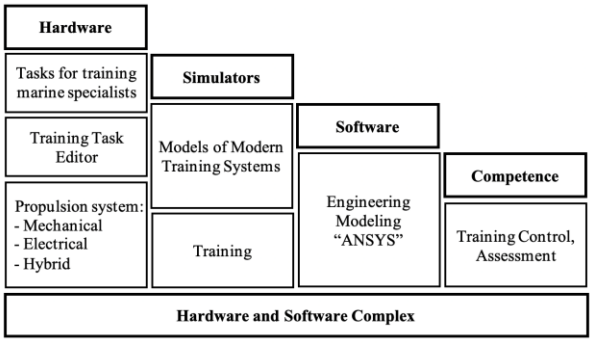

Fig. 2. The architecture of the training complex

3.1. General overview

A distinctive feature of the proposed simulator is an integrated approach, where the platform of the software and hardware complex makes it possible to integrate hardware, simulators, software with high output quality of competence based on a training control and assessment system.

Such multitasking implements high-quality education and training of marine specialists, as well as conducting research after

processing of the results of engineering modeling of structural, thermal power, hydraulic, electrical, electronic, multi-physical and other solutions. The need to use the training complex allows us to form the necessary competence of the engine room personnel, develop methods and criteria for assessing competence, evaluate and demonstrate practical skills.

When decomposing the tasks that are implemented in the hardware and software of the simulator's complex, methods of system analysis were used. Each module of the multifunctional simulator implements certain tasks and goals. The training equipment includes a number of hardware simulators and makes it possible to use a database and a monitoring system for a real ship with subsequent intellectual processing of the received data and modeling of nominal and emergency situations. In fig. 3 the structure of a module of a high-voltage simulator with the electric propulsion system is shown.

Such a simulator complex reproduces most of the ship's operating conditions and allows making training with monitoring, control and management of low-voltage and high-voltage power plants and propulsion systems.

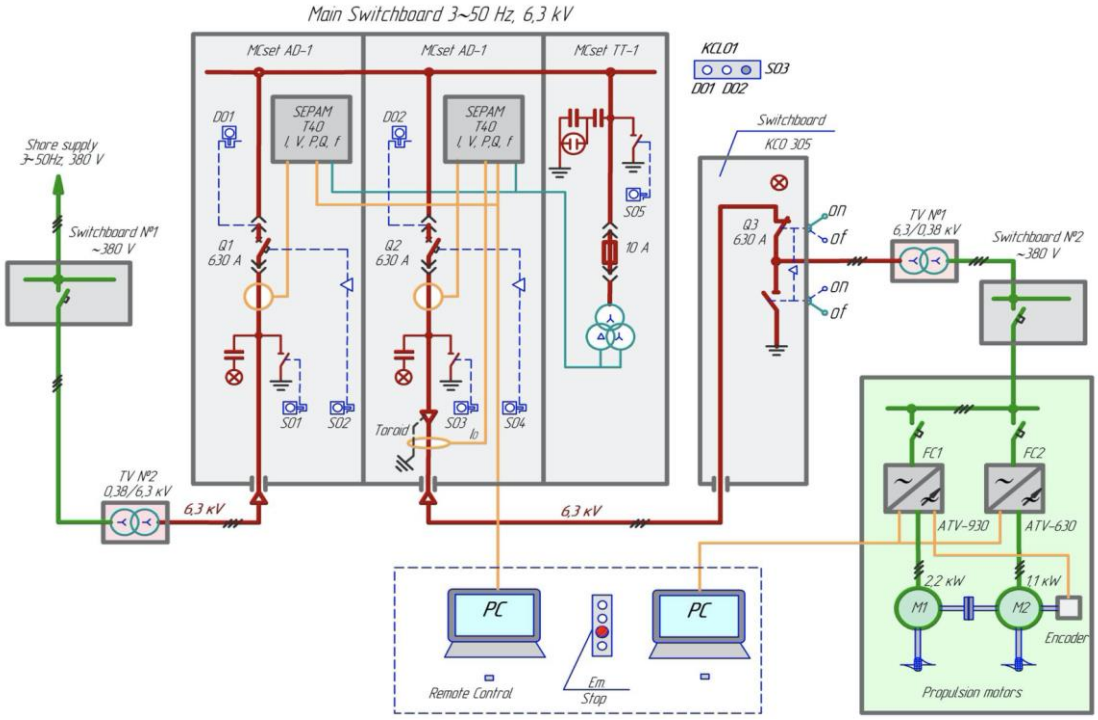

Fig. 3. Structure of electric propulsion high voltage simulator

3.2. Hardware

To ensure the rapid reconfiguration of the multifunctional simulator, designed to simulate the ship operating modes of various classes, it is advisable to use the modular principle in the development of hardware. This allows a simple configuration change. The layout of the hardware of the developed training complex is shown in Fig. 4.

The simulator includes the following equipment:

- two asynchronous electric motors which shafts are rigidly connected by a coupling;
- each electric motor is controlled by a frequency converter;
- software "So Move" (Schneider Electric).

Technical parts of the simulator equipment.

1. Asynchronous motor:
   type: A02-22-2. Δ/Y, 220/380 V, 50 Hz 7.8/4.5 A; 2.2 kW, 2860 rpm, cosφ = 0.8.
2. ATV630 frequency converter (Schneider Electric): 3F, 4 kW, 380-480 V, 50-60 Hz, 6 A at 380 V; output frequency 0.1–500 Hz.
3. Asynchronous motor (3-speed):
   type: AO-6-4-2. 380 V, 50 Hz;
   2p-6 (Y) – 960 rpm, 2.5 A, 0.79 kW, η = 69%, cosφ = 0.67;
   2p-4 (Δ) - 1460 rpm, 2.6 A, 0.9 kW, η = 71%, cosφ = 0.73;
   2p-2 (YY) – 2880 rpm, 2.9 A, 1.1 kW, η = 70%, cosφ = 0.90.
4. ATV930 frequency converter (Schneider Electric):
   3F, 4 kW, 380-480 V, 50-60 Hz, 9.3 A – 380 V; output frequency 0.1–500 Hz.

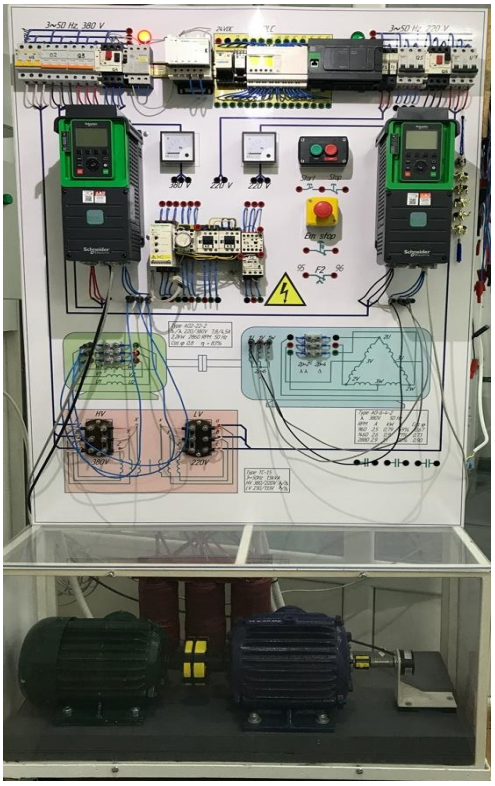

Fig. 4. Hardware of the electric propulsion simulator

One of the motors is controlled by ATV630 like a propulsion motor and the other motor (multi-speed) is controlled by ATV930 like a load with the possibility of controlling the torque on the shaft (propeller simulator with variable pitch propeller (VPP) or fixed pitch propeller (FPP), depending on preset parameters). Thus, the simulator can be used in various modes, changing the speed of rotation of the power plant, as well as changing the load on the power plant.

On this simulator, mainly steady-state modes are analyzed: mechanical performances, curves of changes in frequency, voltage, stator current, etc. with various methods of frequency control. Dynamic modes are studied not only at idle, but also at different values or laws of load change.

The use of bi-directional frequency converters in the hardware of the training complex allows studying of ship power systems in which energy recovery modes are implemented. An example of such ship's power plants are hybrid propulsive complexes, power take-off complexes and others that can improve the energy efficiency of the marine industry through the rational use of fuel combustion energy. The implementation of such installations, on the one hand, leads to increase of technical means survivability and reduction of harmful emissions into the environment, and on the other hand, equipment control algorithms are significantly complicated. This leads to an increase in requirements for marine personnel competence.

To change the configuration of the hardware of the electric propulsion to hybrid propulsion, it is enough to integrate the module with energy storage and change the algorithms of the propulsion system at the software level.

3.3. Software

Various algorithms for the operation of programmable controllers, depending on the configuration of the hardware, allow flexible enough to choose the optimal operating modes of the propulsion system in accordance with the goals and objectives. Such a solution makes it possible to carry out complex modeling of various modes using databases from real ships, on which it has possibilities to record all monitoring parameter data into an integrated automation system (IAS).

On the proposed multifunctional simulator, the propulsion system using the So Move software is controlled.

Using the "So Move" software from the simulator operator panel (Fig. 5) it is possible to implement various speeds and load modes with the ability to observe and register all processes, record parameters, and form the graphical and screw characteristics of the propulsion system [2].

Using the operator panel, the following basic operations are performed:

- setting and editing the parameters of the frequency of the converter;
- visual display of the state of parameters and variable drives;
- automatization of the experimental research;
- oscillography of the measured coordinates;
- intellectual processing of the experimental research results and modeling of the standard and emergency situations [16].

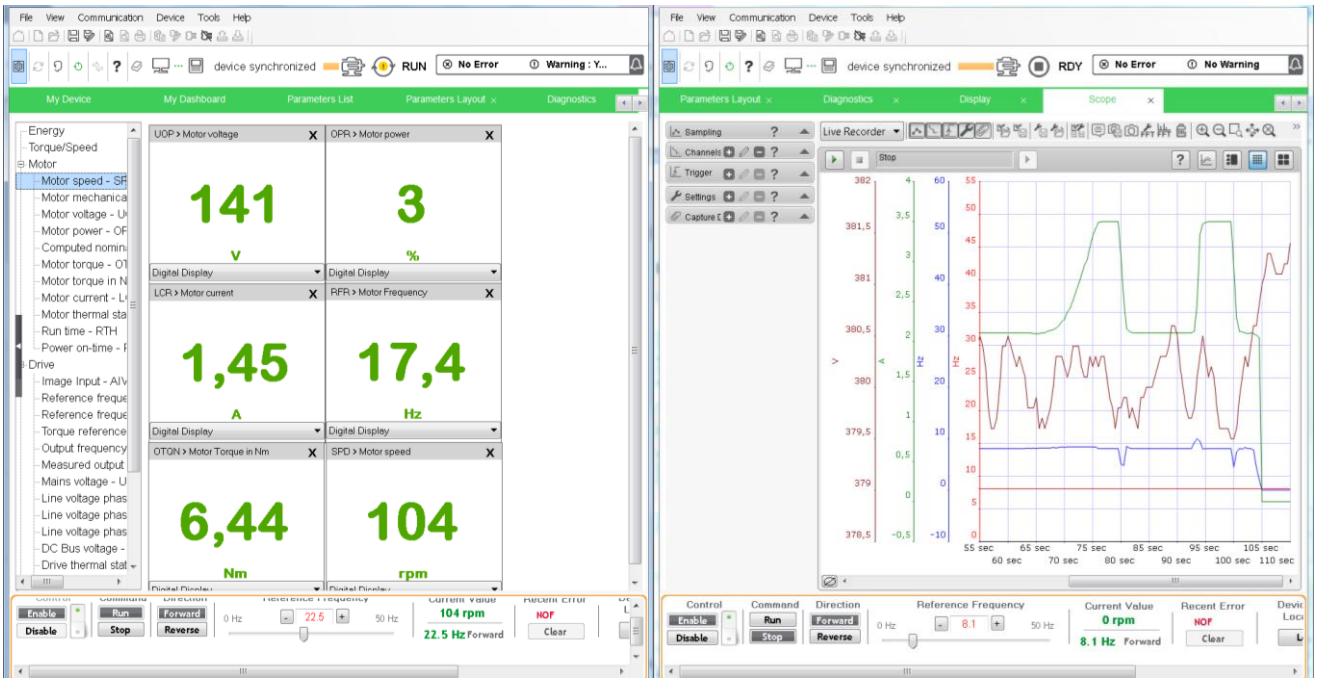

Fig. 5. Software on the operator's panel

3.4. Results of simulations

Modern ships use up-to-date technologies, and in particular, IAS (Integrated Automation System) implemented automated control system of ship's electric power plant gives possibilities to record the history of numerous monitoring parameters of the power management system.

In case of malfunctions or system failures, it is always possible to track which parameters of the system have gone out of operating range and analyse what happened as a result.

For example, let us consider a diesel-electric propulsion 3D class seismic vessel with wide stern for streamer towing (equipment for a seismic survey). Power of aft azimuth thrusters is 2×4000 kW, bow thruster is 1×2000 kW and the power system of the vessel includes four main diesel generator sets of 3355 kW each, the main switchboard (MSB) consist starboard (STBD) and port side (Port) sections, the nominal voltage of 4160 V and frequency of 60 Hz.

In this case, a module of the electric propulsion system integrates into the multifunctional simulator. The module includes a propulsion motor (PM) operated by a frequency converter and a propeller (asynchronous motor) that is a load (torque) for PM operated by another frequency converter.

Fig. 6 shows a general view of the main components of the Power Management System:

– main generators, which are located in STBD and Port engine rooms, separated by a watertight bulkhead.
– the switchboards with high and low Volt are physically segregated in port and starboard switchboard rooms and

equipped with a segregated, PS & SB redundant UPS system supplying all vital consumers.

– the 2 different propulsion lines powered by 3 separate electro motors with double stator windings and ABB ACS 6000 redundant drives. Electric motors and all their vital auxiliaries are located in 2 separate propulsion rooms. The 2 of individual main propulsion units use to mitigate the above situation if one propeller unit failure and in addition an independently steerable azimuth thruster in the bow.

The general structure of Integrated Automation System (IAS) are shown in Figure 7. It includes several operation stations in various ship rooms, such as the engine control room (main operation station), the bridge, the starboard and portside main switchboards, the auxiliary equipment room, the offices of the captain and chief engineer. All vital parts of the system have dual power supply from each of the two central UPS systems. If one of the redundant power supplies is lost, the system will hot-swap to live power supply without a power drop.

All vital communication in IAS system is done with dual, redundant communication bus. The system consists of several servers and computers with dual redundancy of the data received to increases reliability.

In figure 8 the separate windows with data and information on the current status of the propulsion system are displayed. It gives wide opportunities to the crew personnel to carry out the appropriate maintenance, to analyze the state of the ship propulsions, to take measures to prevent malfunctions and as well as to display the playback history of parameter changes when various malfunctions and emergencies occur.

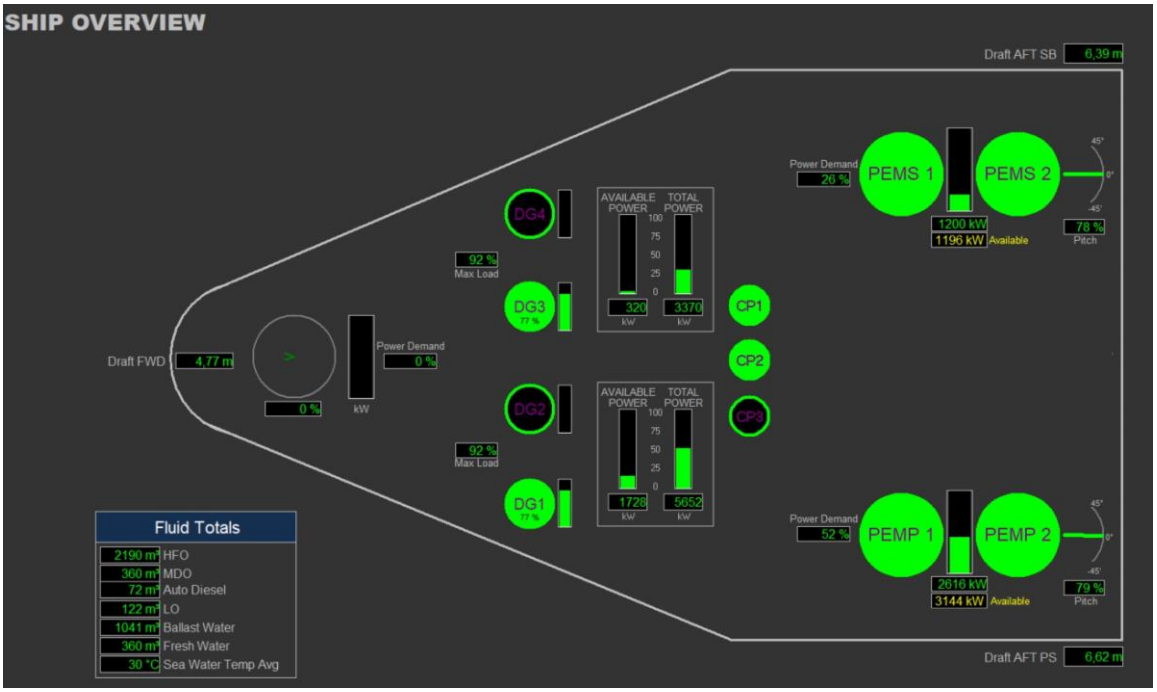

Fig. 6. Power Management system overview

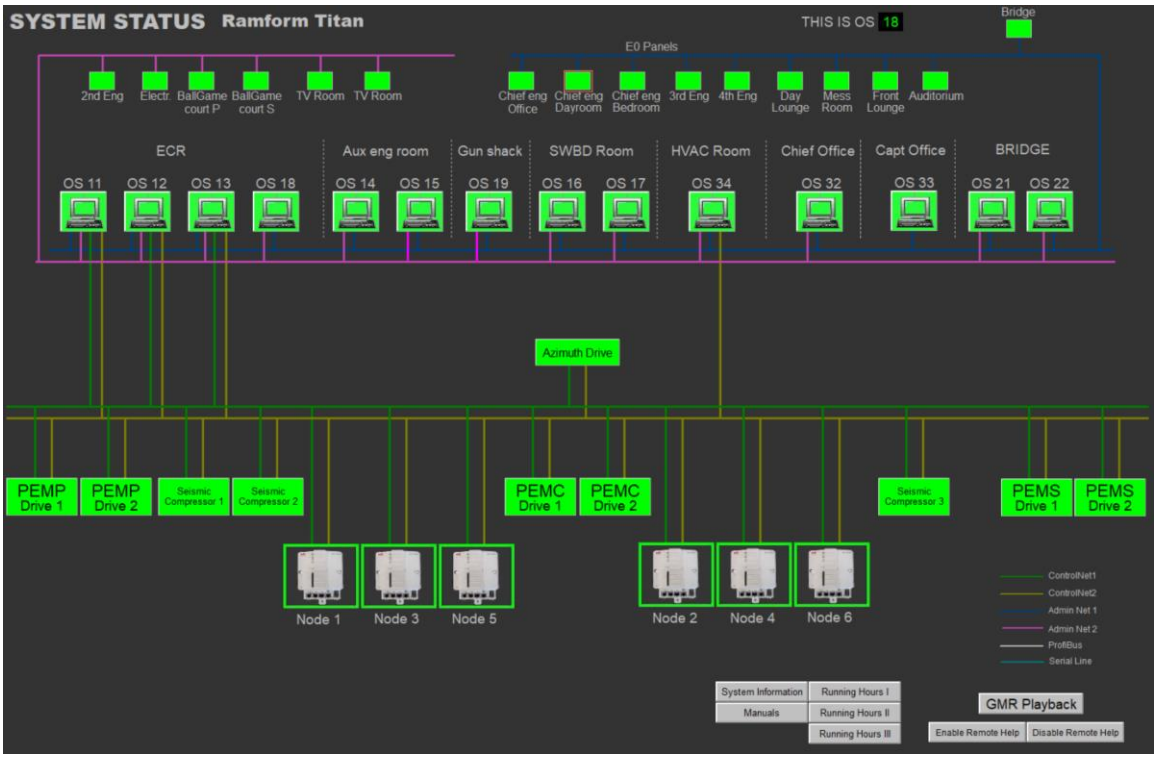

Fig. 7. Structure of integrated automation system

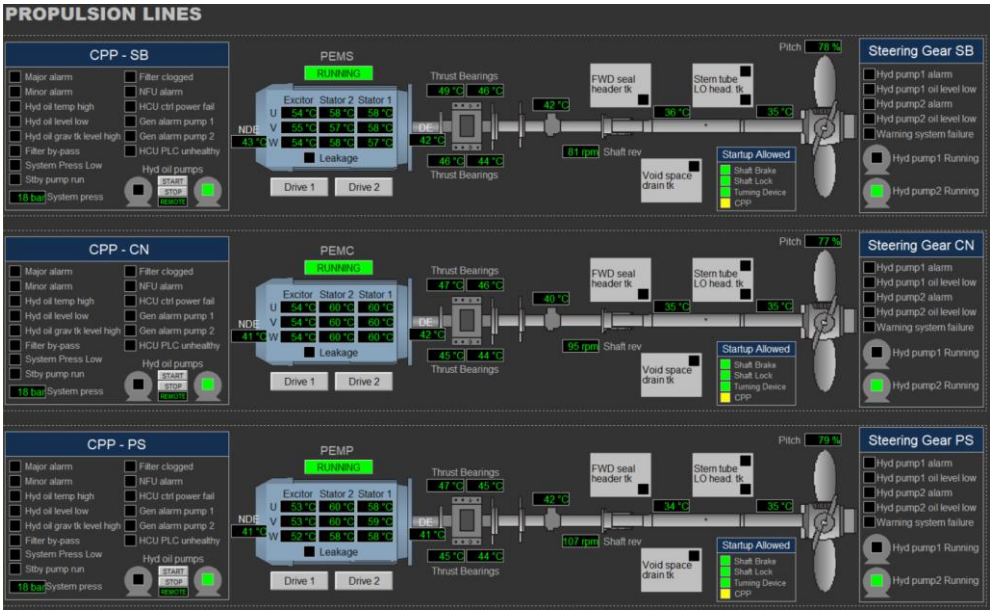

a) propulsion mnemonic

b) parameters propulsion drive system

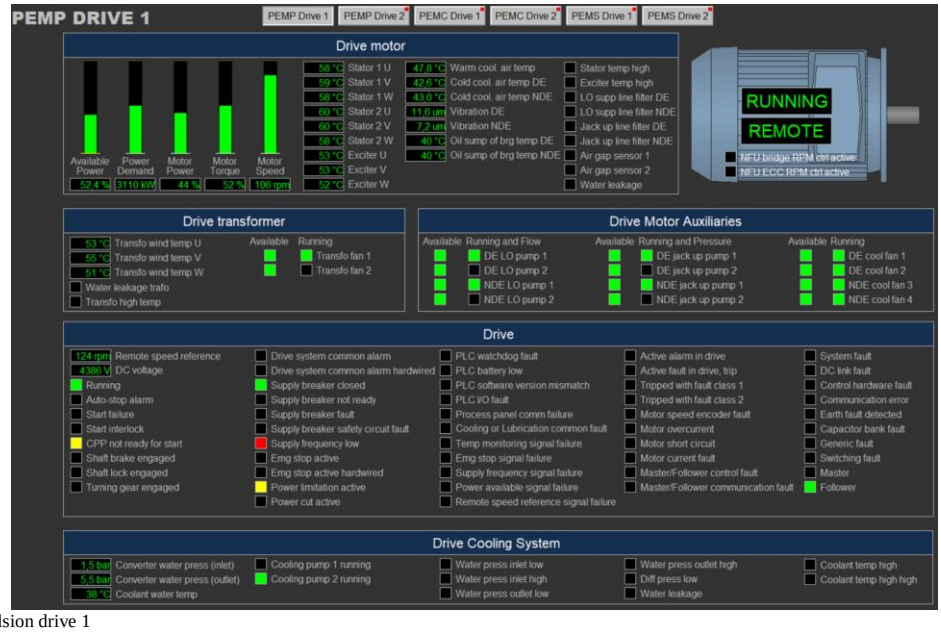

c) detailed data for propulsion drive 1

Fig. 8. Propulsion monitoring system

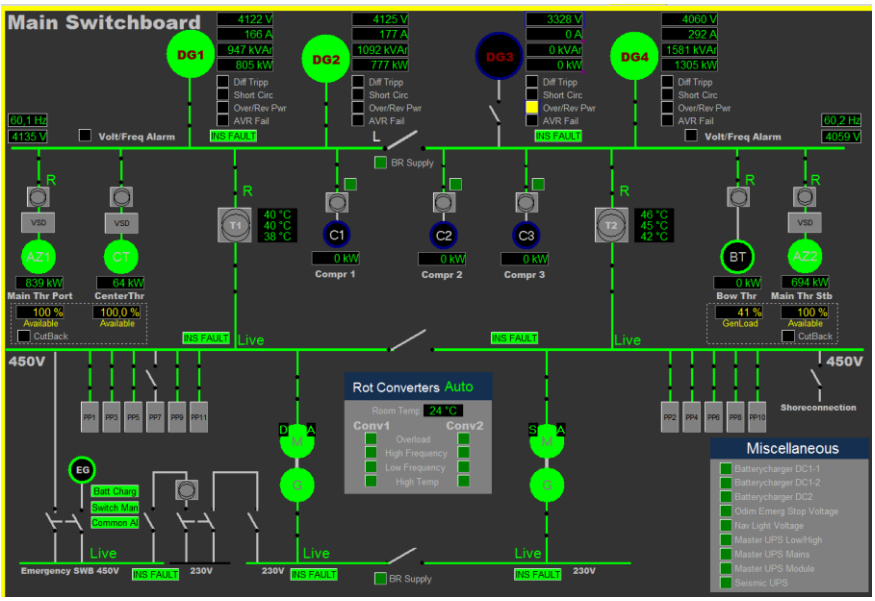

Fig. 9. Mnemonic of High Voltage Main Switchboard

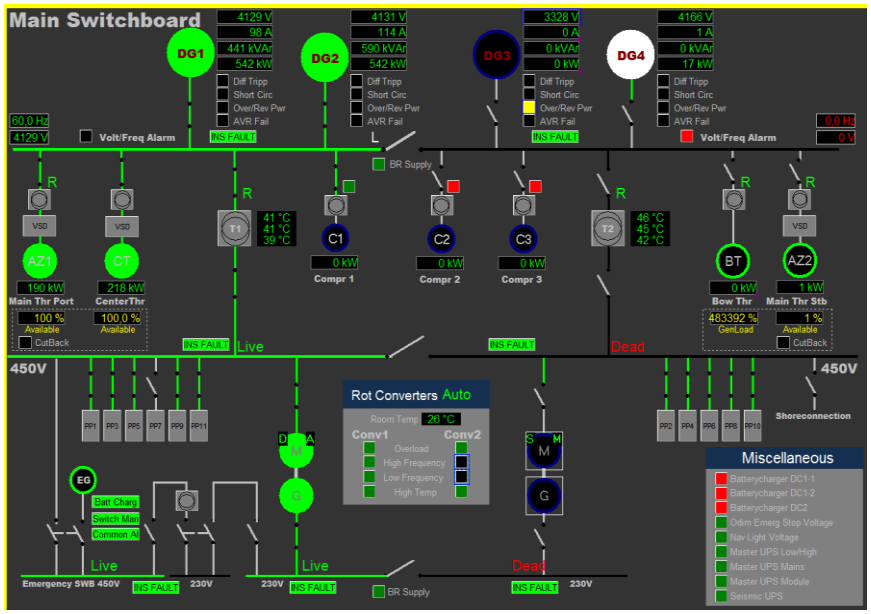

Fig. 10. Emergency situation and partial blackout

Each parameter displayed on the screen is recorded in a database, which stored on servers for an average of 3 to 6 months. Where applicable, the recording history can be retrieved to playback, save or analyze the system status.

By means of control algorithms on the multifunctional simulator, different modes of operation (nominal and emergency) are implemented. The simulator gives various loading ranges, which reproduce general operation of the propulsion system, simulation of overloads, suddenly increase and decrease loads and emergencies that occurred or would occur on the diesel-electric propulsion vessels.

Simulation of high voltage PMS of dynamic positioning (DP) diesel-electric propulsion of seismic vessel in the operating mode under the rough state of the sea with wave height up to 8 meters was performed.

A particular feature of this operation mode is that during the seaway of a vessel, propellers are exposed which cause the sudden changes of load for propulsions. Monitoring system window in this situation is shown in figure 9. It can be seen that the loads on the generator sets and thrusters are distributed extremely unevenly.

In this case, trainees should pay attention to the understanding of processes in operating the propulsion system, such as static, dynamic characteristics of power units, parameters of operation modes and character of transient processes.

Based on the analysis of the current load and the dynamics of its change, the operator must make a decision to reconfigure the power system in order to avoid overloading or an emergency situation in the future.

Any loss of electrical power, propulsion or steering functions must immediately be brought to the attention of the Chief Engineer and Master.

The vessels are equipped with back-up systems for all safety-critical equipment including electrical power, propulsion and steering. Vessel specific checklists for the operation of these systems must be followed to restore the lost functions as quickly as possible. Blackout recovery procedure is described in [15].

The result of simulation of such an emergency when the operator took the wrong decision is shown in Fig. 10.

Untimely or wrong actions of the operator resulted partial blackout of STBD HV switchboard and all power consumers are supplied from this side and emergency shutdown of the propulsion motors. The training complex also allows simulating elimination of emergency.

4. Control of the training process

Monitoring of training process is necessary to implement rational management of the process and form an individual trajectory to increase the effectiveness of training.

The management system of training quality, which is based on the competency-based approach, should consist of three interconnected modules: a subsystem for assessing the results of a delegate's activity, a subsystem for identifying his psychophysiological state, and a subsystem for forming a simulator's intellectual information environment.

To determine the level of professional competence, the quality and proficiency of knowledge, skills and abilities assimilation, motivation, activity and successfully completed tasks in solving practical training are evaluated. Training control is traditionally carried out in the form of testing in the practical exercises.

Identification of a person state can be carried out on the basis of determining biological parameters during the execution of different nature operations. To process the measurement results, it is advisable to use the methods of fuzzy logic. That allows us to timely identify critical deviations of the psychophysiological parameters of the delegate and adaptively configure the training process [3].

Individual correction of specialist training contributes to the elimination of erroneous actions, development of positive abilities by adjusting the complexity of tasks, selecting tasks corresponding to the specialization of training, and redistributing the time for their implementation.

5. Conclusions

The uniqueness of the simulator complex is that in addition to real simulators, virtual simulators with various modern models, systems of marine vessels are integrated into the software, and hardware complex, which makes this simulator complex multitask, universal and flexible in achieving a variety of tasks and goals.

Based on "ANSYS" software and engineering modelling, the data and results, obtained during the work and training with hardware simulators, are processed and simulated by heat-power, hydraulic, electrical, electronic or multi-task solutions both for improving the functionality and for research activities.

Training of marine specialists on simulators provides many opportunities for the implementation of various scenarios, as well as training of a whole team of navigational and engine room officers.

References

[1] Geertsma R., Negenborn R., Hopman J.: Design and control of hybrid power and propulsion systems for smart ships: A review of developments. Elsevier 2017.
[2] Ivanov A.A., Lebedenko Yu.A., Rozhkov S.A., Kolosov I.V.: Electric Propulsion Ship's Training Simulator Based on Intelligent system. International scientific journal Electronics and Control Systems 2(60), 2019, 53–60.
[3] Kuznetsov M., Rudakova H., Kolosov I.: The application of fuzzy logic to identify the personal state of the human operator. Computer-integrated technologies in the present: a collection of scientific works of young scientists, Kherson 2016, 15–19.
[4] DNV GL Standard. DNVGL-ST-0033. Maritime simulator systems. Edition: March 2017.
[5] IMO: International Convention on Standards of Training, Certification and Watchkeeping for Seafarers, (STCW Code). London 2017.
[6] IMO: Marpol, AnnexVI and NTC 2008. London 2017.
[7] IMO: Marpol. London, 2017.
[8] IMO: MEPC 63/23 Annex9. London 2012.
[9] IMO: Model Course 2.07 Engine-Room Simulator. London 2017.
[10] IMO: Model Course 4.05 Energy Efficiency Operation of ship. London 2014.
[11] IMO: Model Course 7.02 Chief Engineer Officer and Second Engineer Officer. London 2014.
[12] IMO: Model Course 7.04 Officer in Charge of an Engineering Watch. London 2014.
[13] IMO: Model Course 7.08 Electro-Technical Officer. London 2014.
[14] https://www.kongsberg.com/digital/products/maritime-simulation/k-sim-engine/ (available 26.01.2020).
[15] https://www.pgs.com/marine-acquisition/tools-and-techniques/the-fleet/ (available 26.01.2020).
[16] https://www.se.com/ww/en/product-range-presentation/2714-somove/#tabs-top (available 26.01.2020).
[17] https://www.wartsila.com/marine/optimise/simulation-and-training (available 26.01.2020).

M.Sc. Artem Ivanov
e-mail: artiva1978@gmail.com

Ph.D. student of Kherson State Maritime Academy, Department of Ship Electrical Equipment and Automatic Devices Operation. Head of department of courses in ship's marine engineering Kherson Maritime Specialized Training Centre. Research Interests: marine engineering, software engineering, energy systems.

http://orcid.org/0000-0002-1919-2570

M.Sc. Igor Kolosov
e-mail: ikolosov@marlow.od.ua

Graduated in 1998 from Odessa Maritime Academy as a maritime navigator. While studying at the Academy, he began his career at sea and got position Chief officer. Since 2003 works at Marlow Navigation Ukraine and holds the position Director of Crewing Department.
Research interest: optimization of training process management of marine personnel.

http://orcid.org/0000-0001-9572-587X

M.Sc. Vadim Danyk
e-mail: vadymdanyk@gmail.com

Assistant of Department of Ship Electrical Equipment and Automatic Devices Operation, Kherson State Maritime Academy.
The field of scientific interest is hybrid marine propulsion systems, marine power systems.

http://orcid.org/0000-0002-4439-0309

M.Sc. Sergey Voronenko
e-mail: vr.sergey@ukr.net

Assistant of the Department Operation of Marine Electric Equipment and Means of Automation of Kherson State Maritime Academy.
Research interest: optimization of control of ship complex electric power turbo compressor units.

http://orcid.org/0000-0002-3880-9556

Ph.D. Yurii Lebedenko
e-mail: lebedenko@kntu.net.ua

Assistant professor of Department of Automation, Robotics and Mechatronics, Kherson National Technical University.
The fields of scientific interest are adaptive and optimal control systems, marine power systems. The author of more than 80 scientific papers.

http://orcid.org/0000-0002-1352-9240

Prof. D.Sc. Hanna Rudakova
e-mail: rudakova.ganna@ kntu.net.ua

Professor of Department of Automation, Robotics and Mechatronics, Kherson National Technical University.
The fields of scientific interest are modeling of complex systems, automation of control processes, identification of critical operating modes of equipment.

http://orcid.org/0000-0002-8053-4218

otrzymano/received: 08.04.2020 *przyjęto do druku/accepted: 26.06.2020*

http://doi.org/10.35784/iapgos.931

MODEL PREDICTIVE CONTROL APPLICATION IN THE ENERGY SAVING TECHNOLOGY OF BASIC OXYGEN FURNACE

Oleksandr Stepanets, Yurii Mariiash
National Technical University of Ukraine "Igor Sikorsky Kyiv Polytechnic Institute", Department of Automation of heat-and-power engineering processes, Kyiv, Ukraine

Abstract. *The fulfilment of the condition for the simultaneous achievement of the desired chemical composition and temperature of the metal is ensured by controlling the oxygen consumption and the position of the oxygen impeller lance. The method for solving Model Predictive Control with quadratic functionality in the presence of constraints is given. Implementation of the described solutions will contribute to increasing the proportion of scrap and reducing the melting period without changing of technological process.*

Keywords: model predictive control, basic oxygen furnace, optimal control, energy saving

ZASTOSOWANIE MODELU STEROWANIA PREDYKCYJNEGO W ENERGOOSZCZĘDNEJ TECHNOLOGII PROSTEGO PIECA TLENOWEGO

Streszczenie. *Spełnienie warunku jednoczesnego osiągnięcia pożądanego składu chemicznego i temperatury metalu jest zapewnione poprzez kontrolę zużycia tlenu i położenia palnika tlenowego. Zaprezentowano metodę rozwiązania Modelu Sterowania Predykcyjnego z funkcjonalnością kwadratową w obecności ograniczeń. Wdrożenie opisanego rozwiązania przyczyni się do zwiększenia udziału złomu i skrócenia czasu topnienia bez zmiany procesu technologicznego.*

Słowa kluczowe: model sterowania predykcyjnego, prosty piec tlenowy, optymalna kontrola, oszczędność energii

Introduction

Steel production is a complex process that requires the use of a complex of technological, energy and transport equipment, each of which requires appropriate automation. Today, carbon steel is mainly produced using blast furnace route where basic oxygen furnace (BOF) basic oxygen furnace has an important role [8].

The intensification and complication of technological processes, increasing the capacity of units and increasing the quality requirements of finished products make it impossible to manage the units without improving the structure of automatic control systems. Despite the significant popularity of the classical theory of control with PID-controllers [9], the main part of the research conducted today is the use of process optimization [1] and improvement of predictive models [2].

Automation of the BOF involves obtaining high quality steel, which is possible while achieving the desired chemical composition and metal temperature [2, 6]. This condition is ensured by controlling the flow of oxygen and the position of the lance of the oxygen converter, so solving the problem of controlling the purge of the converter bath is the main task. That is why the task of implementing modern control methods in the conditions of stochasticity, non-stationarity and limitations of technological processes is an urgent problem today [10]. Classical approaches are designed for the thermal mode, which determines the software trajectory of the control effects. Today, more and more research is focused on steelmaking raw materials and energy optimization [1]. One modern advanced control method is control theory using predictive models, such as Model Predictive Control (MPC). Model Predictive Control is an optimal control strategy based on numerical optimization [7].

1. The aim and objectives of the study

The purpose of the work is to develop an automatic control system for basic oxygen furnace-smelting, which would provide the specified quality indicators in conditions of unsteadiness of the rate of decompression and perturbations associated with changes in oxygen consumption for purging and introduction of loose. To achieve the objective, the following tasks were formulated:
to study the dynamic properties of the process of changing the rate of decarbonization of metal;
obtain a predictive model of the degree of carbon oxidation to the carbon dioxide of the oxygen-converter process;
to solve the problem of MPC-control with quadratic functional in the presence of restrictions.

2. Mathematical model of oxygen converter process

The transient process of changing the rate of decarburization from changing the distance of the lance to the level of a quiet bath is described by the transfer function (1) of the form [3]:

$$W_{v_c}(s) = \frac{k_{v_c}}{T_{v_c} s + 1} \tag{1}$$

where $k_{v_c}\ \left[t/(h \cdot m)\right]$ – the transmission coefficient through the channel distance of lance to the level of a quiet bath – the rate of decarburization; $T_{v_c}\ [\mathrm{s}]$ – time constant.

The time constant (2) is non-stationary and also depends on the melting period. It can be described functions [3]:

$$T_{v_c} = \begin{cases} 1.143 + 4.446\tau - 0.484\tau^2, \text{ 1 period} \\ 11.267, \text{ 2 period} \\ 11.267 - 4.446(\tau - 16) + 0.484(\tau - 16)^2, \text{ 3 period} \end{cases} \tag{2}$$

where $\tau\,[\min]$ – purging time.

Changing the rate of decarburization leads to a change in the degree of carbon oxidation to carbon dioxide in the converter cavity. This process is also described by the first-order transfer function (3) of the form [3]:

$$W_{\gamma_{CO_2}}(s) = \frac{k_{\gamma_{CO_2}}}{T_{\gamma_{CO_2}} s + 1} \tag{3}$$

where $k_{\gamma_{CO_2}}\left[\%_{CO_2} \cdot \min \cdot t^{-1}\right]$ is the transmission rate through the channel of the speed of carbonation – the degree of carbon oxidation to CO_2; – it is time. According to the results of experimental studies [5], the transmission rate of the channel is the carbonation rate – the degree of carbon oxidation to CO_2 is determined from the balance equation of the purge flow rate $k_{\gamma_{CO_2}}$=3.33 $\%_{CO_2} \cdot \min \cdot t^{-1}$.

The two links are connected in series (4) and the transfer function of the system in which the input value of the lance distance to the level of a quiet bath and the output – the degree of carbon oxidation to CO_2:

$$W_{v_c}(s) = \frac{k_{v_c} \cdot k_{\gamma_{CO_2}}}{(T_{v_c} s + 1)(T_{\gamma_{CO_2}} s + 1)} = \frac{k^H_{\gamma_{CO_2}}}{(T_{v_c} s + 1)(T_{\gamma_{CO_2}} s + 1)} \tag{4}$$

where $k_{v_c}\left[\%_{CO_2}\cdot m^{-1}\right]$ – the transmission coefficient through the channel distance of lance to the level of a quiet bath – the degree of carbon oxidation to CO_2.

The system on the channel "position of the swing flap – vacuum in the caisson" has a transfer function (5):

$$W_v(s)=\frac{0,55}{5s+1}e^{-s} \tag{5}$$

where $W_v(s)$ – a transfer function on the channel "position of the swing flap – vacuum in the caisson".

3. MPC controller design and control system modelling

The design of a quadratic-functional MPC controller with constraints was performed using the Matlab MPC Designer package [11]. The design of the MPC controller (Fig. 1) used the mathematical model of the oxygen converter process, which is described in section 2.

The predictive model (6) of the oxygen converter process for the second purge period of the oxygen converter process is obtained:

$$x_{i+1}=Ax_i+Bu_i,$$
$$y_i=Cx_i,$$
$$i=k+j,\ j=0,1,2...,$$

where k – tact number, $x_i\in E^n$ – the state of the object, $y_i\in E^r$ – measurements, $u_i\in E^m$ – control action,

$$A=\begin{pmatrix}-1.613 & 0 & 0 & 0 & 0\\ 0 & -0.0887 & 0 & 0 & 0\\ 9.677 & 0 & -0.2924 & 0 & 0\\ 0 & 0 & 0 & -0.2 & 0\\ 0 & 0.3426 & 0.00146 & 0 & -0.466\end{pmatrix},$$

$$B=\begin{pmatrix}1 & 0 & 0\\ 0 & 1 & 0\\ 0 & 0 & 0\\ 0 & 0 & 1\\ 0 & 0 & 0\end{pmatrix}, \tag{6}$$

$$C=\begin{pmatrix}9.677 & 0 & 0 & 0 & 0\\ 0 & 0 & 0 & 0 & 1.522\\ 0 & 0 & 0 & 0.11 & 0\end{pmatrix}$$

The dynamic properties of the actuators was introduced into the MPC-controller as the constraints on the input values (Fig. 2).

The quality of control is characterized by a linear-quadratic functional (7):

$$J_k=J_k(\bar{y},\bar{u})=$$
$$=\sum_{j=1}^{P}\left[\left(y_{k+j}-r_{k+j}\right)^T R_{k+j}\left(y_{k+j}-r_{k+j}\right)+u_{k+j-1}^T Q_{k+j}u_{k+j-1}\right] \tag{7}$$

where R_{k+j} and Q_{k+j} – positively defined symmetric matrices.

Auxiliary vectors (8):

$$\bar{y}=(y_{k+1}\ y_{k+2}\ ...\ y_{k+P})^T\in E^{rP}$$
$$\bar{u}=(u_k\ u_{k+1}\ ...\ u_{k+P-1})^T\in E^{mP} \tag{8}$$

Given that the movement of the system (6) on the clock is only determined, then. The problem of optimization (9) with respect to the functional (7) can be formulated:

$$J_k(\bar{u})\to\min_{\bar{u}\in E^{mP}} \tag{9}$$

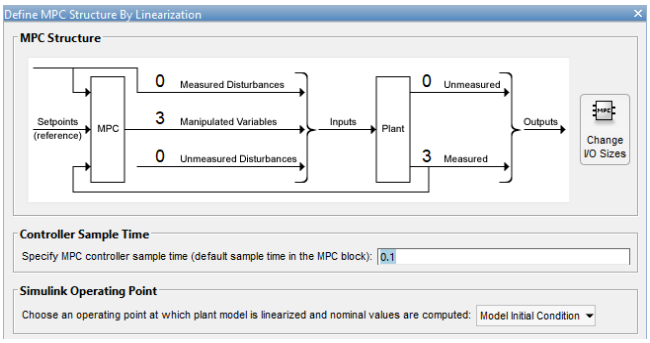

Fig. 1. Description of the structure of the MPC controller

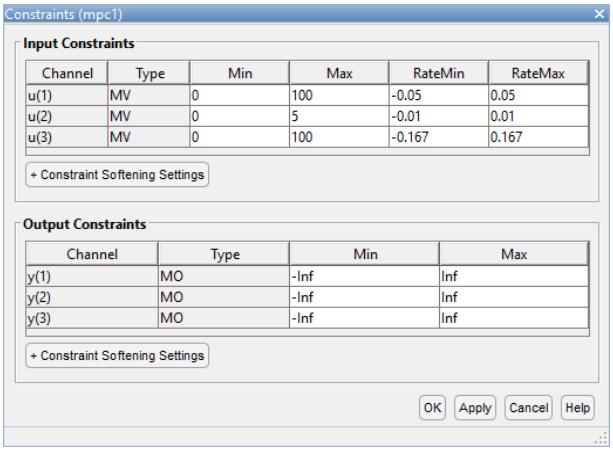

Fig. 2. Constraints to input values introduced in the MPC controller

The solution to problem (9) found, the functional (7) presented in the form (10):

$$J_k=J_k(\bar{u})=\left(\bar{y}-\bar{r}\right)^T R\left(\bar{y}-\bar{r}\right)+\bar{u}^T Q\bar{u}$$
$$y_{k+1}=Cx_{k+1}=CAx_k+CBu_k$$
$$y_{k+2}=Cx_{k+2}=CAx_{k+1}+CBu_{k+1}=CA^2x_k+CABu_k+CBu_{k+1}$$
e.t.c. $y_{k+P}=Cx_{k+P}=CA^Px_k+CA^{P-1}Bu_k+CBu_{k+1}$
$$\Rightarrow\bar{y}=Lx_k+M\bar{u}\text{, where}$$

$$L=\begin{pmatrix}CA\\ CA^2\\ .....\\ CA^P\end{pmatrix}\quad \text{M}=\begin{pmatrix}CB & 0 & \cdots & 0\\ CAB & CB & \cdots & 0\\ .... & .... & \cdots & \\ CA^{P-1}B & CA^{P-2}B & \cdots & CB\end{pmatrix}\Rightarrow$$

$$J_k=J_k(\bar{u})=\left(Lx_k+M\bar{u}-\bar{r}\right)^T R\left(Lx_k+M\bar{u}-\bar{r}\right)+\bar{u}^T Q\bar{u}$$
$$\frac{\partial J_k}{\partial\bar{u}}=\frac{\partial}{\partial\bar{u}}\left[\left(Lx_k+M\bar{u}-\bar{r}\right)^T R\left(Lx_k+M\bar{u}-\bar{r}\right)+\bar{u}^T Q\bar{u}\right]=0$$
$$\frac{\partial J_k}{\partial\bar{u}}=M^T R\left(Lx_k+M\bar{u}-\bar{r}\right)+Q\bar{u}=0$$
$$\Rightarrow\bar{u}^*=\bar{K}x_k+\bar{T}\bar{r}$$
$$\bar{K}=-(M^TRM+Q)^{-1}M^TRL,\bar{T}=(M^TRM+Q)^{-1}M^TR$$

Matrix search algorithm:

1. Having matrices *A*, *B*, *C* and forecast horizon *P* to form matrices *L* and *M*.
2. Using the input data in the form of matrices *R* and *Q* calculate additional matrices $\bar{K}$ and $\bar{T}$ from (10).
3. Select the upper blocks in size *m*n* and *m*r* according to the matrices $\bar{K}$ and $\bar{T}$.

According to the MPC strategy, the behaviour of the system is predicted and the resulting structure is optimized to find the optimal control of the oxygen converter. The obtained optimal control is applied at the current step, after which the forecast horizon shifts and the described sequence of actions is repeated [4]. The approach takes into account the constraints imposed on both control variables and control variables.

The simulation procedure was performed in the Matlab Simulink environment. An algorithm for solving the equations ode23s (stiff / mod. Rosenbrock) was chosen with variable-step change. The absolute and relative accuracy of the calculations is 0.0001.

For a control system of oxygen consumption, a perturbation of a task of 15 m^3/min (Fig. 3) relative to the nominal value of oxygen consumption is typical during purging. The obtained system quality indicators are shown in Table 1.

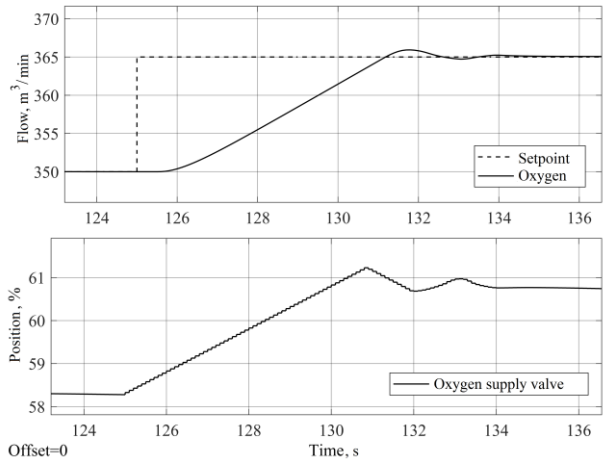

Fig. 3. Oxygen purge control system overflow position of oxygen supply valve – oxygen flow

Table 1. Quality indicators of SAR oxygen consumption

Quality indicators	Value
Static error	0
Dynamic Error	0.067
Adjustment time	8 s
The attenuation index	0.95
Overshoot	6.67%

For the control system of CO_2 content, the main task is the problem of stabilization (Fig. 5) in the event of disturbances: changes in the flow rate of oxygen, change in the rate of decarburization, introduction of bulk, etc. Transitions through the perturbation-output channel are shown in Fig. 4. The obtained system quality indicators are shown in Table 2.

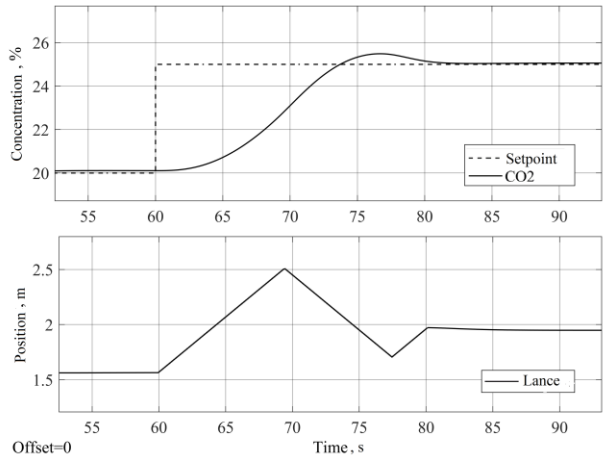

Fig. 4. Intermittent process of control system in the second period of purging through channel position of lance-CO2 content in flue gases

Table 2. Quality indicators of SAR of disturbances CO_2 content

Quality indicators	Value
Static error	0%
Dynamic Error	0.1
Adjustment time	18 s
The attenuation index	1
Overshoot	10%

Transitions through the disturbances for perturbation-output channel are shown in Fig. 5. The obtained system quality indicators are shown in Table 3.

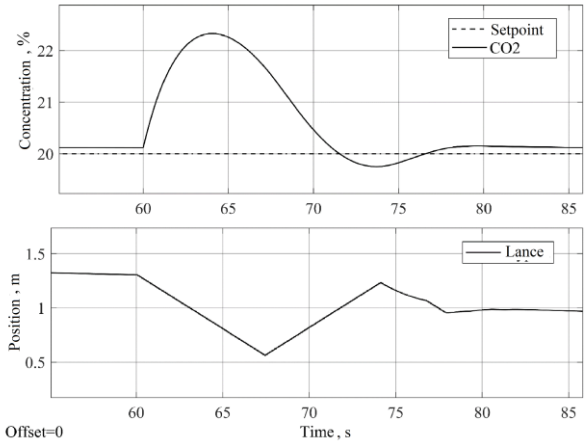

Fig. 5. Interrupting the process of the control system in the second period of purging through the channel change in the rate of decarburization – CO2 content in the flue gases

Table 3. Quality indicators of SAR CO_2 content

Quality indicators	Value
Static error	0,1%
Dynamic Error	2,25
Adjustment time	16 s
The attenuation index	0.92
Overshoot	13.3%

To discharge the converter gases, a small (6–50 Pa) vacuum should be maintained in the caisson above the converter. Adjustment of pressure in a caisson is carried out by influence on a rotary damper in a gas-purifying tube. For the perturbation control system there is a converter gas recovery system. The transients of the system of automatic control of the vacuum on the channel vacuum-output are shown in Fig. 6, obtained system quality indicators are shown in Table 4.

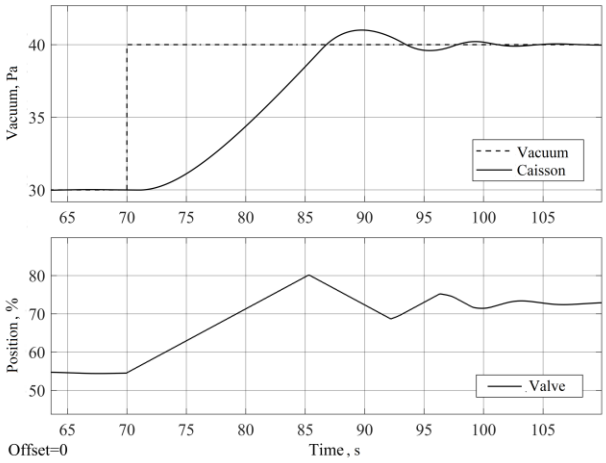

Fig. 6. Intersection process of the automatic control system on the vacuum channel by the gas-vacuum system in the caisson

Table 4. Quality indicators of SAR vacuum in the caisson

Quality indicators	Value
Static error	0
Dynamic Error	0.09
Adjustment time	27 s
The attenuation index	0.91
Overshoot	9%

Transitions through the disturbances of the vacuum channel are shown in Fig. 7. The obtained system quality indicators are shown in Table 5.

Table 5. Quality indicators of SAR the disturbances of vacuum in the caisson

Quality indicators	Value
Static error	0
Dynamic Error	0.52 Pa
Adjustment time	18 s
The attenuation index	0.8
Overshoot	0%

The simulation of oxygen transients during purging for a 160-ton converter in the second purging period using an oxygen flow control algorithm aimed at ensuring the reliability of the equipment and adjusting the position of the lance by the energy-saving technology of combustion of CO to CO_2 (Fig. 8). The obtained transients of the automatic control system of the basic oxygen furnace process using the MPC-strategy provide the requirements to the quality of the system.

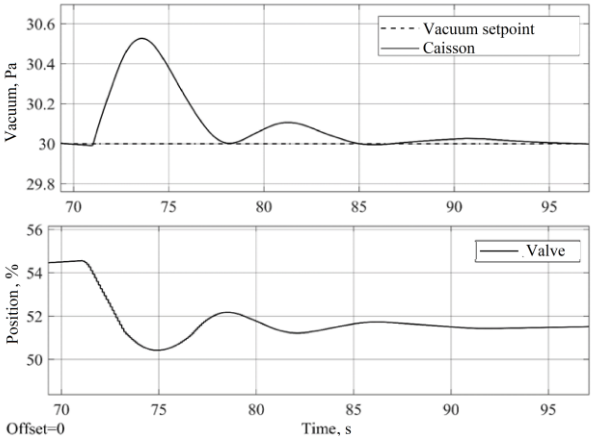

Fig. 7. Intersection process of the automatic control system on the vacuum channel by the gas-vacuum system in the caisson

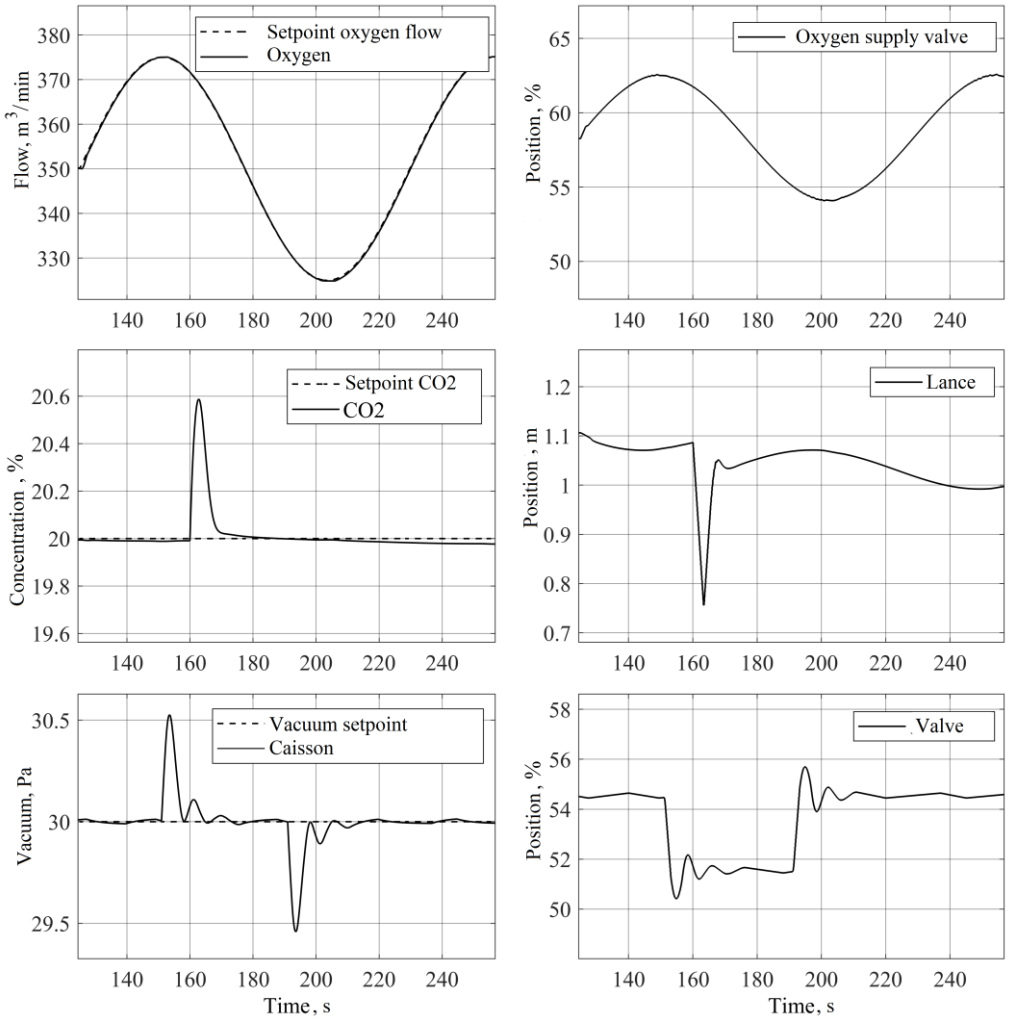

Fig. 8. Front processes of the automatic control system for oxygen converter melting during the second purge period

4. Conclusions

An advanced process control of the refining and heating processes of the metal with reliable blast mode during the purge of the converter bath is described. The using of Model predictive control approach with taking into account the set requirements for quality of operation and provide high operations reliability is proposed.

It is known that at a certain chemical composition of iron, the thermal regime of the process depends on the rate of decarburization, the degree of combustion of CO to CO_2 and the amount of iron oxides in the slag, which, in turn, depend on the distance of the lance to the level of a quiet bath. Adjustment of the lance position is carried out according to the economic regime, based on the increased degree of combustion of CO to CO_2 in the converter cavity. The non-stationary of the melting processes is shown and explained. It makes the use of classical control methods irrational.

It is recommended to use the MPC strategy to solve those processes synchronization problem under physical and technical constraints. The approach minimizes the functionality that characterizes the quality of the adjustment process in real time. The predicted behaviour of a dynamic system will generally be different from its actual motion. Math models of processes are built. The decarburization process is represented as non-stationary first-order inertial transfer function, the gain and time constant of which depends on the melting period and the purge duration. The change in the degree of supplementation of CO to CO_2 is also described by the such model type. The non-stationary oscillatory link describes the system in which the input value of the lance distance to the level of a quiet bath and the initial – the degree of carbon oxidation to CO_2 .

The behaviour of the system is predicted by MPC and the resulting structure is optimized to find the optimal control of the oxygen converter process. The approach takes into account the constraints imposed on both control variables and control variables.

In order to work in real time, it is necessary that the solution of the optimization problem is carried out fairly quickly. The proposed approach was modeled in dynamics in the corresponding software environment. The simulation results show the achievement of the required quality indicators.

References

[1] Backman J., et al.: Methods and Tools of Improving Steel Manufacturing Processes: Current State and Future Methods. International Federation of Automatic Control PapersOnLine 52(13)/2019, 1174–1179 [http://doi.org/10.1016/j.ifacol.2019.11.355].
[2] Bogushevskiy V.S., et al.: System for the BOF Process Control. The Advanced Science Open Access Journal 5/2013, 23–27.
[3] Bogushevskiy V.S., Zuboka C.M.: Mathematical modeling of the converter process by energy-saving technology. Technological complexes 2/2013, 32–38.
[4] Camacho E.F., Bordons A.: Model Predictive Control. 2nd ed, Springer-Verlag London 2007.
[5] Cherneha D.F., et al.: Fundamentals of metallurgical production of metals and alloys. High School, Kyiv 2006.
[6] Ghosh S., et al.: BOF process dynamics. Mineral Processing and Extractive Metallurgy 128(1)/2018, 1–17 [http://doi.org/10.1080/25726641.2018.1544331].
[7] Kouvaritakis B., Cannon M.: Model Predictive Control Classical, Robust and Stochastic. Springer-Verlag, London 2016.
[8] Ruuska J., et al.: Mass-balance Based Multivariate Modelling of Basic Oxygen Furnace Used in Steel Industry. International Federation of Automatic Control PapersOnLine 50(1)/2017, 13784–13789 [http://doi.org/10.1016/j.ifacol.2017.08.2065].
[9] Stepanets O., Mariiash Y.: Analysis of Influence of Technical Features of a PID – controller Implementation on The Dynamics of Automated Control System. Eastern-European Journal of Enterprise Technologies 3(2)/2018, 60–69 [http://doi.org/10.15587/1729-4061.2018.132229].
[10] Zhang J.: Optimal Control Problem of Converter Steelmaking Production Process Based on Operation Optimization Method. Discrete Dynamics in Nature and Society 2015, Article ID 483674 [http://doi.org/10.1155/2015/483674].
[11] MathWorks. Design Controller Using MPC Designer. http://www.mathworks.com/help/mpc/gs/introduction.html?ue (available 5.09. 2018).

Ph.D. Oleksandr Stepanets
e-mail: stepanets.av@gmail.com

Associate professor of Department of Automation of heat-and-power engineering processes of National Technical University of Ukraine "Igor Sikorsky Kyiv Polytechnic Institute".
Engages in the practical automation of complex objects; Industrial Internet of Things; adaptive control systems, model predictive control, fuzzy logic. Responsible for the scientific direction of the department.

http://orcid.org/0000-0003-4444-0705

M.Sc. Yurii Mariiash
e-mail: mariahyuriy@gmail.com

The Ph.D. student of Department of Automation of heat-and-power engineering processes of National Technical University of Ukraine "Igor Sikorsky Kyiv Polytechnic Institute".
The topic of his scientific research is Model Predictive Control. The research focuses on implementation issues for Model Predictive Controllers and intends to present easy ways of implementing them in industry.

http://orcid.org/0000-0002-0812-8960

otrzymano/received: 22.12.2019 *przyjęto do druku/accepted: 26.06.2020*